



National Library  
of Canada

Acquisitions and  
Bibliographic Services Branch

395 Wellington Street  
Ottawa, Ontario  
K1A 0N4

Bibliothèque nationale  
du Canada

Direction des acquisitions et  
des services bibliographiques

395, rue Wellington  
Ottawa (Ontario)  
K1A 0N4

*Your file - Votre référence*

*Ab file - Note de référence*

## NOTICE

The quality of this microform is heavily dependent upon the quality of the original thesis submitted for microfilming. Every effort has been made to ensure the highest quality of reproduction possible.

If pages are missing, contact the university which granted the degree.

Some pages may have indistinct print especially if the original pages were typed with a poor typewriter ribbon or if the university sent us an inferior photocopy.

Reproduction in full or in part of this microform is governed by the Canadian Copyright Act, R.S.C. 1970, c. C-30, and subsequent amendments.

## AVIS

La qualité de cette microforme dépend grandement de la qualité de la thèse soumise au microfilmage. Nous avons tout fait pour assurer une qualité supérieure de reproduction.

S'il manque des pages, veuillez communiquer avec l'université qui a conféré le grade.

La qualité d'impression de certaines pages peut laisser à désirer, surtout si les pages originales ont été dactylographiées à l'aide d'un ruban usé ou si l'université nous a fait parvenir une photocopie de qualité inférieure.

La reproduction, même partielle, de cette microforme est soumise à la Loi canadienne sur le droit d'auteur, SRC 1970, c. C-30, et ses amendements subséquents.

Canada

**Vehicle Structure Characterization  
Using  
Experimental Modal Testing Techniques**

**Gaëtan Lebel**

**A Thesis  
in  
The Department  
Of  
Mechanical Engineering**

**Presented in Partial Fulfillment of the Requirements  
for the Degree of Master of Engineering at  
Concordia University**

© Gaëtan Lebel, 1993



National Library  
of Canada

Acquisitions and  
Bibliographic Services Branch

395 Wellington Street  
Ottawa, Ontario  
K1A 0N4

Bibliothèque nationale  
du Canada

Direction des acquisitions et  
des services bibliographiques

395, rue Wellington  
Ottawa (Ontario)  
K1A 0N4

*Your file - Votre référence*

*Our file - Notre référence*

**The author has granted an irrevocable non-exclusive licence allowing the National Library of Canada to reproduce, loan, distribute or sell copies of his/her thesis by any means and in any form or format, making this thesis available to interested persons.**

**L'auteur a accordé une licence irrévocable et non exclusive permettant à la Bibliothèque nationale du Canada de reproduire, prêter, distribuer ou vendre des copies de sa thèse de quelque manière et sous quelque forme que ce soit pour mettre des exemplaires de cette thèse à la disposition des personnes intéressées.**

**The author retains ownership of the copyright in his/her thesis. Neither the thesis nor substantial extracts from it may be printed or otherwise reproduced without his/her permission.**

**L'auteur conserve la propriété du droit d'auteur qui protège sa thèse. Ni la thèse ni des extraits substantiels de celle-ci ne doivent être imprimés ou autrement reproduits sans son autorisation.**

ISBN 0-315-87272-1

**Canada**

ABSTRACT

Vehicle Structure Characterization  
Using  
Experimental Modal Testing Techniques

Gaëtan Lebel

Vehicle Structure Characterization by estimating the modal parameters such as modal frequencies, modal dampings, and mode shapes can be used to formulate a modal model in order to describe and understand its structural dynamic behavior. It can be carried-out by using an experimental testing method based upon modal analysis theory. This method is called EMTT (Experimental Modal Testing Techniques). In this thesis, EMTT are used to characterize small and large vehicle structures. For this purpose, a detailed mathematical review which includes EMTT assumptions, structural response representations, SDOF and MDOF mathematical definitions, and FRF (Frequency Response Function) display formats are presented. A discussion on various hardware requirements for measurement, rules of thumb to measure meaningful data, types of error encountered, data averaging methods, and response and excitation systems is also presented.

A step-by-step procedure is illustrated to characterize two cases of vehicle structures studied, namely, a small and three large vehicle structures. A Finite Element Analysis (FEA) was carried-out on the small vehicle structure and the modal results were validated.

In summary, the thesis establishes the step-by-step procedure to carry-out EMTT, on both small and large vehicle structures, using single exciter method, and discusses the method of carrying out a comparative evaluation of modal testing results with Finite Element Analysis.

En mémoire, de toi, Dad

ACKNOWLEDGEMENTS

The author is sincerely grateful to his supervisor, Professor Seshadri Sankar, with whom he has had the pleasure and privilege of studying and working for some five years. His support, encouragement and suggestions have culminated in this thesis.

Thanks are also due to other members of faculty and staff of the CONCAVE Research Centre, Department of Mechanical Engineering, Concordia University, for their time and assistance during the course of this work.

The financial support received by the FCAR, Fonds pour les chercheurs et l'aide à la recherche, is gratefully acknowledged.

The author is greatly indebted to his brother, Jean-François, for his support and encouragement during this endeavor.

The author wishes to thank his family and the family of his sister Reine for their understanding and support during the course of this research.

Lastly, the author wishes to thank his wife and her family for their encouragement and understanding during the course of this work.

TABLE OF CONTENTS

LIST OF FIGURES	xi
LIST OF TABLES	xix
NOMENCLATURE	xxi
CHAPTER 1      INTRODUCTION, LITERATURE SURVEY AND OBJECTIVES	1
1-1 Introduction	2
1-2 Literature Survey	4
1-3 Scope of the Thesis	13
CHAPTER 2      THE BASIC CONCEPTS OF EXPERIMENTAL MODAL ANALYSIS	15
2-1 General	16
2-2 Modal Testing Assumptions	18
2-3 Structural Response Representations	20
2-4 Review of Laplace Transform and Graphical Representation of Modal Parameters	22
2-4-1 Mathematical Representation of a SDOF System	23
2-4-2 Frequency Response Function (FRF)	37
2-4-3 Display Formats for FRF	40
2-4-4 Hysteretic (Structural) Damping	54
2-5 Multiple-Degree-of-Freedom (MDOF) Models	55
2-5-1 Undamped Free Vibration Eigenvalues & Eigenvectors	58
2-5-2 Orthogonal Properties of Eigenvectors	62
2-5-3 Generalized Mass and Generalized Stiffness	63



2-5-4	Normalization of Mode Shapes	64
2-5-5	Forced Vibration - Modal Coordinates	65
2-5-5-1	Undamped System	65
2-5-5-2	Residue and Eigenvector Relationship	69
2-5-5-3	Damped System - Proportional Damping	74
2-5-5-4	Damped System - Non-Proportional Damping	77
2-6	Conclusion	80
<b>CHAPTER 3</b>	<b>MECHANICAL FRF MEASUREMENT TECHNIQUES</b>	<b>81</b>
3-1	General	81
3-2	Measurement Hardware	83
3-3	Frequency Response Function (FRF) Estimation	84
3-4	Coherence Function	88
3-5	Signal-To-Noise Ratio Function	90
3-6	Random and Bias Errors	93
3-7	Aliasing Error	95
3-8	Resolution Bias Error	98
3-9	Discrete Fourier Transform Error	102
3-10	Overlapping Analysis	102
3-11	Averaging Methods	106
3-12	Frequency Bandwidth of Interest	108
3-13	Nonlinearities in Experimental Modal Testing	109
3-14	Response Transducer System	111
3-14-1	Accelerometer Selection	117
3-14-2	Accelerometer Mounting	118

3-14-3	Accelerometer Location	121
3-15	Excitation Waveforms	126
3-15-1	Pure Random	126
3-15-2	Pseudo-Random	130
3-15-3	Periodic Random	133
3-15-4	Sinusoidal	135
3-15-5	Transient	138
3-16	Conclusion	151
 <b>CHAPTER 4 EXPERIMENTAL MODAL TESTING: CASE STUDIES</b>		<b>152</b>
4-1	General	153
4-2	Case I: Modal Testing of the Snowmobile Frame Structure	154
4-2-1	Step 1 - Setting Up the Modal Test	159
4-2-1-1	Choosing the Degrees of Freedom (DOF) and Laying Out the Test Points onto the Structure	159
4-2-1-2	Preparation of the Test Structure	165
4-2-1-3	Choosing the Excitation Technique	166
4-2-1-4	Setting Up the FFT Analyzer	169
4-2-1-5	Calibration of the Force/Response Transducer Combination	172
4-2-1-6	Exciter and Load-Cell Positioning and Connection	179
4-2-1-7	Mounting the Response Transducer (Accelerometer)	184
4-2-1-8	Checking the Measurement Set-Up	187
4-2-2	Step 2 - Making the Measurements	202

4-2-3	Step 3 - Estimating the Modal Parameters by Curve-Fitting	211
4-2-4	Documenting the Test Results	212
4-3	Case II: Modal Testing of Large Vehicle Structures	260
4-4	Conclusion	271
<b>CHAPTER 5 MODAL ANALYSIS OF A SNOWMOBILE FRAME STRUCTURE USING FINITE ELEMENT ANALYSIS (FEA)</b>		<b>272</b>
5-1	General	273
5-2	The ANSYS-PC/LINEAR Finite Element Software	275
5-2-1	General Finite Element Concepts	276
5-2-2	Understanding Static and Modal Structural Analysis Types	284
5-3	Modal Analysis of the Snowmobile Frame Structure Using FEA	285
5-4	Comparison between Experimental and Analytical Modal Results	286
5-5	Conclusion	296
<b>CHAPTER 6 CONCLUSIONS AND RECOMMENDATIONS FOR FUTURE WORK</b>		<b>297</b>
6-1	General	298
6-2	Conclusions and Highlights of the Present Work	300
6-3	Recommendations for Future Work	301
<b>REFERENCES</b>		<b>303</b>

LIST OF FIGURES

2-1	Structural Response Representation of a Single-Span Uniform Beam with End Conditions Hinged-Hinged in Different Domains	21
2-2	Generalized Analytical SDOF System	24
2-3	Free-Body Sketch of the Model shown in Fig. 2-2 ( $\delta x$ = Static Deflection of the Spring, $k\delta x = mg$ )	24
2-4	Transient Motion of the System shown in Fig. 2-2	26
2-5	Time, Frequency, and Laplace Domain Relationships	28
2-6	An s-Plane Representation for a SDOF System	31
2-7	FRF Magnitude, $\ H(j\omega)\ $ , Versus Frequency Ratio $\omega / \omega_0$ for Various Values of the Damping Ratio, $\zeta$ ; System shown in Fig. 2-2	32
2-8	Phase Lag of Displacement Behind Excitation, $\phi$ , for Various Values of the Damping Ratio, $\zeta$ ; System shown in Fig. 2-2	33
2-9	Representation of Equations (2-27) and (2-29)	36
2-10	Typical Receptance FRF Magnitude and Phase Plots for a SDOF System	41
2-11	Log-Log Receptance, Mobility, and Inertance Plots for Undamped System [2]	43
2-12	Nyquist Plot for SDOF System with Viscous Damping Mobility-FRF, (Eq. (2-42))	45
2-13	Nyquist Plot for SDOF System with Viscous Damping Receptance-FRF, (Eq. (2-50))	48
2-14	Plot of Eqs. (2-52) and (2-53)	50
2-15	Plot of Eq. (2-53)	51
2-16	Typical Co-Quad Plots for a Damped SDOF System [2] a) Receptance-FRF, b) Mobility-FRF, c) Inertance-FRF	52
2-17	Typical Nichols Plot of a Lightly Damped SDOF System	53

2-18	Modulus of Eq. (2-56) as a Function of $\omega / \omega_0$ for Various Values of Hysteretic Damping, $\gamma = h^0/k$ [3]	56
2-19	Phase of Eq. (2-56) as a Function of $\omega / \omega_0$ for Various Values of Hysteretic Damping, $\gamma = h/k$ [3] <sup>0</sup>	56
2-20	Nyquist Plot of the Receptance-FRF for Hysterecally-Damped SDOF System, (Eq. (2-57))	57
2-21	Two-Degrees-of-Freedom System	59
2-22	Undamped SDOF System in the Modal Domain, Eq. (2-86)	68
2-23	Typical Mode Shapes: a) Normal, b) Complex [8]	79
3-1	Schematic Hardware Requirement for Mobility Measurement Techniques	85
3-2	Typical Comparison between: a) $H$ and $H_1$ , b) $H$ and $H_2$	89
3-3	Typical FRF Measurement and its Corresponding Coherence Function	91
3-4	Normalized Random Error Versus Number of Averages [6]	94
3-5	Representation of the Resolution Bias Error	99
3-6	Time Histories and their Corresponding FRF	100
3-7	Example Comparing $H_1$ and $H_2$ with Leakage for Two Different Spectral Resolutions [5]	101
3-8	Concepts of Discrete Fourier Transform Error [7]	103
3-9	Selection of Different Degrees of Overlap [6]	104
3-10	Typical Force Versus Displacement Characteristics for Some Symmetrical Spring Arrangements: a) Hardening Type Spring, b) Linear Type Spring, c) Softening Type Spring	112
3-11	Typical Resonance Curves for Various Levels of Excitation: a) Hardening Type Spring, b) Linear Type Spring, c) Softening Type Spring	113
3-12	Typical Resonance Curve for a Hardening Type Showing the Region of Instability (Hatched Areas)	114

3-13	Resonance Curves for a Hardening Type Measured for Various Levels of Excitation of an Analog Model System [12]	115
3-14	Schematic Measurement Transducer and Signal Conditioner/Amplifier Sequence	116
3-15	Graphical Illustration of Transverse Sensitivity	119
3-16	Accelerometer Attachment Methods and their Corresponding Frequency Response Limits	120
3-17	Correct Clamping of an Accelerometer Cable to Minimize Cable Noise Due to Cable Whip	122
3-18	Accelerometer Mass Loading Effect [5]	124
3-19	Possible Driving-Point Response Measurements [5]	125
3-20	Random Signal and its Amplitude Probability Density	128
3-21	Auto-Spectrum of a Random Signal Versus Number of Averages	129
3-22	Baseband and Zoom Analysis	131
3-23	Quasi-Flat Spectrum	132
3-24	Comparison of Pure Random, Pseudo-Random, and Periodic Random Waveforms [20]	134
3-25	FRF Measurement by Sine Sweep Test - Distortion Effect of Sweep Rate [2]	137
3-26	Effect of Hammer Bounce on the Force Spectrum	141
3-27	Effect of Hammer Bounce on the FRF Measurement	142
3-28	Typical Signal Versus Crest Factor Values	143
3-29	Typical Impact Force Signal and its Corresponding Spectrum	144
3-30	Frequency Spectra of Three Pulses of Equal Energy [13]	146
3-31	Effects of Different Impact Hammer Configurations [5]	148
3-32	Cosine Taper Force Window [10]	149

3-33	Window for Response from Impact [5]	150
4-1	Pictorial View of the Snowmobile Frame Structure	155
4-2	First Large Vehicle Structure [14]	156
4-3	Second Large Vehicle Structure [14]	157
4-4	Third Large Vehicle Structure [14]	158
4-5	Schematic 3-D Model of the Snowmobile Frame Structure	164
4-6	Bruël & Kjaer Electrodynamic Shaker with its Sine Performance Chart [15]; Head Type 4812 and Exciter Body Type 4801	168
4-7	Simplified Block Diagram for Dual Spectrum Averaging Mode of the Bruël & Kjaer FFT Analyzer, Model 2032 [6]	171
4-8	Schematic Set-Up of the Force Transducer Accelerometer System Calibration for Shaker Excitation Sensitivities $S_A$ and $S_F$ are Calculated as Follow: $S_A = (101,3 \text{ mV/g}) * (1) * (g/9,81 \text{ m/s}^2) = 10,3 \text{ mV/m/s}^2$ $S_F = (0,01 \text{ V/lbf}) * (1\text{lbf}/4,45 \text{ N}) = 2,25 \text{ mV/N}$	174
4-9	Pictorial View of the Force Transducer-Accelerometer for System Calibration	175
4-10	Inversed Measured Inertance-FRF of System shown in Figure 4-9	176
4-11	Coherence Function of System shown in Figure 4-9	177
4-12	Signal-To-Noise Ratio of the System shown in Figure 4-9	178
4-13	Calibration Process for Impact Hammer Testing	180
4-14	Inversed Equalization Function	181
4-15	Stored Equalization Function	182
4-16	Pictorial View of the Shaker and Load-Cell Positioning	185

4-17	Accelerometer Mounting for: a) $H_{1z/-1y}$ Measurement, b) $H_{-1y/-1y}$	186
4-18 a	Equipment Used to Carry-out the Modal Test on the Snowmobile Frame Structure	188
4-18 b	Impact Blow Hammer Used for Exploratory Testing	189
4-19	Output Signal from the Accelerometer When Most Higher Harmonics Died Down - Frequency Around 41 Hz	190
4-20	Auto-Spectrum of the Input Force Signal	191
4-21	Computed Functions at the Driving point: a) Coherence Function, b) Signal-To-Noise Ratio	192
4-22	Co-Quad Display Format of the Inertance-FRF Measured at the Driving Point	193
4-23	Log-Magnitude with Phase Information of the Inertance-FRF Measured at the Driving Point	195
4-24	Magnitude Comparison of FRF-Measurements Measured at -1Y/-1Y and 1Z/-1Y	196
4-25	Magnitude Comparison of FRF-Measurements Measured at -1Y/-1Y and 1X/-1Y	197
4-26	Magnitude Comparison of FRF-Measurements Measured at 1X/-1Y and 1Z/-1Y	198
4-27	Magnitude Comparison of FRF-Measurements Measured at -1Y/-1Z and 1Z/-1Z	199
4-28	Magnitude Comparison of FRF-Measurements Measured at -1Y/-1Z and 1X/-1Z	200
4-29	Magnitude Comparison of FRF-Measurements Measured at 1Z/-1Z and 1X/-1Z	201
4-30	Comparing Reciprocity of FRF-Measurements Measured at -1Y/-3Y and -3Y/-1Y	203
4-31	Comparing Reciprocity of FRF-Measurements Measured at -1Y/-1Y and -1Z/-1Y	204
4-32	Comparing FRF-Measurements Measured at Symmetrical Points: -3Y/-3Y and -1Y/-1Y	205



4-33	Comparing FRF-Measurements Measured at Symmetrical Points: -23Z/-1Y and -23Z/-3Y	206
4-34	3-D Plot of the Twenty Five Measurements Measured Along the Y-Axis	208
4-35	3-D Plot of the Twenty Five Measurements Measured Along the Z-Axis	209
4-36	Typical FRF Measurement with Both Light and Heavy Modal Coupling [4]	213
4-37	Typical FRF Measurement Having Four Modes	215
4-38	Phase and Log-Mag. Display Formats of the Inertance-FRF Measurement Measured at 23Z/-3Y	220
4-39	Imaginary and Real Display Formats of the Inertance-FRF Measurement Measured at 23Z/-3Y	221
4-40	Phase and Log-Mag. Display Formats of the Inertance-FRF Measurement Measured at -23Y/-3Y	222
4-41	Imaginary and Real Display Formats of the Inertance-FRF Measurement Measured at -23Y/-3Y	223
4-42	Plot of the Fifty FRF Measurements in the Imaginary Display Format	224
4-43	Computed Composite Spectrum Using the First Computation Method	226
4-44	Computed Composite Spectrum Using the Fourth Computation Method	227
4-45	Comparison of Measurement at -1Y/-1Y and its Synthesized One Based on Local Curve-Fitting Method	228
4-46	Comparison of Measurement at -1Y/-1Y and its Synthesized One Based on Global Curve-Fitting Method	229
4-47	Comparison of Synthesized FRF Based on Local and Global Curve-Fitting Methods	230
4-48	Isometric View - Mode #1 (30,7 Hz) Local Bending of Rear Section	236
4-49	Isometric View - Mode #2 (40,5 Hz) Longitudinal Twist	237

4-50	Isometric View - Mode #3 (77,1 Hz) Twisting of Front End Only	238
4-51	Isometric View - Mode #4 (78,8 Hz) Twisting of Front End with Small Local Bending of the Rear End	239
4-52	Isometric View - Mode #5 (81,2 Hz) Twisting of Front End with Local Bending of the Rear End	240
4-53	Isometric View - Mode #1 (30,7 Hz) Local Bending of Rear Section	242
4-54	Isometric View - Mode #2 (40,5 Hz) Longitudinal Twist	243
4-55	Isometric View - Mode #3 (77,1 Hz) Local Bending of Left Side Member with Small Twisting of Front End	244
4-56	Isometric View - Mode #4 (78,8 Hz) Local Bending of Right Side Member	245
4-57	Isometric View - Mode #5 (81,2 Hz) Combination of Modes 1, 2, and 3	246
4-58	Time Signals: a) Impulse Signal with a Rectangular Window, b) Response Signal with an Exponential Window	257
4-59	Based on Impact Hammer Techniques: a) FRF Measurement Measured at DOFs -1Y/-1Y, b) Coherence Function Computed at DOFs -1Y/-1Y	258
4-60	Schematic 3-D Model of the First Large Vehicle Structure [17]	263
4-61	Schematic 3-D Model of the Second Large Vehicle Structure for Vertical Excitation [18]	265
4-62	Schematic 3-D Model of the Second Large Vehicle Structure for Lateral Excitation [18]	267
4-63	Schematic 3-D Model of the Third Large Vehicle Structure [19]	269
5-1	Element Summary by Types Available In ANSYS-PC/LINEAR	278

5-2	Element Summary by Types Available In ANSYS-PC/LINEAR	279
5-3	Plot of Equations (5-2), (5-3), and (5-3) [20]	283
5-4	FEM of the Snowmobile Frame - Isometric View	287
5-5	FEM of the Snowmobile Frame - Top View	288
5-6	Master DOF's Selected for Modal Analysis	289
5-7	Isometric View - Mode #1 (30,3 Hz) Local Bending of Rear Section	290
5-8	Isometric View - Mode #2 (44,7 Hz) Longitudinal Twist	291
5-9	Isometric View - Mode #3 (75,5 Hz) Lateral Bending of the Side Steel Pipes (Out-of-Phase)	292
5-10	Isometric View - Mode #4 (89,2 Hz) Lateral Bending of the Side Steel Pipes (In-Phase)	293

LIST OF TABLES

2-1	Values of $\frac{\omega_d}{\omega_0}$ and $\frac{\omega_{peak}}{\omega_0}$ Versus $\zeta$	38
2-2	Different Forms of FRF for Mechanical Systems	39
3-1	Best Estimator ( $H_1$ or $H_2$ ) Versus Classe of Errors	96
3-2	Measuring Time for 100 Averages with Different Degrees of Overlap and $T = 2$ sec. (i.e. Freq. Span = 400 Hz) [6]	105
3-3	Characteristics Comparison Between Excitation Waveforms [5] and [19]	127
4-1	Coordinates of the Test Points (Snowmobile Frame)	162
4-2	Connectivity of the Test Points (Snowmobile Frame)	163
4-3	FFT Analyzer Configuration	170
4-4	Modal results Using Different Cursor Bands	217
4-5	Extracted Modal Parameters: a) Based on Global Curve-Fitting, b) Based on Local Curve-fitting	231
4-6	Cursor Bands and Fit Methods Used to Estimate the Pole Locations and the Residues at All Points	233
4-7	Estimated Modal Parameters	233
4-8	Mode Shape Values - Mode #1 (Based on Y-FRF Data Only)	247
4-9	Mode Shape Values - Mode #2 (Based on Y-FRF Data Only)	248
4-10	Mode Shape Values - Mode #3 (Based on Y-FRF Data Only)	249
4-11	Mode Shape Values - Mode #4 (Based on Y-FRF Data Only)	250

4-12	Mode Shape Values - Mode #5 (Based on Y-FRF Data Only)	251
4-13	Mode Shape Values - Mode #1 (Based on Y- and Z-FRF Data)	252
4-14	Mode Shape Values - Mode #2 (Based on Y- and Z-FRF Data)	253
4-15	Mode Shape Values - Mode #3 (Based on Y- and Z-FRF Data)	254
4-16	Mode Shape Values - Mode #4 (Based on Y- and Z-FRF Data)	255
4-17	Mode Shape Values - Mode #5 (Based on Y- and Z-FRF Data)	256
5-1	Comparison of Analytical and Experimental Centroid of Mass and Total Mass	295

NOMENCLATURE

The following is a list of frequently used symbols and their descriptions. Others are defined where used.

<u>Symbol</u>	<u>Description</u>
$A, A_1, A_2$	Constants
$\alpha$	Indicates Proportionality
$\alpha, \beta$	Rayleigh Damping Constants
$c$	Viscous Damping coefficient
$[C]$	Viscous Damping Matrix
$[\bar{C}]$	Diagonal Modal Damping Matrix
$\delta x$	Static Deflexion of a Spring Element
$e$	Exponential ( $e^1 = 2,71828\dots$ )
$\epsilon_r$	$r^{\text{th}}$ Modal Constant
$f(t)$	Excitation Function of Time
$\{f\}$	Time-Varying Force Vector
$F$	Excitation Amplitude
$\mathbb{F}(j\omega)$	Input Excitation Vector in the Frequency Domain
$\{\phi\}_r$	$r^{\text{th}}$ Mode Shape Vector
$[\tilde{\Phi}]$	Mass-Normalized Eigenvector Matrix
FRF	Frequency Response Function
$\gamma^2$	Coherence Function
$\{\Gamma\}$	Modal Force Vector
$\Gamma_i$	$i^{\text{th}}$ Modal Force Vector

$g(t)$	Time Function
$G(j\omega)$ or $\mathbb{G}(j\omega)$	Fourier Transform of $g(t)$
$G(s)$	Laplace Transform of $g(t)$
$h$	Hysteretic Damping Coefficient
$[H]$	Hysteretic Damping Matrix
$h(t)$	Impulse Response
$H(j\omega)$	Receptance Frequency Response Function (FRF) Matrix
$H_1$	Lower Bound Estimate of the True FRF
$H_2$	Upper Bound Estimate of the True FRF
$H_A(j\omega)$	Inertance FRF Matrix
$H_M(j\omega)$	Mobility Matrix
$ H(j\omega) $ or $\ H(j\omega)\ $	Denotes Modulus of $H(j\omega)$
$[I]$	Identity Matrix
$\text{Im}$	Denotes Imaginary
$j$	$\sqrt{-1}$
$\psi$	Angle in Radian
$\{\psi\}_r$	$r^{\text{th}}$ Mode Shape Vector (Eigenvector)
$[\Psi]$	Eigenvector Matrix
$k$	Stiffness Coefficient
$[K]$	Stiffness Matrix
$[\bar{K}]$	Diagonal Modal Stiffness Matrix
$K_r$	$r^{\text{th}}$ Modal Stiffness
$\mathcal{L}$	Laplace Transform
$\lambda_r$	$r^{\text{th}}$ Eigenvalue
$[A]$	Eigenvalue Matrix

$m$	System Mass
$[M]$	Mass Matrix
$[M]$	Diagonal Modal Mass Matrix
$M_r$	$r^{\text{th}}$ Modal Mass
$p$	Pole Location
$\pi$	Constant ( $\pi = 2.14159\dots$ )
$q_i$	$i^{\text{th}}$ Modal Coordinate
$\{q\}$	Modal Vector Coordinates
Re	Denotes Real
R	Residue
s	Laplace Operator
$S/N(j\omega)$	Signal-To-Noise Ratio Function
$\sigma_i$	$i^{\text{th}}$ Modal Damping
t	Time
$\omega$	Angular Frequency
$\omega_i$ or $\omega_r$	$i^{\text{th}}$ or $r^{\text{th}}$ Natural Frequency
$\omega_0$	Natural Frequency
$\omega_d$	Modal Frequency
$\omega_{di}$	$i^{\text{th}}$ Modal Frequency
$x(t)$	Displacement Function of Time
$\dot{x}(t)$	Velocity Function of Time
$\ddot{x}(t)$	Acceleration Function of Time
$\{x\}$	Displacement Vector
$\{\dot{x}\}$	Velocity Vector
$\{\ddot{x}\}$	Acceleration Vector



$x_c(t)$	Free-Vibration Response
$x_p(t)$	Forced Vibration Response
$X$	Displacement Amplitude
$X(s)$	Laplace Transform of $x(t)$
$X(j\omega)$	Response Vector in the Frequency Domain
$\zeta$	Damping Factor
$( )^*$	Denotes conjugate

**CHAPTER 1**

**INTRODUCTION, LITERATURE SURVEY AND OBJECTIVES**

## CHAPTER 1

### INTRODUCTION, LITERATURE SURVEY AND OBJECTIVES

#### 1-1 Introduction

Structural analysis is an integral part of any design process. Designing of vehicles, mechanical structures, machine tools, spacecraft, buildings require response calculations (static and dynamic) and natural frequencies and mode shapes (modal parameters), which are obtained through structural analysis.

Initially, it was carried-out by constructing either a lumped-mass or distributed model of the system. The system properties, such as mass, stiffness, and damping are first estimated, and then, the equations of motion are formulated by applying Newton's second law. The  $n$  sets of differential equations of motion obtained (for a  $n$  degree-of-freedom system) are then solved to obtain the response either by numerical methods or by modal analysis approach (eigenvalues problem) after modal parameter evaluation.

However, through the above approach, it was difficult to model quickly and accurately complex systems. The development of the finite element method has made it possible to model complex systems. In industries where such approach is used more frequently, such as in

aerospace, the finite element analysis (FEA) and the interpretation of results have been well documented and accepted as a practice tool.

Although FEA is recognized as an acceptable tool for structural design, the confidence in the results of the FEA is still sometimes questionable because of several simplifications in the model and uncertainties due to localized effects in the structure. Hence confidence in the analytical results most often depends on the experience of the analyst who builds the Finite Element Model (FEM).

However, the rapid development of Fast Fourier Transform (FFT) analyzers has contributed to major advances in experimental modal analysis (also known as modal testing) testing techniques which are currently used in several industries to validate their FEM. The validation of the FEM is carried-out by comparing the modal parameters (natural frequency and mode shape) predicted by the analytical model with the ones obtained by testing the system. Experimental modal analysis can also estimate the modal damping of the system which can be incorporated in the FEM for response calculations.

Although, the most common application of modal testing is to validate analytical models, it can be used to understand fatigue problems, to prevent failure in a system, to carry-out advanced analysis, such as sensitivity analysis, etc.

In this thesis, the basics of experimental modal testing are presented, step-by-step, to take full advantage of this testing

technique. Two case studies are presented to highlight the approach.

## 1-2 Literature Survey

Fundamentals and applications of vibration theory and modal testing methods have been presented by Francis S. Tse, Ivan E. Morse, and Rolland T. Hinkle [1] and D.J. Ewins [2]. Reference [2] presents an overview of the testing method in a reasonably detailed coverage, the following subjects: theoretical basis; mobility measurement techniques; modal parameter extraction methods; derivation of mathematical models; and some applications. K. Zaveri [3] has also presented materials related to modal testing: theory and experimental methods. Both single and multiple exciter techniques are discussed.

Modal 3.0 SE Version 6.00 software [4] is a commercially available modal testing software comprising of three modules, namely Modal, SDM and FRS. MODAL software processes measured data and estimates and displays the modal parameters (modal frequencies, modal damping, and animated mode shapes). "What if" investigations can be carried-out with SDM (Structural Dynamics Modification) to determine the effects of potential structural changes in the mass, stiffness, or damping in the structure. It can also synthesize any element in the FRF matrix model and determine the new modal properties of the structure by adding a tuned mass-spring-damper vibration absorber. The last module, FRS (Forced Response Simulation) can predict a structure's response to

specific input forcing functions.

A booklet by Ole Dossing [5] introduces the theoretical background to modal analysis and structural dynamics. Emphasis has been placed on the broadband testing technique using a dual-channel FFT analyzer.

The instruction manual by Brüel & Kjaer [6] provides easy-to-follow, step-by-step procedures for quickly learning the general operation and use of the dual channel signal analyzer type 2032. This manual has two guided tours which is directly related to modal testing: frequency response function and modal parameter identification.

The modal testing chapter in the book by Inman [7] is totally dedicated to topics associated with dynamic measurement and testing of structures.

Another booklet by Ole Dossing [8] presents the theoretical and practical backgrounds to experimental modal analysis. It is a continuation to the first booklet [5].

The handbook by Mark Serridge and Torben R. Licht [9] presents practical guide to making accurate vibration measurements with piezoelectric accelerometers.

Ramsey [10] introduced and used the structural dynamics model for presenting the basic mathematics related to modal analysis and the representation of modal parameters in the Laplace domain. Also, he

described the basic theoretical concepts for calculating transfer and Coherence functions using a digital analyzer.

The ANSYS dynamic seminar notes [11] presents theory and exercises suited for quickly carrying out dynamic analysis, such as modal analysis, harmonic analysis, random vibration analysis, just to name a few, using ANSYS software.

The handbook by Jens Trampe Broch [12] describes measurement data and techniques necessary to characterize vibration and shock.

The major errors encountered in the application of the impulse technique due to measurement noise, shape and time duration of the impulse signal, nonlinearities in structures, and signal processing are presented by Halvorsen and Brown [13]. Effects of weighting functions applied to force and response signals are presented along with zoom transform. Equipments required, measurement set-up, load-cell calibration by "equalization", and measurement procedures are discussed. Frequency Response Functions (FRF) measured between the workpiece and the cutting tool of a milling machine with swept-sine and impulse excitations are compared. Also FRFs measured on hydrodynamic grinder are compared with stationary and rotating spindles.

The Brüel & Kjaer catalogue [15] gives technical informations and specifications on their electronic instruments.

Three confidential reports [16], [17], and [18] present the

experimental modal testing results of three different Eurotunnel wagons. The procedures used to carry-out the three body vibration surveys are also given. General data, features, and physical characteristics of the three wagons tourist cars, purchased by Gie Transmanche Construction and operated by Eurotunnel, are presented in the pamphlet produced by Bombardier Inc. [14].

Ramsey [19] discussed and characterized five different excitation methods namely: Pure Random, Pseudo-Random, Periodic Random, Impact and Swept Sine or Chirp. Also, he discussed the BSFA (Band Selectable Fourier Analysis), the so-called "Zoom" transform versus the Baseband Fourier Analysis (BFA). Results from a single-degree-of-freedom (SDOF) system tested with each of the five excitation methods mentioned above are compared using various analysis techniques (with-and-without distortion, BFA, and BSFA with Pure Random only).

A discussion on modal analysis methods based upon the measurement and post-test processing of FRF in digital form is given by Richardson [20]. In the first section of his paper, he reviewed the Laplace transform of a physical system described by a set of simultaneous second-order linear differential equations and illustrated the real part of a typical transfer function plotted as a function of the  $s$ -variable. Then he derived the transfer matrix in terms of structured modes of vibration; i.e. in terms of modal damping, modal frequency and modal vectors. Also, he showed that the complete modal model can be obtained by measuring only one row or one column of the transfer matrix. In the second section of his paper, he discussed methods of measuring transfer



functions using a two-channel Fast Fourier Transform (FFT) Analyzer with sine wave, transient (hammer or shaker), and random excitations. In addition, digital techniques for obtaining improved and meaningful measurements, including Hanning windowing, exponential smoothing, computation of Coherence function, computation of FRF in the presence of noise, and increasing frequency resolution (BSFA versus BFA) are discussed. Measurement requirements for single- and multi-point excitations are also presented. Modal parameter identification methods are outlined in the last section of his paper for single degree-of-freedom and multiple degrees-of-freedom models. The methods presented based upon single degree-of-freedom models are mode shape by quadrature response, circle fitting, complex division, and by a difference formula. When the overlap between modes is large, multi-degree-of-freedom identification technique must be used. The techniques presented in that case are least squares estimation, and complex exponential algorithm.

New modal testing methods using multiple references and frequency domain curve fitting algorithms are addressed by Shye, Vankarsen, Richardson and Structural Measurement Systems Inc. [21]. Two cases are studied in their paper. The first case studied is an automobile body-in-white tested with two exciters acting in the vertical direction attached to the structure, and with twenty triaxial accelerometers positioned on the structure to measure responses. Random-transient waveforms were used to excite the structure. In order to verify the accuracy of the method, the second case selected was a simple square plate structure from which theoretical natural frequencies and mode

shapes can be calculated. The plate was tested in a "free-free" condition with three accelerometers mounted normal to its surface, and excited by an impact hammer. The methods were extended to account for the effects of "out-of-band" modes. The advantages offered by multiple references are also highlighted.

Mechanical design problems, dynamic analysis techniques, combined with experimental modal testing are discussed by Richardson, Ramsey and Structural Measurement Systems Inc. [22]. The use of a structural dynamic model to perform several analyses such as load analysis, dynamic simulation, modal analysis, and structural modifications are given. Normal mode and transfer function testing methods are presented and compared. A flow-chart is given to show how modal testing and finite element modeling can be combined to solve noise and vibration problems. A sequence of typical steps to follow in case of noise and vibration problems which occur in prototype designs or operational hardware are presented. Dynamic analysis of an automobile drivetrain problem, operational improvement of a computer disc drive servo-control through dynamic analysis, and structural failure analysis of military avionics equipment are examples solved using modal testing techniques.

Structural Measurement Systems Inc. [23] introduced in their paper the concepts of structural dynamics modification in relation with their module SDM discussed earlier. Modal truncation and measurement implications are also discussed. Two examples are also presented in this paper to illustrate the various capabilities of their SDM module. The first example used is a simple two-degree-of-freedom, lumped parameter

system which consists of two masses on rollers connected together by linear springs and dampers. The second one is a cantilever beam, an actual structure, that was tested using an impact testing method.

Ramsey, Structural Measurement Systems Inc., Firmin, and H. G. Engineering Ltd. [24] discussed how FEA and modal testing techniques can be used together to tackle noise and vibration problems. Combined testing and SDM is compared to traditional method of "trial and error" testing through flow-charts. This paper concludes with an example combining analysis and test using SDM module and FESDEC FEA program

A cantilever beam structure is taken as an example by Herbert, Kientzy and Structural Measurement Systems Inc. [25] to illustrate the four basic functional capabilities (hardware modification, resonance specification, substructuring, and dynamic model synthesis) of SDM system developed by Structural Measurement Systems Inc.

Richardson, Formenti, and Structural Measurement Systems Inc. [26] centered their discussion on the reformulation of the solution equations in terms of orthogonal polynomials, and generation of the polynomials themselves using the analytical rational fraction form of the frequency response function. An alternative formulation, to estimate the characteristic polynomial from multiple measurements is also included. Finally, common curve fitting problems are discussed such as measurement noise, frequency resolution, and effects of resonances which lies outside of the analysis band.

Bourdon, Brunelle, Hardy, and Lavigne [27] conducted experimental modal analysis on power transmission line dampers and spacer dampers to estimate quantitatively their dynamic characteristics. Different excitation methods such as impulse hammer excitation using different hammer weights, broadband random and pseudo-random noise at various levels, and constant peak velocity sinusoidal sweep excitation are explored. Because of the non-linearity in those devices, the latest one was selected with three different levels of excitations which correspond to the typical range of aeolian vibration levels encountered on Hydro-Quebec transmission lines. Experimental results are compared to the ones acquired and processed by a Nicolet 6602 Structural Analysis System. In addition, recommendations to improve the accuracy of the technique are identified.

Global curve-fitting of frequency response measurements using rational fraction polynomial method is addressed by Richardson, Formenti and Structural Measurement Systems Inc. [28]. Global frequency and damping and global mode shape steps are discussed. The method is compared with the local curve-fitting (most commonly used today) through a test case with heavy modal coupling (MDOF case) and additive random noise. Also, are given advantages and disadvantages of several curve-fitting methods, such as Local- SDOF, Local-MDOF, Global, and Poly-reference.

Snoeys, Sas, Heylen, and Van Der Auweraer [29] reviewed in their paper, the current trends of various excitation techniques and parameter estimation methods with special emphasis on the use and limitations of

those. The parameter extraction methods are classified as time domain or frequency domain methods. The second part of their paper, discusses applications and use of modal parameters for optimal solution, through flow-charts, in techniques such as structural modification, fatigue, and acoustic analysis.

Dobson [30] developed a new technique, called straight-line, for extracting modal properties from frequency response data. Linear relationships are derived from the inverted standard form used in the analysis of receptance data based upon an Argand diagram ( $1/\text{receptance} = \text{dynamic stiffness}$ ). The technique is tested using synthesized and measured data from systems having "well-separated" and closely coupled modes. Also, the Argand diagram approach is compared to this new technique.

Boentgen, Behring, Allen, and Yeh [31] conducted modal testing on a prototype trashrack panel to confirm the mode shapes and natural frequencies predicted by the Finite Element Model (FEM), and also to verify that assumed damping values used in the FEM to compute the dynamic stresses in the structure are conservative. The structure's dimensions are about 6 meters wide by 2 meters high by 2,5 meters depth, and with a mass of about 38000 Kg. A series of tests was performed using a roving impact excitation, and a hand-held impactor for different structure configurations and test conditions. There is no indication in this paper on the method used to select and extract the modal properties from the frequency response measurements.

Braccesi, and Carfagni [32] illustrated in their paper the usefulness of experimental Structural Dynamic Modifications (SDM) through several application examples simulating structural stiffness modifications. Experimental and theoretical results, including mode shapes and frequencies, are compared for each case studied.

A method to correlate the results from both finite element and modal test studies of a structure is presented by Sidhu and Ewins [33]. Basically, the method consists of comparing the spatial properties (mass and stiffness matrices) obtained from the mathematical model with those calculated using the reduced mass-normalised mode shape vectors and eigenvalues from experimental tests. The discrepancy in those matrices can be directly related to parts of the structure which are poorly modelled. Two examples are studied to indicate the validity of this method.

### 1-3 Scope of the Thesis

The objective of the present research work is to highlight rules of thumb or heuristic knowledge to carry-out experimental modal analysis (modal testing) on small and large vehicle structures.

The thesis is organized in six chapters presenting the basic definitions, concepts, and practical aspects of experimental modal analysis. Overall objective of the thesis and a detailed literature

survey are presented in Chapter 1.

In Chapter 2, mathematical background information is presented to understand the limitations and assumptions of experimental modal analysis.

In Chapter 3 mobility measurement techniques are discussed to obtain meaningful results.

In Chapter 4, two cases studies (small and large vehicle structures) are presented to illustrate the step-by-step procedures to construct, with confidence, an experimental modal model.

In chapter 5, the modal analysis results of finite element analysis (FEA) of the small vehicle structure are compared to the ones obtained from modal testing.

Finally, in Chapter 6, conclusions and highlights of the present work, and recommendations for future work are presented.

**CHAPTER 2**

**THE BASIC CONCEPTS OF EXPERIMENTAL MODAL ANALYSIS**



## CHAPTER 2

### THE BASIC CONCEPTS OF EXPERIMENTAL MODAL ANALYSIS

#### 2-1 General

In general, to carry-out free and forced vibration analyses of a structure, an analytical model is created in terms of its mass, stiffness and damping properties. The first analysis estimates the structure's modal properties (natural frequency, modal damping and mode shape), and the second one predicts the frequency response characteristics of the structure. In many cases, prior to the use of those results, experimental validation of the theoretical model is desirable or mandatory. One can be tempted to measure in laboratory the mass and stiffness distributions of the structure and compare them with the ones used to construct the mathematical model. This approach is not possible since we cannot measure directly those physical properties on the structure. There is a technique called experimental modal analysis, also known as modal testing, which enables an engineer to validate dynamically their analytical mathematical models.

Experimental modal analysis is an experimental testing method based upon modal analysis theory to identify within a frequency range of interest, the inherent dynamic properties of a structure, in terms of its modal parameters such as modal frequency (damped natural frequency), modal damping, and mode shape.

The method consists of exciting and measuring the response behavior of the structure at various locations, and identifying and evaluating all resonances, and mode shapes, from the measured data. Hence, the theoretical model can be validated by comparing the results of the modal analysis to the experimental ones.

The model can be further validated through computer simulations using the experimental modal data. Indeed, an experimental mathematical model can be constructed using the modal parameters identified in the laboratory. Structural Dynamics Modification (SDM) and Forced Response Simulations (FRS) are computer analyses that can be studied using any of the two mathematical models (experimental and analytical). SDM evaluates the effects of changing the dynamic properties due to physical modifications, such as adding or subtracting mass, stiffness, and damping to the structure. FRS predicts the response to assumed input excitations. Thus, high confidence in the theoretical model can be achieved through those different levels of validation.

SDM can also estimate the combined behavior when two or more structural components (substructures) are connected together as one single structure. The substructures can be composed of a combination of structural components for which the modal models have been experimentally built and of tuned mass- spring-damper vibration absorbers. They can be connected together at several points by any combination of scalar springs, dampers, or rigid links.

In this chapter, basic definitions and concepts are presented to

highlight the process and limitations of the modal testing method. Although these simple mathematical definitions can be found in several books and technical papers, they are reviewed here in order to highlight useful rules of thumb in experimental modal testing method and to be able to apply them efficiently.

## 2-2 Modal Testing Assumptions

Modal testing assumes that the structure under test can be adequately modeled by a set of single degree-of-freedom (SDOF) models; characterized by a set of linear second order differential equations. This implies that the structural motions or the dynamic response will always be proportional to the input excitations; i.e.

$$X(j\omega) \propto F(j\omega)$$

or

$$X(j\omega) = H(j\omega) \cdot F(\omega) \quad (2-1)$$

where

$X(j\omega)$  = Response Vector in the Frequency Domain

$H(j\omega)$  = Frequency Response Function (FRF) Matrix

$F(j\omega)$  = Input Excitation Vector in the Frequency Domain

$\omega$  = Angular Frequency

$j$  =  $\sqrt{-1}$

Equation (2-1) to be linear requires that the properties of the structure ( $H(j\omega)$ ) obey the superposition, homogeneity, and reciprocity definitions. Superposition implies that the measured FRF are independent on the type of excitation waveform technique used to excite the structure. Also, if the structure is excited simultaneously by several exciters, the total response will be the sum of the individual ones measured or calculated for each exciter acting separately. Homogeneity demands that the measured FRF do not vary with the level of excitation. Reciprocity holds for all linear systems, and is described by Maxwell's Reciprocity Theorem [1]. The theorem states that the structure exhibits symmetry; in other words, the FRF measured between any two points is independent of which of them is used for excitation or response; i.e.

$$H_{ij} = H_{ji} \quad (2-2)$$

where  $H_{ij}$  is the ratio of the response at point  $i$  in a particular direction (e.g. along X-axis) due to an excitation at  $j$  acting along a particular direction (e.g. along Y-axis); i.e.

$$H_{ij} = \frac{X_{xi}}{F_{yj}} \quad (2-3)$$

Modal testing also assumed that the structure is causal, stable and time-invariant. A causal structure will not start to vibrate before it is excited. The vibrations of a stable structure will die out when the excitation is removed. Lastly, the dynamic properties ( $H(j\omega)$ ) of a time-invariant structure will remain constant during the test period.

In addition, the modal properties should not vary significantly from one part of the structure to another, and only one mode shape should exist at each modal frequency.

### 2-3 Structural Response Representations

There are four different domains in which the response of a structure can be represented. Those are physical domain, time domain, frequency domain, and modal domain, and are illustrated in Figure 2-1.

In the physical domain, the response of a vibrating structure is shown as a complex geometrical deflected pattern defined in terms of its physical coordinates. That physical pattern can also be represented as a sum of simpler, independent deflected patterns called mode shapes and are defined in terms of modal coordinates (q's). Each mode shape or modal deflection is typical of the response of a single-degree-of-freedom (SDOF) structure.

The response in the time domain is shown as a time history or a time signal,  $x(t)$ , and can be measured easily by an accelerometer or motion sensor. This time history can also be defined as a sum of decaying sinusoids, each described by a modal coordinate,  $q_1$ , and a modal damping parameter,  $\sigma_1$ .

In the frequency domain, a Fast Fourier Transform (FFT) analyzer is

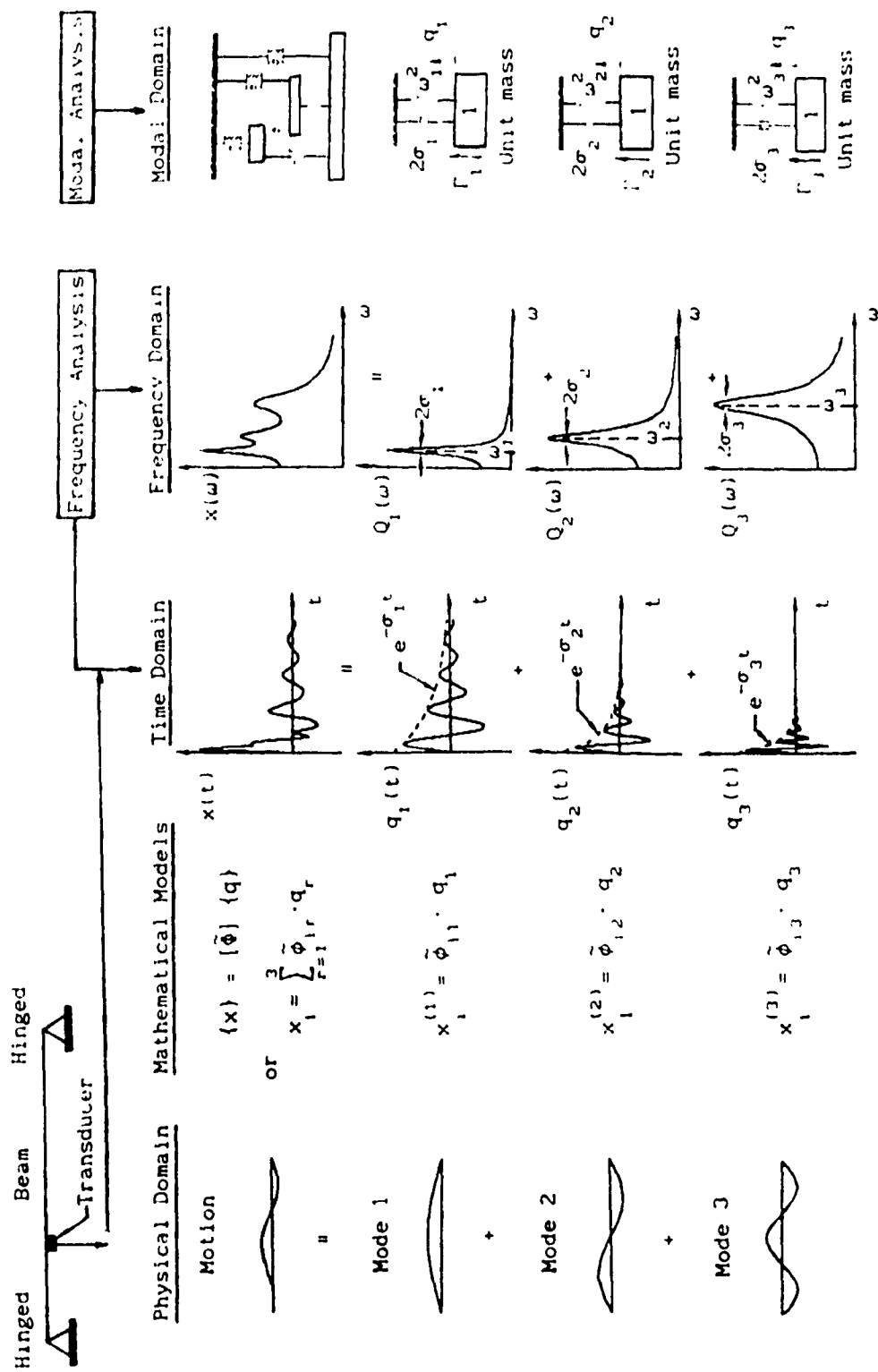


Figure 2-1: Structural Response Representation of a Single-Span Uniform Beam with End Conditions Hinged-Hinged in Different Domains

usually used to compute the frequency spectrum, also called Frequency Response Function (FRF) of a given time signal. A spectrum has basically several resonance and anti-resonance peaks within a selected frequency range, which can also be represented by a set of SDOF response spectra. Each of the spectra is also described by a set of modal parameters.

In the case of a modal domain, a lumped-parameter model is constructed from a set of SDOF models to obtain the overall response of the model.

In summary, the dynamic response of a structure can be described by an infinite set of SDOF models ( $i = 1, \dots, \infty$ ), where each of them is defined by three modal parameters, namely, a modal frequency ( $\omega_{d1}$ ), a modal damping ( $\sigma_1$ ), and a mode shape vector ( $\{\phi\}_1$ ).

#### **2-4 Review of Laplace Transform and Graphical Representation of Modal Parameters**

In the cases of modal analysis and modal testing, it is very important to understand the vibration characteristics of a SDOF system and their relations from one domain to another since the inherent dynamic properties of a complex structure are defined as a linear superposition of a set of SDOF modal parameters.

### 2-4-1 Mathematical Representation of a SDOF System

The generalized model for the SDOF system is shown in Fig. 2-2, and consists of a point mass ( $m$ ), supported by a massless linear spring ( $k$ ) and connected to a linear viscous dashpot ( $c$ ). The mass can only move along the  $x$  direction and will start to oscillate (vibrate) if an external force (excitation) ( $f(t)$ ) is applied on the mass along the same direction.

The equation of motion is found by applying Newton's second law to the free-body sketch in Fig. 2-3 (note: the gravity force cancels out with the static deflection of the spring):

$$f(t) - kx(t) - c\dot{x}(t) = m\ddot{x}(t) \quad (2-4)$$

or

$$m\ddot{x} + c\dot{x} + kx = f(t) \quad (2-5)$$

Equation (2-5) is a second-order non-homogeneous differential equation. It can be shown that the general solution  $x(t)$  of that equation is the sum of the complementary function (free-vibration response,  $x_c(t)$ ) and the particular integral (forced vibration response,  $x_p(t)$ ), that is,

$$x(t) = x_c(t) + x_p(t) \quad (2-6)$$



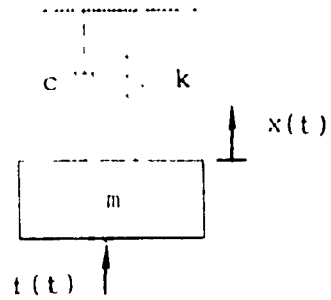


Figure 2-2: Generalized Analytical SDOF System

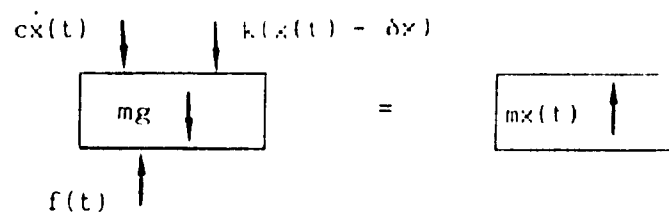


Figure 2-3: Free-Body Sketch of the Model shown in Fig. 2-2  
 ( $\delta x$  = Static Deflection of the Spring,  $k\delta x = mg$ )

Defining the following physical quantities:

$$\omega_0^2 = \frac{k}{m} \quad \text{and} \quad \zeta = \frac{c}{2m\omega_0} \quad (2-7)$$

where  $\omega_0$  is the natural frequency of the system and  $\zeta$  is the damping factor, and using them to rewrite Eq. (2-5) with  $f(t)$  set to zero, we get,

$$\ddot{x} + 2\zeta\omega_0\dot{x} + \omega_0^2 x = 0 \quad (2-8)$$

The solution of the homogeneous equation in Eq. (2-8) corresponds to the complementary function  $x_c(t)$ , and for  $\zeta < 1$  (the underdamped case) is of the form

$$x_c(t) = \exp(-\zeta\omega_0 t) (A_1 \cos \omega_d t + A_2 \sin \omega_d t) \quad (2-9)$$

or

$$x_c(t) = A \exp(-\zeta\omega_0 t) \sin(\omega_d t + \psi) \quad (2-10)$$

where  $A_1$  and  $A_2$  are real constants to be evaluated by the initial conditions, and  $A = \sqrt{A_1^2 + A_2^2}$  and  $\psi = \tan^{-1}(A_1/A_2)$ . The harmonic motion described by Eq. (2-10) is shown in Fig. 2-4. This motion is often referred to as the transient motion of the system. The damped natural frequency,  $\omega_d$ , is defined as

$$\omega_d = \omega_0 \sqrt{1 - \zeta^2} \quad (2-11)$$

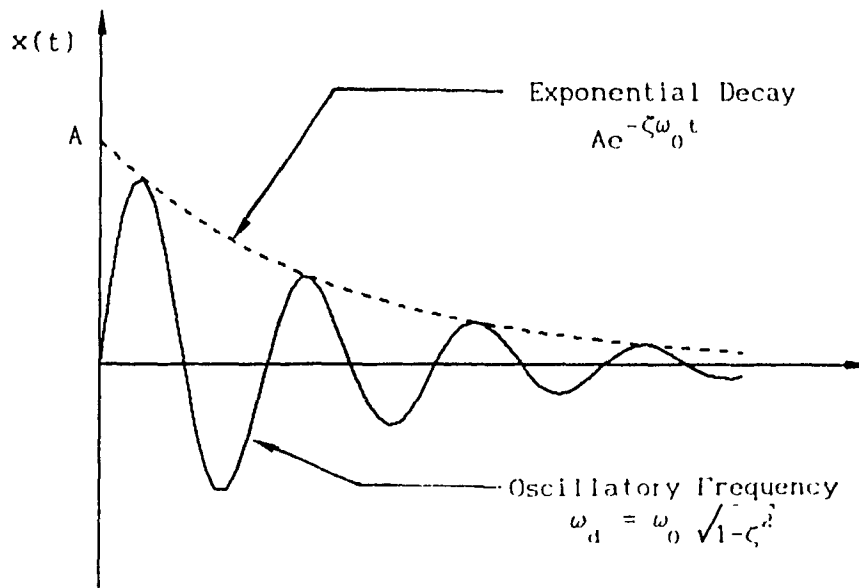


Figure 2-4: Transient Motion of the System shown in Fig 2-2

The modal damping ( $\sigma$ ) is defined as the product of the damping factor ( $\zeta$ ) and the natural frequency ( $\omega_0$ ).

$$\sigma = \zeta \omega_0 \quad (2-12)$$

Hence, in the time domain, the free-vibration response of a SDOF system is described by Eq. (2-10) and its modal parameters are defined by Eqs. (2-11) and (2-12) with Eq. (2-7).

When a harmonic excitation ( $f(t)$ ) is considered, the particular integral or forced response ( $x_p(t)$ ) gives the steady-state response with the complimentary function ( $x_c(t)$ ) becoming zero. For a given harmonic excitation of constant amplitude ( $F$ ) and frequency ( $\omega$ ) of the general form:

$$f(t) = F \exp(j\omega t) \quad (2-13)$$

the steady-state response will be in a similar form as

$$x(t) = x_p(t) = X \exp(j\omega t + \phi) \quad (2-14)$$

where  $X$  is the amplitude of the motion and  $\phi$  is the phase angle of the response relative to the excitation force.

The system can also be studied in the frequency domain or in the Laplace domain. Figure 2-5 shows the relationship between time, frequency and Laplace domains. The Laplace Transform  $\mathcal{L}$  of a time

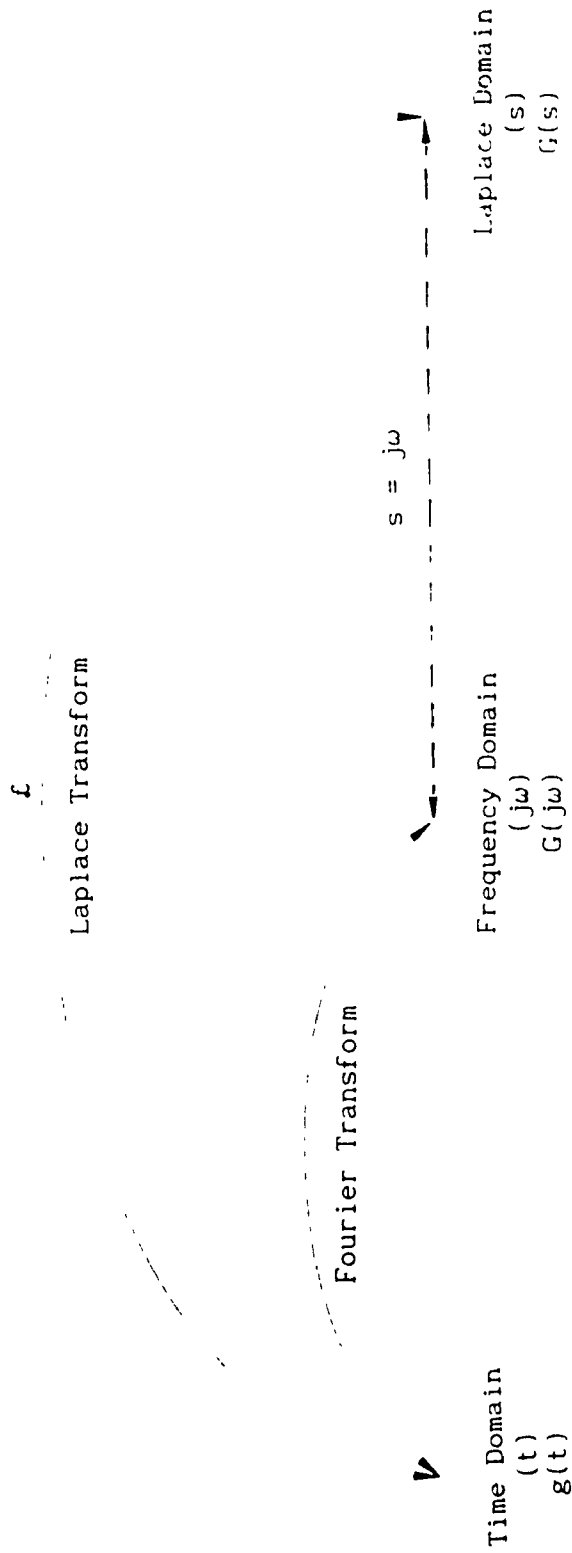


Figure 2-5 Time, Frequency, and Laplace Domain Relationships

function  $g(t)$  is defined as:

$$\mathcal{L}(g(t)) = G(s) \quad (2-15)$$

where

$$G(s) = \int_0^{\infty} g(t) \exp(-st) dt \quad (2-16)$$

and

$$s = \sigma + j\omega \quad (2-17)$$

Hence, the Laplace transform converts a problem from the time domain (real) into the  $s$  domain (complex). As we will see, this conversion or transformation simplifies the mathematics when solving ordinary differential equations (physical system). Another advantage is that the parameters and the behavior of a damped linear system are easier to visualize in the  $s$ -domain.

It can be shown that the Laplace transform of Eq. (2-5) is a simple algebraic equation, where  $s$  is called the Laplace operator and is:

$$(ms^2 + cs + k) X(s) = F(s) \quad (2-18)$$

The compliance transfer function ( $H(s)$ ) relates the displacement to the force and is expressed mathematically as,

$$H(s) = \frac{X(s)}{F(s)} = \frac{1}{ms^2 + cs + k} \quad (2-19)$$

The Fourier transform or the Frequency Response Function (FRF) is obtained by substituting  $j\omega$  for  $s$  in Eq. (2-19):

$$H(j\omega) = \frac{X(j\omega)}{F(j\omega)} = \frac{1}{-m\omega^2 + j\omega c + k} \quad (2-20)$$

The roots of the polynomial denominator of Eq. (2-20) are the poles or singularities of the system:

$$j\omega_{1,2} = -\sigma \pm j\omega_d \quad (2-21)$$

or

$$p = -\sigma + j\omega_d \quad \text{and} \quad p^* = -\sigma - j\omega_d \quad (2-22)$$

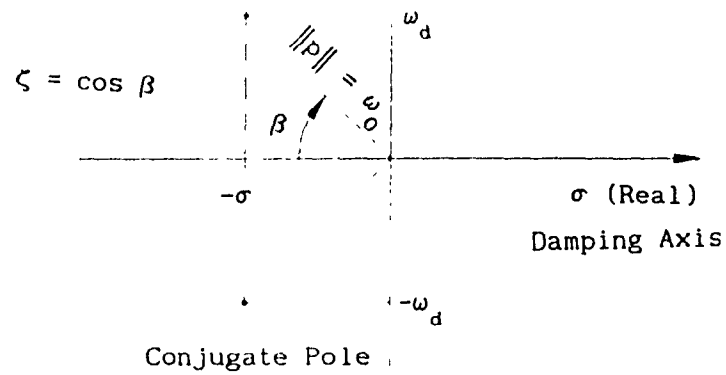
where  $\sigma$  and  $\omega_d$  are defined by Eqs. (2-7), (2-11), and (2-12). The modal parameters ( $\sigma$  and  $\omega_d$ ) determine the character of the time response and are shown on the  $s$ -plane in Fig. 2-6.

Equation (2-20) is a complex-valued function of frequency and can be represented by its real (coincident or in-phase response) part and its imaginary (quadrature or out-of-phase response) part or equivalently by its magnitude and phase. The latter representation is shown in Figs. 2-7 and 2-8. It is observed in Fig. 2-7 that the magnitude of the resonance peak decreases as the damping in the system increases and in Fig. 2-8 that the phase is always  $90^\circ$  at the resonance; i.e. when the ratio of the excitation frequency ( $\omega$ ) to the natural frequency ( $\omega_0$ ) is equal to one:

## s-PLANE

Pole location:  $s = \sigma + j\omega$ ▲  $j\omega$  (Imaginary)

Frequency Axis



$$\text{Note: } \|p\| = \sqrt{\sigma^2 + \omega_d^2} = \sqrt{\omega_0^2 \zeta^2 + \omega_0^2 (1 - \zeta^2)} = \omega_0$$

Figure 2-6: An s-Plane Representation for a SDOF System



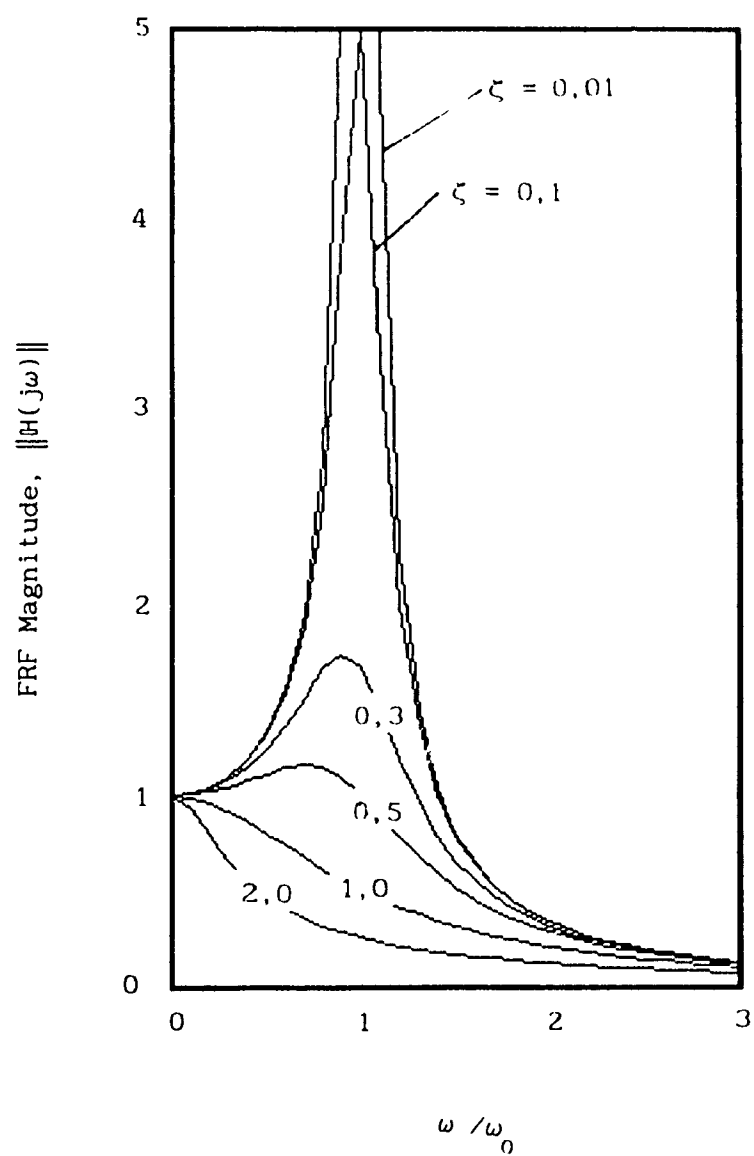


Figure 2-7: FRF Magnitude,  $\|H(j\omega)\|$ , Versus Frequency Ratio  $\omega / \omega_0$  for Various Values of the Damping Ratio,  $\zeta$ ; System shown in Fig. 2-2

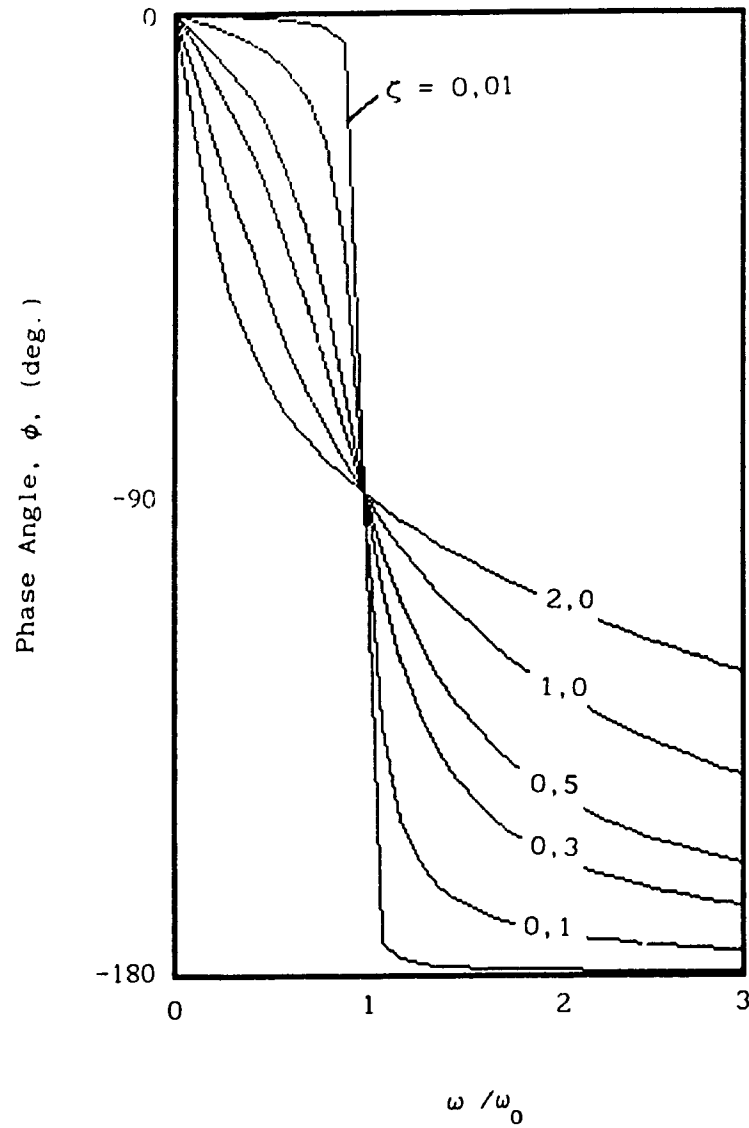


Figure 2-8: Phase Lag of Displacement Behind Excitation,  $\phi$ , for Various Values of the Damping Ratio,  $\zeta$ ; System shown in Fig. 2-2

$$\frac{\omega}{\omega_0} = 1 \quad (2-23)$$

Equation (2-20) can always be written in a partial fraction form as:

$$H(j\omega) = \frac{a}{(j\omega - p)} + \frac{a^*}{(j\omega - p^*)} \quad (2-24)$$

where  $a$  and  $a^*$  are complex constants and  $*$  denotes the conjugate. It can be shown that the value of the constants commonly called the residues are given by:

$$a = R = -j \frac{1}{2m\omega_d} \quad \text{and} \quad a^* = R^* = j \frac{1}{2m\omega_d} \quad (2-25)$$

Therefore Eq. (2-23) becomes

$$H(j\omega) = \frac{R}{(j\omega - p)} + \frac{R^*}{(j\omega - p^*)} \quad (2-26)$$

Hence, the FRF ( $H(j\omega)$ ) can be defined in terms of the pole location ( $p$ ) and the residue ( $R$ ) - and their complex conjugates ( $p^*$  and  $R^*$ ) where  $p$  and  $R$  are defined in terms of spatial parameters. Due to the symmetry of the FRF, Eq. (2-26), FFT (Fast Fourier Transform) analyzers only record the data for positive frequencies, i.e. along the positive  $j\omega$  axis. In addition, in the vicinity of a positive frequency peak, the majority of the FRF, for lightly damped systems, is described by the single pole formula:

$$H(j\omega) = \frac{R}{(j\omega - p)} \quad (2-27)$$

and at the resonance peak ( $\omega \approx \omega_d$ ) the FRF is approximately equal to the ratio of the residue to the modal damping:

$$H(j\omega) \approx \frac{R}{\sigma} \quad (2-28)$$

The residue is sometimes called the pole-strength and dividing it by the modal damping gives the response magnitude to unit force (Eq. (2-28)).

It can be shown that the inverse Laplace transformation of the FRF of a SDOF system is the impulse response and has the form:

$$h(t) = 2 \|R\| \exp(-\sigma t) \sin(\omega_d t) \quad (2-29)$$

Equations (2-27) and (2-29) are illustrated in Fig. 2-9. The real part of the pole location ( $\sigma$ ) is the modal damping and, in the time domain, it represents the rate at which a damped oscillation decays. In the frequency domain,  $\sigma$  represents half the -3 dB bandwidth of the FRF peak. The imaginary part of the pole location is the damped frequency ( $\omega_d$ ) for a free decaying oscillation. It can be shown that the peak of the FRF occurs at

$$\omega_{\text{peak}} = \omega_0 \sqrt{(1 - 2\zeta^2)} \quad (2-30)$$

which indicates that the maxima does not occur neither at the undamped natural frequency ( $\omega_0$ ) nor at the damped frequency ( $\omega_d$ ). However, for

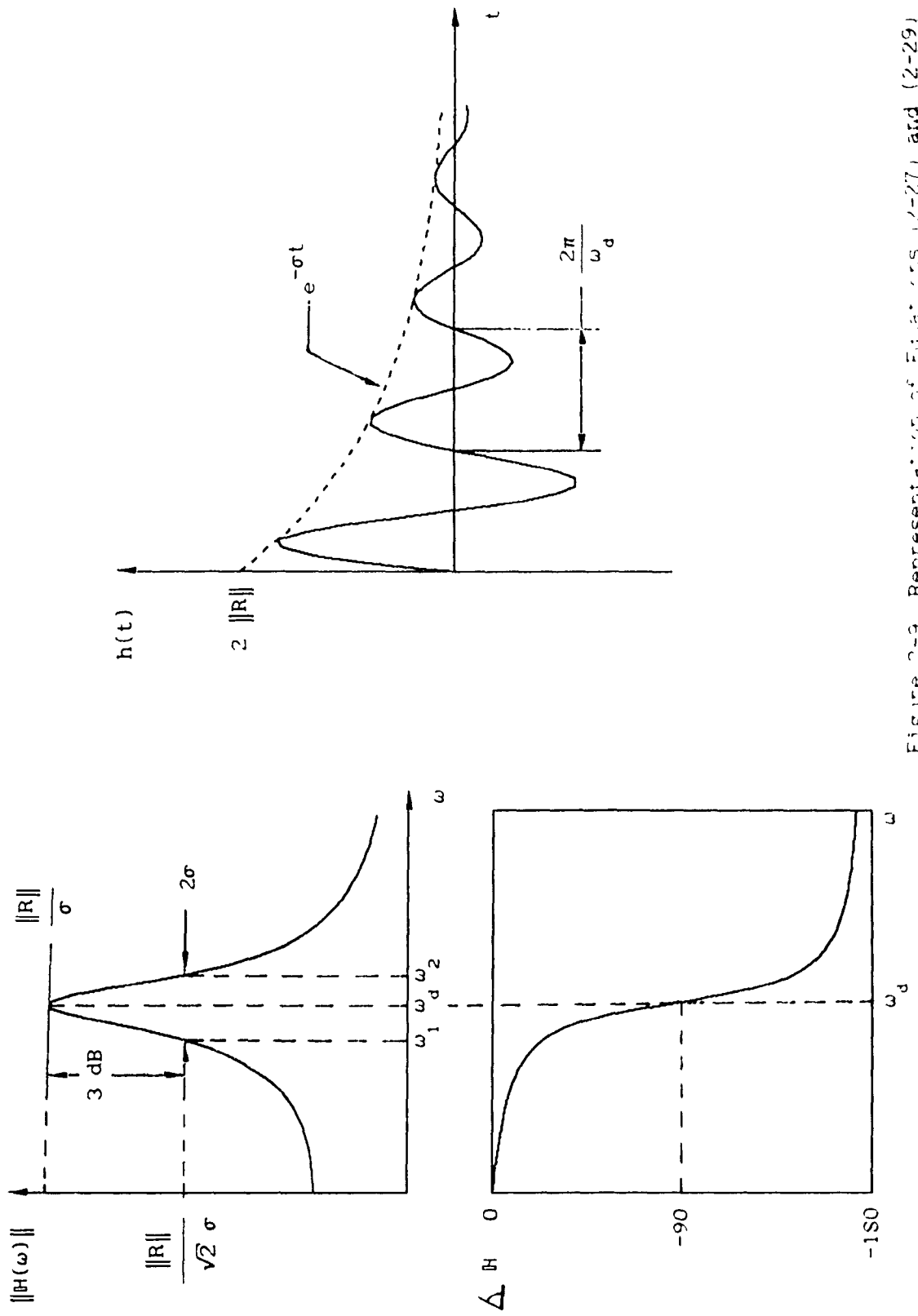


Figure 2-9 Representation of Equations (2-27) and (2-29)

$\zeta \leq 0.1$ , Table 2-1 shows that the peak frequency given by Eq. (2-30) is approximately equal to the damped frequency  $\omega_d$  and the undamped frequency ( $\omega_0$ ).

Using an FFT analyzer, both the pole location and residue can be extracted from FRF measurements. The pole location is a quantitative measure of the dynamic properties of the system and is defined by two modal parameters ( $\omega_d$  and  $\sigma$ ). The residue is a qualitative measure of the system behavior and as we will see in Section 2-5-6, it is related to the third modal parameter, the mode shape.

#### 2-4-2 Frequency Response Function (FRF)

There are different forms of Frequency Response Function (FRF) used to represent the behavior of mechanical systems. Those are summarized in Table 2-2. When considering a harmonic excitation as defined by Eq. (2-13), the velocity and acceleration are related to the displacement by the following simple relationships:

$$x(t) = X \exp(j\omega t + \phi) \quad (2-31)$$

$$\dot{x}(t) = j\omega X \exp(j\omega t + \phi) = j\omega x(t) \quad (2-32)$$

$$\ddot{x}(t) = -\omega^2 X \exp(j\omega t + \phi) = -\omega^2 x(t) \quad (2-33)$$

Thus, the relationships for FRF will be:

$$H(j\omega)_{\text{velocity}} = j\omega H(j\omega) \quad (2-34)$$

Table 2-1: Values of  $\frac{\omega_d}{\omega_0}$  and  $\frac{\omega_{peak}}{\omega_0}$  Versus  $\zeta$

$\zeta$	$\frac{\omega_d}{\omega_0} = \sqrt{1 - \zeta^2}$	$\frac{\omega_{peak}}{\omega_0} = \sqrt{1 - 2\zeta^2}$	Comments
> 1,0	—	—	Over damped (No Oscillation, $\omega_d = 0$ )
1,00	0	*	Critically Damped
0,80	0,60	*	
$1/\sqrt{2}$	$\sqrt{1/2}$	0	
0,50	0,87	$\sqrt{1/2}$	Under damped, ( $\zeta < 1$ )
0,30	0,95	0,91	
0,20	0,98	0,96	
0,15	0,99	0,98	
0,10	0,99	0,99	
			$\omega_{peak} \cong \omega_0$
0	1	1	Undamped, ( $\omega_{peak} = \omega_0$ )

\* = No Real Solution

Table 2-2: Different Forms of FRF for Mechanical Systems

Response Parameter X	Standard FRF X/F	Inverse FRF F/X
Displacement, X	Receptance Admittance Compliance Dynamic Flexibility	Dynamic Stiffness
Velocity, $\dot{X}$	Mobility	Mechanical Impedance
Acceleration, $\ddot{X}$	Inertance Accelerance	Apparent Mass



or

$$H(j\omega)_{\text{accelerance}} = -\omega^2 H(j\omega) \quad (2-35)$$

These relationships show that the mobility and the accelerance are out-of-phase with the displacement by  $90^\circ$  and  $180^\circ$  respectively.

Although the amplitude and phase vary from one form of FRF to another, we will see that any of them can be used to extract the modal parameters.

### 2-4-3 Display Formats for FRF

It is always useful to display the Frequency Response Function (FRF) in a format which is best suited to the particular application in hand. The most common type of display format is the modulus in terms of receptance (ratio of displacement to force) and phase versus frequency. In this display format, resonances occur as peaks and the width of each peak is proportional to its damping value. An example of this format for a typical SDOF system is shown in Figure 2-10. The static deflection is taken by the spring stiffness alone. At low frequencies, the response is controlled by the spring (line of constant dynamic stiffness of zero slope) and in phase with the excitation. The inertial force of the mass increases with  $\omega$ , and at the peak frequency ( $\omega_{\text{peak}}$ ) it cancels out with the spring term so that the response is limited only by the damping term. At that frequency, the response lags the excitation by exactly  $90^\circ$ . When the response ( $x(t)$ ) lags the excitation by  $180^\circ$ , the system behaves like a simple mass and ( $\ddot{x}(t)$ ) is in phase

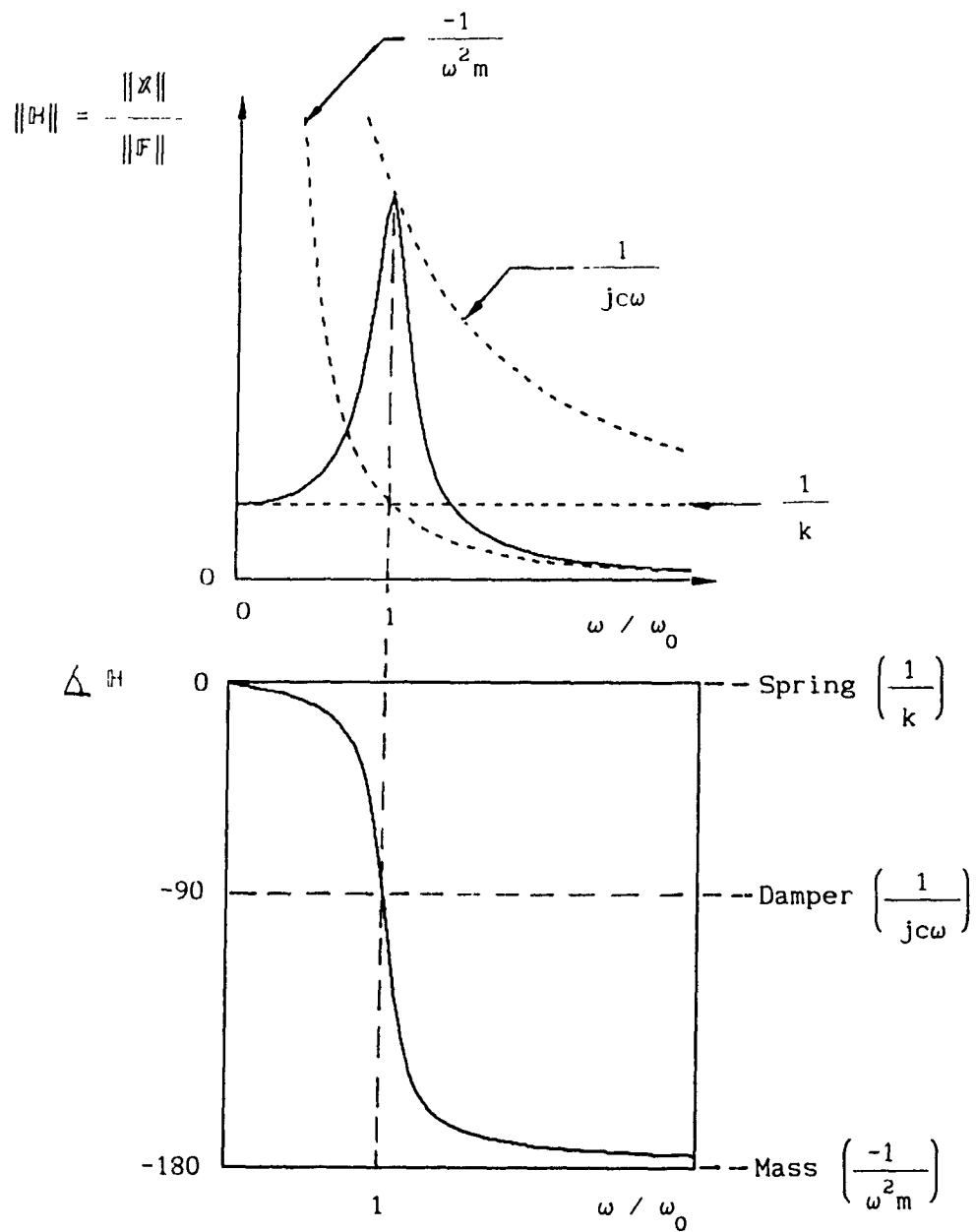


Figure 2-10: Typical Receptance FRF Magnitude and Phase Plots for a SDOF System

with  $f(t)$ ). If logarithms of both modulus and frequency are considered, the two plots are called the Bode plot. The Bode plot is convenient when the data is spread over a wide range of values of modulus and frequencies. This display format first requires that the modulus is transformed in a nondimensional quantity by dividing it by a reference value and then expressed in decibels (dB). The decibel expression is given by:

$$\text{dB} = 20 \log \| H(j\omega) \| \quad (2-36)$$

where

$$\| H(j\omega) \| = \frac{1 / k}{\sqrt{(1 - r^2)^2 + (2\zeta r)^2}} \quad (2-37)$$

A typical Log-Log plot of an undamped SDOF system with corresponding plots for the mobility and inertance of the same system are shown in Figure 2-11. We see that mass and stiffness properties appear as straight lines in the three plots. It can be shown that any of the three plots can be used to estimate the modal properties of a system. However, when it is desired to carry-out Structural Dynamic Modification (SDM) analyses, the bode plot should be used to extract the modal properties in order to keep the units consistent.

An other display format of the FRF is by plotting in the complex plane, the coincident (real part) versus the quadrature (imaginary part) of the FRF, the plot is nearly a circle arc with frequency increasing clockwise around the arc. This display format is called Nyquist plot or Argand plot. For viscously-damped systems, the mobility has particular FRF form of FRF that traces out an exact circle in the Nyquist plane.

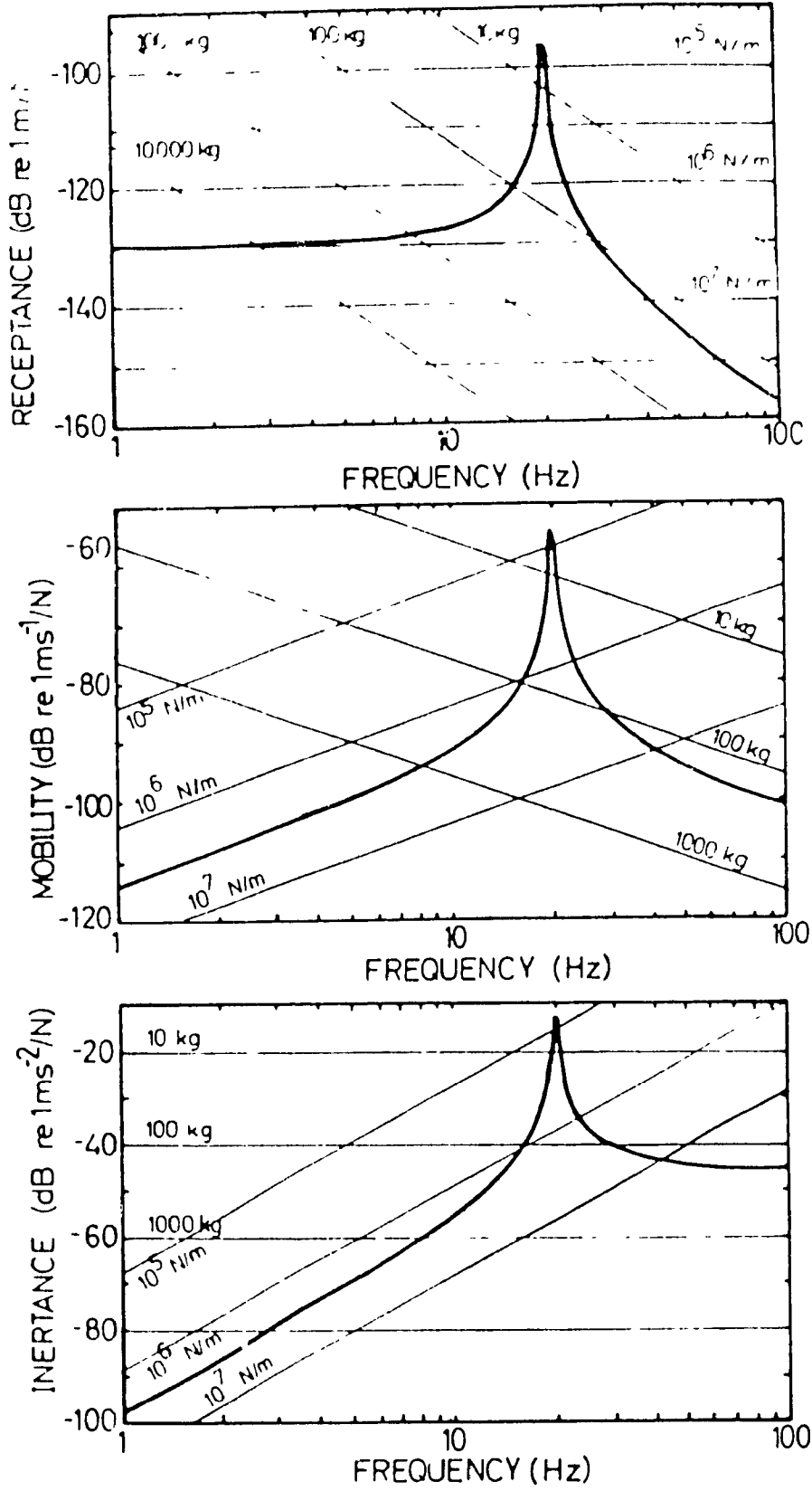


Figure 2-11. Log-Log Receptance, Mobility, and Inertance Plots for Undamped System [2]

Other FRF's such as receptance and inertance trace out a distorted circle, and the degree of distortion will become negligible as the damping decreases [2]. From Eqs. (2-20) and (2-32) the mobility FRF is

$$H_M(j\omega) = \frac{\dot{X}(j\omega)}{F(j\omega)} = \frac{j\omega}{(k - m\omega^2) + j\omega c} \quad (2-38)$$

or

$$H_M(j\omega) = \frac{\dot{X}(j\omega)}{F(j\omega)} = \text{Re}[H(j\omega)] + j\text{Im}[H(j\omega)] \quad (2-39)$$

where

$$\text{Re}[H_M(j\omega)] = -\frac{\omega^2 c}{(k - \omega^2 m)^2 + (\omega c)^2} \quad (2-40)$$

$$\text{Im}[H_M(j\omega)] = \frac{\omega(k - \omega^2 m)}{(k - \omega^2 m)^2 + (\omega c)^2} \quad (2-41)$$

and subscript M denotes mobility.

It can be shown that equations (2-40) and (2-41) form the following relationship:

$$\left[ \text{Re}[H_M(j\omega)] - \frac{1}{2c} \right]^2 + \left[ \text{Im}[H_M(j\omega)] \right]^2 = \left[ \frac{1}{2c} \right]^2 \quad (2-42)$$

Hence, Eq. (2-42) is the equation of a circle of radius  $1/2c$  and with its centre at  $(\text{Re} = 1/2c, \text{Im} = 0)$ , as illustrated in Figure 2-12.

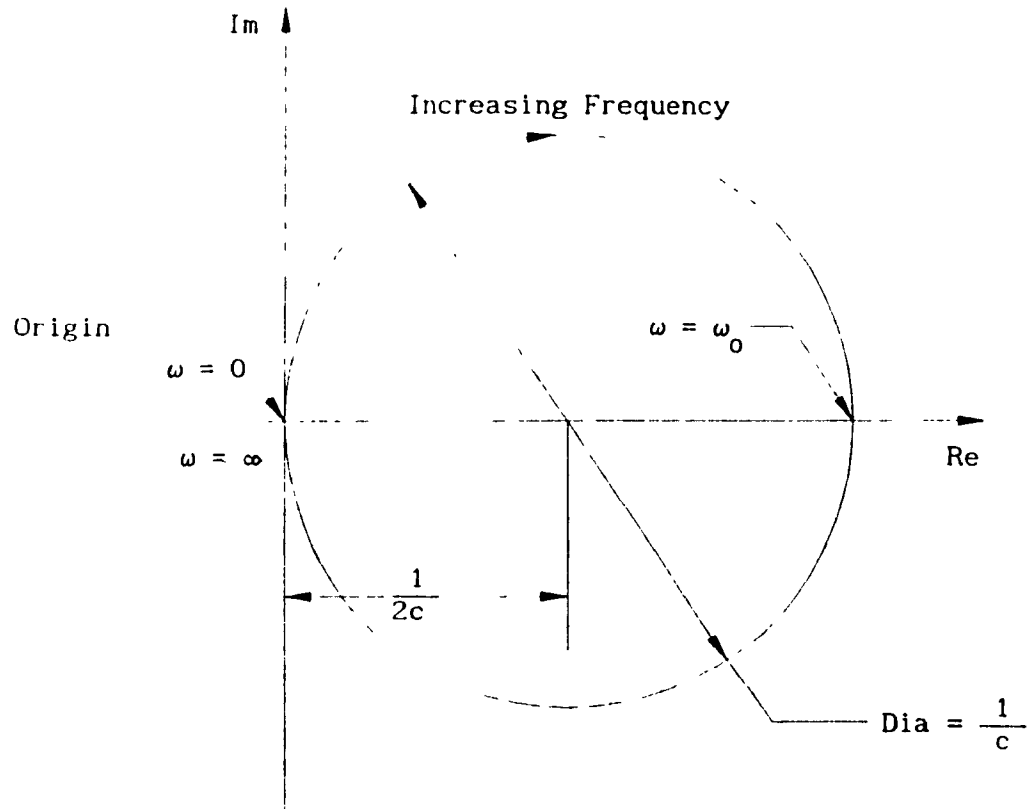


Figure 2-12: Nyquist Plot for SDOF System with Viscous Damping Mobility-FRF, (Eq.(2-42))

In the case of lightly damped systems ( $\zeta \leq 0.20$ ), the second term of Eq. (2-26) in the receptance FRF can be neglected in the vicinity of a modal resonance, so that

$$H(j\omega) \approx \frac{R}{(j\omega - p)} \quad (2-43)$$

The residue  $R$  is almost always real valued and can be identified by picking the quadrature response value (imaginary value) of the FRF at the modal frequency. Eq. (2-43) can also be expressed as:

$$H(j\omega) \approx \frac{\bar{R}}{2j(j\omega - p)} \quad (2-44)$$

where  $\bar{R}$  is a complex constant. Equation (2-44) can also be written in a polar form

$$H(j\omega) \approx \frac{\|\bar{R}\| \exp(j\beta)}{2j(j\omega - p)} \quad (2-45)$$

where  $\|\bar{R}\|$  is the modulus of the complex residue, and  $\beta$  is the phase of the complex residue. If we assume that  $\bar{R}$  is real valued and one unit magnitude, Eq. (2-45) gives:

$$H(j\omega) \approx G(j\omega) = \frac{1}{2j(j\omega - p)} \quad (2-46)$$

and substituting Eq. (2-22) into (2-46) and rearranging gives:

$$G(j\omega) = \text{Re}[G(j\omega)] + j \text{Im}[G(j\omega)] \quad (2-47)$$

where

$$\text{Re}[G(j\omega)] = \frac{(\omega_d - \omega)}{2[(\omega_d - \omega)^2 + \sigma^2]} \quad (2-48)$$

and

$$\text{Im}[G(j\omega)] = \frac{-\sigma}{2[(\omega_d - \omega)^2 + \sigma^2]} \quad (2-49)$$

It can be shown that equations (2-48) and (2-49) form the following relationship:

$$\left[ \text{Re}[G(j\omega)] \right]^2 + \left[ \text{Im}[G(j\omega)] + \frac{1}{4\sigma} \right]^2 = \left[ \frac{1}{4\sigma} \right]^2 \quad (2-50)$$

Hence, for this case, the receptance FRF of a SDOF system forms a circle in the Nyquist plane whose center is displaced  $1/4 \sigma$  down from the real axis and with diameter  $1/2 \sigma$  as shown in Figure 2-13. It can be noted that this circle is similar to the one formed by the mobility FRF but rotated clockwise about the origin by  $90^\circ$  and with a radius augmented by a factor  $m$ , the mass of the system.

Now if we assume that  $\bar{R}$  is an arbitrary complex residue, Eq. (2-45) can be rewritten as

$$H(j\omega) \approx \|G(j\omega)\| \exp(j\phi) \times \|\bar{R}\| \exp(j\beta) \quad (2-51)$$



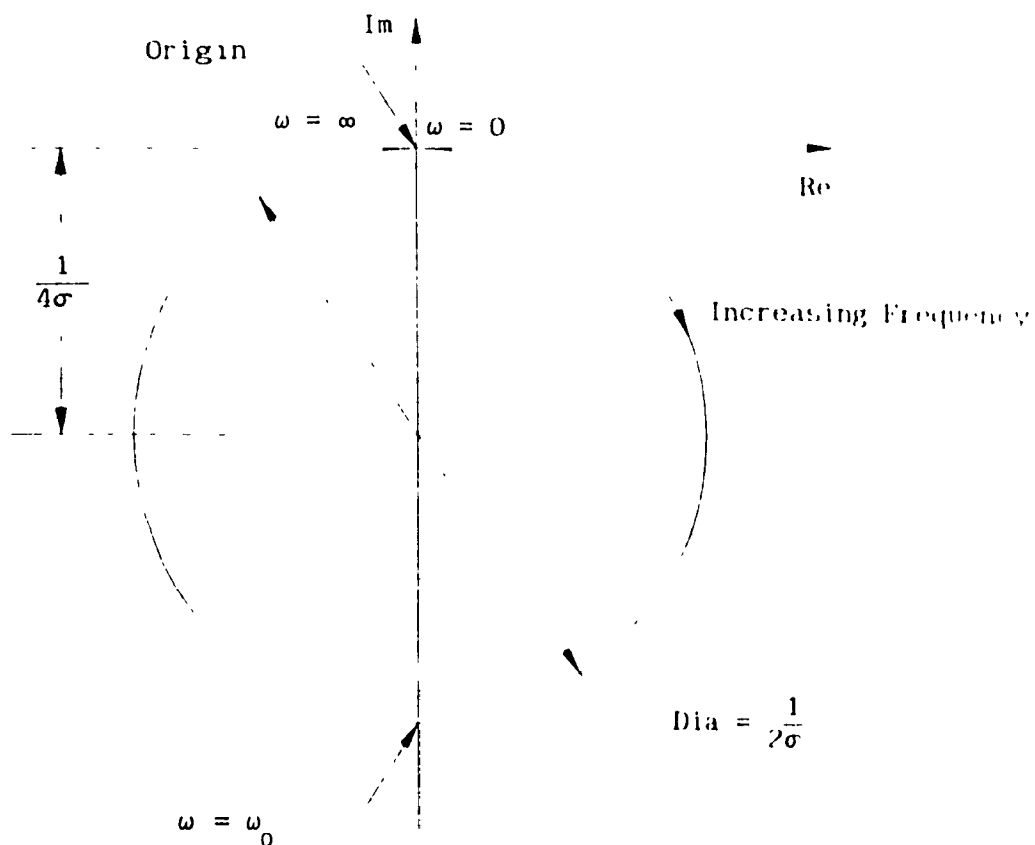


Figure 2-13: Nyquist Plot for SDOF System with Viscous Damping, Receptance-FRF, (Eq. (2-50))

or

$$H(j\omega) \approx \|G(j\omega)\| \|\bar{R}\| \exp[j(\phi+\beta)] \quad (2-52)$$

or

$$H(j\omega) \approx \|G(j\omega)\| \|\bar{R}\| \exp(j\gamma) \quad (2-53)$$

where  $\gamma = \beta$  and it represents the phase angle of  $H(j\omega)$  relative to the transfer function  $G(j\omega)$  of real unit residue as illustrated in Figure 2-14. By comparing Eq. (2-53) with Eq. (2-46) we see that the complex constant  $\bar{R} = \|\bar{R}\| \exp(j\gamma)$  expands the diameter of the circle in Figure 2-13 by  $\|\bar{R}\|$  and rotates this circle counterclockwise about the origin by an angle  $\gamma$  as shown in Figure 2-15.

Another interesting plot is the Co-Quad plot. It is a plot of the real and imaginary parts of a FRF versus frequency. The "Co-" stands for the "coincident" waveform and represents the portion of the response which is in-phase with the input, and "Quad" stands for the "quadrature" and represents the portion of the response which is  $90^\circ$  out-of-phase with the input. Typical Co-Quad plots for a damped SDOF system are shown in Figure 2-16 a, b, and c.

Finally, when plotting the log magnitude versus the phase angle of a FRF we get the Nichols plot. This particular display format is not commonly used for modal analysis but has been widely used to analyze servo-mechanisms. A typical Nichols plot of a lightly damped SDOF system is displayed in Figure 2-17.

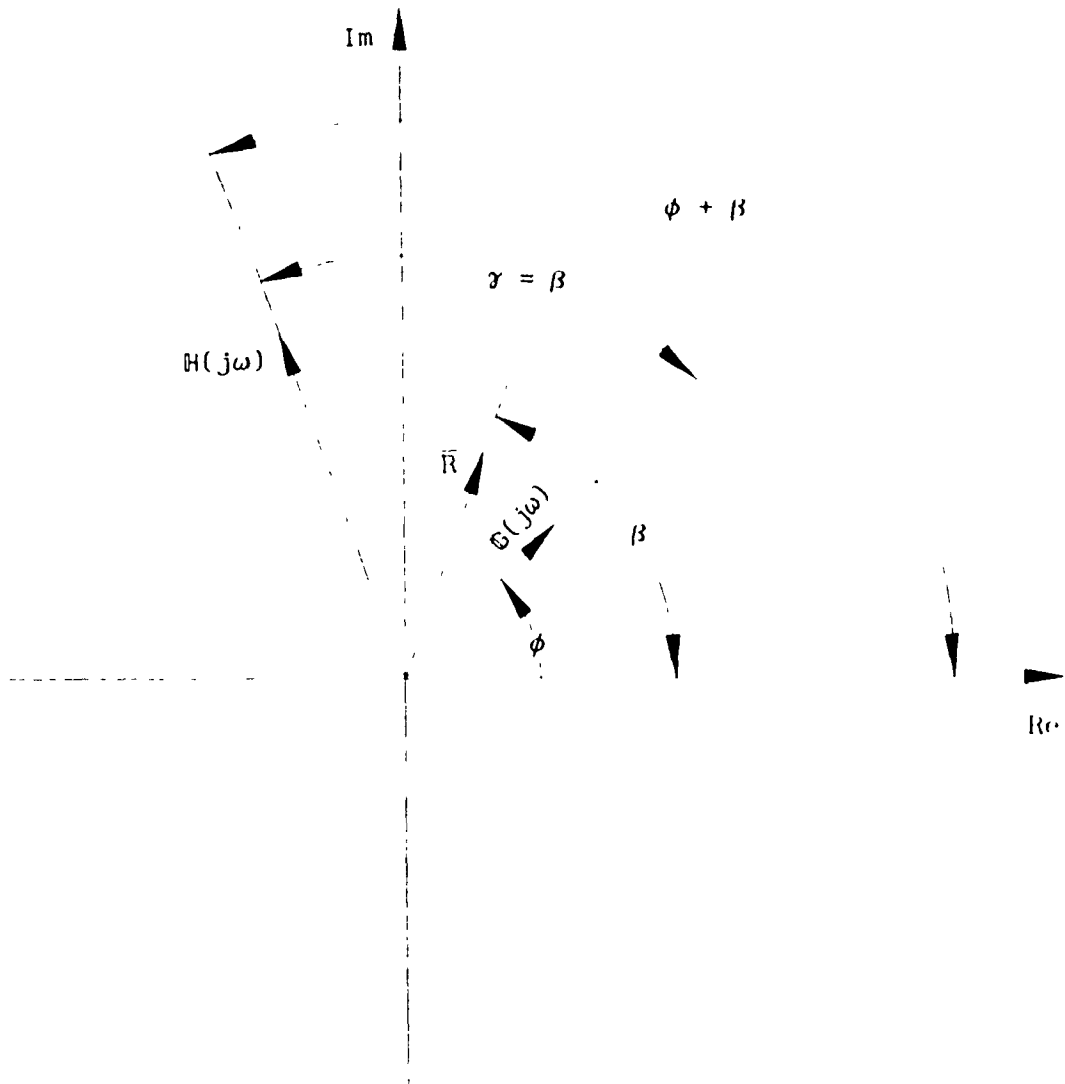


Figure 2-14: Plot of Eqs. (2-52) and (2-53)

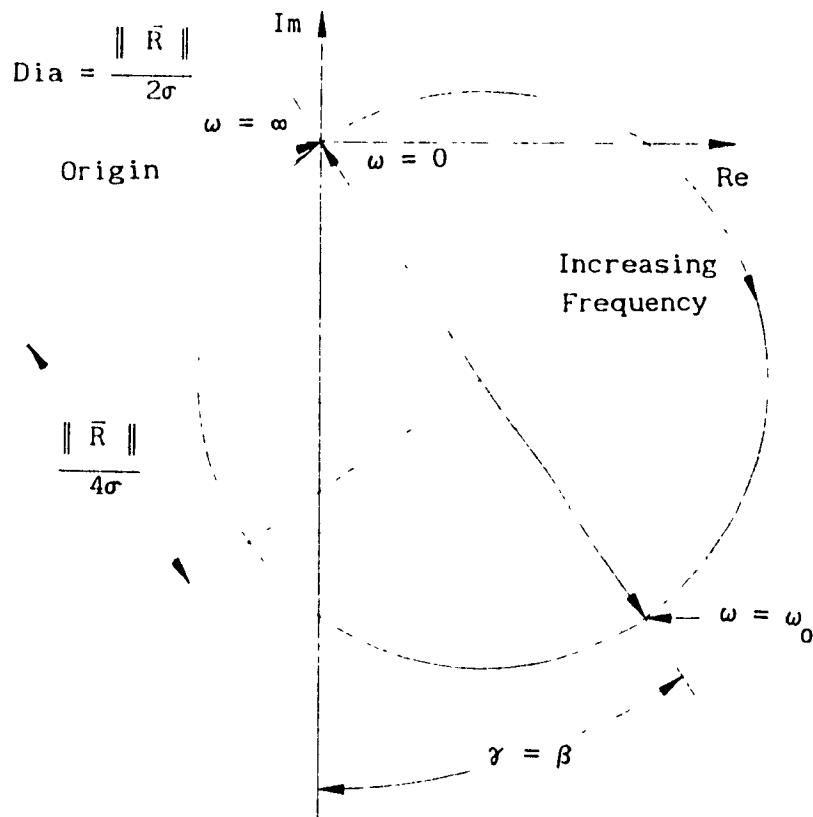


Figure 2-15: Plot of Eq. (2-53)

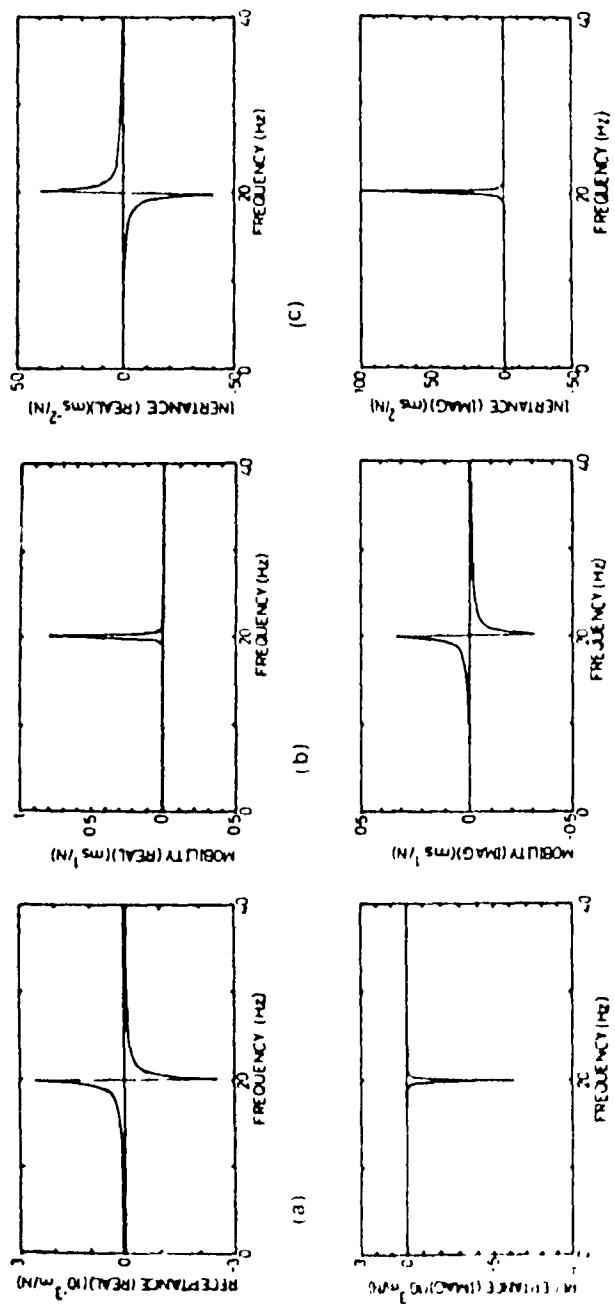


Figure 2-16: Typical Co-Quad Plots for a Damped SDOF System [2]  
 a) Receptance-FRF, b) Mobility-FRF, c) Inertance-FRF

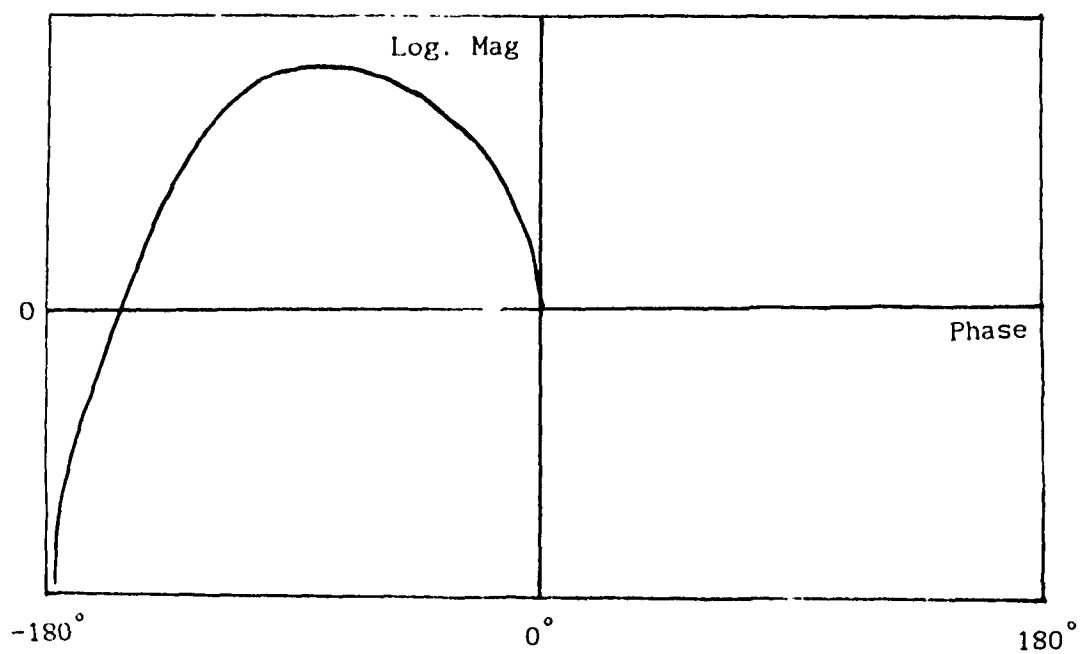


Figure 2-17: Typical Nichols Plot of a Lightly Damped SDOF System

#### 2-4-4 Hysteretic (Structural) Damping

The SDOF analysis presented so far is based upon viscous damping model. However, when studying the behaviour of real structures, viscous damping ( $c$ ) is not representative and damping process used is hysteretic damping ( $h$ ). If we assume that the hysteretic damping force ( $F_{HD}$ ) is in phase with the relative velocity (condition for energy dissipation) but proportional to the relative displacement across the damper, for simple harmonic motion,  $F_{HD}$  is given by

$$F_{HD} = jhx = j\gamma kx = \gamma k\dot{x}/\omega \quad (2-54)$$

where  $\gamma$  is a constant varying from 0 to 1.

It can be shown that the equivalent viscous damping is a frequency-dependent damping whose rate varies inversely with frequency, i.e.

$$c = \frac{h}{\omega} = \frac{\gamma k}{\omega} \quad (2-55)$$

and often gives a better approximation of the damping process.

Substituting Eq. (2-54) into Eq. (2-20), the receptance FRF becomes:

$$H(j\omega) = \frac{X(j\omega)}{F(j\omega)} = \frac{1}{-m\omega^2 + jh + k} \quad (2-56)$$

The modulus and phase of Eq. (2-56) are plotted against  $\omega/\omega_0$  for various values of  $\gamma$  in Figs. 2-18 and 2-19 respectively. By comparing them with Figs. 2-7 and 2-8 for viscous damping, we can see some minor differences. For hysteretic damping the maxima occurs exactly at the undamped natural frequency,  $\omega_0$ , and is independent of the damping  $h$ , whereas for viscous damping it occurs at  $\omega_{peak}$  defined by Eq. (2-30). At low frequencies the response depends on  $h$  since the stiffness is complex and defined as  $k(1 + jh/k)$  whereas for viscous damping it is taken by the spring stiffness alone. Also the phase angle at low frequency tends to  $\tan^{-1}(h/k)$  whereas it is zero for viscous damping.

Similarly for hysteretic damping it can be shown that the real and imaginary of the receptance FRF (Eq. (2-56)) form the following relationship:

$$\left[ \operatorname{Re}[H(j\omega)] \right]^2 + \left[ \operatorname{Im}[H(j\omega)] + \frac{1}{2h} \right]^2 = \left[ \frac{1}{2h} \right]^2 \quad (2-57)$$

Hence, it is the receptance FRF for hysteretically-damped SDOF system that forms an exact circle in the Argand plane (radius  $(1/2h)$  and centre  $(0, -1/2h)$ ) as shown in Fig. 2-20 while for viscously-damped system, it is the mobility which does so.

## 2-5 Multiple-Degree-of-Freedom (MDOF) Models

Previous sections have been limited to the SDOF model with a single



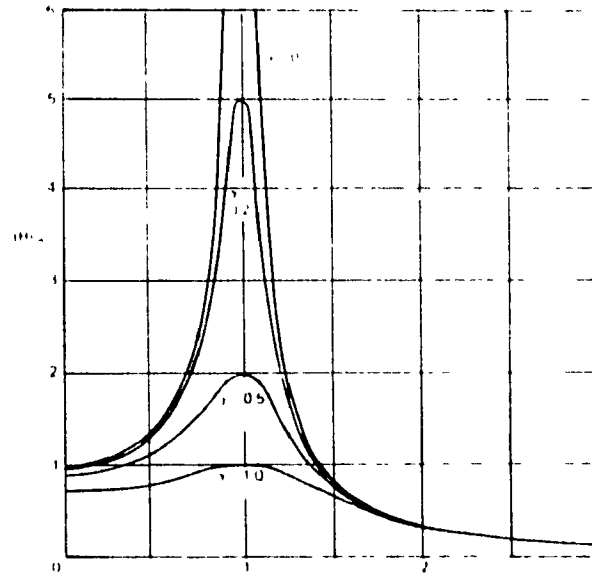


Figure 2-18: Modulus of Eq. (2-56) as a Function of  $\omega/\omega_0$  for Various Values of Hysteretic Damping,  $\gamma = h/k$  [3]<sup>0</sup>

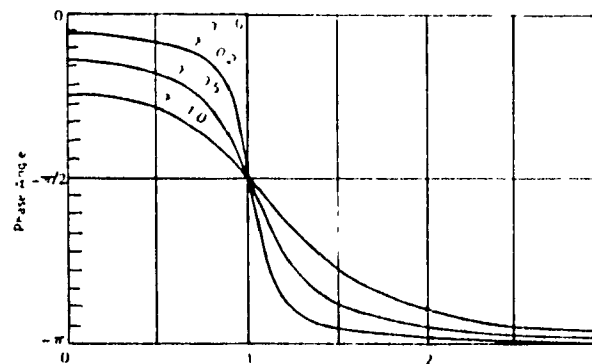


Figure 2-19: Phase of Eq. (2-56) as a Function of  $\omega/\omega_0$  for Various Values of Hysteretic Damping,  $\gamma = h/k$  [3]<sup>0</sup>

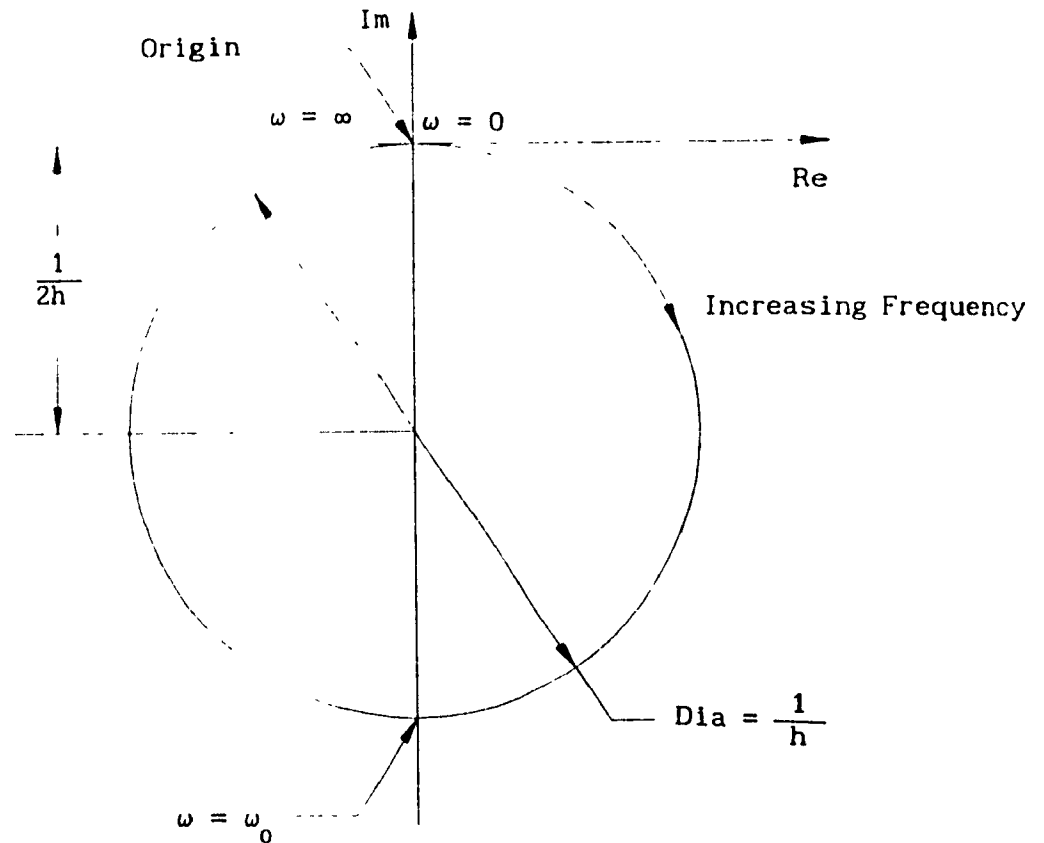


Figure 2-20: Nyquist Plot of the Receptance-FRF for Hysterecally-Damped SDOF System, (Eq. (2-57))

mass, damper and spring elements as shown in Fig. 2-2. Fig. 2-1 illustrates that real structures can be described as an infinite set of SDOF models. This section presents this concept which form the basis for applying experimental modal testing techniques to real structures - MDOF systems.

### 2-5-1 Undamped Free Vibration - Eigenvalues & Eigenvectors

The equations of motion for a two degree-of-freedom system shown in Fig. 2-21 can be obtained by applying Newton's second law to each of the masses. In matrix form, they are:

$$[M] \{\ddot{x}\} + [C] \{\dot{x}\} + [K] \{x\} = \{f\} \quad (2-58)$$

where

$$[M] = \begin{bmatrix} m_1 & 0 \\ 0 & m_2 \end{bmatrix} = \text{Mass Matrix, (2 x 2)}$$

$$[C] = \begin{bmatrix} c_1 + c_2 & -c_2 \\ -c_2 & c_2 + c_3 \end{bmatrix} = \text{Damping Matrix, (2 x 2)}$$

$$[K] = \begin{bmatrix} k_1 + k_2 & -k_2 \\ -k_2 & k_2 + k_3 \end{bmatrix} = \text{Stiffness Matrix, (2 x 2)}$$

$$\{x\} = \begin{Bmatrix} x_1 \\ x_2 \end{Bmatrix} \quad \text{and} \quad \{f\} = \begin{Bmatrix} f_1 \\ f_2 \end{Bmatrix} = \text{Time-Varying Displacements and Forces Vectors, (2 x 1)}$$

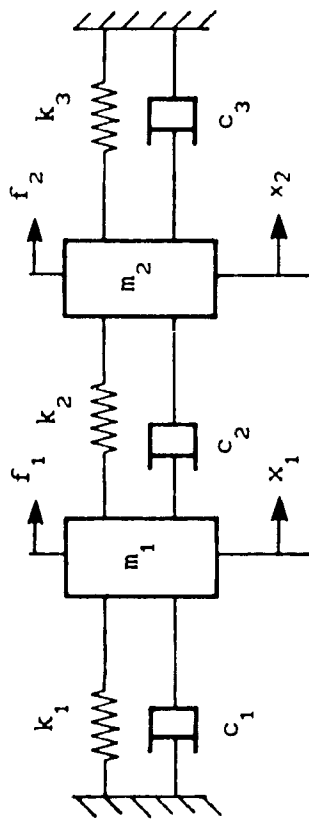


Figure 2-21: Two Degrees-of-Freedom System

For the general n-degree-of-freedom system,  $[M]$ ,  $[C]$ ,  $[K]$  and  $\{\ddot{x}\}$ ,  $\{\dot{x}\}$ ,  $\{x\}$ ,  $\{f\}$  will be  $(n \times n)$  matrices and  $(n \times 1)$  vectors respectively.

The natural frequencies  $(\omega_i, i = 1, \dots, n)$  of this general n-degree-of-freedom system and the corresponding mode shape vectors,  $(\{\psi\}_r, r = 1, \dots, n)$ , can be evaluated by considering the undamped free-vibration; i.e.

$$[M] \{\ddot{x}\} + [K] \{x\} = \{0\} \quad (2-59)$$

Assuming that the system is capable of vibrating at a single frequency,  $\omega$ , a general solution is of the form

$$\{x\} = \{X\} \exp(j\omega t) \quad (2-60)$$

and

$$\{\ddot{x}\} = -\lambda \{X\} \exp(j\omega t) = -\lambda \{x\} \quad (2-61)$$

where

$$\lambda = \omega^2 \quad (2-62)$$

Eq. (2-59) leads to

$$\left[ [K] - \lambda [M] \right] \{X\} \exp(j\omega t) = \{0\} \quad (2-63)$$

since  $\exp(j\omega t) \neq 0$ , Eq. (2-63) can be expressed as:

$$\left[ [K] - \lambda [M] \right] \{X\} = \{0\} \quad (2-64)$$

Premultiplying Eq. (2-64) by  $[M]^{-1}$  and rearranging we obtain

$$\left[ [M]^{-1}[K] - \lambda[I] \right] \{X\} = \{0\} \quad (2-65)$$

where  $[I] = [M]^{-1}[M]$  is the identity matrix, and  $[M]^{-1}[K]$  is called the dynamic matrix. Equation (2-65) is a set of simultaneous algebraic equations in  $X_i$  and for non-trivial solution ( $\{X\} \neq \{0\}$ ), the determinant of the coefficients must be zero; i.e.

$$\det \left[ [M]^{-1}[K] - \lambda [I] \right] = \{0\} \quad (2-66)$$

Expanding Eq. (2-66) gives a polynomial in  $\lambda$  of order  $n$

$$\lambda^n + a_1 \lambda^{n-1} + a_2 \lambda^{n-2} + \dots + a_n = 0 \quad (2-67)$$

and is known as the characteristic equation. The  $n$  roots  $\lambda_i$  of this equation are called the eigenvalues of the system. The natural circular frequencies are calculated from Eq. (2-62); i.e.

$$\omega_i^2 = \lambda_i \quad (2-68)$$

By substituting back any one of these roots  $\lambda_r$  into Eq. (2-65) we get a corresponding set of relative values for  $\{X\}_r$ ; i.e.  $\{\psi\}_r$ , the so-called mode shape or modal vector corresponding to the natural frequency  $\omega_r$ . The vector  $\{\psi\}_r$  is also known as eigenvector of mode  $r$ . Hence the modal properties of a MDOF system can be expressed in two matrices ( $n \times n$ ) called the eigenmatrices as

$$\left[ \Lambda \right]_{\text{diag.}} \quad \text{and} \quad \left[ \Psi \right] \quad (2-69)$$

where  $\lambda_i$ 's form the diagonal elements of  $\left[ \Lambda \right]_{\text{diag.}}$ .

### 2-5-2 Orthogonal Properties of Eigenvectors

It has been shown in the previous section that the solution of Eq. (2-64) yields the eigenmatrices. Thus a particular eigenvalue  $\lambda_r$  and its corresponding eigenvector  $\{\psi\}_r$  will satisfy Eq. (2-64); i.e.

$$[K] \{\psi\}_r = \lambda_r [M] \{\psi\}_r \quad (2-70)$$

Premultiplying Eq. (2-70) by the transpose of another eigenvector  $\{\psi\}_p^T$ , gives

$$\{\psi\}_p^T [K] \{\psi\}_r = \lambda_r \{\psi\}_p^T [M] \{\psi\}_r \quad (2-71)$$

Similarly, we can write the equation for the  $p^{\text{th}}$  mode and premultiply it by the transpose of the  $r^{\text{th}}$  eigenvector  $\{\psi\}_r^T$ ; i.e.

$$\{\psi\}_r^T [K] \{\psi\}_p = \lambda_p \{\psi\}_r^T [M] \{\psi\}_p \quad (2-72)$$

Since  $[K]$  and  $[M]$  are symmetric matrices and are identical to their transposes, we have

$$\{\psi\}_r^T [K] \{\psi\}_p = \{\psi\}_p^T [K] \{\psi\}_r$$

and

$$\{\psi\}_p^T [M] \{\psi\}_r = \{\psi\}_r^T [M] \{\psi\}_p$$

Subtracting Eq. (2-72) from Eq. (2-71) we obtain

$$0 = (\lambda_p - \lambda_r) \{\psi\}_r^T [M] \{\psi\}_p \quad (2-73)$$

If  $\lambda_p \neq \lambda_r$ , Eq.(2-73) can only be satisfied if

$$\{\psi\}_r^T [M] \{\psi\}_p = 0 \quad (2-74)$$

and from Eq. (2-72), it can be seen that

$$\{\psi\}_r^T [K] \{\psi\}_p = 0 \quad (2-75)$$

Equations (2-74) and (2-75) are the orthogonality properties of the eigenvectors with respect to the system mass and stiffness matrices respectively.

### 2-5-3 Generalized Mass and Generalized Stiffness

For the special cases where  $\lambda_p = \lambda_r$  in Eq. (2-73), Eqs. (2-74) and (2-75) do not apply and it is clear that Eq. (2-74) is equal to a scalar constant other than zero; e.g.  $M_r$



$$\{\psi\}_r^T [M] \{\psi\}_r = M_r \quad r = 1, \dots, n \quad (2-76)$$

and from Eq. (2-72) it follows that

$$\{\psi\}_r^T [K] \{\psi\}_r = \lambda_r M_r = \omega_r^2 M_r = K_r \quad r = 1, \dots, n \quad (2-77)$$

The scalar constants  $M_r$  and  $K_r$  are called the generalized mass or modal mass and generalized stiffness or modal stiffness respectively.

#### 2-5-4 Normalization of Mode Shapes

Since a mode shape ( $\{\psi\}_r$ ) defines the relative displacement of each DOF, the ratio between any two elements ( $\psi_{ir} / \psi_{jr}$ ) has to be constant. Hence, the mode shapes can be scaled or normalized (denoted  $\{\phi\}_r$ ) using any particular process. Among the several scaling processes, there are four which are most often used by eigenvalue extraction routines; The mode shapes can be normalized such that:

- 1: The modal mass  $M_r$  in Eq. (2-76) is set to unity.
- 2: The largest element of the mode shape is set to unity.
- 3: A particular element of the mode shape is set to unity.
- 4: The length of the mode shape vector is set to unity.

The second method is convenient for plotting the mode shape but the first one has the most relevance to modal testing since Eq. (2-77) will yield directly the eigenvalues and thus the natural frequencies. A modal vector scaled by the first method is called a weighted modal

vector ( $\{\tilde{\phi}\}_r$ ) and as we will see later it is related to the residue of that mode by its modal constant. This process is called mass-normalization ( $M_r = 1$ ). The mass-normalized eigenvector matrix or weighted modal matrix is denoted  $[\tilde{\Phi}]$  and have the particular property that

$$[\tilde{\Phi}]^T [M] [\tilde{\Phi}] = [I] \quad \text{and} \quad [\tilde{\Phi}]^T [K] [\tilde{\Phi}] = [\Lambda] \quad (2-78)$$

This matrix can also be obtained by dividing the natural modes ( $\{\psi\}_r$ ) by the square root of their respective modal masses calculated in the previous section; i.e.

$$\{\tilde{\phi}\}_i = (M_i)^{-1/2} \{\psi\}_i \quad (i = 1, \dots, n) \quad (2-79)$$

## 2-5-5 Forced Vibration - Modal Coordinates

### 2-5-5-1 Undamped System

The equations of motion for the two-degree-of-freedom system shown in Fig. 2-21 without damping can be written in matrix form as

$$[M] \{\ddot{x}\} + [K] \{x\} = \{f\} \quad (2-80)$$

where  $[M]$  and  $[K]$  are defined in Eq. (2-56). The equations were derived based on the coordinates chosen at each mass point. For that selected coordinates system, we see that both the mass ( $[M]$ ) and stiffness ( $[K]$ )

matrices are symmetric but only [M] is diagonal; i.e. the off-diagonal terms of [[K] are non-zero. The coupling is seen by that fact and it is called elastic coupling or static coupling. If the chosen coordinate system had been the extensions of each spring, [K] would have been diagonal and not [M]. In this case the coupling is called inertial coupling or dynamic coupling. Thus, the equations of motion of a lumped mass system will always be coupled independently of the physical coordinates system chosen to derive them and consequently the derivation of the system response is complicated.

Modal transformation is a mathematical device that converts the problem from physical domain into the modal domain as illustrated in Fig. 2-1. It decouples the equations of motion into a set of independent SDOF models and each of them can be solved as discussed in Section 2-4.

The modal transformation is as follows

$$\{x\} = [\Psi] \{q\} \quad (2-81)$$

or

$$x_i = \sum_{r=1}^n \psi_{ir} q_r \quad (2-82)$$

where  $[\Psi]$  is an eigenvector matrix or simply the modal matrix and  $\{q\}$  is the new coordinates system called principal coordinates, normal coordinates or modal coordinates.

Substituting the coordinate transformation, Eq. (2-81) into Eq. (2-80) yields

$$[M] [\Psi] \{\ddot{q}\} + [K] [\Psi] \{q\} = \{f\} \quad (2-83)$$

Premultiplying Eq. (2-82) by the transpose of the modal matrix,  $[\Psi]^T$ , we get

$$[\Psi]^T [M] [\Psi] \{\ddot{q}\} + [\Psi]^T [K] [\Psi] \{q\} = [\Psi]^T \{f\} \quad (2-84)$$

From Section 2-5-3, Eq. (2-83) can be written in terms of diagonal modal mass matrix  $[\bar{M}]$  and diagonal modal stiffness matrix  $[\bar{K}]$  as

$$[\bar{M}] \{\ddot{q}\} + [\bar{K}] \{q\} = [\Psi]^T \{f\} = \{\Gamma\} \quad (2-85)$$

where  $\{\Gamma\}$  is called the modal force vector. Equation (2-85) represents  $n$  SDOF equations and the  $r^{\text{th}}$  one is

$$\bar{M}_r \ddot{q}_r + \bar{K}_r q_r = \Gamma_r \quad (2-86)$$

or

$$\ddot{q}_r + \omega_r^2 q_r = \Gamma_r / \bar{M}_r \quad (2-87)$$

Equation (2-86) is the equation of motion for SDOF systems without damping as shown in Fig. 2-22. Hence, the solution (time responses) can be obtained for each modal degree-of-freedom,  $q_1$ , using Eqs. (2-6), (2-10) and (2-14). The solution in terms of the original coordinates (physical ones) can be obtained by transforming back; i.e. substituting

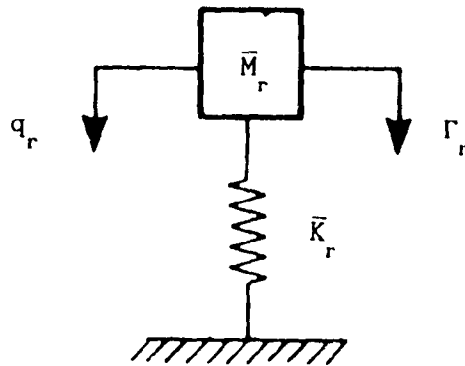


Figure 2-22: Undamped SDOF System in the Modal Domain (Eq. (2-86))

for  $q$ 's in Eq. (2-82).

We can see that if the weighed modal matrix ( $[\tilde{\Phi}]$ ) had been used in Eq. (2-83) instead of the modal matrix ( $[\Psi]$ ), Eq. (2-85) would have been

$$\ddot{q}_r + \omega_r^2 q_r = \Gamma_r \quad (2-88)$$

### 2-5-5-2 Residue and Eigenvector Relationship

Referring to Figure 2-9, the peak amplitude of the receptance-FRF ( $\|H_{ijr}(j\omega)\|_{\omega=\omega_{dr}}$ ), for a SDOF system, is related to the residue by Equation (2-28). Since that residue is a local property, for MDOF system, that relation will become

$$H_{ijr}(j\omega) \Big|_{\omega = \omega_{dr}} \approx \frac{R_{ijr}}{\sigma_r} \quad (2-89)$$

or

$$\|H_{ijr}(j\omega)\| \Big|_{\omega = \omega_{dr}} \approx \frac{\|R_{ijr}\|}{\sigma_r} \quad (2-90)$$

where subscript  $r$  represents the  $r^{\text{th}}$  mode, subscripts  $i$  and  $j$  represent the response and excitation points respectively, and  $\omega_{dr}$  is the  $r^{\text{th}}$  damped frequency.

It can be shown that the  $r^{\text{th}}$  residue subscripts  $i$  and  $j$  is proportional to the product of the  $i^{\text{th}}$  and  $j^{\text{th}}$  elements of the  $r^{\text{th}}$  eigenvector matrix, i.e.

$$\|R_{ijr}\| \propto \psi_{ir} \cdot \psi_{jr} \quad (2-91)$$

or

$$\|R_{ijr}\| = \epsilon_r \psi_{ir} \cdot \psi_{jr} \quad (2-92)$$

and for a driving point, i.e.  $i=j$ , Equation (2-92) will be

$$\|R_{j jr}\| = \epsilon_r \psi_{jr}^2 \quad (2-93)$$

where  $\epsilon_r$  is a complex constant of proportionality. It is sometimes called the modal constant and its value is derived below.

Recalling the definition of the  $r^{\text{th}}$  modal mass, that is

$$\bar{M}_r = \langle \psi \rangle_r^T [\bar{M}] \langle \psi \rangle_r \quad (2-94)$$

For SDOF, the modal mass will be given by

$$M = \langle \psi \rangle_{1 \times 1} m \langle \psi \rangle_{1 \times 1} = \psi m \psi \quad (2-95)$$

Equating Equation (2-25) with Equation (2-92), we have

$$R = \frac{1}{2j\omega_d m} = \epsilon \psi \psi \quad (2-96)$$

Hence,

$$\epsilon = \frac{1}{2j\omega_d M} \quad (2-97)$$

Therefore, for MDOF, the  $r^h$  constant,  $\epsilon_r$ , will be given by

$$\epsilon_r = \frac{1}{2j\omega_{dr} \bar{M}_r} \quad (2-98)$$

If the mass-normalized eigenvector matrix elements ( $\check{\phi}_{1r}$  and  $\check{\phi}_{jr}$ ) are used instead of the eigenvector matrix elements ( $\psi_{1r}$  and  $\psi_{jr}$ ) in the previous equations, the modal mass,  $\bar{M}_r$ , will be unity and  $\epsilon_r$  will be defined as

$$\epsilon_r = \frac{1}{2j\omega_{dr}} \quad (2-99)$$

Using Equations (2-90), (2-92), (2-93), and (2-99), the scaled mode shapes,  $[\check{\Phi}]$ , can be estimated using the following procedures.

1) Measure at least one row or one column of the FRF measurements matrix (minimum data requirement). You must have at least as many DOF as the number of modes of interest.

2) Since, generally, inertance-FRF ( $A_{1jr}(j\omega)$ ) measurements are measured, Equation (2-89) can be written as:

$$A_{1jr}(j\omega) \approx \frac{R_{1jr} (j\omega)^2}{\sigma_r} \quad (2-100)$$



substituting Equations (2-92) and (2-99) in Equation (2-100) gives

$$A_{1jr}(j\omega) \Big|_{\omega = \omega_{dr}} \approx \frac{\epsilon_r \tilde{\phi}_{1r} \cdot \tilde{\phi}_{jr}}{\sigma_r} (-\omega_{dr}^2) = j \frac{\tilde{\phi}_{1r} \cdot \tilde{\phi}_{jr}}{2 \sigma_r} \omega_{dr} \quad (2-101)$$

or

$$\|A_{1jr}\| \Big|_{\omega = \omega_{dr}} \approx \frac{\|R_{1jr}(\omega = \omega_{dr})\|}{\sigma_r} (-\omega_{dr}^2) \quad (2-102)$$

Equation (2-101) gives the basis for quadrature picking technique, through which we can determine the mode shapes. Indeed, the FRF appears to become purely imaginary at all modal frequencies,  $\omega_{dr}$ . Its amplitude is proportional to the residue (Equation (2-102)), and its sign is positive if displacement is in phase with the excitation.

Alternatively, since most FFT analyzers come with built-in integrators, receptance-FRF measurements can easily be obtained by integrating twice the inertance-FRF measurements. In that case, Equation (2-90) can be used instead of Equation (2-102).

- 3) Identify the modes of interest
- 4) Evaluate  $\sigma_r$  for all the modes of interest using the half power method (refer to Figure 2-9).
- 5) Calculate the residues,  $\|R_{1jr}(\omega = \omega_{dr})\|$ , for all modes using the appropriate equation, i.e.

If receptance-FRF measurements are used:

$$\|R_{1jr}\| \Big|_{\omega = \omega_{dr}} \approx \sigma_r \|H_{1jr}(j\omega)\| \Big|_{\omega = \omega_{dr}} \quad (2-103)$$

If inertance-FRF measurements are used:

$$\|R_{1jr}\| \Big|_{\omega = \omega_{dr}} \approx (-\omega_{dr}^2) \sigma_r \|A_{1jr}(j\omega)\| \Big|_{\omega = \omega_{dr}} \quad (2-104)$$

6) Calculate the constants  $\epsilon_r$  for all the modes of interest using Equation (2-99).

7) Calculate  $\tilde{\phi}_{jr}$  for all the modes

$$\tilde{\phi}_{jr} = \sqrt{\frac{\|R_{j jr}(\omega = \omega_{dr})\|}{\epsilon_r}} \quad (2-105)$$

8) Calculate the remaining eigenvector matrix elements  $\tilde{\phi}_{1r}$

$$\tilde{\phi}_{1r} = \frac{\|R_{1 jr}(\omega = \omega_{dr})\|}{\epsilon_r \tilde{\phi}_{jr}} \quad (2-106)$$

However, formal curve fitting, discussed in Chapter 4, is preferred to the above estimation procedure since it gives a better estimate of the modal damping and thus more accurate mode shapes. Indeed, most curve fitting methods are based on least squared method.

### 2-5-5-3 Damped System - Proportional Damping

All materials have internal damping which is commonly referred to as solid damping, hysteretic damping, or structural damping. However, a particular structure may have other damping characteristics resulting from a combination of several types of damping, such as hysteretic, viscous, coulomb, aerodynamic, etc.

Most mechanical systems are inherently lightly damped [3] and certain simplifying assumptions can be made.

If we assume that the damping type is viscous (i.e., the damping force is proportional to the velocity), the equations of motion for an n degree-of-freedom system can be written, in a matrix form, as

$$[M] \{\ddot{x}\} + [C] \{\dot{x}\} + [K] \{x\} = \{f\} \quad (2-107)$$

where  $[M]$ ,  $[C]$ ,  $[K]$  and  $\{\ddot{x}\}$ ,  $\{\dot{x}\}$ ,  $\{x\}$ ,  $\{f\}$  will be  $(n \times n)$  matrices and  $(n \times 1)$  vectors respectively.

If we also assume that the damping matrix  $[C]$  is proportional, it implies that the matrix  $[C]$  can be written as a linear combination of the mass and stiffness matrices, i.e.

$$[C] = \alpha [M] + \beta [K] \quad (2-108)$$

Because of the assumption of proportionality, we can see that the modal transformation, discussed in Section 2.5.5.1, will also decouple the equations of motion (Eq. (2-89)) into a set of  $n$  independent SDOF models and each of them can be solved as discussed in Section 2-4.

Hence, in the modal domain, Eq (2-89) is expressed in terms of diagonal modal mass matrix  $[ \bar{M} ]$ , diagonal modal damping matrix  $[ \bar{C} ]$ , and diagonal modal stiffness matrix  $[ \bar{K} ]$  as

$$[ \bar{M} ] \{ \ddot{q} \} + [ \bar{C} ] \{ \dot{q} \} + [ \bar{K} ] \{ q \} = \{ \Gamma \} \quad (2-109)$$

where

$$[ \bar{C} ] = [ \Psi ]^T [ C ] [ \Psi ] = \alpha [ \bar{M} ] + \beta [ \bar{K} ] \quad (2-110)$$

and  $[ \Psi ]$  is the modal matrix evaluated for the free undamped case. The  $r^{\text{th}}$  equation of motion of Eq (2-91) is

$$\bar{M}_r \ddot{q}_r + \bar{C}_r \dot{q}_r + \bar{K}_r q_r = \Gamma_r \quad (2-111)$$

or

$$\ddot{q}_r + (\bar{C}_r / \bar{M}_r) \dot{q}_r + \omega_r^2 q_r = \Gamma_r / \bar{M}_r \quad (2-112)$$

and using Eqs. (2-7) and (2-12), Eq (2-94) becomes

$$\ddot{q}_r + 2\sigma_r \dot{q}_r + \omega_r^2 q_r = \Gamma_r / \bar{M}_r \quad (2-113)$$

For mass-normalization ( $\bar{M}_r = 1$ ) and Eq. (2-95) becomes

$$\ddot{q}_r + 2\sigma_r \dot{q}_r + \omega_r^2 q_r = \Gamma_r \quad (2-114)$$

Equation (2-96) is illustrated in Figure 2-1.

Hysteretic damping was discussed in Section 2-4-4 under one degree-of-freedom system but it can be extended to multiple degree-of-freedom system. The damping vector ( $\{F_{HD}\}$ ) will be given by

$$\{F_{HD}\} = j[H]\{x\} = \gamma[K]\{\dot{x}\}/\omega \quad (2-115)$$

and its equivalent viscous damping matrix will be given by

$$[C] = \frac{[H]}{\omega} = \frac{\gamma}{\omega} [K] \quad (2-116)$$

where  $[H]$  is the hysteretic damping matrix.

Comparing Eq. (2-80) with Eq. (2-98), we have

$$\alpha = 0 \text{ and } \beta = \frac{\gamma}{\omega} \quad (2-117)$$

Hence, the equations of motion can be uncoupled and solved as discussed previously.

Considering the general case of proportional damping, i.e. the damping in the system is of the form given by Eq. (2-90), it can be shown that the  $r^{\text{th}}$  eigenvalue and eigenvector, for a viscously damped system, will be as follow:

$$\lambda_r^2 = \omega_r^2 \sqrt{1 - \rho_r^2} \quad , \quad \rho_r = \alpha/(2\omega_r) + (\beta\omega_r)/2 \quad (2-118)$$

and

$$\{\psi\}_r^{\text{damped}} = \{\psi\}_r^{\text{undamped}} \quad (2-119)$$

In the case of Hysteritic damping, considering the general case of proportional damping, i.e.

$$[H] = \alpha [M] + \beta [K] \quad (2-120)$$

the mode shapes for the damped system are again identical to those of the undamped system and the eigenvalues take the complex form.

$$\lambda_r^2 = \omega_r^2 (1 + j\eta_r^2) \quad (2-121)$$

where

$$\omega_r^2 = \bar{K}_r / \bar{M}_r \quad ; \quad \eta_r = \beta + \alpha / (\omega_r^2) \quad (2-122)$$

Thus, both undamped and proportionally damped systems behave in a similar manner. The various parts of both systems move either in phase or  $180^\circ$  out of phase with each other. This means that the modes have well defined modal points or lines and appear as a standing wave, i.e. all points on the system pass through their equilibrium position simultaneously. The modes characterized by this property are classified as normal modes.

Normal modes should be expected in structures that have very light ( $\zeta_r < 0.2$ ) or no damping, or when the damping is distributed in the same way that the inertia and stiffness are (proportional damping).

#### 2-5-5-4 Damped System - Non-Proportional Damping

When the damping is not proportional, the modal matrix obtained

from the undamped system will not diagonalize the damping matrix. In this case, the equations of motion can be solved simultaneously or uncoupled by using the state space method.

Basically, the state space method converts the set of  $n$  second order differential equations to an equivalent set of  $2n$  first order.

The mode shapes of such systems are complex . They can be considered as propagating waves with no stationary nodal points and nodal lines as shown in Figure 2-23. These can be expected in systems that have localized damping, such as structures with spot welds and discrete isolators/dampers.

In order to carry-out experimental modal testing on such structures, multiple exciter techniques should be used.. The main reason is that larger amount of vibration energy can be fed more uniformly into the structure than with single excitation. In addition, closely spaced modes are often encountered in these structures and this technique will be able to isolate each principal mode. Hence, the modal testing results based on one exciter position may not agree with those based on another exciter position.

Since, Experimental modal testing based on multiple exciter techniques is beyond the scope of this thesis, it is not presented here.

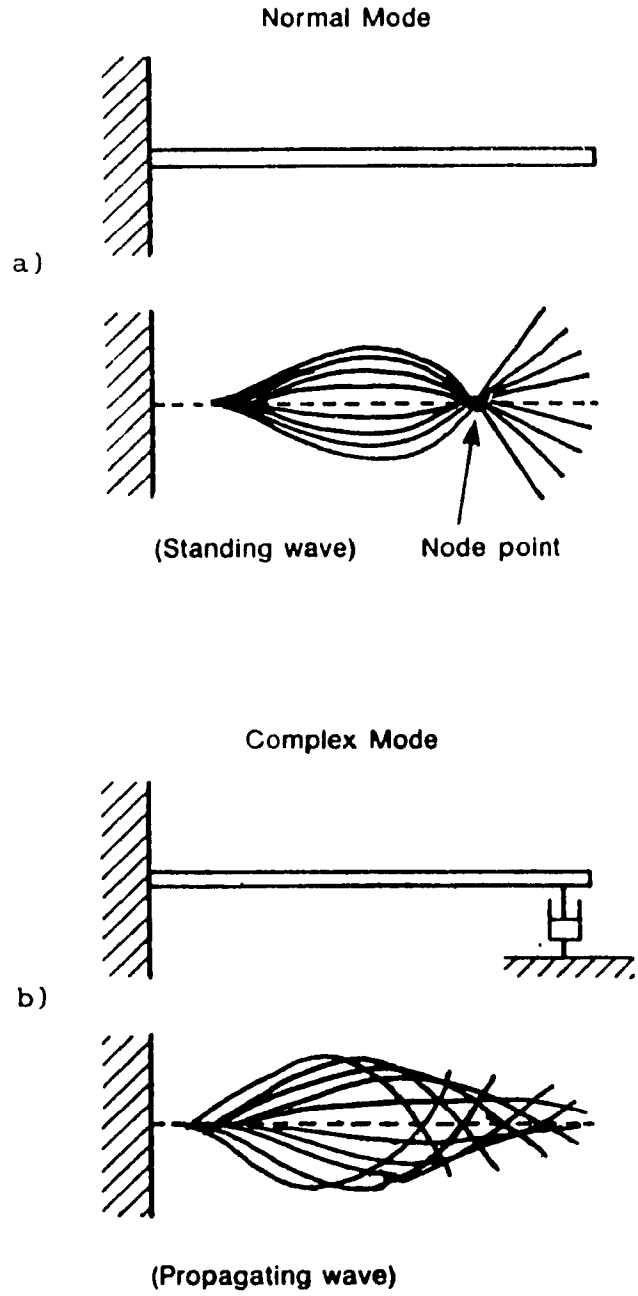


Figure 2-23: Typical Mode Shapes [8]  
a) Normal, b) Complex



## 2-6 Conclusion

In this chapter, basic definitions and concepts of experimental modal analysis are presented. The modal testing assumptions are discussed. The structural response of a single-span uniform beam with end conditions hinged-hinged is shown in five different domains: physical, mathematical, time, frequency and modal domains. A complete review of a SDOF system is presented discussing the relations between the mathematical domain and the modal domain for both viscous and hysteretic damping. Multiple-degree-of-freedom models are then discussed in relation with the definitions and concepts.

## CHAPTER 3

### MECHANICAL FRF MEASUREMENT TECHNIQUES

## CHAPTER 3

### MECHANICAL FRF MEASUREMENT TECHNIQUES

#### 3-1 General

In the previous chapter, mathematical dynamic models of SDOF and MDOF were derived. Equations of motion were derived in terms of  $[M]$ ,  $[C]$ , and  $[K]$  and their solutions or responses (FRF) were described by a set of three modal parameters. Experimental modal analysis is the inverse of this; i.e. to extract the modal parameters from the measured FRF and to identify the system matrices.

There are two types of vibration measurement for experimental structural analysis, namely, signal and system analyses. Signal analysis consists of measuring only one variable (usually a response level) at one or several points on a system under operating conditions to identify the source(s), in the case of noise or vibration (also called trouble-shooting), or to monitor the response levels to prevent a mechanical failure (also called mechanical monitoring).

In the case of system analysis, both input(s) and response(s) are measured to determine the inherent dynamic properties (FRF), and to

extract from them the experimental dynamic model, modal model, or modal parameters. This experimental analysis is also known as modal testing. It can be carried-out by using either a single or multiple exciter techniques. The mechanical frequency response function (FRF) measurement techniques are often referred to as mobility measurement techniques.

In this chapter, the different measurement techniques which are currently used for experimental modal testing are discussed. Since the important aspect of the experiment is to measure meaningful data, for the purpose of building the experimental modal model, rules of thumb are highlighted to minimize the most common errors that can occur in measuring input and output signals and in computing frequency response functions.

### 3-2 Measurement Hardware

Mobility measurement techniques require three basic hardware components: a vibratory excitation mechanism; a transducer for measuring the excitation and response of the system; and a dual-channel Fast Fourier Transform (FFT) analyzer.

The vibratory excitation mechanism provides a known or controlled input to the structure. The response transducer system converts the mechanical motion of the structure into an analog electrical signal. The FFT analyzer converts both the output and input analog signals into digital signals and computes from them various functions such as instant spectrum, auto-spectrum, cross-spectrum, Frequency Response Function (FRF), Coherence function, etc. This hardware requirement is illustrated schematically in Figure 3-1.

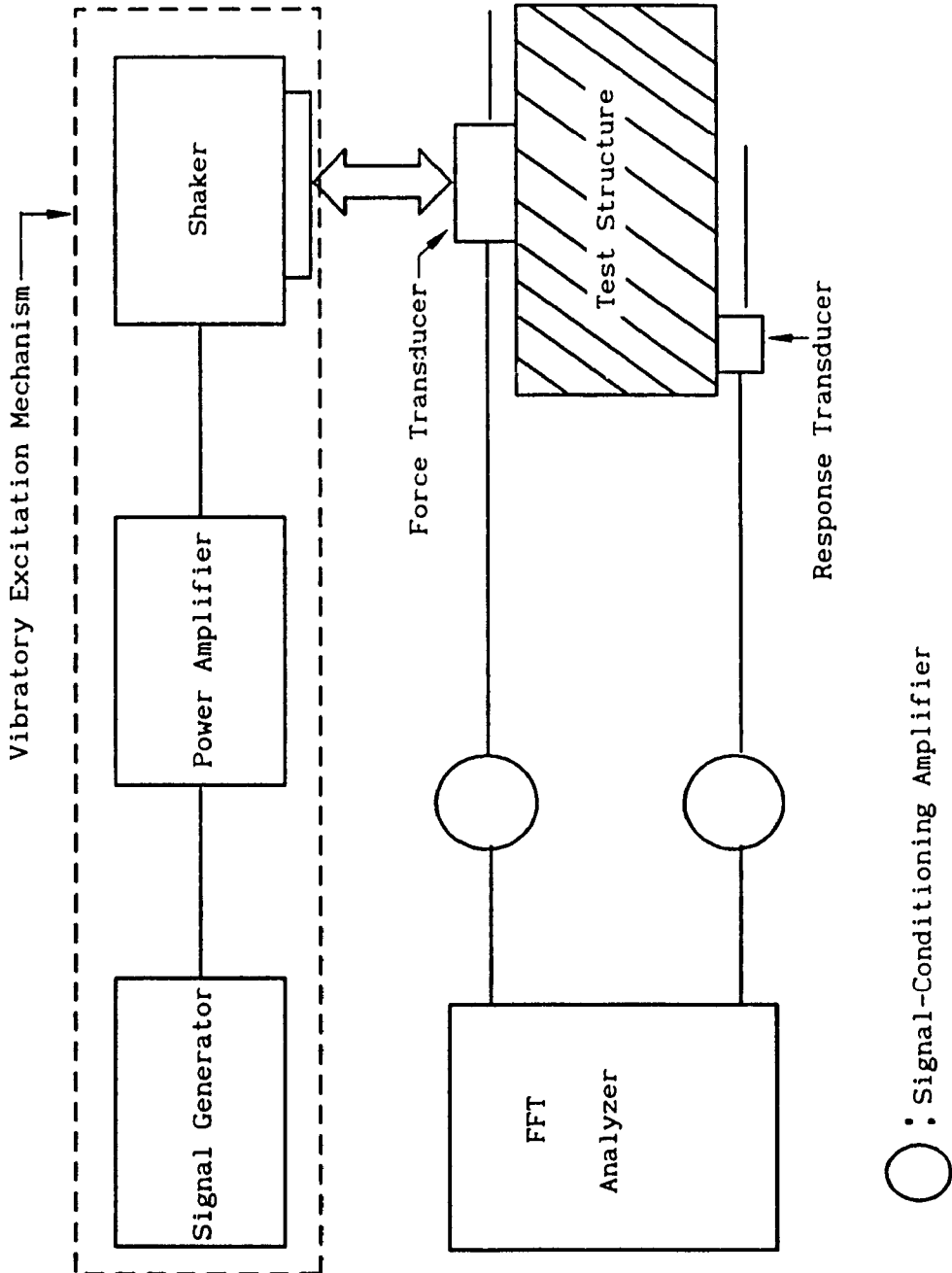
### 3-3 Frequency Response Function (FRF) Estimation

Certainly, one of the most important and crucial phase of experimental modal testing is acquiring meaningful Frequency Response Function (FRF) measurements. The FRF is a complex function and is defined as the ratio of the Fourier Transforms of the system output  $\ddot{x}(t)$  to the system input  $f(t)$ ; i.e.

$$\text{FRF} = H(j\omega) = \frac{\ddot{X}(j\omega)}{F(j\omega)} = \frac{G_x(j\omega)}{G_f(j\omega)} \quad (3-1)$$

where

$$\ddot{X}(j\omega) = G_x(j\omega) = \int_0^{\infty} \ddot{x}(t) \exp(-j\omega t) dt, \text{ spectrum of the output signal}$$



○ : Signal-Conditioning Amplifier

Figure 3-1: Schematic Hardware Requirement for Mobility Measurement Techniques

$$F(j\omega) = G_f(j\omega) = \int_0^{\infty} f(t) \exp(-j\omega t) dt, \text{ spectrum of the input signal}$$

Although the FRF can be computed from Eq. (3-1), in practice, two estimators are used to estimate the true FRF. They are based upon the calculation of the cross-spectrum between of the input and output signals and their auto-spectra.

The first estimator is denoted  $H_1$ , and is derived by premultiplying both the numerator and denominator of Eq. (3-1) by the complex conjugate of the input Fourier transform  $F^*$  to obtain:

$$H_1(j\omega) = \frac{G_{fx}(j\omega)}{G_{ff}(j\omega)} = \frac{G_{fx}(j\omega)}{|F(j\omega)|^2} \quad (3-2)$$

where

$$G_{fx}(j\omega) = F^*(j\omega) \ddot{X}(j\omega), \text{ cross-spectrum}$$

$$G_{ff}(j\omega) = F^*(j\omega) F(j\omega) = |F(j\omega)|^2, \text{ input auto-spectrum}$$

and where \* indicates complex conjugate.

Similarly, the other estimator is obtained by premultiplying by the complex conjugate of the output Fourier transform,  $\ddot{X}^*$ :

$$H_2(j\omega) = \frac{G_{xx}(j\omega)}{G_{xf}(j\omega)} = \frac{|\ddot{X}(j\omega)|^2}{G_{xf}(j\omega)} = \frac{|\ddot{X}(j\omega)|^2}{G_{fx}^*(j\omega)} \quad (3-3)$$

where

$$G_{xx}(j\omega) = \dot{X}^*(j\omega) \dot{X}(j\omega) = |\dot{X}(j\omega)|^2, \text{ output auto-spectrum}$$

$$G_{xf}(j\omega) = \dot{X}^*(j\omega) F(j\omega), \text{ cross-spectrum}$$

$$G_{fx}^*(j\omega) = G_{xf}(j\omega)$$

Equations (3-2) and (3-3) are commonly used by modern FFT analyzer to estimate the Frequency Response Function.

The usefulness of these two forms of FRF can be seen from the fact that the uncorrelated noise, if exit and is significant, can be removed or reduced from the computing of the cross-spectrum through an averaging process so that:

1.  $H_1$  gives the best estimate of the true FRF at low levels (antiresonances) since all the uncorrelated noise at the output is suppressed.
2.  $H_2$  gives the best estimate of the true FRF at high levels (resonances peaks) since all the uncorrelated noise at the input is suppressed.

Hence,  $H_1$  and  $H_2$  are the upper and lower bounds of the true Frequency Response Function (FRF), i.e.

$$H_1 \leq H \leq H_2 \quad (3-4)$$



Figure 3-2 compares graphically  $H$  with  $H_1$ , and  $H$  with  $H_2$ .

From this and other reasons that will be discussed in the other sections,  $H_2$  was selected as the FRF estimator for the cases studied and presented in Chapter 4.

### 3-4 Coherence Function

The Coherence function is a measure of linearity between the input and output signals and is defined as the ratio between the cross-spectrum and the auto-spectra of the input and output signals. It is calculated on a digital Fourier analyzer as:

$$\gamma_{fx}^2(j\omega) = \frac{|G_{fx}(j\omega)|^2}{G_{ff}(j\omega) G_{xx}(j\omega)} = \frac{H_1}{H_2} \quad (3-5)$$

It is used basically in conjunction with Frequency Response Function (FRF) as a means of detecting a number of possible errors in the measurements at any specific frequency.. The bounds for the Coherence function are between 0 and 1, i.e.

$$0 \leq \gamma^2 \leq 1 \quad (3-6)$$

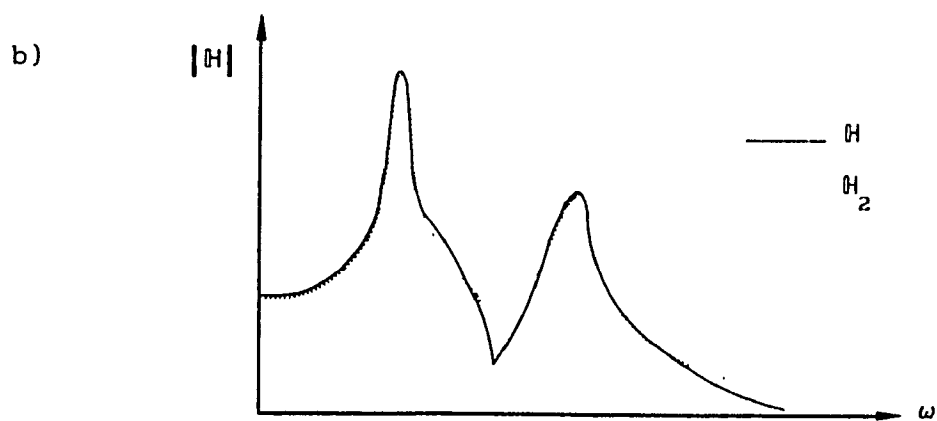
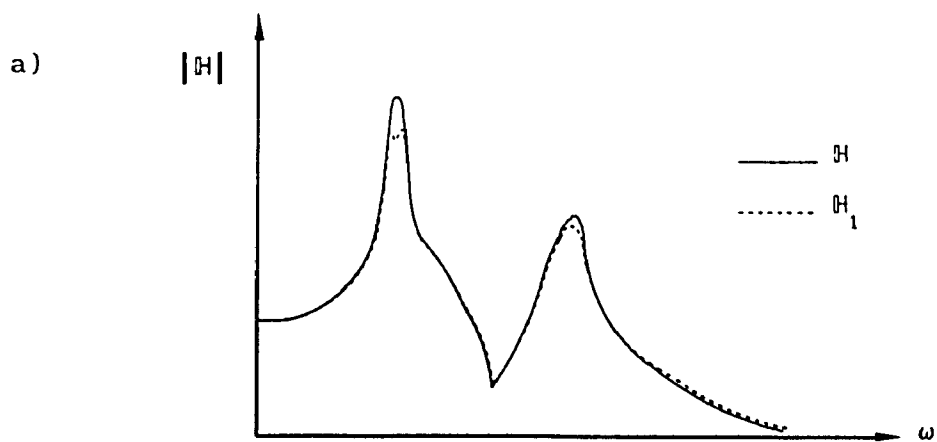


Figure 3-2: Typical Comparison between: a)  $H$  and  $H_1$ , b)  $H$  and  $H_2$

A value of 1 indicates no noise in the measurements and full linear input/output relationship whereas a value of 0 indicates pure noise in the measurement.

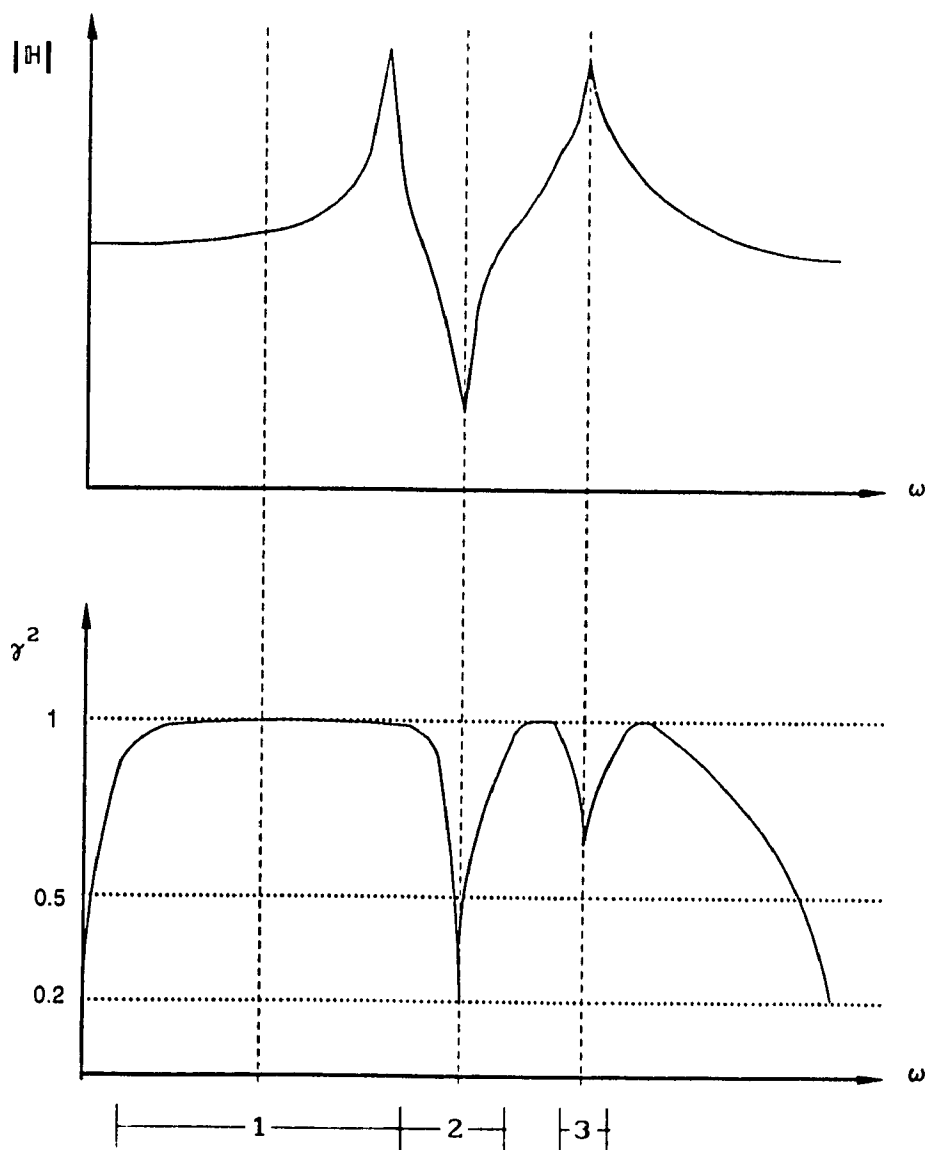
A typical Coherence function of a good FRF measurement shows a value close to 1 (higher than 0,95) [5] at the resonance peaks and values close to 0 at the antiresonances as shown in Figure 3-3. Therefore, attention should be paid only in the resonance frequency regions to accept or reject a measurement.

Coherence less than unity at the resonance peaks can be caused by the following error sources:

- Noise at the output of the system (response to unmeasured excitation forces)
- Aliasing error (discussed in Section 3-7)
- Resolution bias error (discussed in Section 3-8)
- Noise at the input not passing through the system
- Non-linearities of the system (discussed in Section 3-13)
- Scatter of impact point/direction

### 3-5 Signal-To-Noise Ratio Function

As with the Coherence, signal to noise ratio function provides at



- 1: Excellent Input/Output Relationship
- 2: Anti-Resonance Zone where Noise in the Output Measurement is High
- 3: Non-Linear Behavior at Resonance

Figure 3-3: Typical FRF Measurement and its Corresponding Coherence Function

any one frequency an indication of the quality of the measurement by computing the relative system noise. Also, this function is useful to verify if a particular excitor is appropriate to test a given mechanical structure. For example, the selection of an impact blow hammer or a small shaker to test a large complex structure may not be appropriate and this will be seen by a low signal to noise ratio.

This function is defined as the ratio between the coherent output power,  $COP(j\omega)$ , and the non-coherent output power,  $NCOP(j\omega)$ . The coherent output power expresses the power at the output due to the input, whereas the non-coherent output power expresses the power at the output due to system noise and are defined as:

$$COP(j\omega) = \frac{|G_{fx}(j\omega)|^2}{G_{ff}(j\omega)} = \gamma_{fx}^2(j\omega) G_{xx}(j\omega) \quad (3-7)$$

$$NCOP(j\omega) = G_{xx}(j\omega) - COP(j\omega) = (1 - \gamma_{fx}^2(j\omega)) G_{xx}(j\omega) \quad (3-8)$$

Hence, the signal to noise ratio function, is given by:

$$S/N(j\omega) = \frac{COP(j\omega)}{NCOP(j\omega)} = \frac{\gamma_{fx}^2}{1 - \gamma_{fx}^2} \quad (3-9)$$

A rule of thumb to obtain reasonably good accuracy in the actual vibration measurements, the signal to noise ratio should be at least 40 dB.

### 3-6 Random and Bias Errors

Random errors are caused by noise which appear with different magnitude and phase at each observation. These errors can only be minimized by averaging independently the estimator used to compute the FRF measurement. Hence, the accuracy of a measurement showing small values of Coherence and signal to noise ratio can be improved taking more averages. Figure 3-4 shows the relationship between the normalized random error and the number of averages to compute for different values of Coherence. For example, for a Coherence  $\gamma^2 = 0,1$  - approximately 2000 averages are required to get a normalized random error smaller than 5% ( $\sim \pm 0.45$  dB).

On the contrary, bias errors are systematic errors which appear with the same magnitude and phase at each observation. These errors can only be minimized by using a different estimator.

The most common typical error sources encountered when making FRF measurements can be classified into two classes of error (R = Random

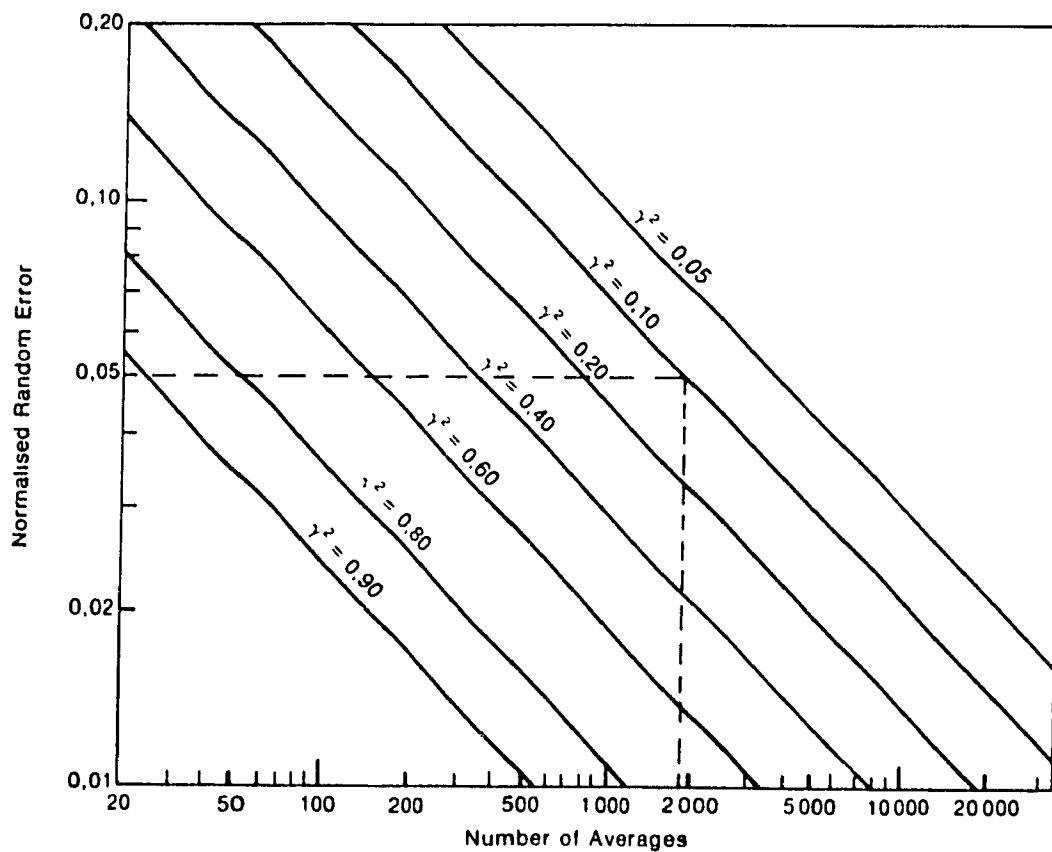


Figure 3-4: Normalized Random Error Versus Number of Averages [6]

error and B = Bias error) along with the best estimator ( $H_1$  or  $H_2$ ) to be used to minimize a particular error source, and also giving an idea about when the Coherence function  $\gamma^2$  can be utilized to detect them. This is shown in Table 3-1.

### 3-7 Aliasing Error

Aliasing error is a bias error which occurs when improper sampling time is used. The sampling time is denoted  $\Delta T$  and is directly proportional to the spectral resolution of an FFT analyzer. The spectral resolution is defined as:

$$\Delta F = \frac{\text{Frequency Span}}{\text{Number of Spectral Lines (N) - 1}} \quad (3-10)$$

Thus, The record length, T, is the inverse of the spectral resolution

$$T = 1 / \Delta F \quad (3-11)$$

Therefore, the sampling time will be the ratio between the record length divided by the number of samples (n) used to convert the data from analog to digital:



Table 3-1: Best Estimator ( $H_1$  or  $H_2$ ) Versus Classe of Errors

Sources of Error	Estimator		Detection of error by estimator $\gamma^2$
	$H_1$	$H_2$	
Noise at the output (response to unmeasured excitation forces)	R	B	YES
Noise at the input	B	R	YES
Non-linear System	Random Excitation	B/R	YES
	Deterministic Excitation	B	NO
Scatter of impact point / direction	R	R	YES
Leakage	Random Excitation	B	(B)
	Deterministic (impact)	B	B
B = Bias error (systematic) R = Random error (minimized by averaging)			

$$\Delta T = \frac{T}{n} \quad (3-12)$$

For example, the digital to analog converter of the Bruel & Kjaer Dual ( Channels A and B) FFT Analyzer - model 2032, digitizes the analog signals (input signals) into 2 x 2048 samples for each record measured in the baseband mode, i.e. not in the zoom mode. These digitized signals are Fourier transformed with a spectral resolution of 801 lines/signal. Hence, by fixing the frequency span, the spectral resolution, record length and sampling time are automatically computed by the analyzer. In our example, if frequency span is set to 200 Hz, the 2032 computes the other parameters to:  $\Delta F = 250$  mHz,  $T = 4$  s, and  $\Delta T = 1,95$  ms.

The sampling theorem, or Shannon's sampling theorem [7], states to avoid leakage, that the sampling time,  $\Delta F$ , must be chosen such to provide at least 2,5 samples per cycle of the highest frequency to be calculated. In our example above, we can show that this analyzer used 2,56 samples per cycle at 200 Hz which is the minimum requirement of the theorem.

However, most modern digital analyzers provide built-in antialiasing filters which cut-off frequency higher than about half the maximum frequency of interest, also called the Nyquist frequency. Hence, as a rule of thumb, the frequency span must be at least twice the maximum frequency of interest. For example, if we are looking for singularities

in the frequency bandwidth of 0 to 100 Hz, the frequency span should be 200 Hz with centre frequency set to baseband.

### 3-8 Resolution Bias Error

Resolution bias error occurs when the peak itself is narrower than the resolution of the analyzer as shown in Figure 3-5. This effect is also called leakage since the impulse response is longer than the record length of the analyzer as shown in Figure 3-6. This error can be detected by a Coherence less than unity. Band selectable Fourier Analysis (BSFA) also called Zoom Transform, or simply Zooming is a technique to improve the measurement in a frequency region by using an increased spectral resolution. This mode can be evoked in the 2032 analyzer by changing the centre frequency from baseband mode to zoom mode and specifying a centre frequency.

Generally, to carry-out modal testing, a white noise spectrum is used to excite all the modes of a structure within a frequency band of interest. Since this type of spectrum can be measured without leakage error, we can experimentally verify that  $H_2$  estimator reduces the error dramatically. Figure 3-7 compares  $H_1$  and  $H_2$  estimates for two different spectral resolutions. We can see that even for a low Coherence ( $\gamma^2 = 0.48$ ),  $H_2$  seems to cancel-out the error. This can be explained by

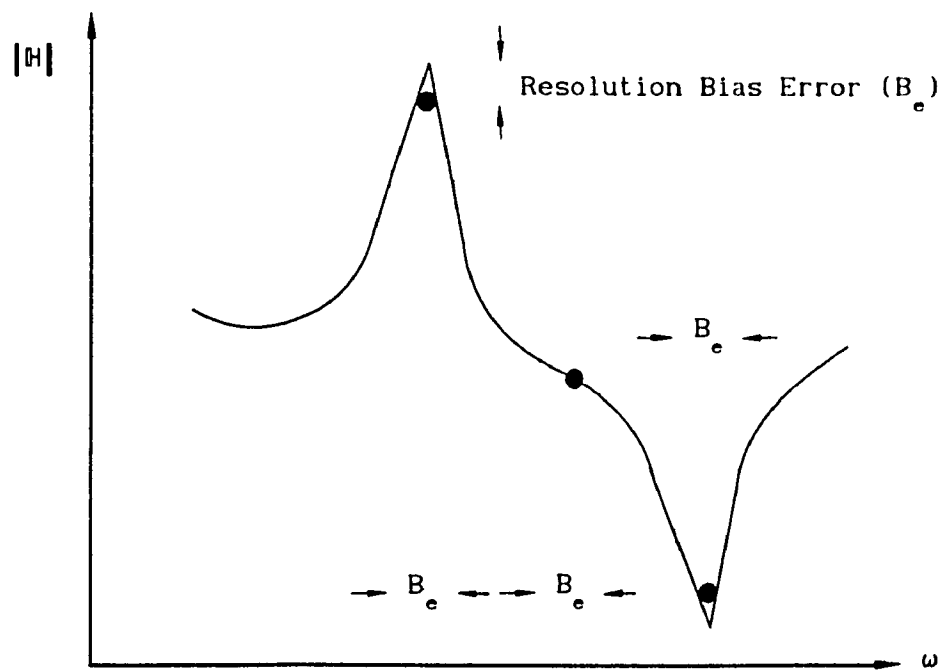
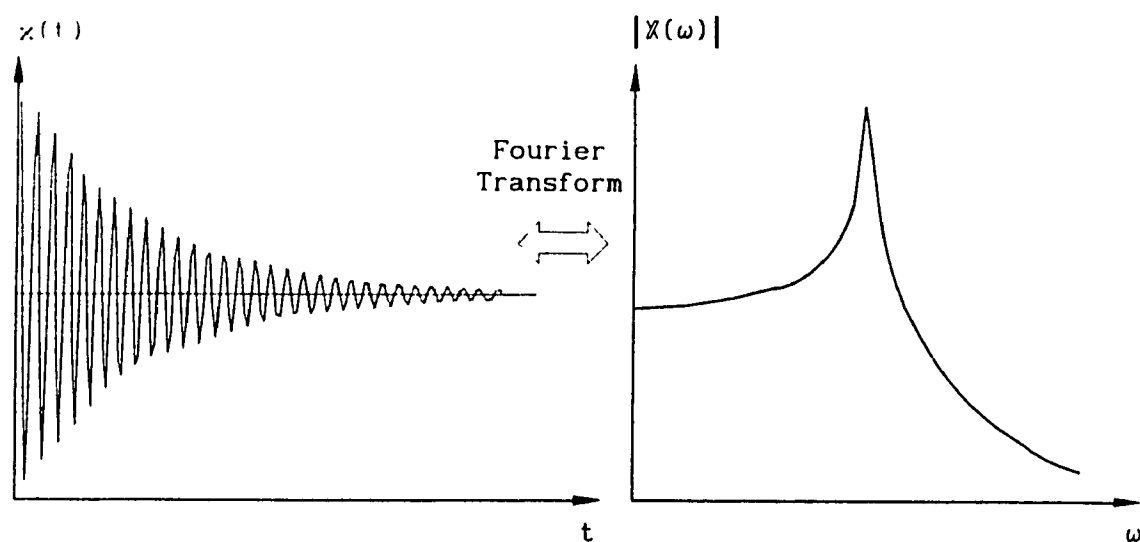


Figure 3-5: Representation of the Resolution Bias Error

a)



b)

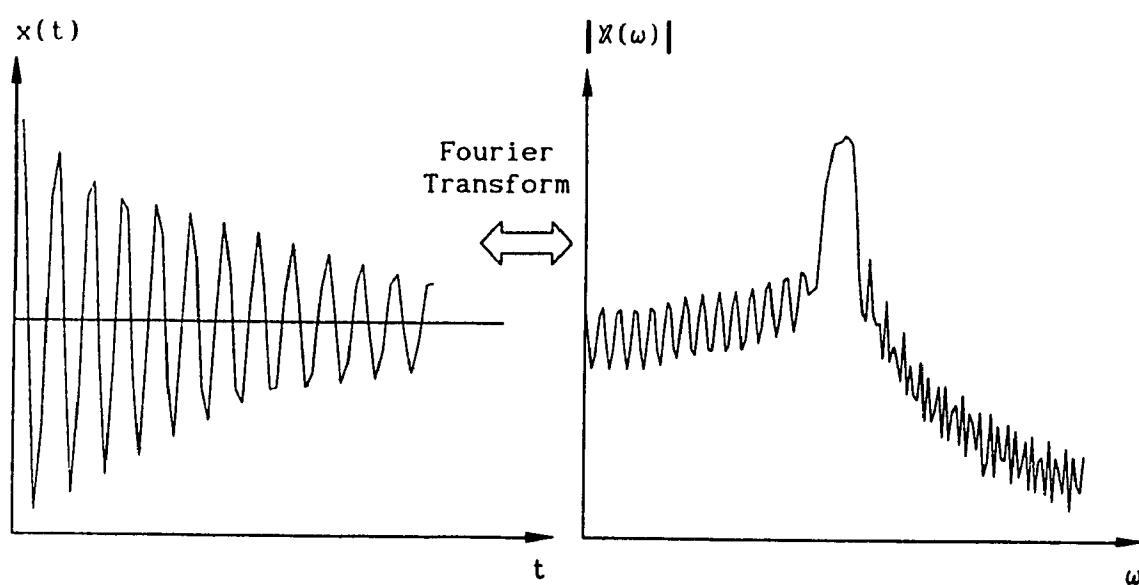


Figure 3-6: Time Histories and their Corresponding FRF

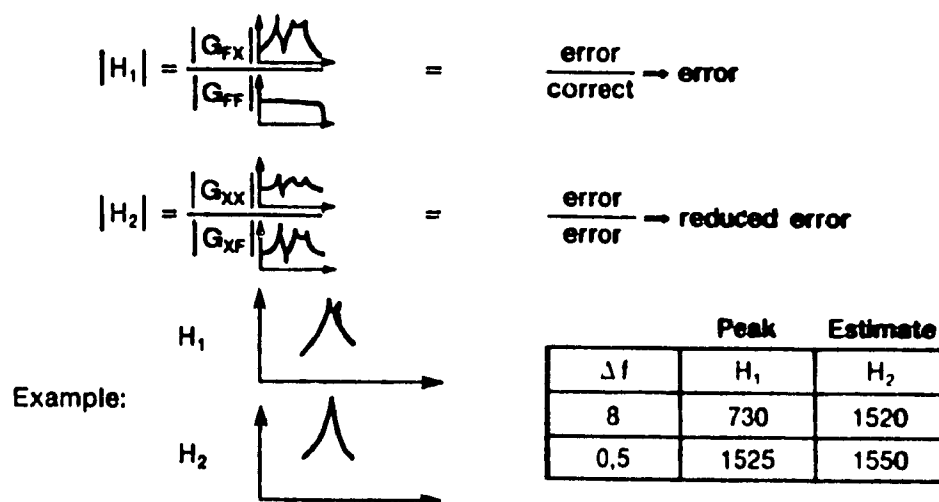


Figure 3-7: Example Comparing  $H_1$  and  $H_2$  with Leakage for Two Different Spectral Resolutions [5]

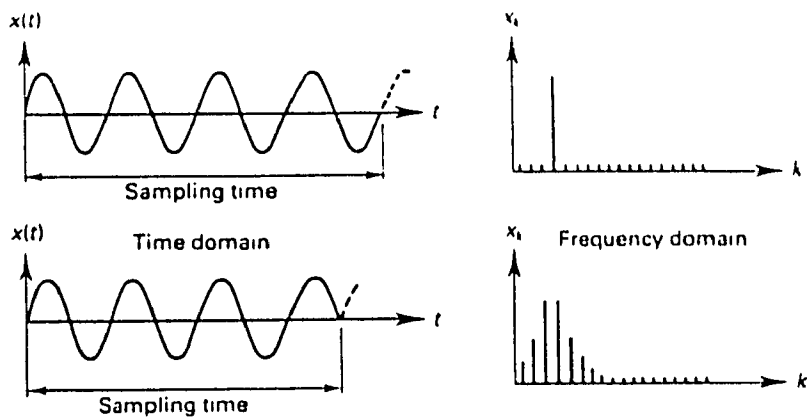
the fact that  $M_2$  is the ratio between two spectra both prone to leakage errors and their ratio reduces the error.  $M_1$ , by contrast is a ratio between a spectrum with leakage and a spectrum without leakage and their ratio does not reduce the error.

### 3-9 Discrete Fourier Transform Error

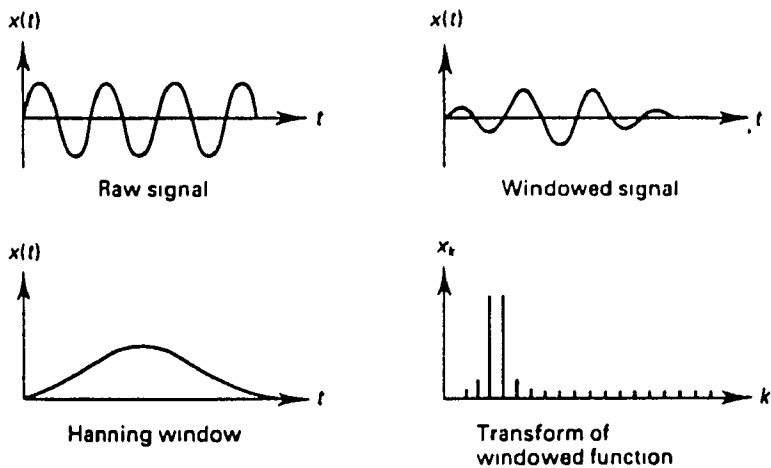
Digital Fourier analysis assumes that the signal is exactly periodic in the record window. When this assumption is violated, leakage occurs and energy leaks into adjacent frequency channels. This effect can be reduced by multiplying each data record in the time domain by a weighting function such as a Hanning window. Figure 3-8 shows these concepts for a sinewave.

### 3-10 Overlapping Analysis

Overlap analysis is a common function of modern analyzer, and it defines the degree of overlap between the time records as shown in Figure 3-9. Hence, the number of statistically independent spectra averaged can be set by this function. Table 3-2 shows the measuring time of the 2032 analyzer for 100 averages with different degree of



a) Sinewave and its Digital Fourier Transform for Two Different Sample Intervals Illustrating Leakage



b) Typical Hanning Window and its Effect on a Sinewave

Figure 3-8: Concepts of Discrete Fourier Transform Error [7]



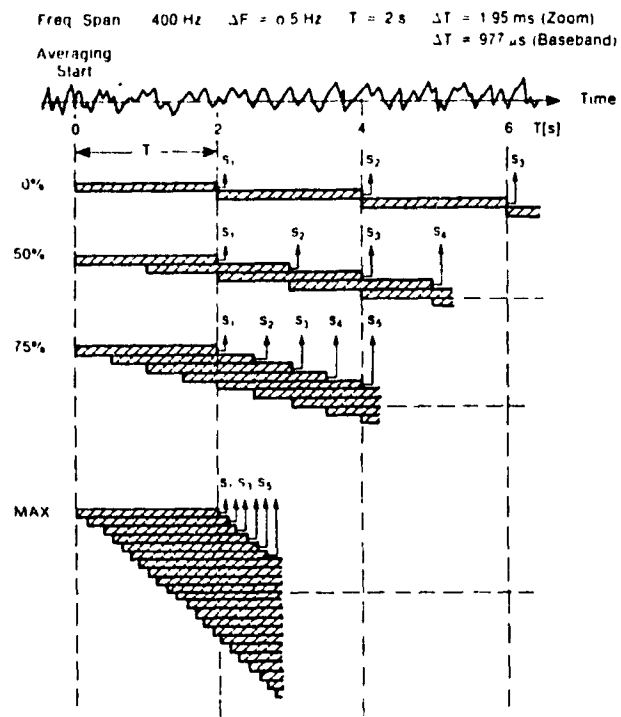


Figure 3-9: Selection of Different Degrees of Overlap [6]

Table 3-2: Measuring Time for 100 Averages with Different Degrees of Overlap and  $T = 2$  sec. (i.e. Freq. Span = 400 Hz) [6]

Degree of Overlap	Sampling Time Period
0%	# A T = 200 s
50%	$T + (\# A - 1) \frac{T}{2} = 101$ s
75%	$T + (\# A - 1) \frac{T}{4} = 51.5$ s
MAX	20 s

overlap and the record length  $T = 2$  s. 0% overlap is also called sequential averaging.

### 3-11 Averaging Methods

Averaging is a statistical method to reduce the variance when analyzing random data and to recover coherent signal buried in noise. The averaging methods currently available in a modern FFT analyzer are: linear, exponential and peak averaging.

Linear averaging is defined as:

$$Y_n = \left( 1 - \frac{1}{n} \right) Y_{n-1} + \frac{X_n}{n} \quad (3-13)$$

where

$Y_n$  = average after  $n$  ensembles

$Y_{n-1}$  = previous average after  $n-1$  ensembles

$X_n$  = the  $n^{\text{th}}$  ensemble

This method calculates a linearly weighted average so that all ensembles have the same influence on the average and the average is always properly scaled. This is the most popular averaging method used by test engineers.

Exponential averaging is defined as:

$$Y_n = \left( 1 - \frac{1}{N} \right) Y_{n-1} + \frac{X_n}{n} \quad (3-14)$$

where

$N$  = total number of ensembles used to calculate the average, and where the other parameters have the same meaning as given for linear averaging.

This method calculates an exponentially weighted average so that the newest ensemble has largest influence on the average and older ensembles are gradually forgotten. Using this type of averaging method with a transient type of excitation will provide weighting to the FRF measurement so that only the fundamental frequency will remain.

In peak averaging, each spectral component from each ensemble is compared with the corresponding peak "averaged" component and the largest value is retained.

The number of total ensembles or averages to use depends on the type of errors present in the measurement and the accuracy required. If most errors in the measurement are bias errors, averaging cannot reduce the errors. On the other hand, random errors can be minimized and in this case Figure 3-4 gives the number of averages to be used to obtain a desired normalized random error for a given Coherence. We must keep in mind that increasing the number of averaging increases the length of

the experiment. Hence, efforts should be made to find the error sources, e.g. replace a bad electrical wiring, in order to record good measurement using a small number of averages. A rule of thumb is to use 3 to 5 averages to verify that the measurement has constant value and its Coherence is close to unity.

### 3-12 Frequency Bandwidth of Interest

In general, for a given FFT analyzer, selecting a high frequency bandwidth reduces the time required to take the measurements due to shorter record length. However, this increases the resolution bias error due to low spectral resolution but decreases the aliasing error due to more samples per cycle are calculated for the highest frequency of interest.

When an experimental modal test specifies the frequency range of interest to evaluate the major modes of vibration of a mechanical structure, the frequency bandwidth must be selected so as to include at least the specified frequencies of interest. If the lower frequency range of the specification is greater than zero Hertz, preliminary testing should be carried-out with the lower frequency bandwidth set at 0 Hz in order to verify that the highest rigid body mode of the test system does not interfere with the lowest flexural mode of the structure

(see Section 4-2-1-2). In addition, to reduce the aliasing error, the upper frequency bandwidth should be selected twice as the one specified in the test requirements as discussed earlier in Section 3-7.

When the purpose of a test experiment is to build a modal model to simulate Structural Dynamic Modifications (SDM), the selection of the frequency bandwidth should be large enough to include all the vibration modes or singularities which contribute to the overall dynamics of the structure, otherwise large errors will incur. These errors are called modal truncation errors. As an analogy, when simulating the dynamics of a mechanical system using Finite Element Analysis (FEA), appropriate master Degrees-Of-Freedom (DOF) should be selected to have confidence in the results. A rule of thumb in FEA is to select the master DOF in such a way to compute twice the number of modes of interest. In modal testing of course, which modes does not cause "significant" errors when left out of the modal data set is a matter of engineering judgement.

### **3-13 Nonlinearities in Experimental Modal Testing**

One of the most important assumption of experimental modal testing is linearity which implies that the measured FRF (i.e., measured properties of the structure) obey the superposition, homogeneity and reciprocity definitions. If non-linear behavior is expected in a

structure or is detected in the FRF measurements, modal testing can only make a linear approximation. In this case, the best linear approximation can be obtained by using a random excitation waveform that will remove the non-linearities through ensemble averaging. However, if it is preferred to describe the non-linear behavior in the structure an excitation waveform that permits maximum amplitude control should be chosen (e.g. sinusoidal excitation). Hence, it is important to understand the various types of non-linearities, and certainly, to detect them in the measured FRF.

The most common types of non-linearities encountered in mechanical systems are due to clearance between parts, non-linear damping, and load-sensitive stiffness. Clearance between parts are frequently encountered in geared systems and shafts mounted on bearings. The usual approach to minimize these errors is to preload the system through a soft spring to take up clearances so that the resonances associated with the preload (rigid modes) lie below the frequency range of interest.

Non-linear damping are usually seen in mechanical systems with joints or mounts, where the damping values are function of the relative displacement at the joint. Hence, if the point of excitation is close to a joint, the relative motion at that location will be high, and thus the apparent damping in the measured FRF will be high.

The last common type of nonlinearity is encountered in mechanical systems where the spring rate ( $dk/dx$ ) of elastic elements either increases (so-called hardening type spring system) or decreases (so-called softening type spring system) with vibration amplitude. Figure 3-10 shows the characteristics for some symmetrical spring arrangements. In the case of hardening type spring system, the resonances are shifted toward the higher frequencies as the dynamic load increases, whereas, in the case of softening spring type system, the resonances are moved toward the lower frequencies. Figure 3-11 illustrates how the resonance curves change for various levels of excitation for both spring types and linear resonant systems. Figures 3-12 and 3-13 show the instability regions and a measured FRF of a typical hardening spring type resonant system respectively. Hence, this non-linearity can be detected by comparing measured FRF for various vibration amplitudes.

### **3-14 Response Transducer System**

The response transducer system is one of the basic hardware component required to carry-out vibration measurements. It is generally composed of two distinct equipments, namely a measurement transducer and a signal conditioner/amplifier as shown in Figure 3-14 and are selected in pairs. The measurement transducer measures the mechanical motion of



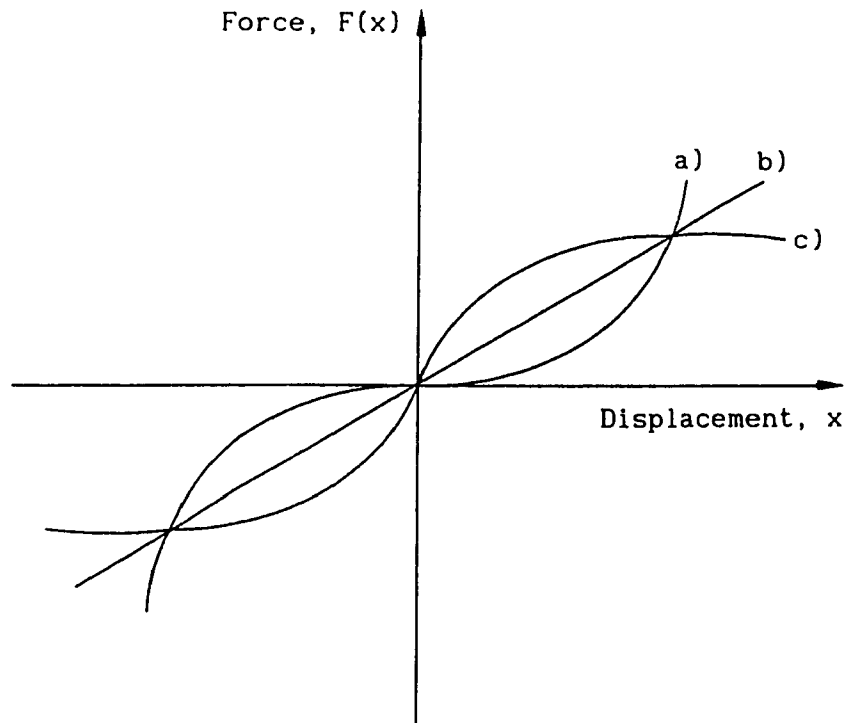


Figure 3-10: Typical Force Versus Displacement Characteristics for Some Symmetrical Spring Arrangements: a) Hardening Type Spring, b) Linear Type Spring, c) Softening Type Spring

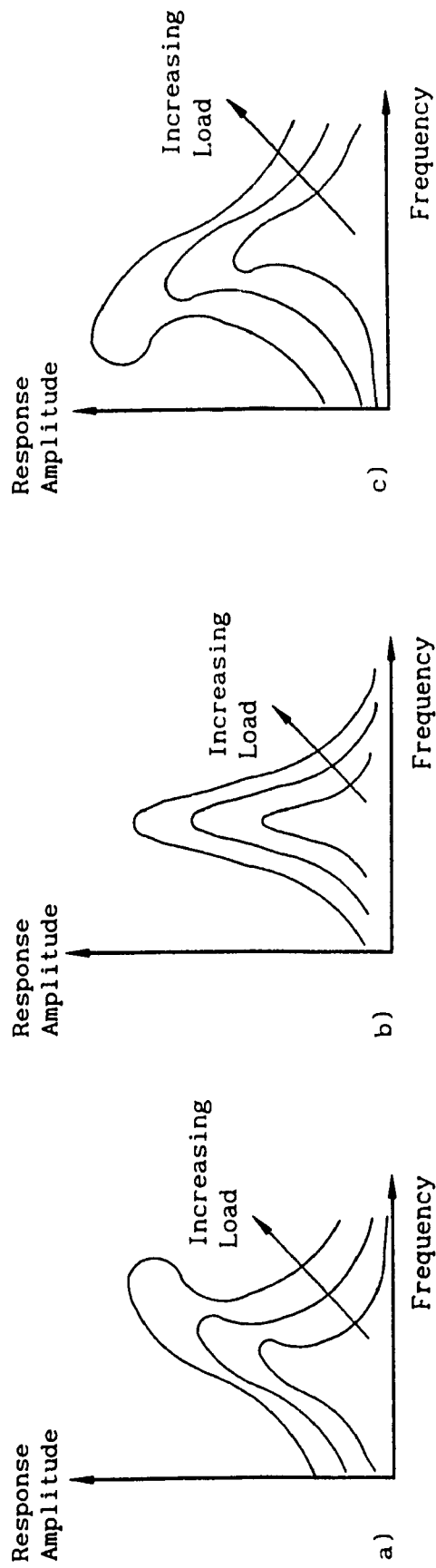


Figure 3-11: Typical Resonance Curves for Various Levels of Excitation:  
 a) Hardening Type Spring, b) Linear Type Spring,  
 c) Softening Type Spring

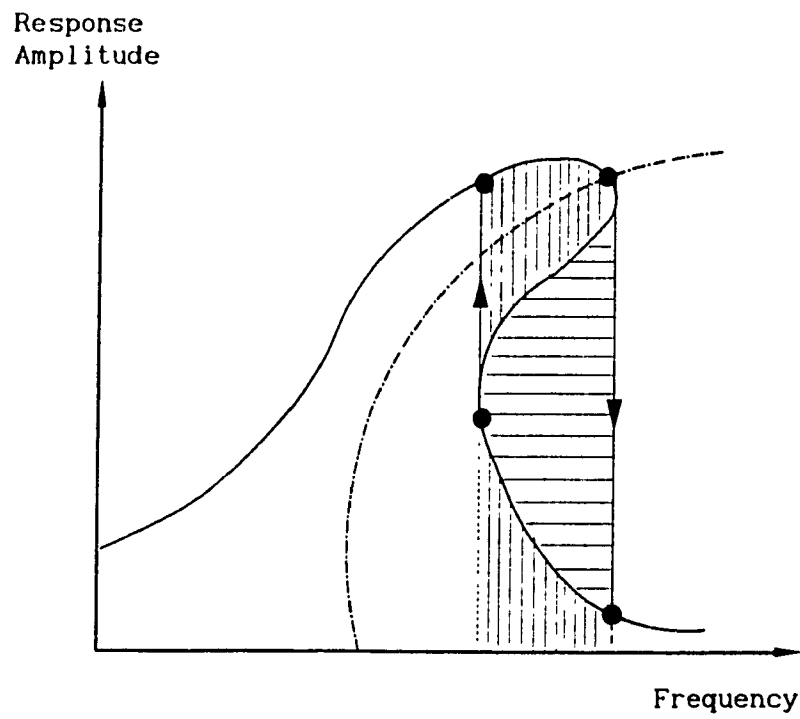


Figure 3-12: Typical Resonance Curve for a Hardening Type Showing the Region of Instability (Hatched Areas)

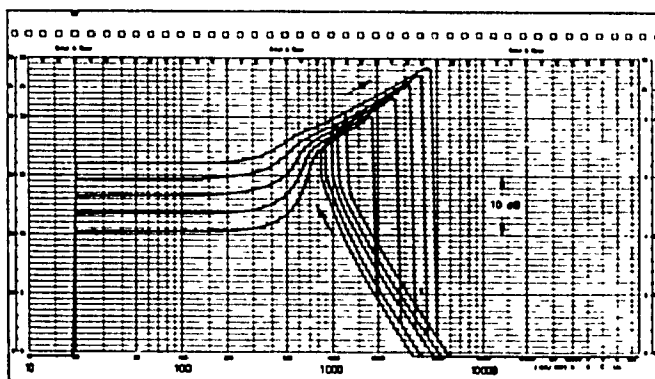


Figure 3-13: Resonance Curves for a Hardening Type Measured for Various Levels of Excitation of an Analog Model System [12]

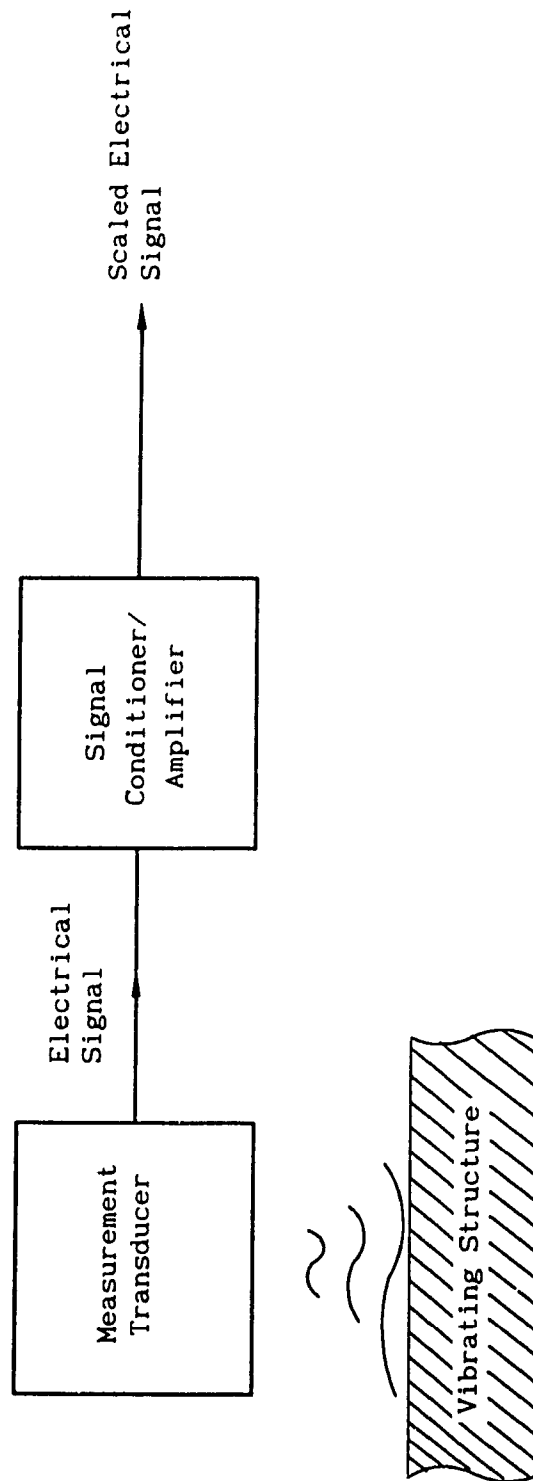


Figure 3-14: Schematic Measurement Transducer and Signal Conditioner/Amplifier Sequence

the structure subjected to vibration in terms of displacement, velocity or acceleration. The signal conditioner/amplifier conditions the output signal generated from the measurement transducer into a measurable signal. For example, a piezoelectric accelerometer is used to measure acceleration and produces an electrical charge proportional to the acceleration to which the transducer is subjected to and the conditioner provides a voltage output signal.

Displacement can be measured with LVDT (Linear Variable Differential Transformers), and displacement proximity probes. Velocity can be measured using an LVT (Linear Velocity Transducer), microphones, and laser velocity-transducer. Acceleration can only be measured using accelerometers. It does not normally matter which quantity is actually measured because these quantities are interrelated by simple differentiation or integration. Accelerometers are small in size and offer a wide useful frequency range compared to the displacement and velocity transducers, and therefore are always used when carrying vibration measurements.

### 3-14-1 Accelerometer Selection

The selection of a suitable accelerometer is principally based upon its useful frequency range and its sensitivity. In general, one should select the most sensitive unit that can operate within the frequency

range of interest. However, higher the sensitivity is, the heavier and larger is the transducer, and thus higher is the interference with the structure (see Section 3-14-3, mass loading effects). A rule of thumb is to use a light accelerometer when testing light structures. Other factors should also be considered such as the transducer operational environment and its sensitivity to environmental changes. In addition, for accurate measurements, especially when testing a structure that is vibrating simultaneously in several directions, the accelerometer cross-axis or transverse sensitivity should be as small as possible, i.e. less than 1-2 per cent of the main sensitivity [9]. A graphical illustration of transverse sensitivity of a typical accelerometer is shown in Figure 3-15.

### 3-14-2 Accelerometer mounting

There are various attachment methods for mounting an accelerometer to the surface of a test structure. The most common methods are: screwed stud, cement stud, wax, adhesive tape, and magnet. In general, as the convenience of the method improves, the stiffness contact between the accelerometer and the structure diminishes which reduces the useful frequency range of the accelerometer as shown in Figure 3-16. However, this rarely gives problems in experimental modal testing since the upper frequency of interest is seldom beyond 100 Hz. Another attachment method that is very convenient is to use "Fun-Tak", a registered

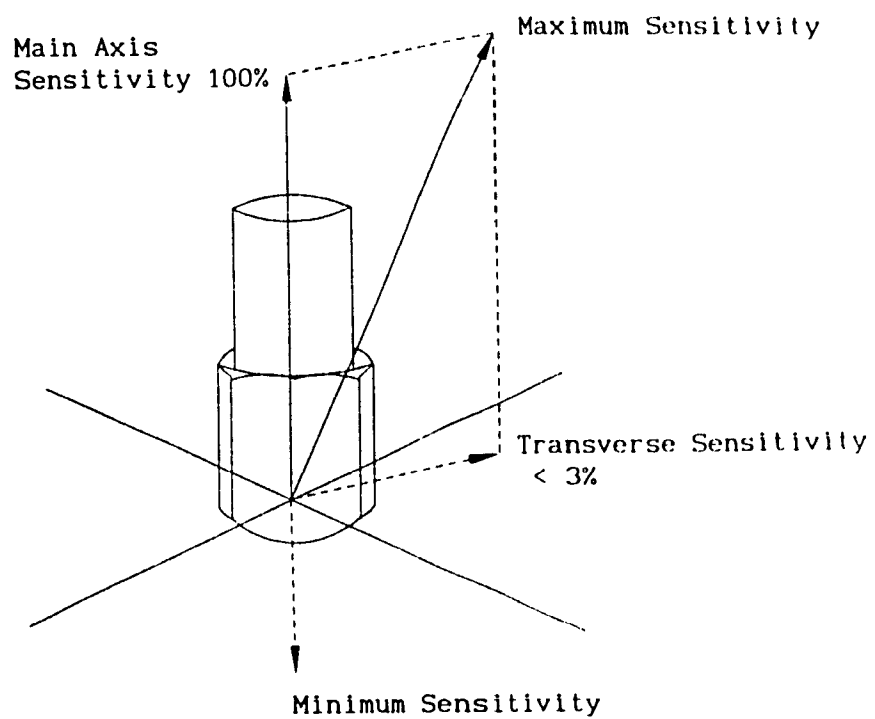


Figure 3-15: Graphical Illustration of Transverse Sensitivity



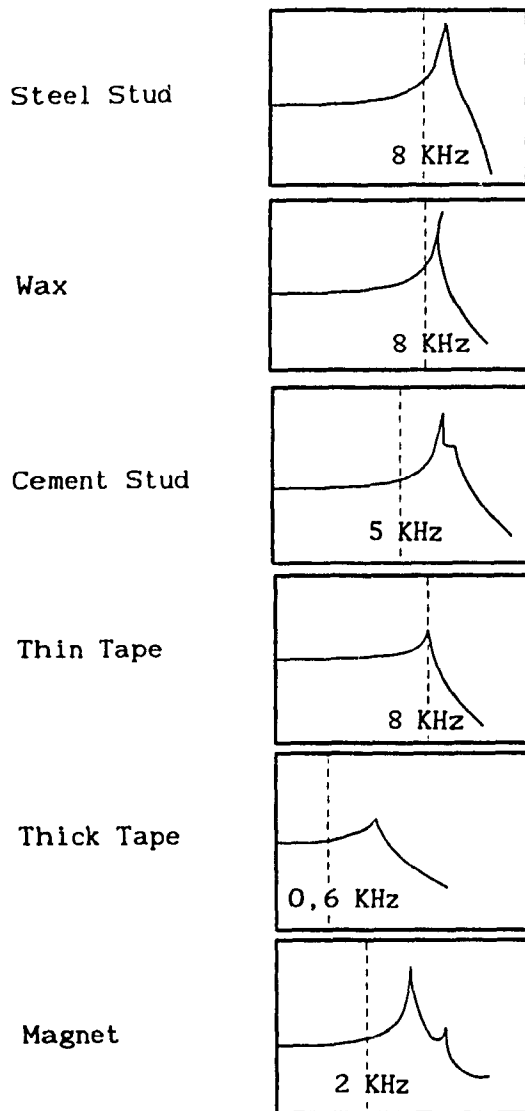


Figure 3-16: Accelerometer Attachment Methods and their Corresponding Frequency Response Limits

trademark of Lepage's Limited. This adhesive is very similar to the modelling wax and can be used repetitively and it adapts to the shape of the structure so that the accelerometer can be mounted at almost any points in any desired directions. The mounting is simple by placing a piece of Fun-Tak on the structure and pressing on it the accelerometer. Elastic rubber band can be used in conjunction with this material to increase the stiffness contact and to hold the accelerometer firmly in place. In addition, the connecting cable should be attached to the test structure to avoid noise due to dynamic bending or compression and tension of the cable as shown typically in Figure 3-17. This mechanically caused noises are sometimes called tribo-electric effects, or simply microphonic noise. Fun-Tak can be conveniently used for this purpose.

### **3-14-3 Accelerometer Location**

The minimum of data to be measured on a structure to identify its modal properties corresponds to the measurement of either one row or one column of the FRF matrix [2]. In the case of measuring a row, all the FRF curves share the same response points (i.e., the accelerometer position is kept constant during the experiment). Conversely, when measuring a column, all the FRF curves share the same excitation point. Hence, if it is decided to measure a row of the FRF matrix, care should be taken to avoid selecting a location at or close to a node of one or

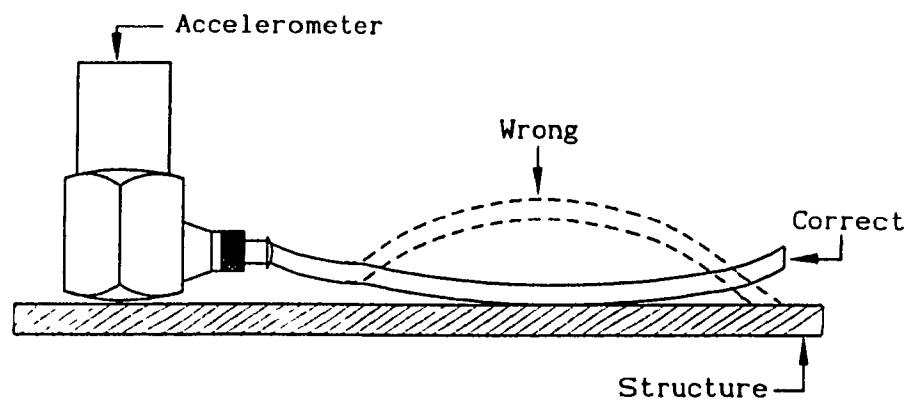


Figure 3-17: Correct Clamping of an Accelerometer Cable to Minimize Cable Noise Due to Cable Whip

more of the structure's modes, otherwise the measurement of that or those modes will not be identified.

In view of this, the accelerometer location should be selected from the FEA results, if exit. If not, measurements should be taken at other DOF's locations to check that all the modes are seen. In general, the selection of an extremity point on the structure is a good choice.

However, mounting an accelerometer away from a node of a given vibration mode increases its mass loading effects which tends to lower the measured resonance frequencies. Figure 3-18 shows the mass loading effect for a free-free beam. Non contact transducers are more appropriate on light structures to give minimum loading.

Also, we should keep in mind before selecting the accelerometer location (or the excitation location) that the measurement of either a row or a column implies a driving point measurement, i.e. exciting the structure and measuring the driving-point response at the same location, and in the same direction. This can be achieved by using an impedance head (an integrated force and response transducer), by placing the force and response transducers in line but on opposite sides of the structure (if permitted) or by measuring the excitation very close to the accelerometer as illustrated in Figure 3-19.

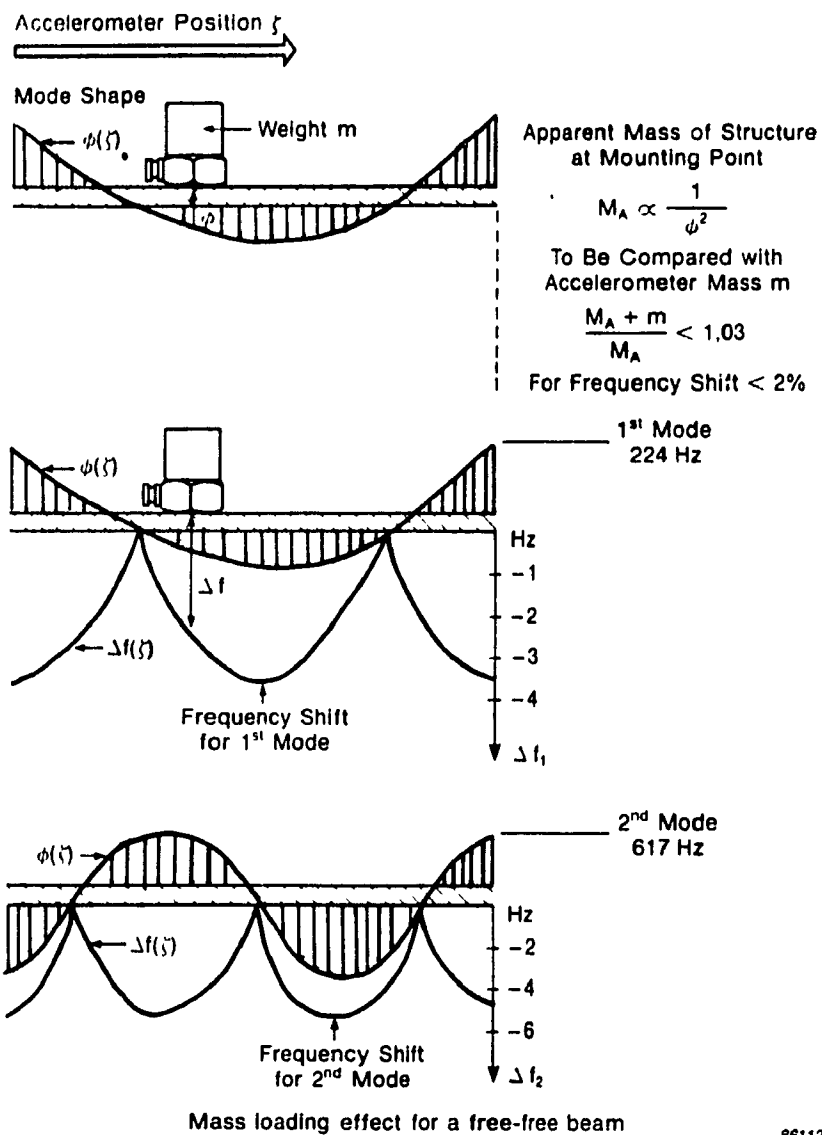


Figure 3-18: Accelerometer Mass Loading Effect [5]

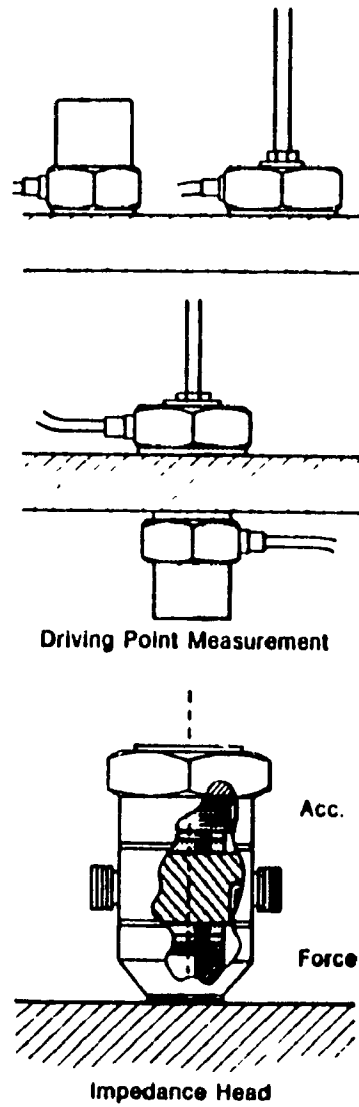


Figure 3-19: Possible Driving-Point Response Measurements [5]

### 3-15 Excitation Waveforms

In this section, five types of excitation forms which can be used for making FRF measurements are discussed. The five types are: (1) pure random, (2) pseudo-random, (3) periodic random, (4) sinusoidal, and (5) transient. Each one possesses a distinct set of characteristics and identified and compared in Table 3-3. A common point between them is that they all require, except for transient excitation waveform, a well-designed fixture and an exciter system (i.e. a shaker and a signal generator).

#### 3-15-1 Pure Random

In statistical terms, a pure random signal has a Gaussian probability distribution as shown in Figure 3-20. Each sample of data, T seconds long, has random amplitude and phase at each frequency. This is the single most attractive characteristic of a pure random signal for FRF measurements. Indeed, the structure is subjected to a wide vibration amplitude, and ensemble averaging randomizes any non-linear effects, and extraneous noise in the measurement data. This excitation method yields the best linear approximation in a mean-square sense.

Its auto-spectrum tends to be a flat spectrum as the number of averaging increases as illustrated in Figure 3-21. Hence, the overall

TABLE 3-3: Characteristics Comparison Between Excitation Waveforms [5] and [19]

WAVEFORM CHARACTERISTICS	Pure Random	Pseudo Random	Periodic Random	Sinusoidal	Transient
Analysis Speed	slow	fast	slow	very slow	fastest
Leakage Error	yes	no	no	no	sometimes
Linear Approximation	yes	no	yes	no	somewhat
$\gamma^2$ - Detects Non-Linearities	yes	no	yes	no	somewhat
$\gamma^2$ - Detects Leakage Errors	yes	no	yes	no	somewhat
Force Level Easily Controlled	yes	yes	yes	yes	no
Force Spectrum Easily Shaped	no	yes	yes	yes	no
Peak-To-RMS Energy Level	no	yes	yes	yes	no
Requires an Exciter System and a Fixture	yes	yes	yes	yes	no
Zoom Analysis	yes	yes	yes	yes	no
Crest Factor S/N Ratio	fair	fair	fair	good	poor



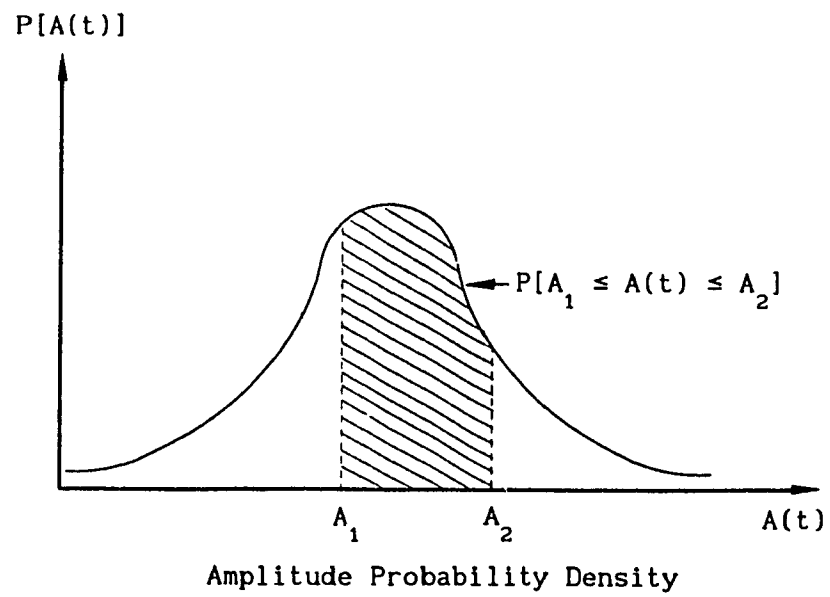
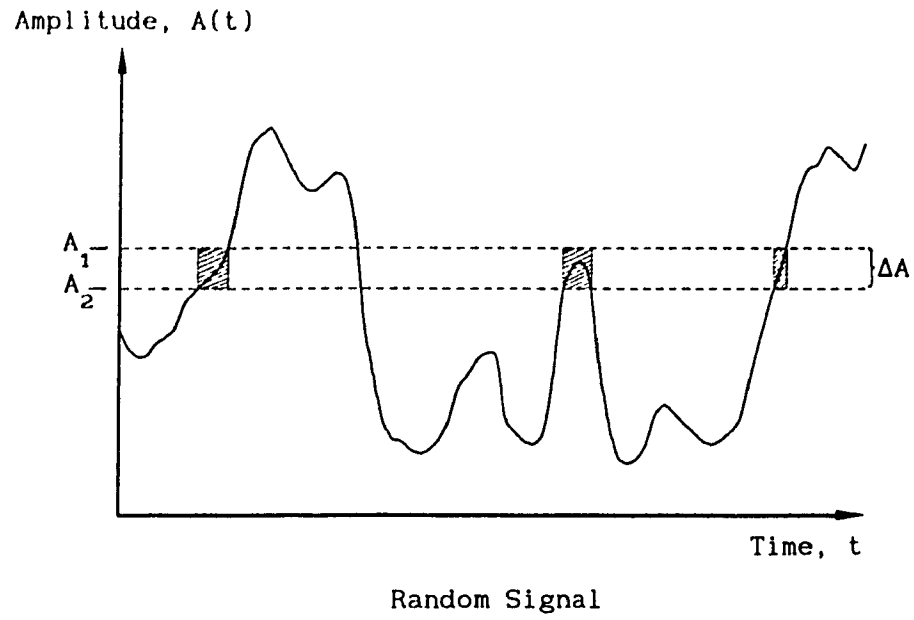


Figure 3-20: Random Signal and its Amplitude Probability Density

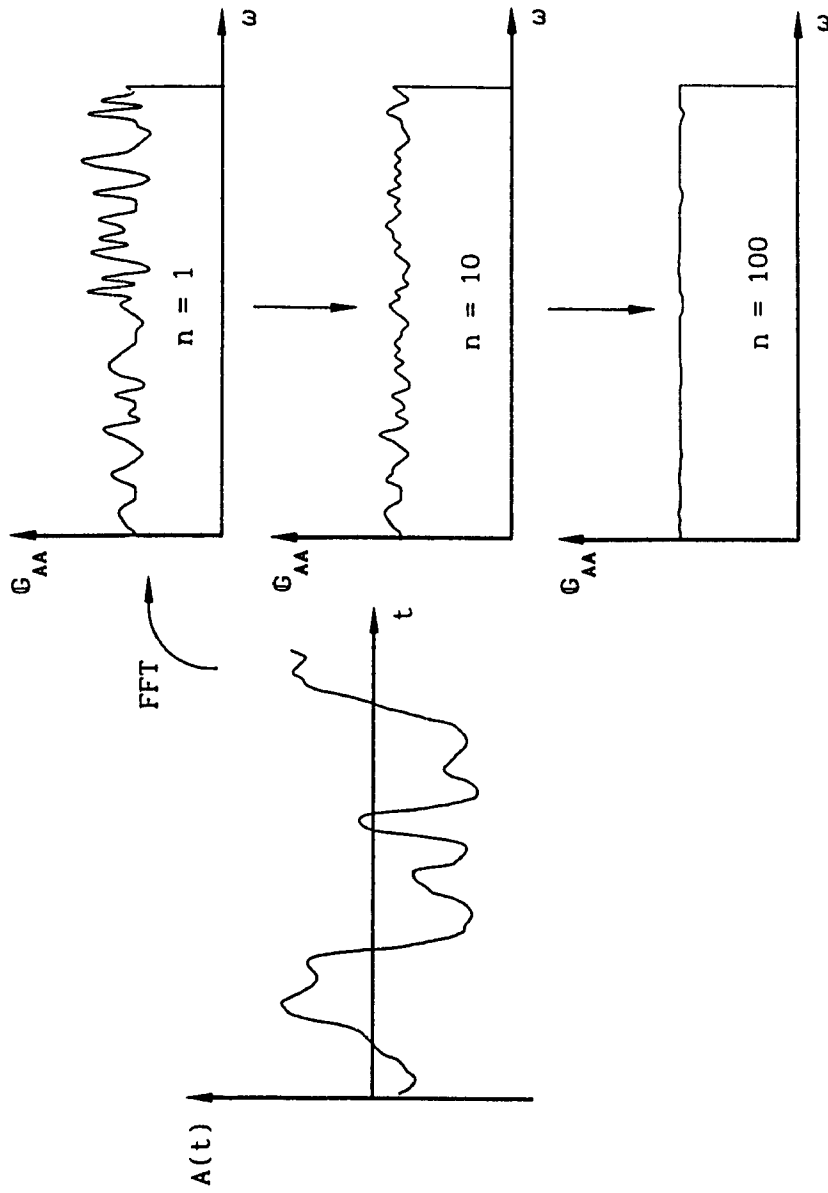


Figure 3-21: Auto-Spectrum of a Random Signal Versus Number of Averages

force level and frequency range can be easily controlled as shown in Figure 3-22. However, due to the impedance mismatch between the shaker head and the structure, the averaged force spectrum measured on the structure at the shaker attachment will be a quasi-flat spectrum as shown in Figure 3-23. The shape of the force spectrum can ideally be improved by using a some form of closed-loop force control system, but practically, it is difficult. Fortunately, when carrying out modal testing, this problem is not important.

The main drawback of this excitation method is that the auto-spectrum contains leakage because the signal is not periodic within the measurement window as discussed in Section 3-9. Hence, a weighting function should be used to minimize the leakage, and the best window function to use is a Hanning window [12].

### 3-15-2 Pseudo-Random

A pseudo-random signal is a periodic random signal of  $T$  seconds which is repeated with every measurement of the analysis. This signal can be seen as a collection of sinusoids with the same amplitudes but random phases. Thus, due to the periodic nature of the signal, the spectrum is leakage-free.

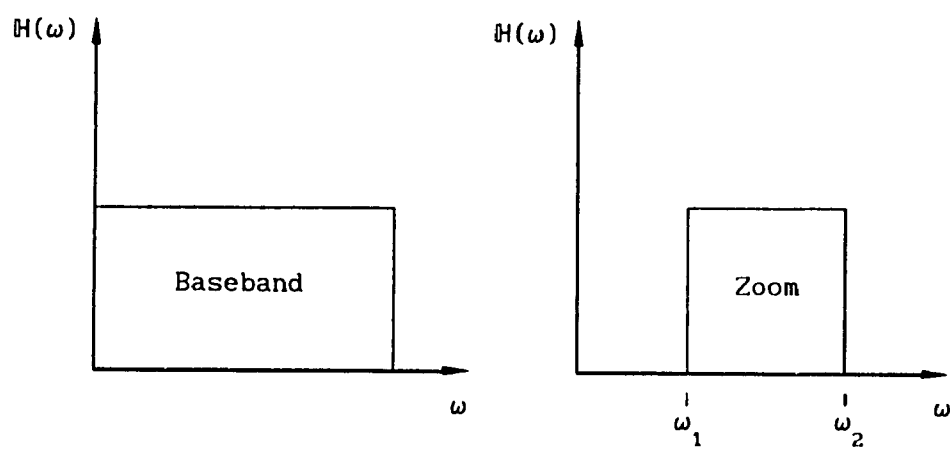


Figure 3-22: Baseband and Zoom Analysis

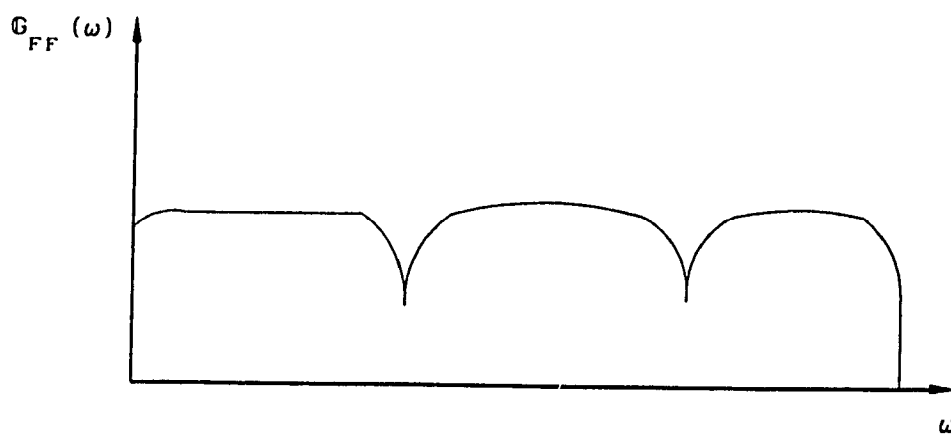


Figure 3-23: Quasi-Flat Spectrum

However, ensemble averaging has no significant effect than reducing the extraneous noise because the structure is excited with the same spectrum (i.e. constant amplitude and phase at each frequency) for every measured FRF measurement.

This technique is the fastest one for making statistically accurate FRF measurements in the case when the measurement is relatively free of extraneous noise and the system behaves linearly.

Since the structure is excited with a constant spectrum, it can be easily shaped to account for the exciter system characteristics by using a compressor.

In order to take advantage of this waveform, it is important to make certain that the signal generator is synchronized with the analyzer measurement window.

### **3-15-3 Periodic Random**

This excitation signal takes the best features of pure random (see Section 3-15-1) and pseudo-random (see section 3-15-2). Indeed, it is a periodic signal and several uncorrelated ones are generated for each FRF measurement taken. Figure 3-24 compares pure random, pseudo random, and periodic random waveforms together. Using an FFT analyzer, the steps to

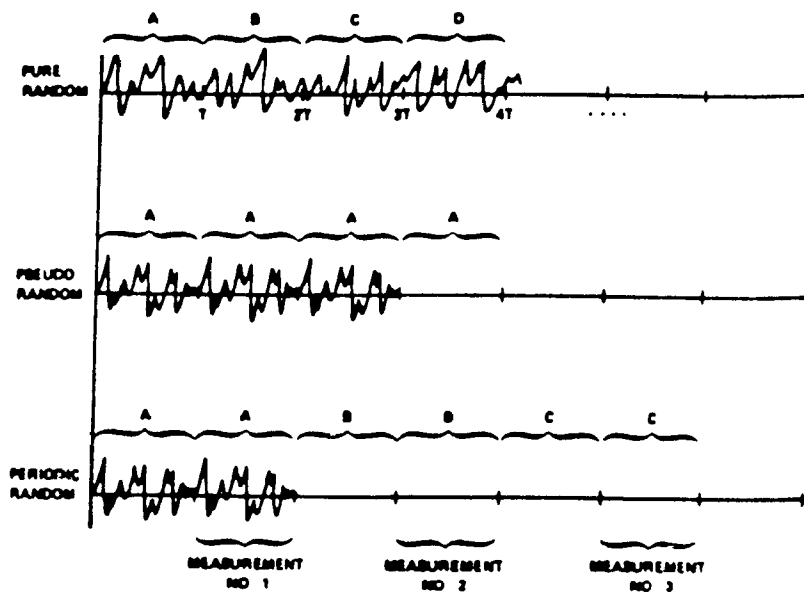


Figure 3-24: Comparison of Pure Random, Pseudo-Random, and Periodic Random Waveforms [19]

take one measurement would be as follow:

- 1) Generate the first pseudo-random signal (" A " signal);
- 2) Excite the structure with that " A " signal;
- 3) When the structure is vibrating in its steady-state condition (i.e., most transient part of the response has died-out), take the first ensemble average measurement (i.e. press start pushkey on the FFT analyzer);
- 4) Remove the excitation signal (for safety and as usual procedure when changing the excitation signal);
- 5) Synthesize the second pseudo-random signal (" B " signal); (this signal is not correlated to the first one);
- 6) At steady-state condition, take the second ensemble average measurement (i.e. press proceed pushkey on the FFT analyzer);
- 7) Repeat steps 4 to 6 for additional averaging.

However, the main drawback of this technique is that it takes much longer time than the pseudo-random approach. Indeed, the time required to remove the excitation signal, to generate and excite the structure with the new signal, and to allow the transient part to die-out before taking a new ensemble averaging (steps 4, 5, and 6) can be very long, especially when using an hydraulic shaker and carrying out several ensemble averages.

### 3-15-4 Sinusoidal

Sinusoidal excitation is a classical method of exciting a



structure. Stepped-sine, slow-sine (linear sweep) and fast-sine (logarithmic sweep) are the most popular sinewave methods for measuring FRF. Each of them have their own merits and drawbacks.

This waveform is not a very effective excitation method to carry-out modal testing for the following reasons:

- Lowest excitation frequency is limited to several Hz
- Analysis speed is very slow
- Less accurate results due to non-linearity, extraneous noise, and leakage errors in the measurements

However, this method is the best of all to investigate structural non-linearities at any specific frequency when the forcing frequency can be controlled manually. Indeed, the excitation force can be controlled accurately and large amounts of energy can be input to the structure at almost any frequency.

Figure 3-25 illustrates the distorting effect on the FRF measurements versus the sweep rate for a given structure. This can be explained by the fact that steady-state response level cannot be attained when the frequency is swept too fast. Therefore, optimum sweep rate should be prescribed for a given structure when carrying out FRF measurements. Fortunately, there is an ISO (International Organization for Standardization) Standard that prescribes maximum linear and logarithmic sweep rates to pass through a resonance and is given in

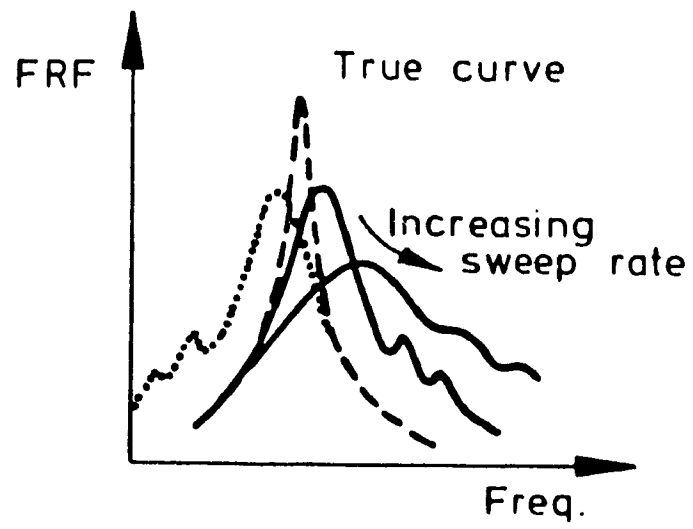


Figure 3-25: FRF Measurement by Sine Sweep Test - Distortion Effect of Sweep Rate [2]

reference [2].

Chirp testing is a logarithmic swept-sine testing whereas the duration of the swept-sinewave is generated in  $T$  seconds which corresponds exactly to the analyzer's measuring window. Hence the signal is periodic, and its spectrum is leakage free. However, this method has the inability to average-out non-linear effects as the pseudo-random excitation. Before using this excitation technique, one should verify that the sweep rate does not violate the ISO Standard.

### 3-15-5 Transient

There are two forms of transient testing, namely, step relaxation and impact testings. Both forms do not require a costly exciter system (shaker and signal generator) and a well designed fixture to attach the exciter to the structure as in the other excitation techniques discussed above.

Step relaxation requires a bit more complicated system set-up than the impact method but it is better adaptable to both too fragile or too heavy structures. Indeed, a lot more energy can be input to the structure without causing local damage. Basically, the structure is preloaded to some acceptable force level through an inextensible, lightweight cable and suddenly the cable is severed. At that instant,

both the transient input force and response are measured.

In the case of impact testing, the structure is excited through the use of an impactor such as an impact hammer, or a sledge hammer. This is the most popular and widely used excitation technique for carrying out modal testing and probably for the following additional reasons: This testing method is:

- Inexpensive compared to other methods.
- Practical for preliminary investigations.
- Convenient for checking accuracy of the modal model.
- Efficient for verifying that the fixed DOF can measure (in the case of a row measurement) or excite (in the case of a column FRF measurement) all the modes of interest.
- Extremely fast for quick test set-up and only a few averages are required.
- Portable and very suitable for field measurements.

There are, however, a number of errors and drawbacks to be considered before using this testing technique. One major error occurs due to the fact that the input force is not easily controlled because it is difficult to maintain the position, orientation, and force level between successive measurements. Hence, the measured FRF will not be a true representation of a point measurement upon which the modal technique is based, but a surface measurement. Also, if the range between the overload and the trigger (underload) levels is set relatively large in the FFT analyzer, non-linearities in the system can

be excited and linear approximation cannot be made for non-linear systems unless large number of averages are taken. But by doing this, we lose its main advantage, i.e. its speed. On the other hand, if this range is set relatively small, non-linearities cannot be excited, thus linear approximation cannot be made for non-linear structures.

Multiple impacts (or hammer bounce) happens when the impactor is too heavy or the experimentalist is not skilled. In this case, the measured FRF will be erroneous as illustrated in Figures 3-26 and 3-27 and must be rejected.

The crest factor describes the "peakiness" of a signal and is defined as the ratio between its peak value and its standard deviation (RMS) as shown in Figure 3-28. Since, this technique has a high crest factor, it may not be well-suited for certain types of structure. For example, the sufficient energy required to measure a good FRF on a large structure might be difficult to apply without damaging the structure locally.

In order to use this technique efficiently, several concepts must be understood before undertaking a complete test.

Figure 3-29 shows a typical impact force signal with its corresponding spectrum. The spectrum is continuous with maximum amplitude at 0 Hz and decaying amplitude with increasing frequency. The

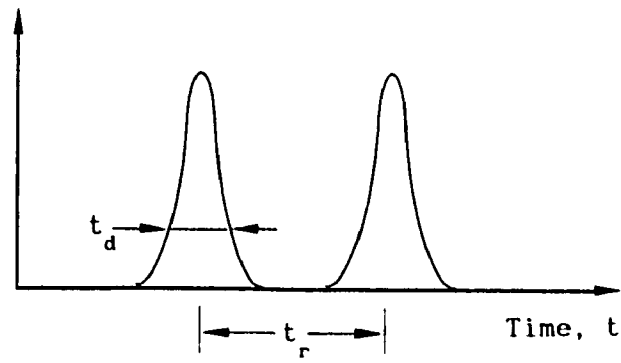
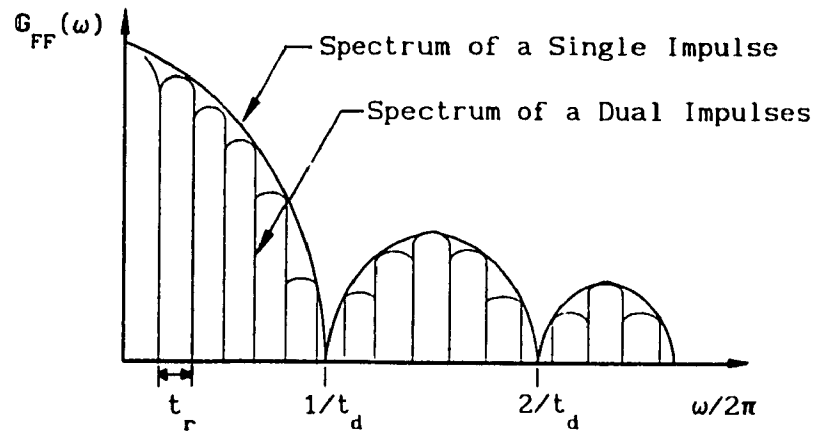
Impact Force,  $f(t)$ Fourier  
Transform

Figure 3-26: Effect of Hammer Bounce on the Force Spectrum

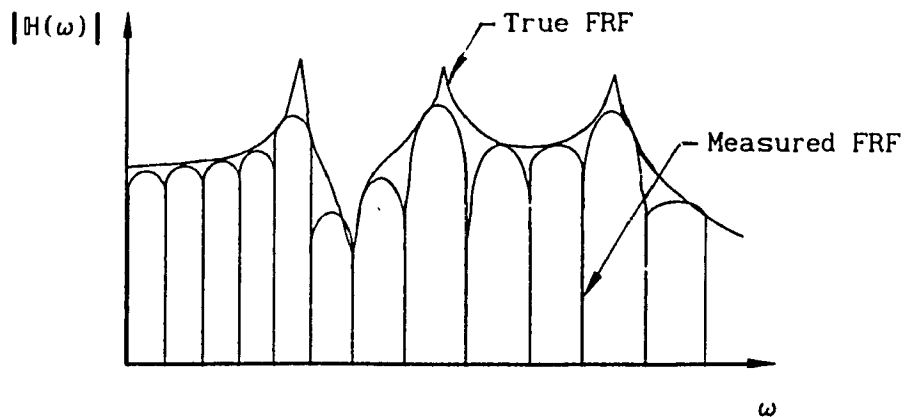


Figure 3-27: Effect of Hammer Bounce on the FRF Measurement

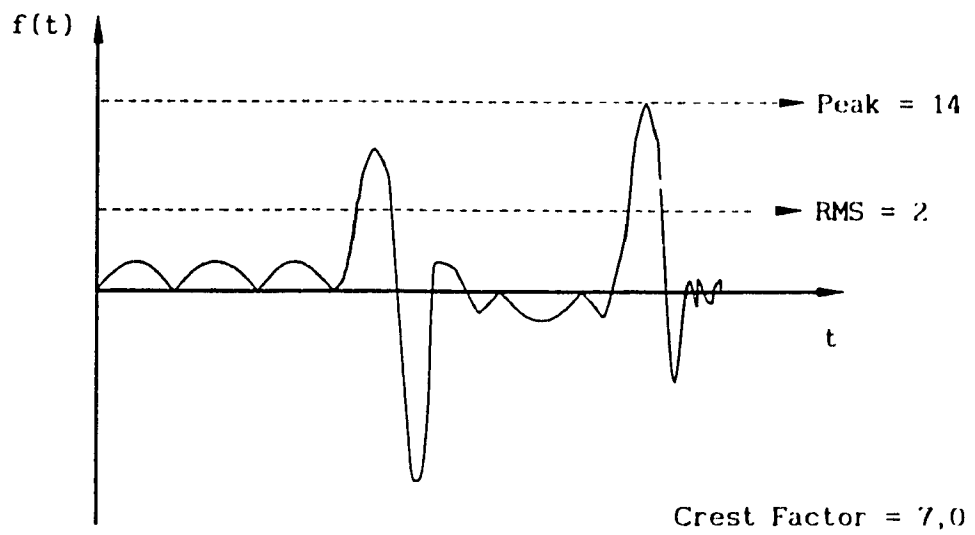
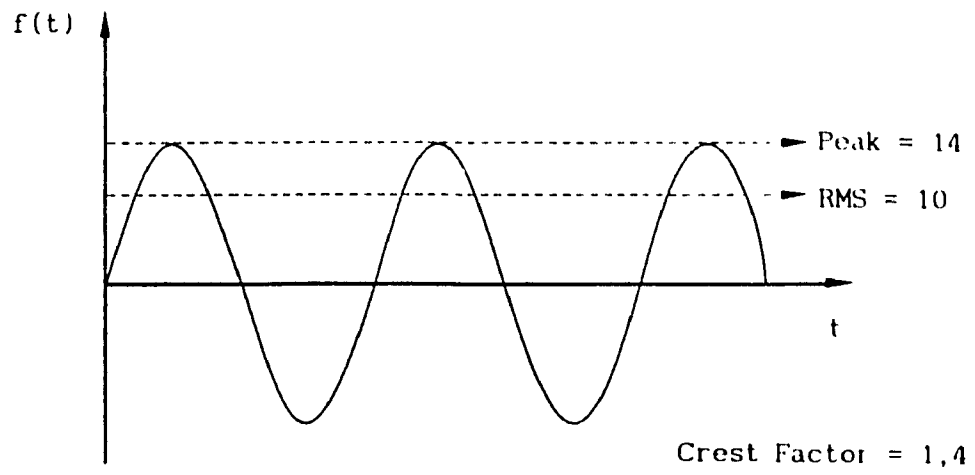


Figure 3-28: Typical Signal Versus Crest Factor Values



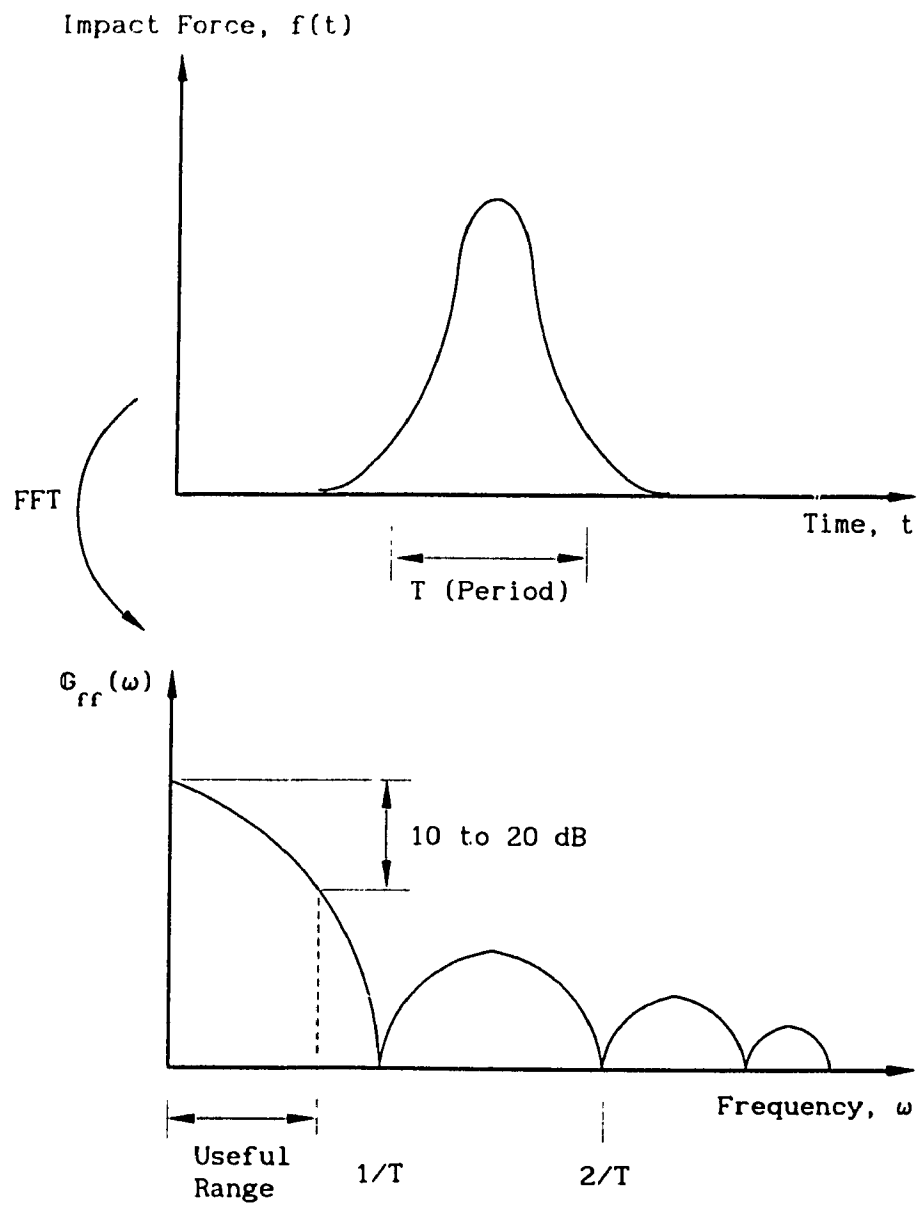


Figure 3-29: Typical Impact Force Signal and its Corresponding Spectrum

useful frequency range is limited at a frequency  $f_c$ , also called the cut-off frequency, at which point the spectrum magnitude has decayed by 10 to 20 dB maximum [13]. There is a direct relation between the first cut-off frequency,  $f_c$ , and the duration of the pulse  $T_c$ . Figure 3-30 shows a square, triangular and half-sine wave pulses of equal energy and time duration along with their respective autospectrum. In the case of a square type pulse, the first zero crossing occurs at a frequency approximately equal to the inverse of the time duration, i.e.

$$f_c \Big|_{\text{square pulse}} = \frac{1}{T_c} \quad (3-15)$$

For a more general pulse, like the half-sine wave, the relation is approximately given as

$$f_c \Big|_{\text{general pulse}} = \frac{2}{T_c} \quad (3-16)$$

We can see from these relations that shorter the pulse length, the higher is the frequency range. Hence, the useful frequency range of an impactor depends on its configuration. Indeed, an impactor can be configured by selecting a tip and a head combination to produce the desired shape and duration of the pulse signal to suit the measurement requirements. A rule of thumb is as follows: stiffer the tip and lighter the impactor mass, the shorter will be the duration of the pulse and thus higher will be the frequency limit of the impactor.

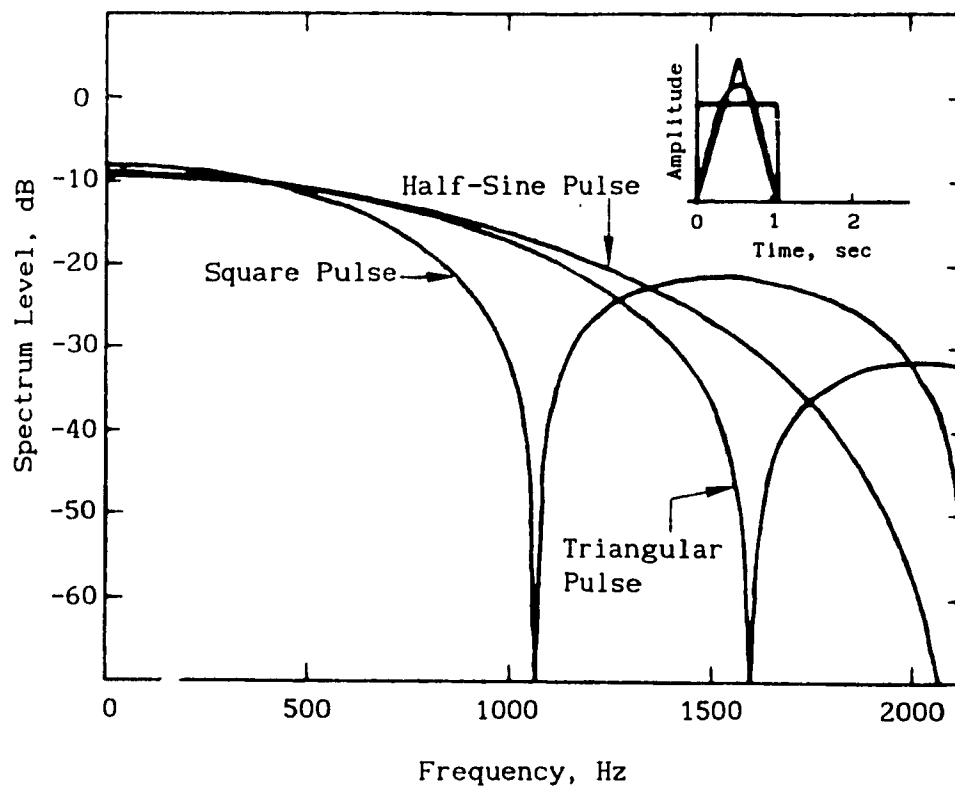


Figure 3-30: Frequency Spectra of Three Pulses of Equal Energy [13]

Figure 3-31 illustrates these concepts.

In terms of signal processing, a good rule of thumb is to insure that the sampling rate ( $\Delta T$ ) set in the FFT analyzer is at least twice the time duration of the impulse. This would put the first  $f_c$  of a square pulse at the Nyquist folding frequency, and the first  $f_c$  of the other pulse shapes above the Nyquist folding frequency [13].

When using this technique to carry-out experimental modal testing, it is recommended to use weighting windows to remove the noise in both the force and response signals, respectively. By applying a rectangular transient window, the noise outside the window length is set to zero. Hence, it is important to choose the length of the force window so that the entire excitation signal is included. For the reasons discussed in [13], the best form of window to select is with unity amplitude for the duration of the impulse and a cosine taper, with a duration of  $1/16$  of the sampling time, from unity to zero as shown in Figure 3-32.

On the other hand, the noise in the response signal generally occurs when the record length is shorter than the decay time. This is typical when testing lightly damped structures. Indeed, the truncation in time signal will be seen in the measurement as leakage in frequency (leakage error) as shown in Figure 3-33. The leakage error can be reduced by weighting the response signal with an exponential window as shown in Figure 3-33. Hence, leakage due to truncation is avoided,

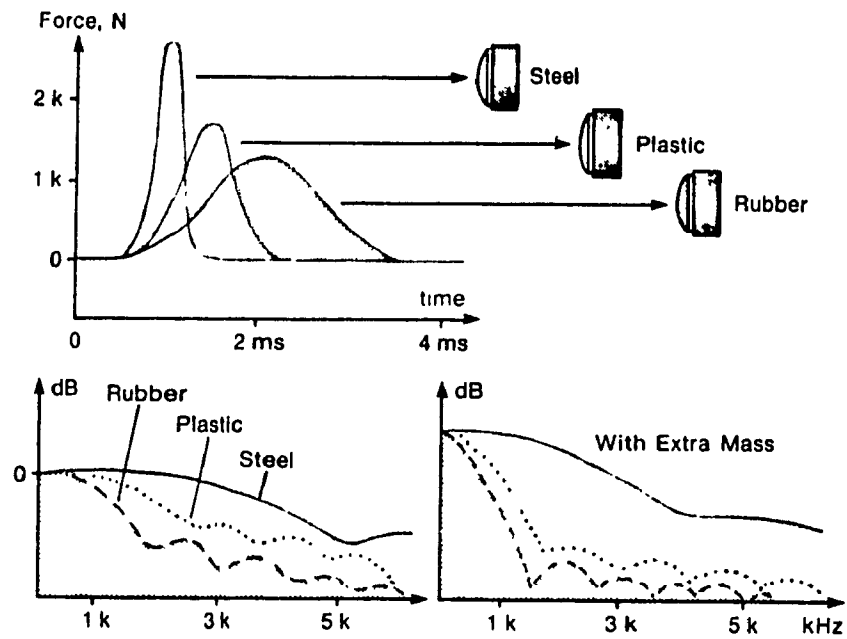


Figure 3-31: Effects of Different Impact Hammer Configurations [5]

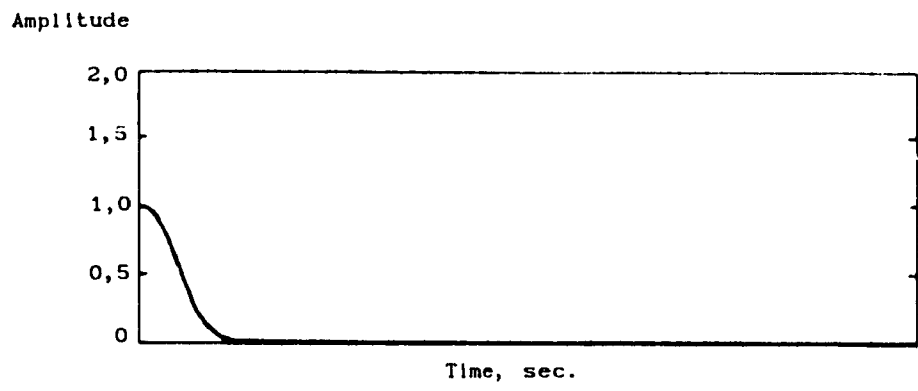


Figure 3-32: Cosine Taper Force Window [10]

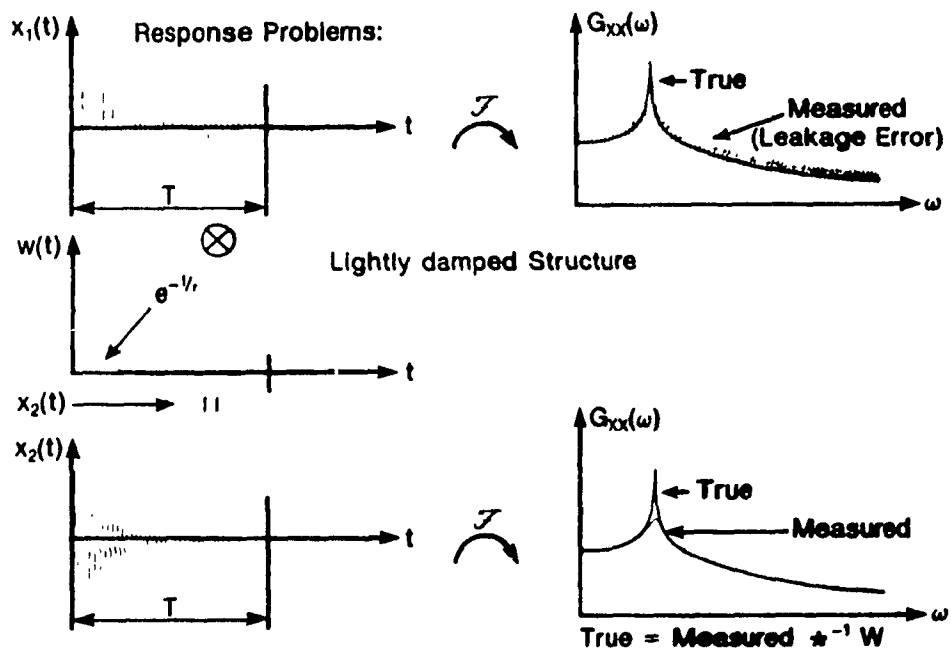


Figure 3-33: Window for Response from Impact [5]

but the apparent damping would be too high in comparison to the existing damping of the structure and thus estimated damping value would have to be corrected as discussed in Chapter 4, at the end of Section 4-2-3.

In the case of heavily damped structures, the record length is generally much longer than the decay time, and the measurement will be contaminated by noise (bias error) as shown in Figure 3-33. This can be detected by a poor signal-to-noise ratio. Hence, an exponential window would remove the noise from the signal. Since, the decay of the response signal is much faster than the weighting function, there is no need to correct the measured damping.

### 3-16 Conclusion

In this chapter, rules of thumb and practical aspects of mechanical mobility measurement techniques are presented. Measurement hardware, FRF estimators, quality of measured data, errors relating to signal processing, non-linearities in structures, response transducer system, and excitation waveforms are discussed in details.



**CHAPTER 4**

**EXPERIMENTAL MODAL TESTING: CASE STUDIES**

## CHAPTER 4

### EXPERIMENTAL MODAL TESTING: CASE STUDIES

#### **4-1 General**

In the previous two chapters, the theoretical aspects of modal testing and the procedures for obtaining FRF (Frequency Response Function) measurements are discussed. Although a good knowledge of all materials presented in the previous two chapters are a prerequisite to understand the experimental modal testing method, a good and an extensive hands-on experience is essential to properly carry-out the modal testing.

In this chapter, step-by-step process involved in carrying out an experimental modal testing, using a computer-aided modal analysis software, is presented by illustrating two case studies: a small and lightweight and three large vehicle structures.

Modal 3.0 SE software developed by Structural Measurement Systems Inc. (SMS), is utilized as the computer-aided modal analysis software to characterize the structures, to accept the FRF measurements from the FFT analyzer, to process the measured data, to estimate the

modal parameters, and to display and animate the mode shapes.

The lightweight structure studied is a snowmobile frame as shown in Figure 4-1. The structure consists of welded steel tubes with straight and curved geometry. Some areas are reinforced using thin steel plates. The structure weight approximately 20 kg and its overall dimensions are 1,0 m long by 0,6 m wide by 0,4 m high.

The large vehicle structures studied are three rail-wagons with some geometrical differences and are shown in Figures 4-2 to 4-4. All three wagons are constructed with stainless steel beams covered with corrugated stainless steel skin. The tare weight of these wagons is approximately 60 000 kg with a maximum payload capacity of 30 000 kg. The overall dimensions of the wagons are: 26,0 m in length, 5,5 m in height, 4,1 m in width.

#### **4-2 Case I: Modal Testing of the Snowmobile Frame Structure**

The objective of this test is to obtain a mathematical description of its dynamic behavior using computer-aided modal analysis software. The mathematical description consists of estimating its basic modal parameters (modal frequency, modal damping, and mode shape) in the frequency range of interest: 0 to 100 Hz.

Soft Elastic String Attached  
to the Ceiling (4 Places)

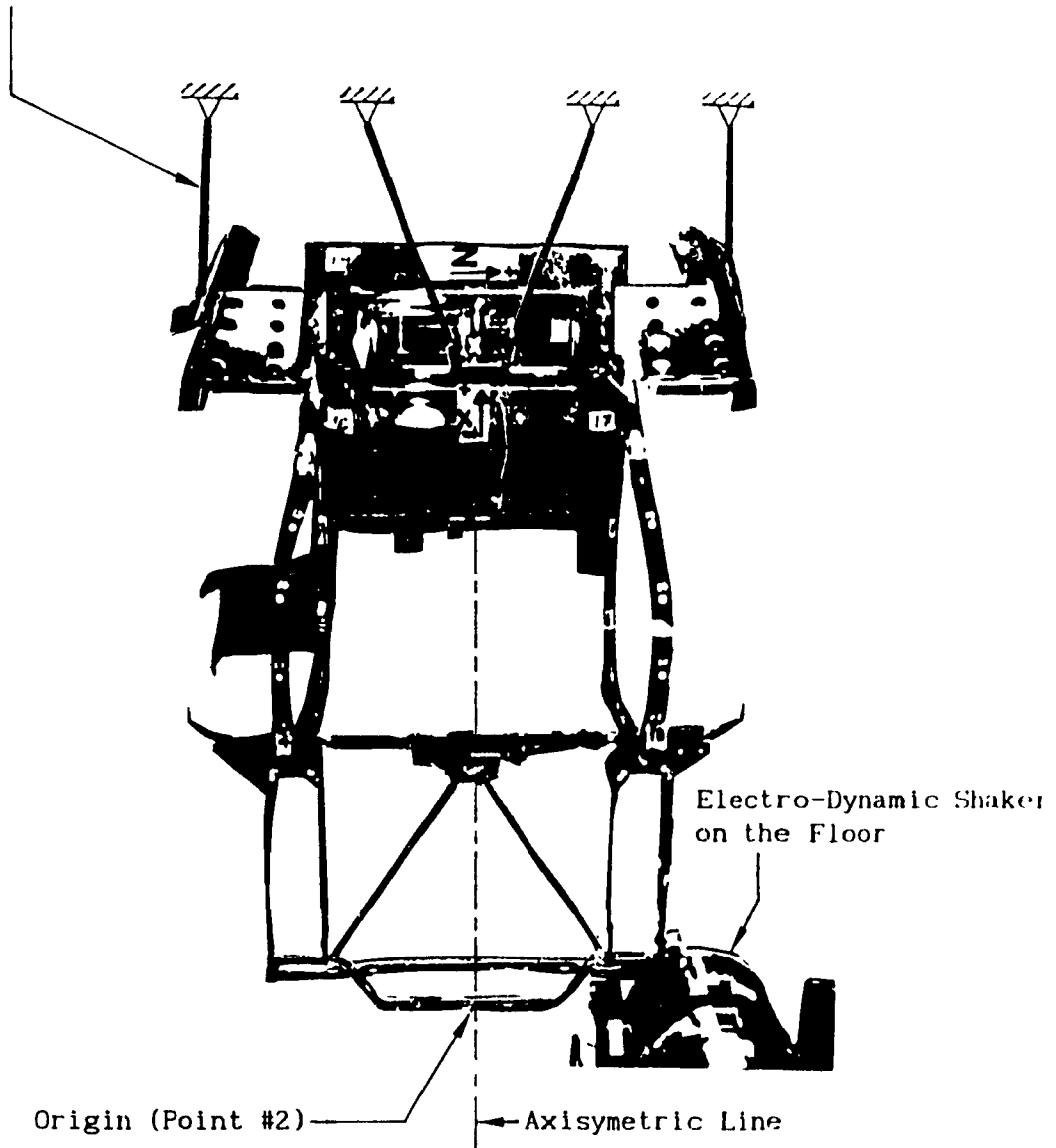


Figure 4-1: Pictorial View of the Snowmobile Frame Structure

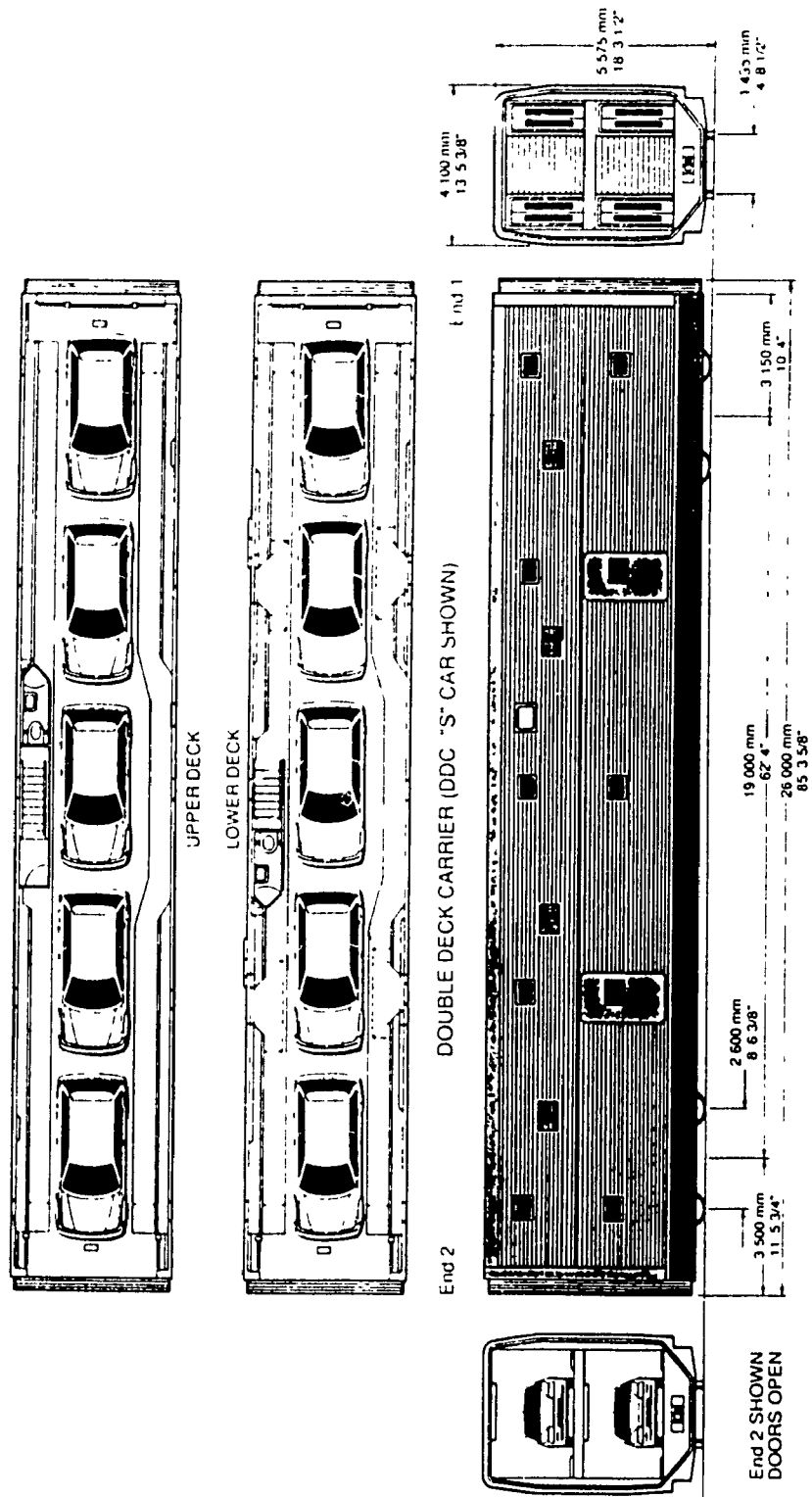


Figure 4-2: First Large Vehicle Structure [14]

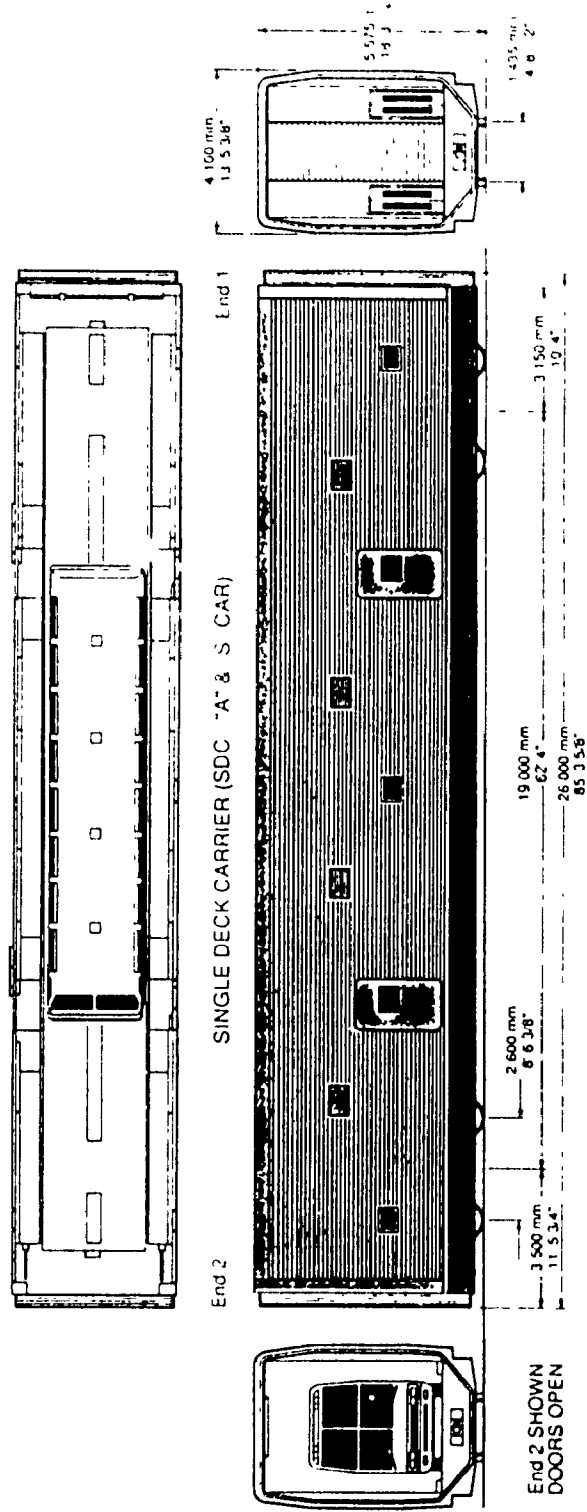


Figure 4-3: Second Large Vehicle Structure [14]

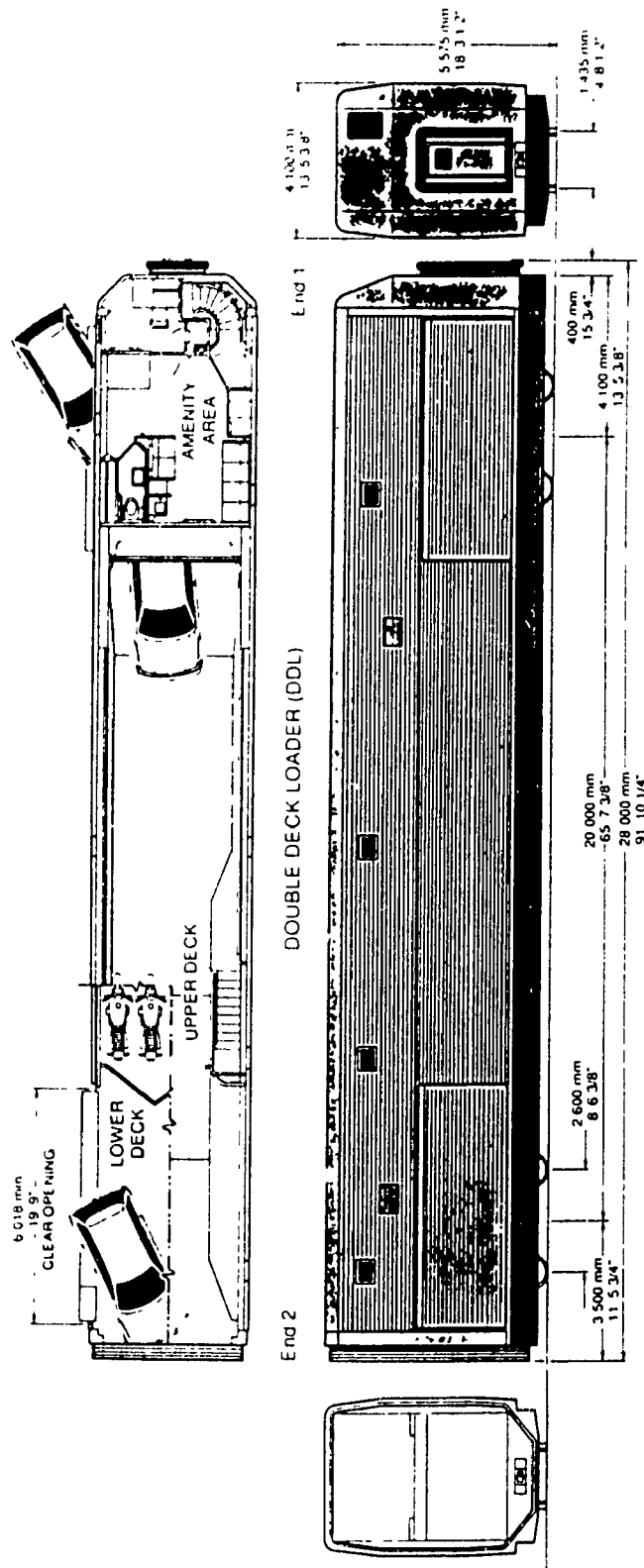


Figure 4-4: Third Large Vehicle Structure [14]

To carry-out this modal test, there are basically four steps involved in the measurement and data analysis procedure and they are examined in details in this section. These steps are :

For measurement

- Step 1 - Setting up the modal test.
- Step 2 - Making the measurements.

For data analysis

- Step 3 - Estimating the modal parameters by curve-fitting.
- Step 4 - Documenting the test results.

#### **4-2-1 Step 1 - Setting Up the Modal Test**

Step 1 can be divided into eight phases and are discussed in detail in Sections 4-2-1-1 to 4-2-1-8.

##### **4-2-1-1 Choosing the Degrees of Freedom (DOF) and Laying Out the Test Points onto the Structure**

In theory, the motion of a free point can be described by



three translations and three rotations for a total of six DOFs. However, in practice rotational DOFs are difficult to measure due to the absence of suitable rotational-transducers but translational DOFs are usually sufficient to describe the motion of a point.

The selection of the test points and the directions that are to be tested or measured depend heavily on the purpose of the experiment. If a test simply consists of estimating the resonances of a structure for validating an analytical model, or predicting the amount of additional damping to be applied (e.g. by spraying) on the structure so as to obtain the desired critical damping, only a few DOFs are required. Also, when troubleshooting a vibration, noise or failure problem, perhaps only a few measurements in the vicinity of the problem area is required.

On the other hand, if a complete mathematical description of the vibrating behavior of the structure (modal model) is sought for a qualitative validation of a Finite Element Model (FEM), then sufficient test points must be used to describe all the mode shapes of the structure within a frequency band of interest. For most practical structures, a set of regularly distributed test points in one or two directions is adequate. If a quantitative comparison of measured (experimental) and predicted (analytical) mode shapes is desired, then the structure should be discretized using the same coordinates used in the theoretical model.

When the experimental modal model is used to carry-out computer analysis for calculating response, and modification and verification simulations, the minimum FRF measurements required is at least one row or one column of the FRF matrix. A column FRF measurement is measured when the exciter is always exciting at the same point (point p) and the responses are measured at all the other test points layed-out on the structure including the excitation point.

It was decided that 25 points are sufficient to describe the motion of the snowmobile structure. These were clearly marked and numbered on the structure using masking tape. Cartesian coordinate system was used to measure the coordinates of all the test points. The origin of the coordinate system was located on an axisymmetric point (point # 2 in Figure 4-1) to facilitate the measurement of the coordinates on the structure. The measured coordinates are listed in Table 4-1. Each line of this table identifies a point on the structure by its point number and its coordinates on the X, Y and Z axes. COORD 1, COORD2 and COORD3 identify the point location on the X-axis, Y-axis and Z-axis respectively. Once this was done, the structure was formed in the software (CRT display) by connecting the points by straight line segments as in FEM where the nodes are connected by elements. Table 4-2 lists the display sequences and Figure 4-5 displays the schematic three-dimensional model of the discretized structure.

Table 4-1: Coordinates of the Test Points (Snowmobile Frame)

POINT	COORD #1	COORD #2	COORD #3
1.	.050	-.055	.320
2.	0.000	0.000	0.000
3.	.050	-.055	-.320
4.	.470	.100	-.280
5.	.430	-.110	-.255
6.	.580	-.200	-.240
7.	.730	-.230	-.245
8.	1.100	-.310	-.240
9.	.890	.090	-.250
10.	.470	.100	.280
11.	.430	-.110	.255
12.	.580	-.200	.240
13.	.730	-.230	.245
14.	1.100	-.310	.240
15.	.890	.090	.250
16.	1.200	-.080	.215
17.	.930	-.080	.215
18.	.930	-.080	-.215
19.	1.200	-.080	-.215
20.	.080	-.055	.225
21.	.080	-.055	-.225
22.	.370	-.175	0.000
23.	.740	-.250	0.000
24.	1.200	-.080	0.000
25.	.930	-.080	0.000

Table 4-2: Connectivity of the Test Points (Snowmobile Frame)

\*\*\* DISPLAY SEQUENCE TABLE \*\*\*

	START POINT	END POINT
	-----	-----
1.	-3	9
2.	4	
3.	-1	
4.	10	15
5.	10	
6.	-11	
7.	22	
8.	5	
9.	-1	
10.	20	
11.	2	
12.	21	
13.	3	
14.	-22	
15.	20	
16.	-22	21
17.	-14	
18.	16	17
19.	25	
20.	18	19
21.	8	
22.	-19	
23.	24	
24.	15	
25.	-17	
26.	13	
27.	-18	
28.	7	
29.	-23	
30.	25	
31.	24	
32.	-7	
33.	23	
34.	13	

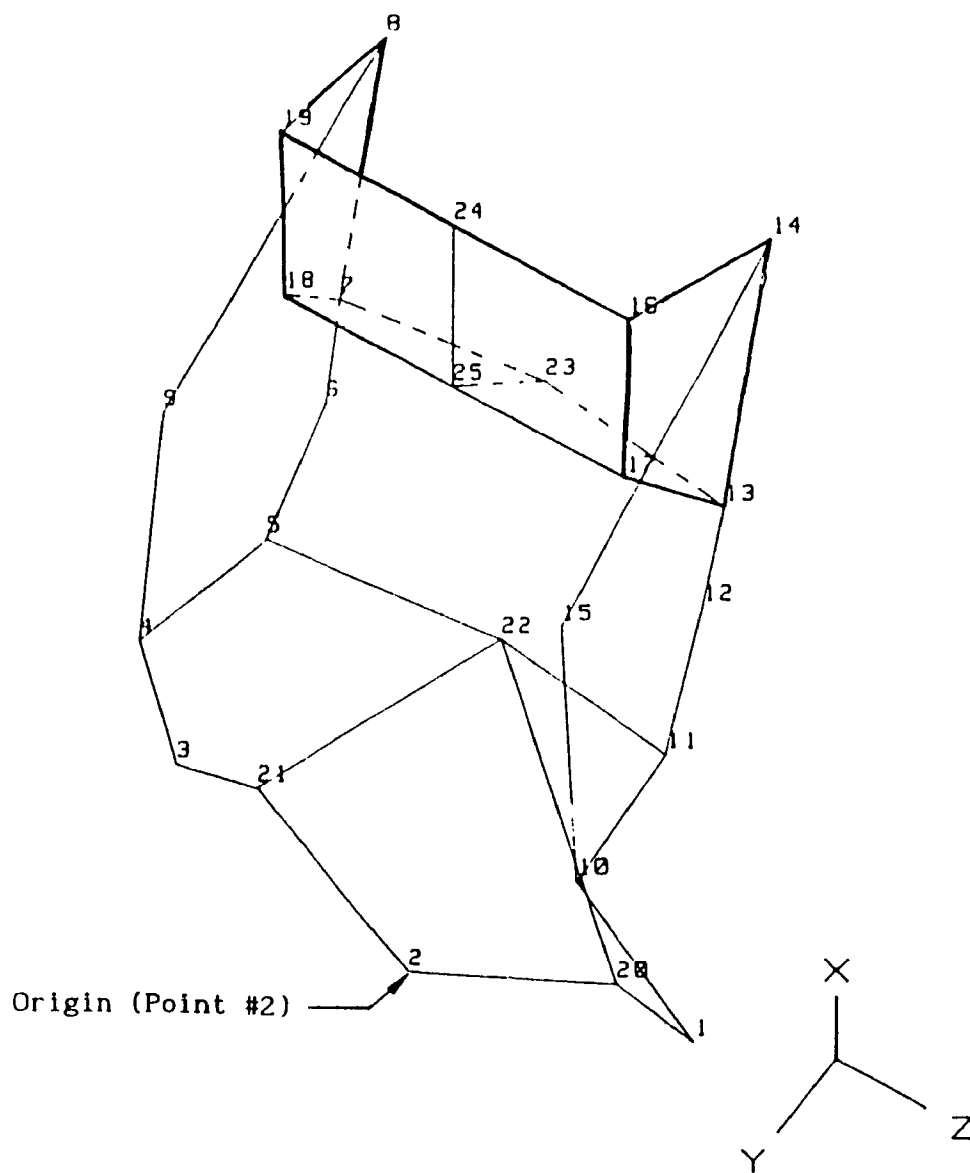


Figure 4-5: Schematic 3-D Model of the Snowmobile Frame Structure

The number of DOFs (test points, and directions) to measure on the structure is a matter of engineering judgement. For the snowmobile frame, simple mode shapes (longitudinal twist, vertical bending and perhaps lateral bending) are expected in the frequency range of interest (0 to 100 Hz). Therefore, these mode shapes can be adequately described by two translations at each point. Hence, the total DOFs were limited to fifty (25 points times 2 directions), measured in the vertical direction (Y-axis) and lateral direction (Z-axis) at all the twenty five points layed out on the structure.

#### 4-2-1-2 Preparation of the Test Structure

The modal test results are directly influenced by the way in which the test structure is prepared. A structure can be prepared in a "free-free" condition or "grounded" condition. It is always preferable to test a structure in a free-free condition due to the fact that the modal test results involve more degrees of freedom, and hence at a later time, some of the DOFs can be deleted to estimate the modal parameters for the "grounded" condition.

Truly free-free condition cannot be achieved but can be approximated by mounting the structure with soft restraints. In this case, the structure will exhibit rigid body modes which are dependent on the mass/inertia property of the structure and the stiffness of the

supports. Hence, the natural frequencies of the rigid body modes will no longer be 0 Hz. Ewins [2], suggests that to minimize the influence of the rigid body modes on the flexural ones, the highest rigid body mode frequency is less than 10-20% of that for the lowest (fundamental) flexural mode.

In the case of the snowmobile frame, the structure was hung from the ceiling by soft elastic strings along its longitudinal axis as shown in Figure 4-1.. It should be noted that this hanging direction is perpendicular to the primary excitation direction, and thus it ensures minimum interference on the flexural modes.

#### 4-2-1-3 Choosing the Excitation Technique

Basically, there are two types of testing techniques which can be performed to carry-out a modal test: hammer testing and shaker testing. The first of these is the simplest and fastest type for obtaining good modal estimates and consists of attaching one response transducer (usually an accelerometer) at one of the points layed-out on the structure along a given direction and then impacting the structure at all the test points and in all directions where the mode shape motion is desired. Hence, one row of the FRF measurement matrix is measured through this approach. It is also possible to measure one column instead of one row of the FRF measurement matrix by exciting always at

the same point and measuring the responses at all points along the desired directions. This second method has no advantage and can only introduce more errors into the modal data and certainly slow down the experiment. However, there are certain types of structure for which hammer testing is ill-suited and shaker testing has to be used.

Generally, shaker testing is preferred because the excitation level and frequency content can be controlled more accurately and thus obtaining better modal estimates. The shaker is normally attached somewhere to the structure, with a load-cell inserted between the shaker and the structure to measure the force input. An accelerometer is used to measure the responses at all the points along the selected directions. Pseudo-random type waveform excitation is the most popular one utilized to drive a shaker since it can cover a wide frequency range and average-out leakage errors as discussed in Chapter 3.

A Brüel & Kjaer electrodynamic exciter body model 4801 with an exciter head model 4812 as shown in Figure 4-6 was utilized to carry out the modal testing on the snowmobile structure. A Pseudo-random waveform generated using a Brüel & Kjaer FFT analyzer model 2032 was used, with power amplification to drive the shaker.



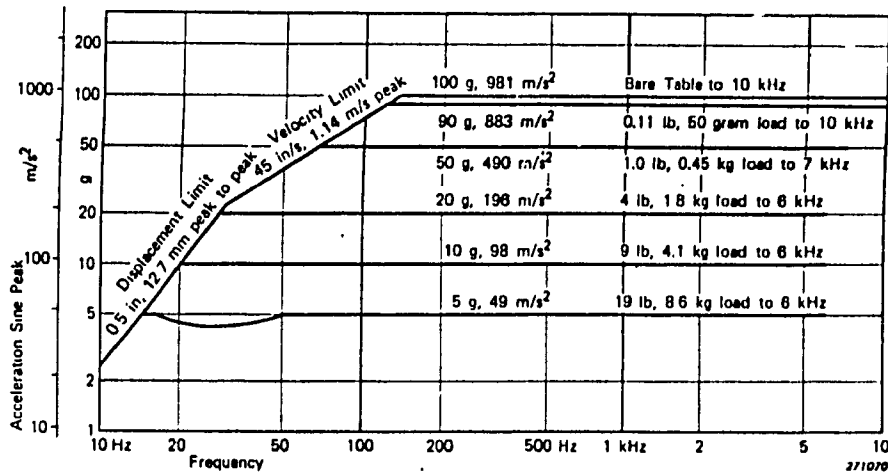
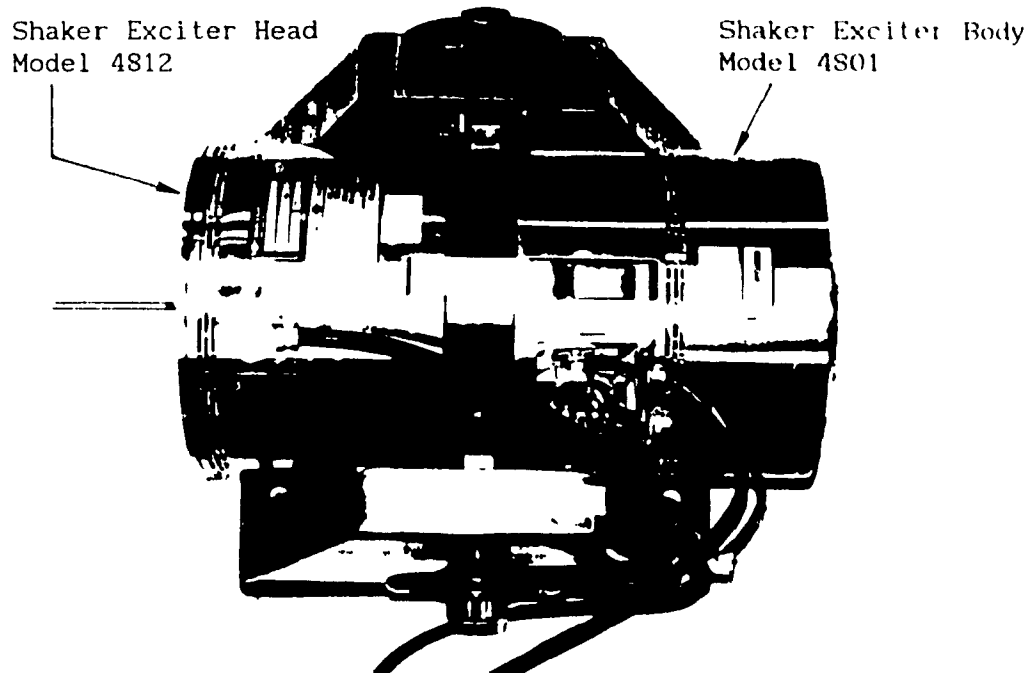


Figure 4-6: Bruel & Kjaer Electrodynamic Shaker with its Sine Performance Chart [15]; Head Type 4812 and Exciter Body Type 4801

#### 4-2-1-4 Setting Up the FFT Analyzer

A dual channel FFT analyzer model 2032, manufactured by Brüel & Kjaer, was utilized to record the input and output signals and to compute several functions such as the inertance-FRF, the Coherence function, the auto-spectra, etc.. The analyzer was configured as shown in Table 4-3. The measurement mode was set to "Dual Spectrum Averaging" for this case study. Figure 4-7 shows a simplified block diagram for this measurement mode. The trigger mode was set to "Generator" so that the trigger input is synchronous with the pseudo-random noise sequence as discussed in chapter 3. The delay between trigger and start of channel A was set to zero milli-second. Linear averaging was set with ten averages per measurement (estimates where satisfactorily smooth after 10 averages). The frequency span was set to 200Hz with center frequency set to baseband, i.e. from 0 to 200 Hz, which corresponds to twice the frequency band of interest. The weighting was set to "rectangular" as recommended when using pseudo-random excitation. Channel A (input force) and channel B (output acceleration) were set in engineering units to 2,25mV/N and 10,3 mV/m/s<sup>2</sup>, which correspond to the sensitivities of the force and response transducers after conditioning.

Table 4-3: FFT Analyzer Configuration

SETUP U12				
MEASUREMENT	DUHL SPECTRUM AVEFAGING			
TRIGGER	GENERATOR			
DELAY	TRIG→A 0 0ms	CH A→B	0 0ms	
AVERAGING	LIN 10			
FREQ SFAM	200Mz	ΔF	250mhz	
CENTER FREQ	BASEBAND		ΔT	1 95ms
WEIGHTING	RECTANGULAR			
CH A	800mv			
CH B	4V	DC-DIRECT	FILT BOTH	
GENERATOR	PSEUDO RANDOM NOISE	DC-DIRECT	FILT BOTH	
			2 25mv/N	
			10 3mv/m/s <sup>2</sup>	

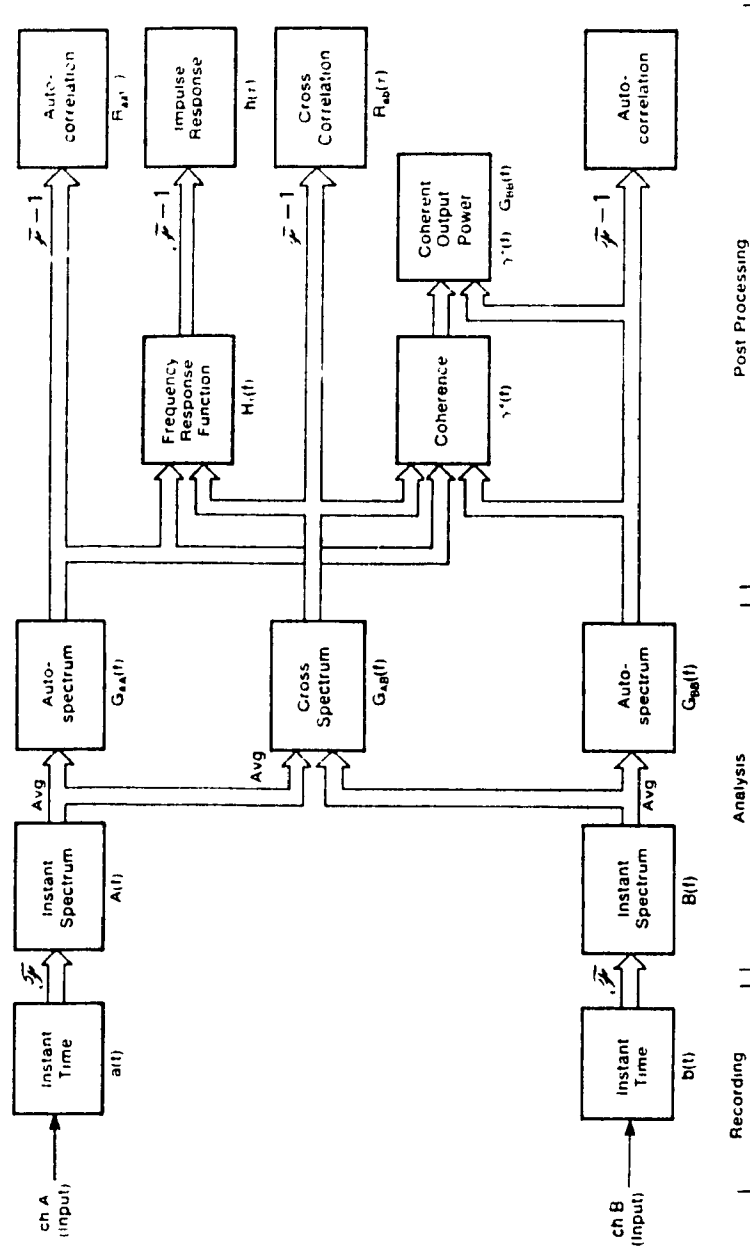


Figure 4-7: Simplified Block Diagram for Dual Spectrum Averaging Mode of the Bruel & Kjaer FFT Analyzer, Model 2032. [6]

#### 4-2-1-5 Calibration of the Force Response Transducer Combination

It is recommended, before carrying-out any experimental testing, to calibrate the equipment or measurement devices which are used to collect the data in order to verify their integrity, and if required, to measure calibrated data. The procedure is strongly recommended if the modal model will be used for carrying out computer analysis.

There are two types of calibration that can be conducted before carrying out a modal test. The first type consists of calibrating the individual transducers (force and response transducers) to verify that their sensitivities are in the same range as those specified by the manufacturer(s), and also to verify that they are behaving linearly with amplitudes in the frequency band of interest without any phase shift. The most commonly used transducers for modal testing are accelerometers and load-cells.

The second type consists of calibrating the force/response transducer combination, to detect any errors in the cables, connectors, conditioner and analyzer, to insure that all gains, polarity and attenuator settings in the system are correct, and to verify that the pair of transducers being used are matched in the frequency band of interest.

A piezo-electric accelerometer manufactured by PCB Piezotronic, model # 308B  $\{S_A = 10,3 \text{ mV}/(\text{m}/\text{s}^2)\}$  was used to measure the responses (accelerations) along the Y- and Z-directions at the 25 selected measurement locations.

A Kistler force transducer model # 912  $\{S_F = 2,25 \text{ mV}/\text{N}\}$  was used to measure the input force signal at the driven point.

An easiest way to calibrate the force/response transducer combination was to measure the inertance-FRF using a known mass as shown in Figures 4-8 and 4-9. From Newton's second law:

$$\text{Force} = \text{Mass} \times \text{Acceleration} \quad (4-1)$$

and the inertance-FRF is defined as:

$$\text{Inertance } (j\omega) = \frac{\text{Acceleration } (j\omega)}{\text{Force } (j\omega)} = \frac{1}{\text{Mass}}$$

Thus, for any frequency, the amplitude of the inertance-FRF should be a constant and equal to  $1/\text{Mass}$  with a phase of 0 degrees. The amplitude of the inverse measured inertance-FRF in Figure 4-10 is 2,32 kg, which corresponds to the total mass (mass of the accelerometer + mass of the calibration block) during the calibration-testing. The Coherence function and the signal-to-noise ratio were also computed to check the quality of the measurement and they are shown in Figures 4-11 and 4-12

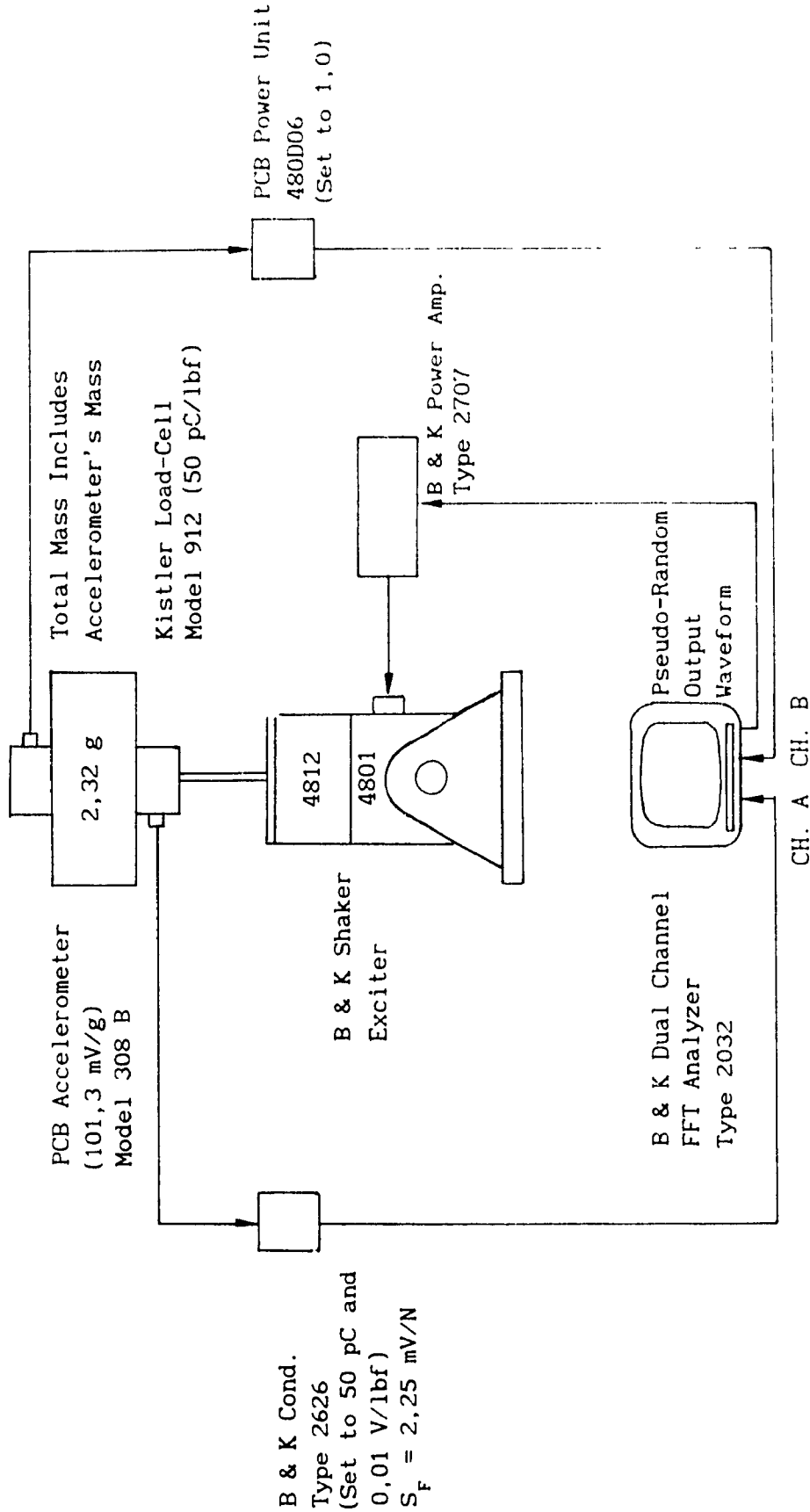


Figure 4-S: Schematic Set-Up of the Force Transducer-Accelerometer System Calibration for Shaker Excitation. Sensitivities  $S_A$  and  $S_F$  are Calculated as Follow:

$$S_A = (101,3 \text{ mV/g}) \cdot (1) \cdot (g/9,81 \text{ m/s}^2) = 10,3 \text{ mV/m/s}^2$$

$$S_F = (0,01 \text{ V/lbf}) \cdot (1 \text{ lbf} = 4,45 \text{ N}) = 2,25 \text{ mV/N}$$

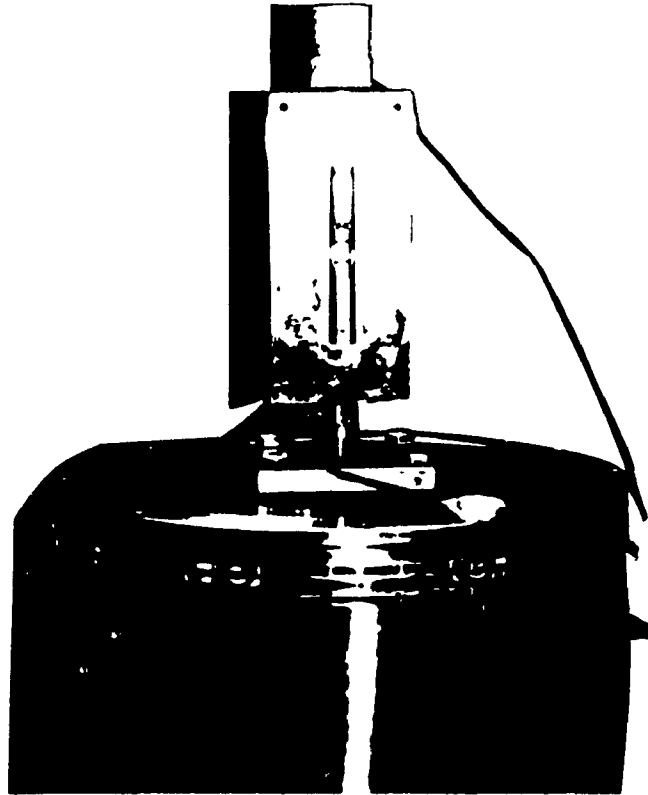


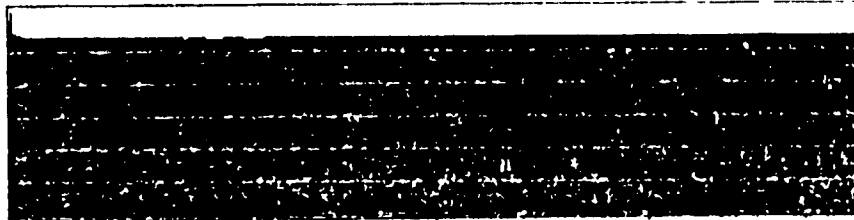
Figure 4-9: Pictorial View of the Force Transducer-Accelerometer for System Calibration



```

W11 1/FREQ RESP HI MAG          MAIN 1 2 32
Y 9 31 30dB                    X 25.00000
X 0 00Hz + 200Hz LIN          L J
                                L J

```



SETUP W12

```

MEASUREMENT    UUHL SPECTRUM AVERAGING
TRIGGER        GENERATOR
DELAY          TRIG→A 0.0ms          CH A+B 0.0ms
AVERAGING      LIN 10

FREQ SPAN      200Hz    ΔF 250mHz    AT 1.45ms
CENTER FREQ    BASEBAND
WEIGHTING      RECTANGULAR

CH A           800mV    UC-DIRECT  FILT BOTH    2.15mV/Hz
CH B           4V      UC-DIRECT  FILT BOTH    10.3mV/Hz
GENERATOR      PSEUDO-RANDOM NOISE

```

--TRIGGERED--

Figure 4-10: Inversed Measured Inertance-FRF of System shown in Figure 4-9

```
W11 COHERENCE          STORED MAIN Y 1 00  
Y 1 20                X 25 30HZ  
X 0 00HZ + 200HZ     LIN  
SETUP S12 *M 10
```



Figure 4-11: Coherence Function of System shown in Figure 4-9

```
W11 SIG/NOISE RATIO          STORED      MAIN 7 59 31B  
V 21.548 12.43  
X 0.00HZ + 200HZ          LIN  
SETUP S12 *H 10
```

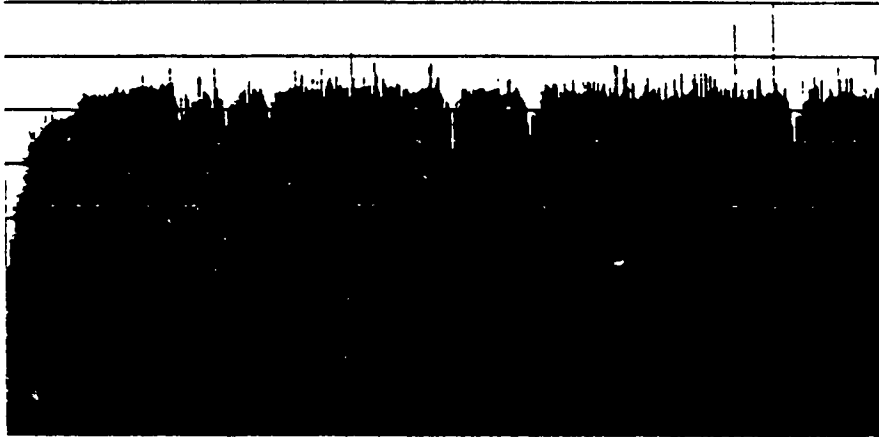


Figure 4-12: Signal-To-Noise Ratio of the System shown in Figure 4-9

respectively. The Coherence function shows a perfect value of 1 and the signal-to-noise ratio shows an average value of 60 dB ( $\gg$  40dB). Hence, the input and output signals are very coherent with low levels of noise.

Similarly, if hammer testing would have been utilized instead of shaker testing, the calibration of the force/response transducer combination could be carried-out by measuring the inertance-FRF using a pendulum system as shown in Figure 4-13.

The measured inertance-FRF can be made into a non-dimensional form by multiplying it by the total mass utilized to calibrate the force/response transducer combination. This was done in the FFT analyzer by dividing the response sensitivity (CH.B) by 2,32 kg and is shown in Figure 4-14. The non-dimensional function (the inverse of the function shown in Figure 4-12) was stored on the computer hard disk for compensating for all measured FRF's at the data analysis stage. This function is shown in Figure 4-15. This process is often referred as equalization process.

#### **4-2-1-6 Exciter and Load-Cell Positioning and Connection**

The selection of the exciter location should be chosen so that all the modes in the bandwidth of interest are stimulated. If the

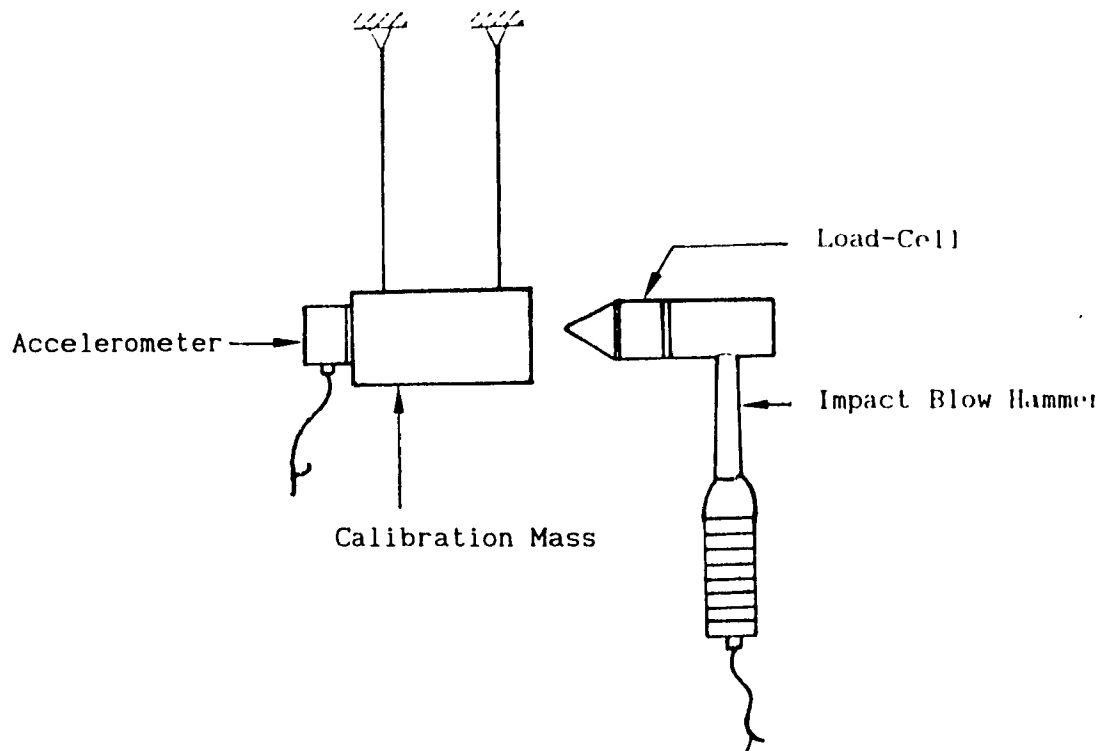
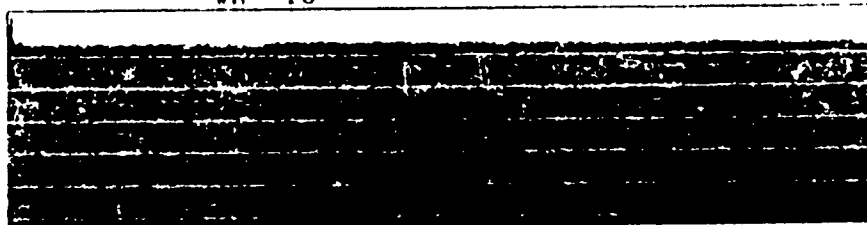


Figure 4-13: Calibration Process for Impact Hammer Testing

#11 1/FREQ RESP HI MAG MAIN Y 998m  
 Y 4 01 30dB X 25 00Hz  
 X 0 00Hz + 200Hz LIN  
 #H 1U



SETUP #12

MEASUREMENT	DUAL SPECTRUM AVERAGING		
TRIGGER	GENERATOR		
DELAY	TRIG→A 0 0ms	CH A→B	0 0ms
AVERAGING	LIN 10		
FREQ SPAN	200Hz	ΔF 250mHz	T 4s
CENTER FREQ	BASEBAND		ΔT 1 35ms
WEIGHTING	RECTANGULAR		
CH A:	300mV + DC-DIRECT	FILT BOTH	2 25mV/V
CH B:	600mV + DC-DIRECT	FILT BOTH	5 33mV/V
GENERATOR	PSEUDO RANDOM NOISE		

Figure 4-14: Inversed Equalization Function

```
M11 FREQ RESP H1 MAG [REDACTED] MAIN Y 1 00  
Y : 00 30dB X 25 00Hz  
K 0 00Hz + 200Hz LIN  
SETUP S12 #A 10
```

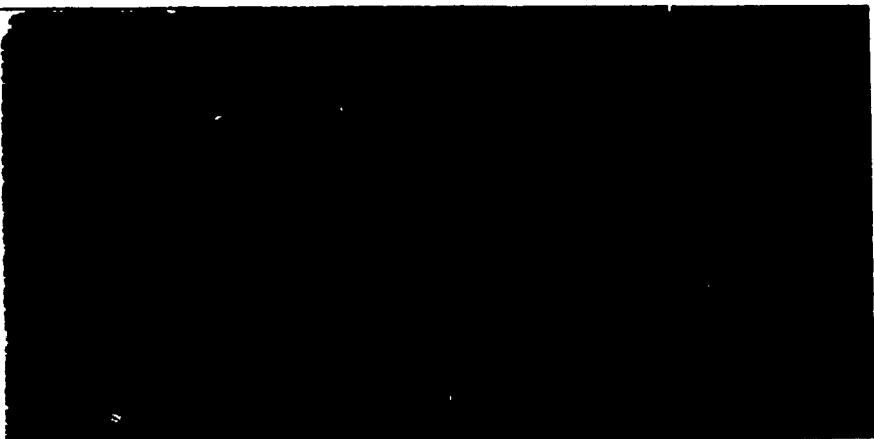


Figure 4-15: Stored Equalization Function

selected location (one of the discretized points) is close to a nodal point, i.e. a node of a particular mode, the corresponding resonance will probably be either difficult to identify or absent from the measured. Generally, the best location for an exciter is at a corner of the structure where both the symmetric and asymmetric modes will exhibit maximum motion.

When simple mode shapes are expected or modal information is available from an analytical model (e.g. FEA) , several good locations can be identified. In this case, the location that should be retained (the optimal location) is the one where the exciter can be easily attached to that point.

It is possible to verify experimentally that the chosen location does not correspond to a nodal point of the structure for the mode shapes of interest. The easiest way to verify it, is to use an impact blow hammer and make a few driving point measurements ( $M_{11}$ ) at other DOFs, i.e. at other points and in different directions, and check if all the resonances identified at those DOFs are seen at the chosen DOF.

Since simple mode shapes were expected in the frequency range of interest for the snowmobile frame (from 0 to 100 Hz), the best location for the exciter was found to be at point # 1 (refer to Figure 4-5) along the Y-direction, i.e. at a corner of the frame. The



Y-direction was chosen as the direction of excitation for two reasons: Maximum motion was expected along that direction for all the expected mode shapes and this direction was convenient for attachment element of shaker to the structure

The load-cell was stud-mounted onto the body frame (through a threaded hole) to measure the input force as close as possible to the structure. The exciter was placed directly on the floor with "Fun Tak" between the floor and the exciter to hold it in place. A 30 cm long, slender push rod was bolted between the load-cell and the exciter head as shown in Figure 4-16.

#### 4-2-1-7 Mounting the Response Transducer (Accelerometer)

An accelerometer described in Section 4-2-1-5 was utilized to measure the vibration at all DOFs. Since, the frequency range of interest was low, "Fun Tak" with elastic rubber was used to hold the accelerometer at the selected points on the structure. Figures 4-17 a and b illustrate pictorially how the accelerometer was mounted for  $H_{1z/-1y}$  and  $H_{-1y/-1y}$  measurements, respectively.

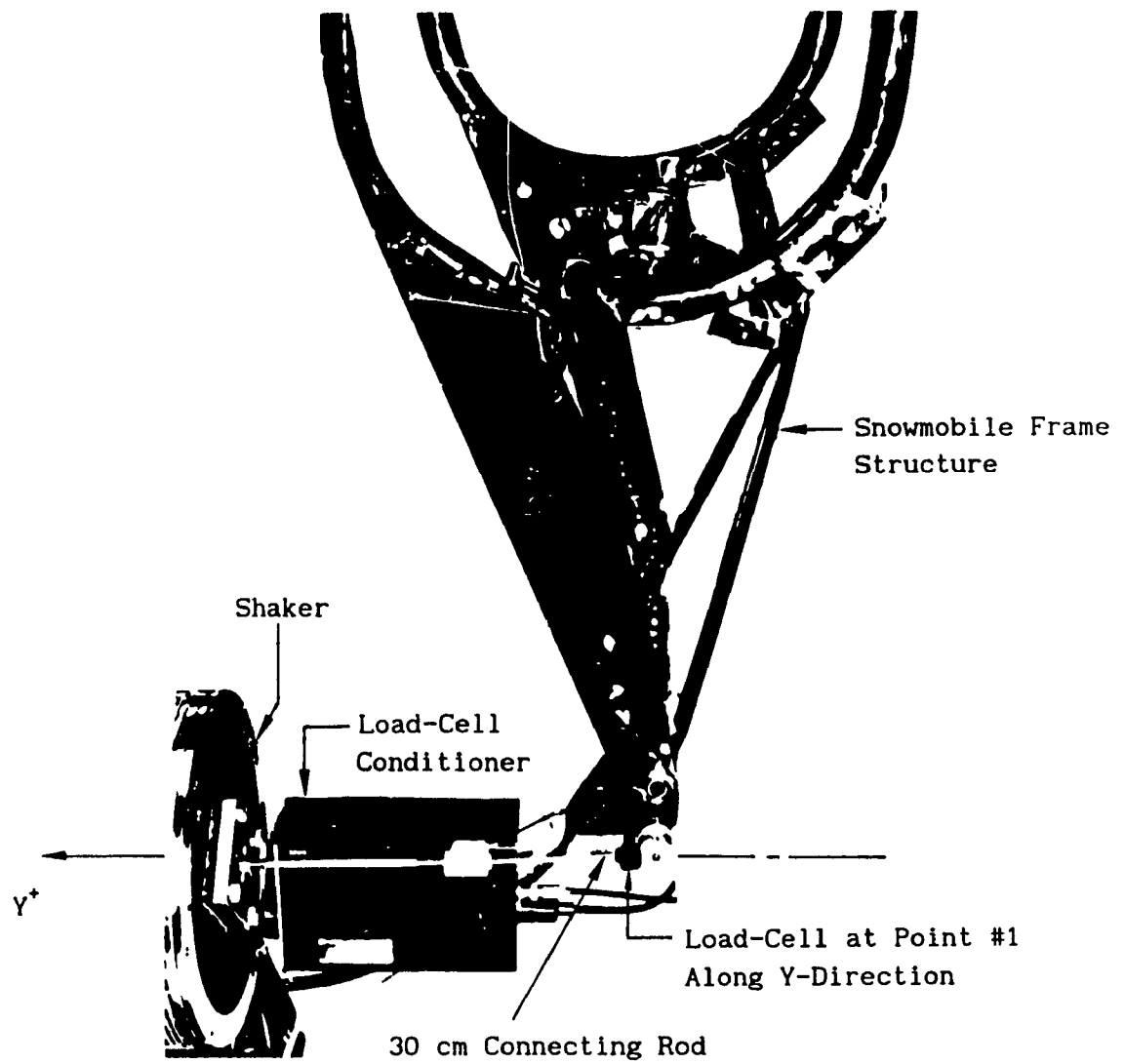


Figure 4-16: Pictorial View of the Shaker and Load-Cell Positioning

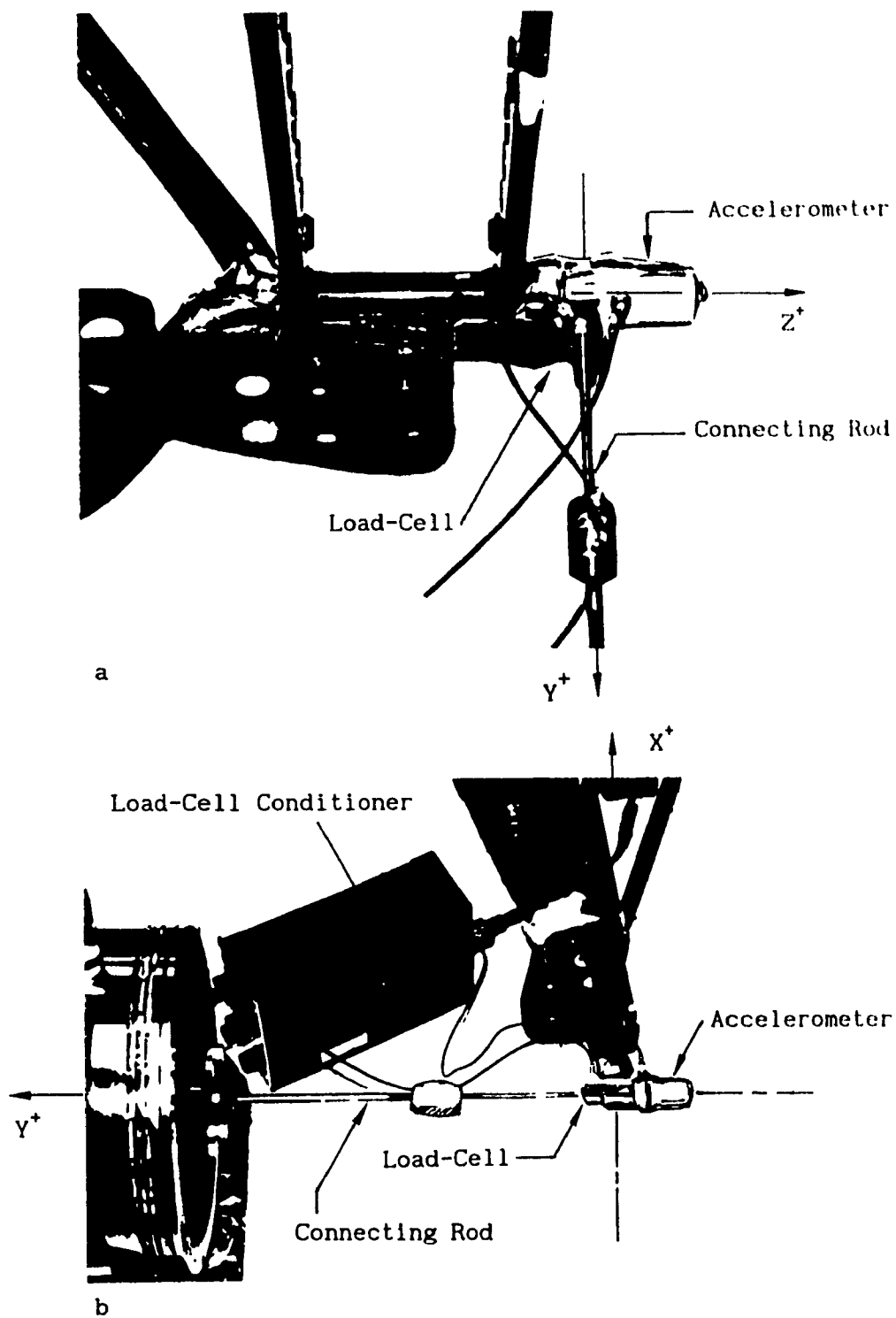


Figure 4-17: Accelerometer Mounting for: a)  $H_{1z/-1y}$  Measurement,  
 b)  $H_{-1y/-1y}$

#### 4-2-1-8 Checking the Measurement Set-Up

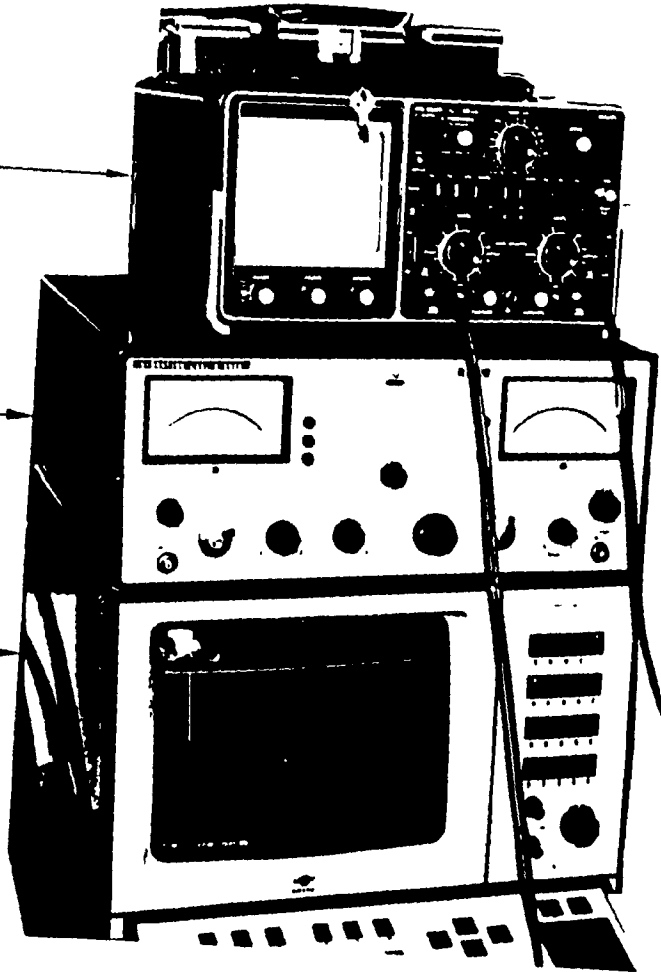
Figures 4-18 a and b show the equipments used to carry-out the modal test on the snowmobile frame structure. At this stage, it is important to verify that the shaker does not change the system significantly. In order to verify that, the structure was first excited at -1Y using an impact blow hammer without the shaker attached. An accelerometer was used to display on an oscilloscope the response at -1Y. From this display, fundamental frequency of vibration was read directly when most of the higher harmonics have died-down. Figure 4-19 shows a picture of the scope taken at that moment. We can see that the fundamental frequency of the frame structure is approximately 41 Hz. Using the modal test set-up, the inertance-FRF was computed for impact hammer testing. The inertance-FRF was measured at the same DOFs using now the shaker with a pseudo-random waveform.

In addition, before taking the complete FRF measurements, several functions were computed for the driving point inertance-FRF measurement. The following functions were observed for each of them. The auto-spectrum of the input force signal shown in Figure 4-20 is a satisfactorily flat force spectrum. The Coherence function and the signal-to-noise ratio, shown in Figure 4.21 a and b are acceptable. The Co-Quad display format of the inertance-FRF is shown in Figure 4-22. It can be observed in the quadrature plot, the magnitude is zero except at the modal frequencies which indicates that the modes would be normal.

Phillips  
Oscilloscope

B & K Power  
Amplifier

B & K FFT  
Analyzer 2032



Computer Hardware (HP3000)  
with SMS Software Modal 3.0 SE

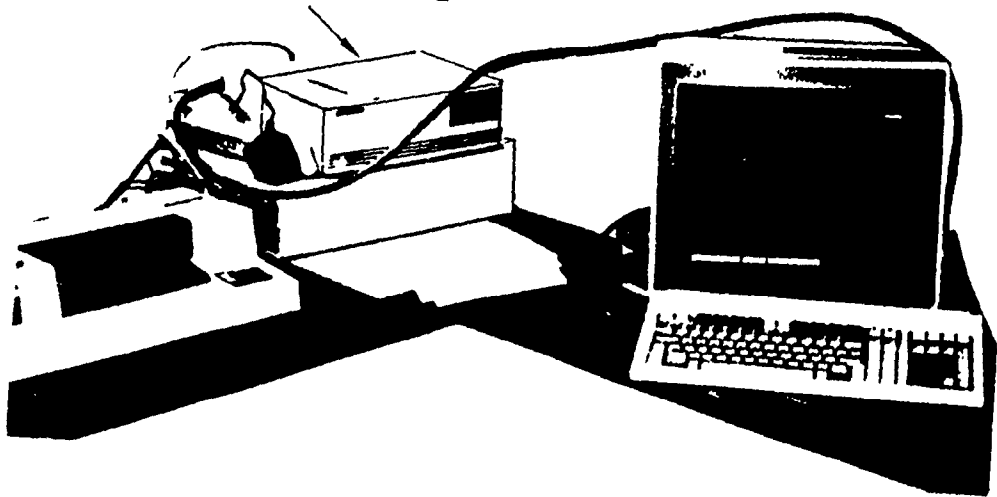


Figure 4-18 a: Equipment Used to Carry-out the Modal Test on the Snowmobile Frame Structure

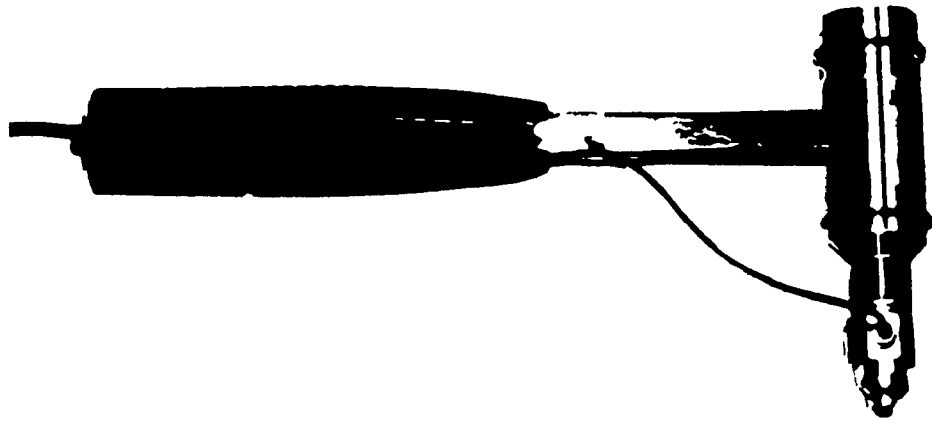


Figure 4-18 b: Impact Blow Hammer Used for Exploratory Testing

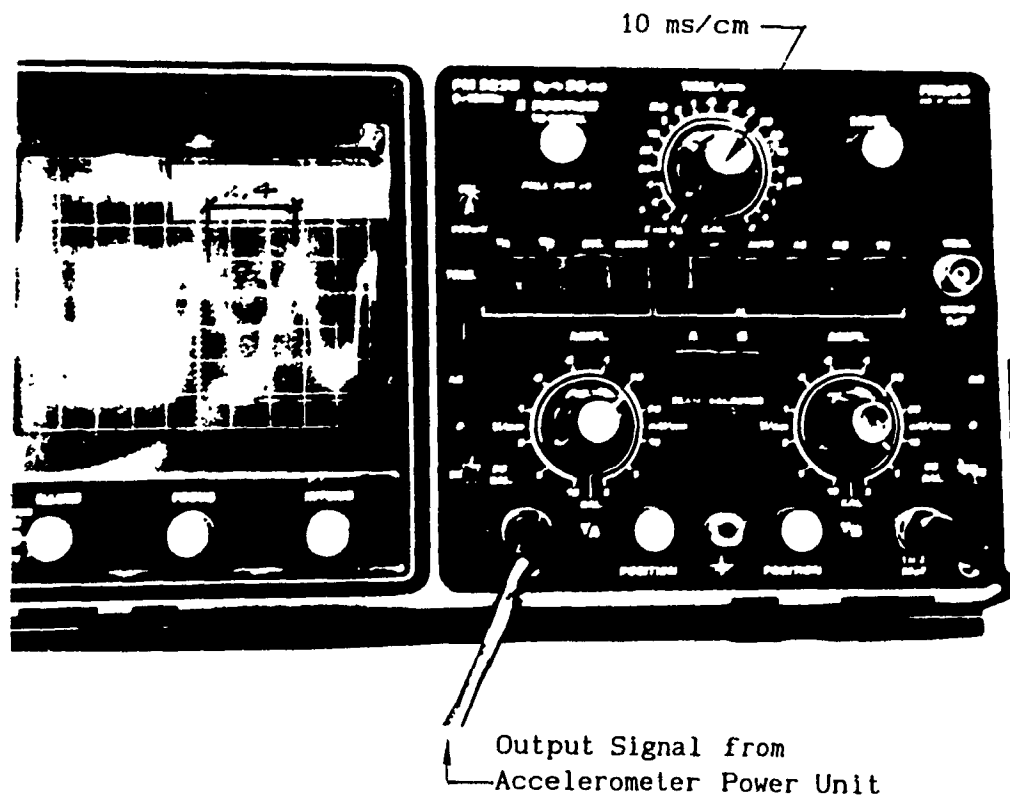
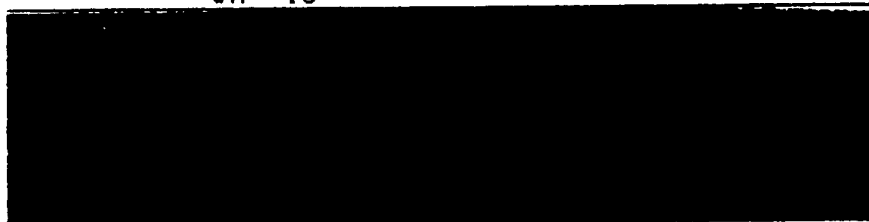


Figure 4-19: Output Signal from the Accelerometer When Most Higher Harmonics Died Down - Frequency Around 41 Hz

```

011 AUTO SPEC CH A [ ] INPUT MAIN Y: 24 1dB
Y 25.7dB / 1.00u RMC 20dB X 41.00Hz
X 0.00Hz + 200Hz LIN
    10

```



SETUP W12

```

MEASUREMENT          DUAL SPECTRUM AVERAGING
TRIGGER              GENERATOR
DELAY:              TRIG→A 0.0ms          CH A→B 0.0ms
AVERAGING           LIN 10
FREQ SPAN           200Hz          ΔF 250mHz          T 4s          ΔT 1.95ms
CENTER FREQ        BASEBAND
WEIGHTING          RECTANGULAR
CH A:              800mV + DC-DIRECT   FILT: BOTH     2.25mV/N
CH B:              4V + DC-DIRECT    FILT: BOTH     10.3mV/m/s²
GENERATOR          PSEUDO RANDOM NOISE

```

--TRIGGERED--

Figure 4-20: Auto-Spectrum of the Input Force Signal



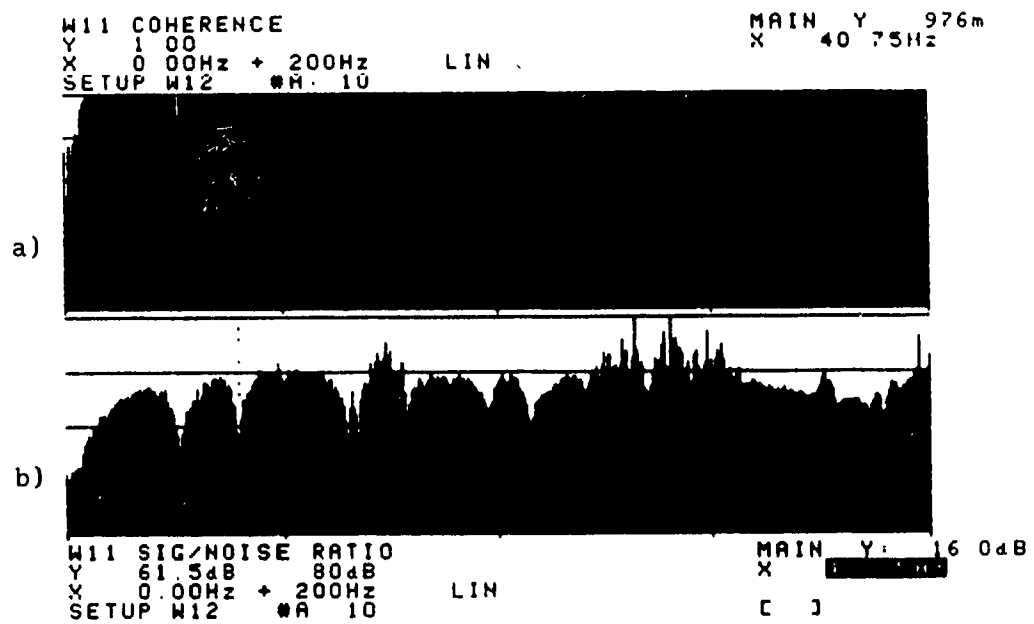


Figure 4-21: Computed Functions at the Driving point: a) Coherence Function, b) Signal-To-Noise Ratio

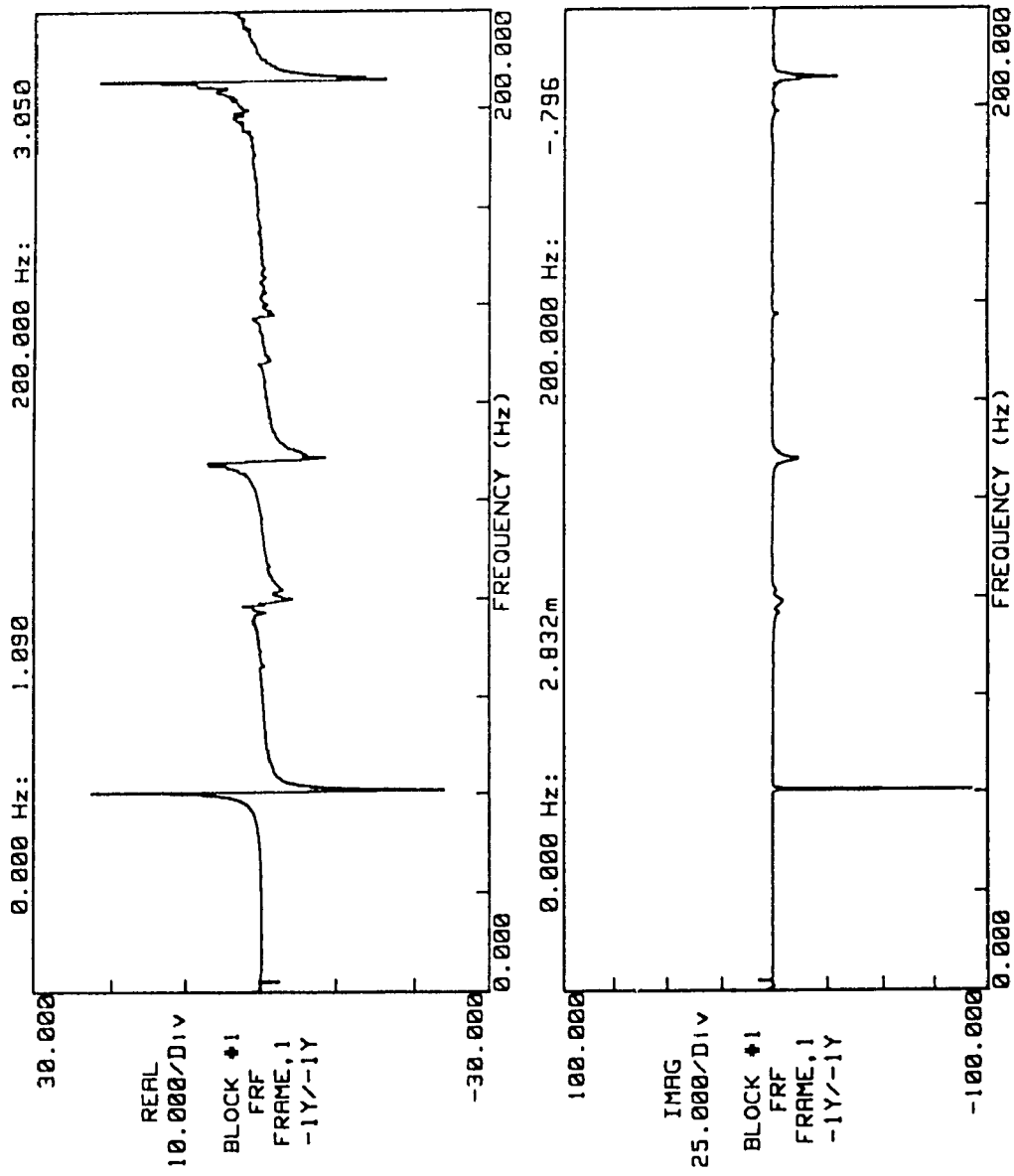


Figure 4-22: Co-Quad Display Format of the Inertance-FRF Measured at the Driving Point

Note that the coincident (in phase response) goes to zero at the quadrature peaks. Finally, the inertance-FRF shown in Figure 4-23 shows anti-resonance peaks between resonances.

Another aspect in the measurement set-up is to verify whether the frequency of the lowest flexural mode (41 Hz) is greater than 5 to 10 times of that for the highest rigid body mode. The highest rigid body mode frequency was identified from Figures 4-22 or 4-23 to be approximately 2 Hz. In order to verify this, the frame was excited at that frequency using a sinusoidal waveform, and found to cause the frame to vibrate in a vertical rigid bounce mode. Hence, the above condition was met.

Finally, other FRF measurements were taken to compare the magnitude of the inertance-FRF along the three axes, and to verify for the reciprocity and symmetricity of the frame structure. For comparing the magnitude, FRF measurements were taken along each axis for two different excitation DOFs (-1Y and -1Z). Figures 4-24 to 4-26 and 4-27 to 4-29 compare the magnitude along one direction with another for the two different excitation DOFs respectively. From the results, it can be concluded that Y is the dominant vibrational axis. The 2<sup>nd</sup> dominant axis can be either Z- or X-axis and it depends on a particular mode.

For checking the reciprocity, four FRF measurements were taken at the following DOFs: -1Y / -3Y, -3Y / -1Y, -1Y / -1Z, and -1Z / -1Y.

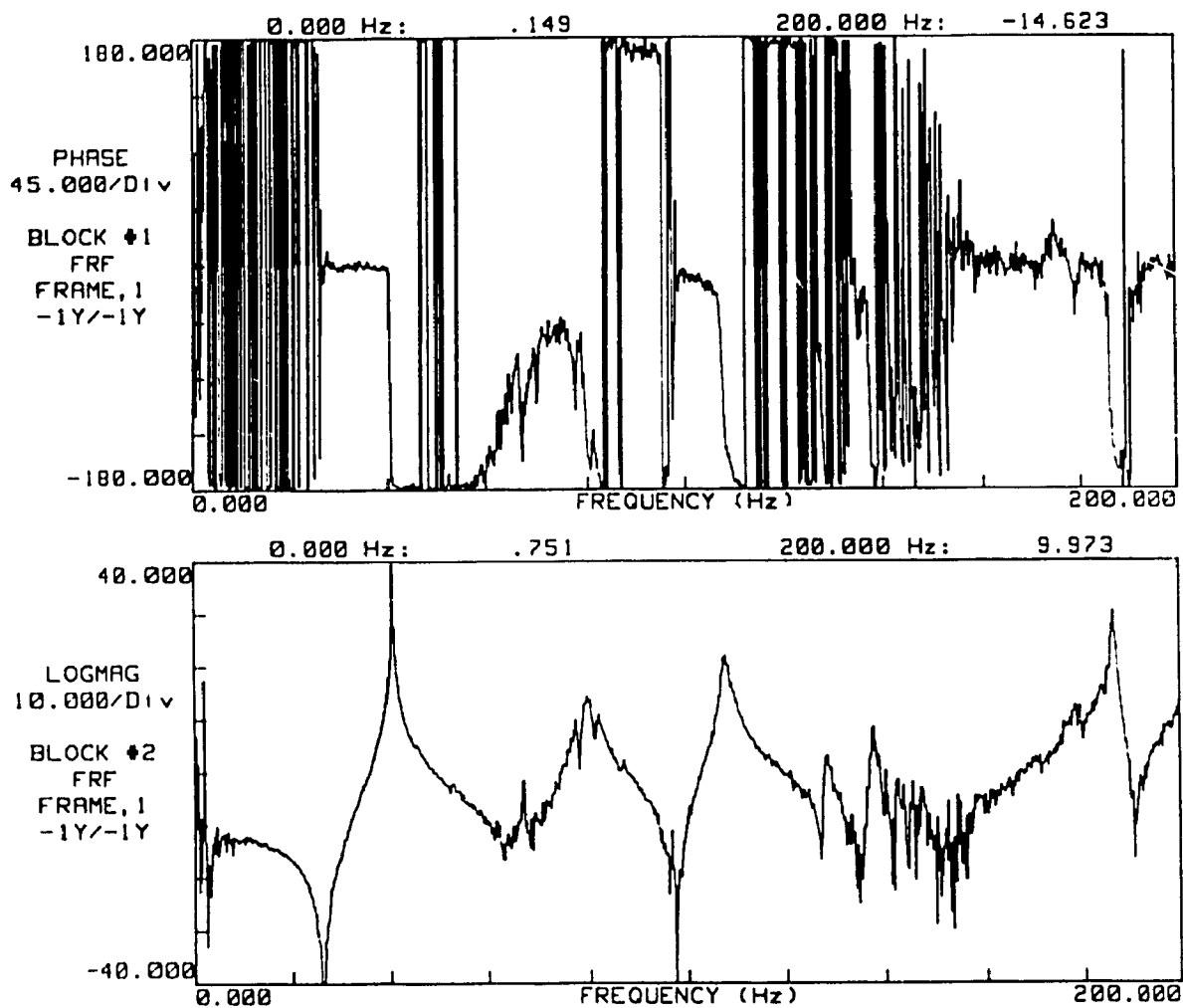


Figure 4-23: Log-Magnitude with Phase Information of the Inertance-FRF Measured at the Driving Point

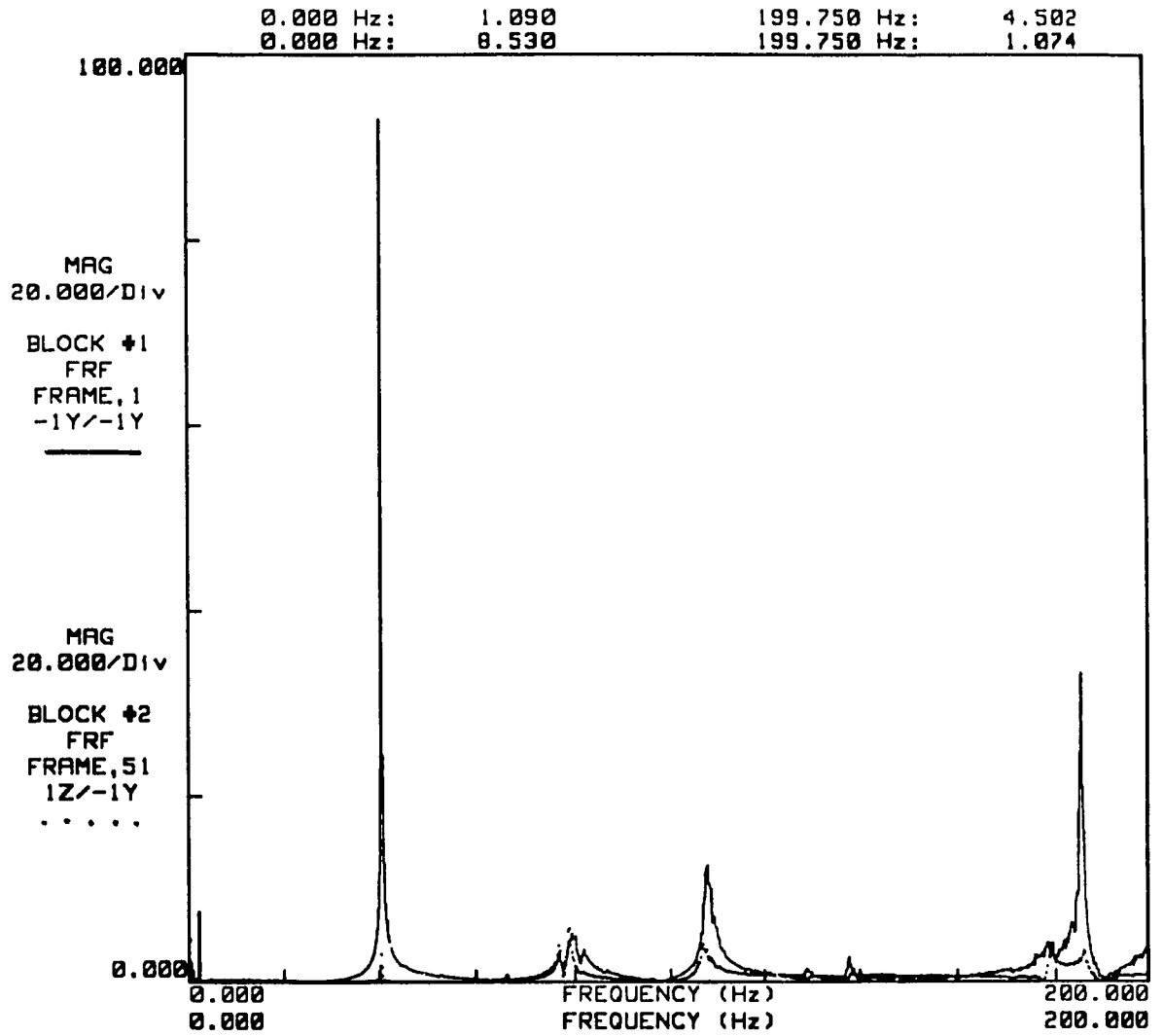


Figure 4-24: Magnitude Comparison of FRF-Measurements Measured at -1Y/-1Y and 1Z/-1Y

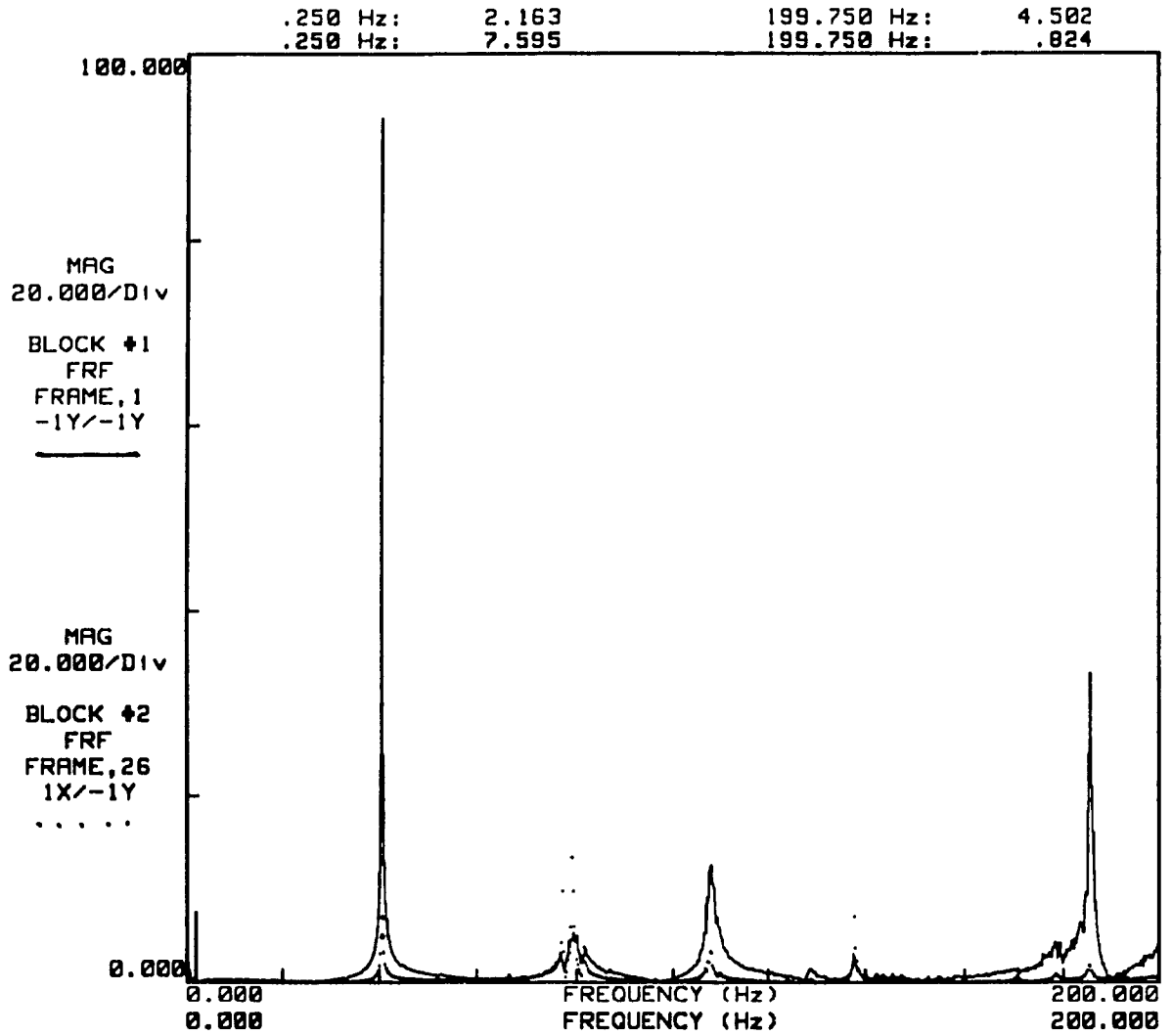


Figure 4-25: Magnitude Comparison of FRF-Measurements Measured at -1Y/-1Y and 1X/-1Y

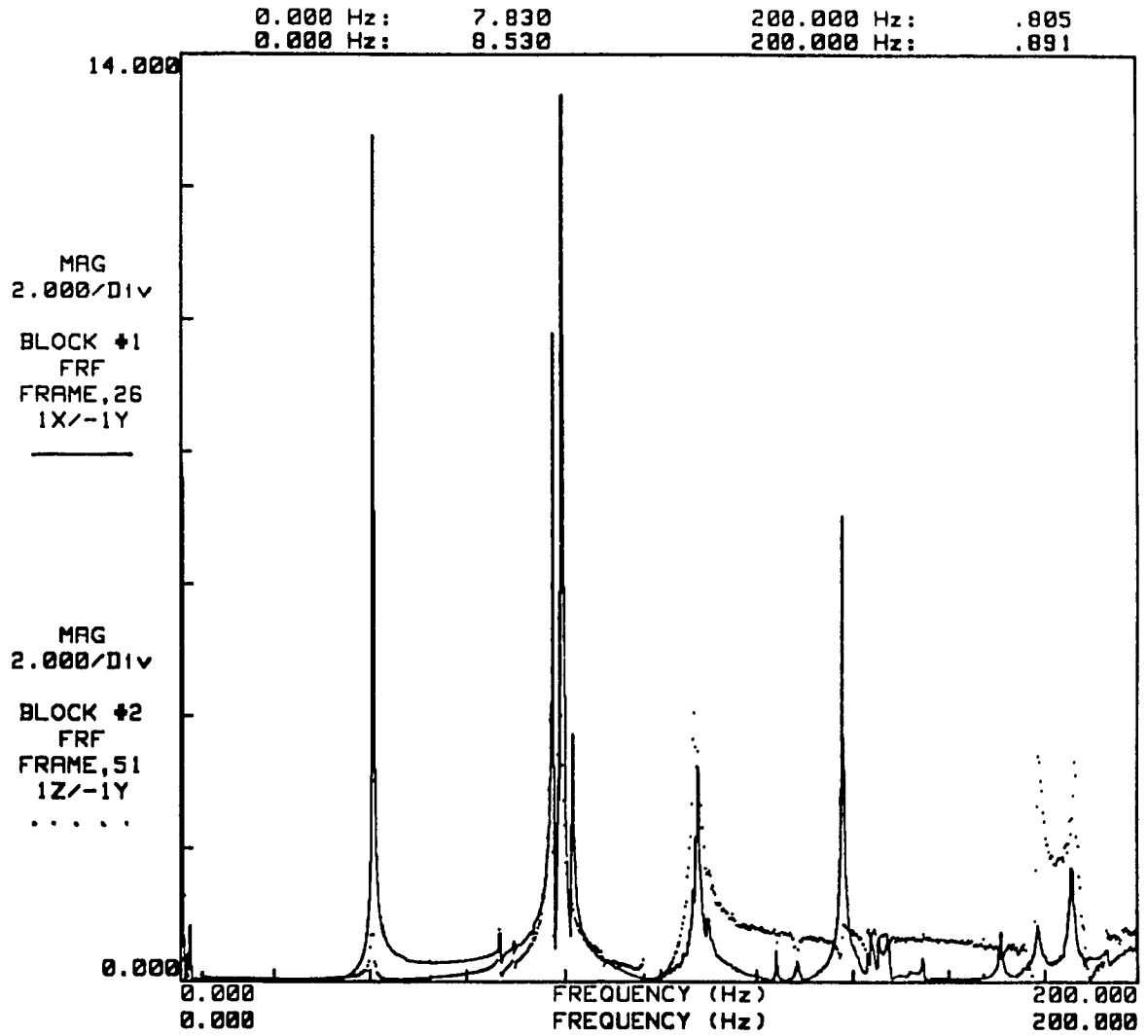


Figure 4-26: Magnitude Comparison of FRF-Measurements Measured at 1X/-1Y and 1Z/-1Y

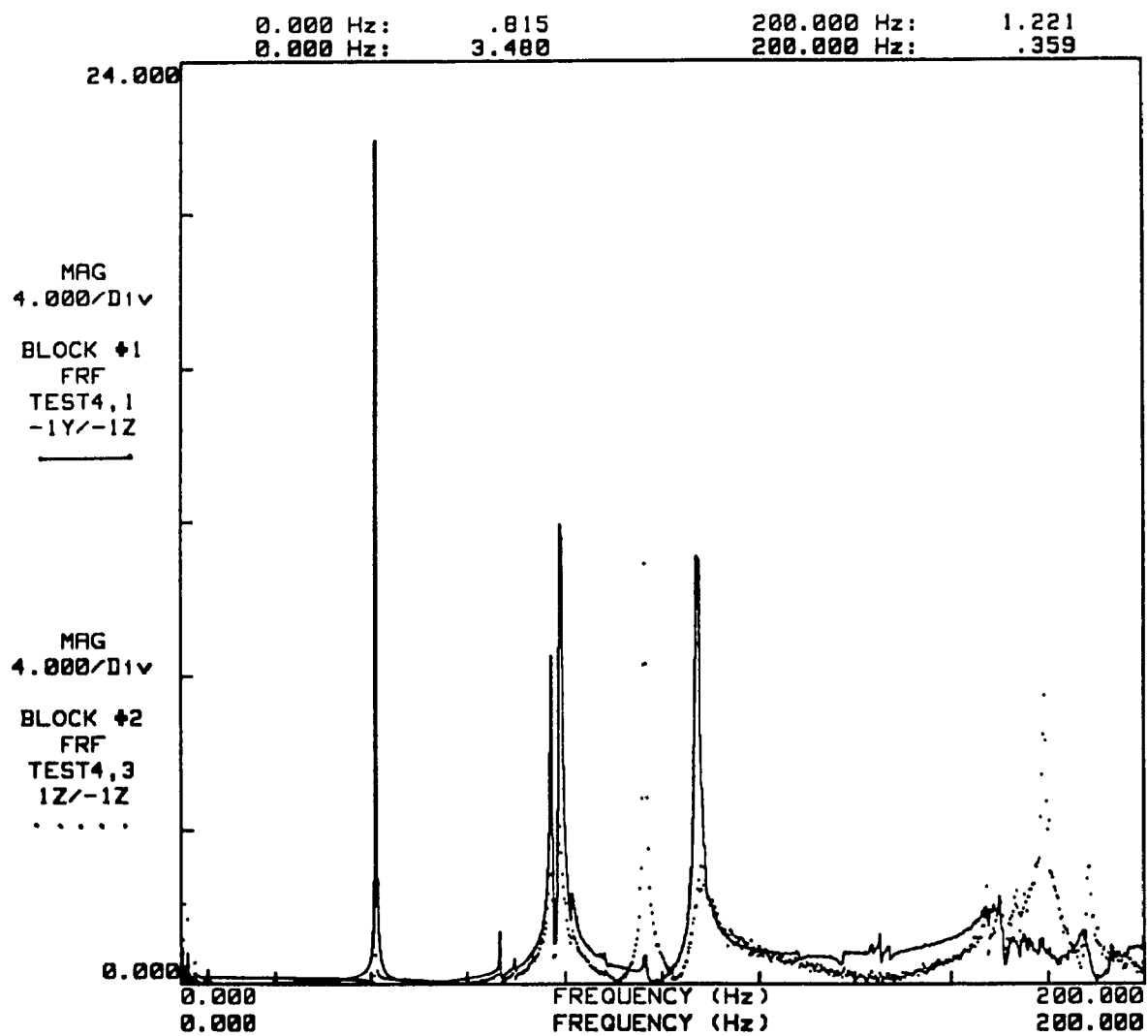


Figure 4-27: Magnitude Comparison of FRF-Measurements Measured at -1Y/-1Z and 1Z/-1Z



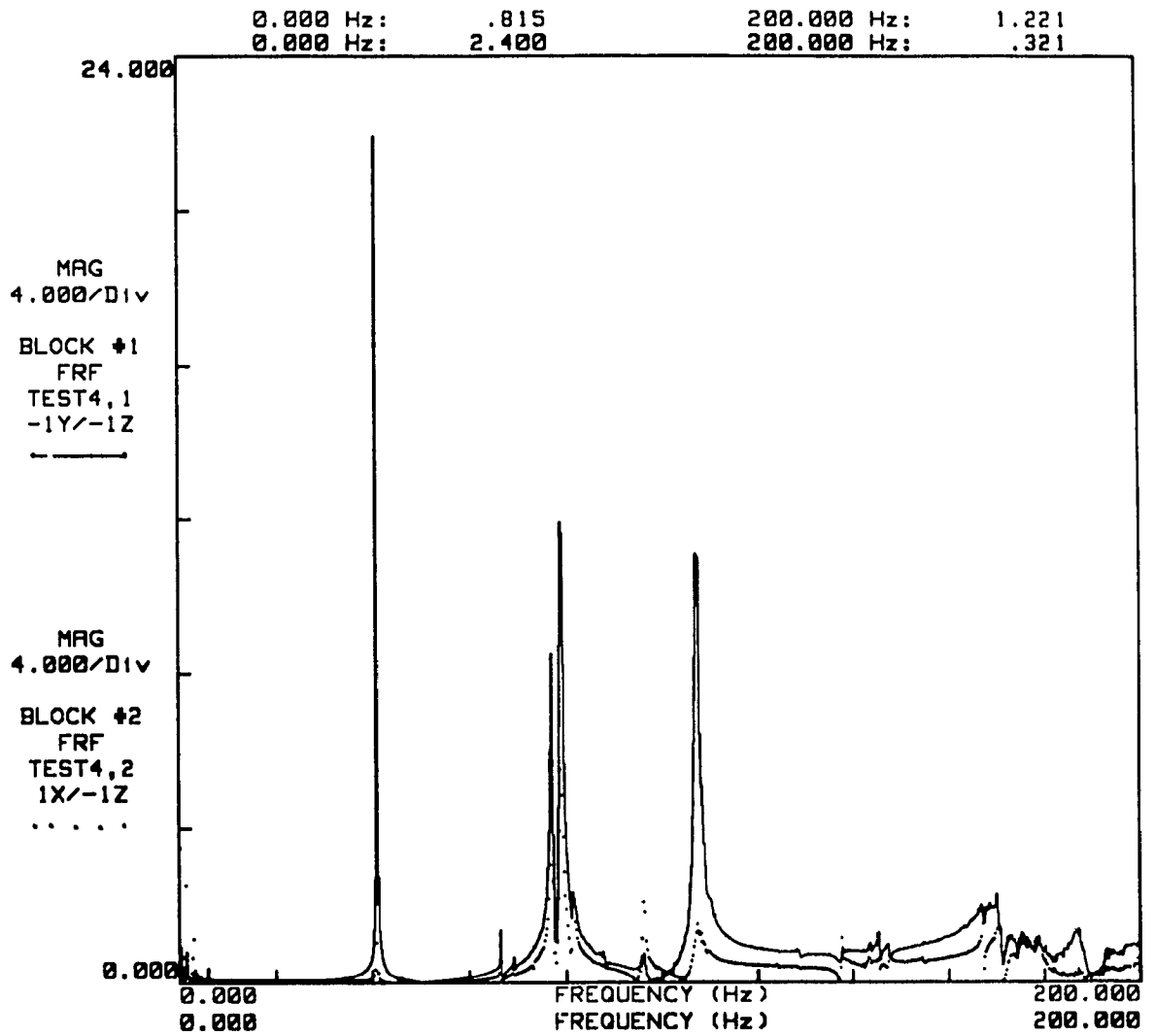


Figure 4-28: Magnitude Comparison of FRF-Measurements Measured at -1Y/-1Z and 1X/-1Z

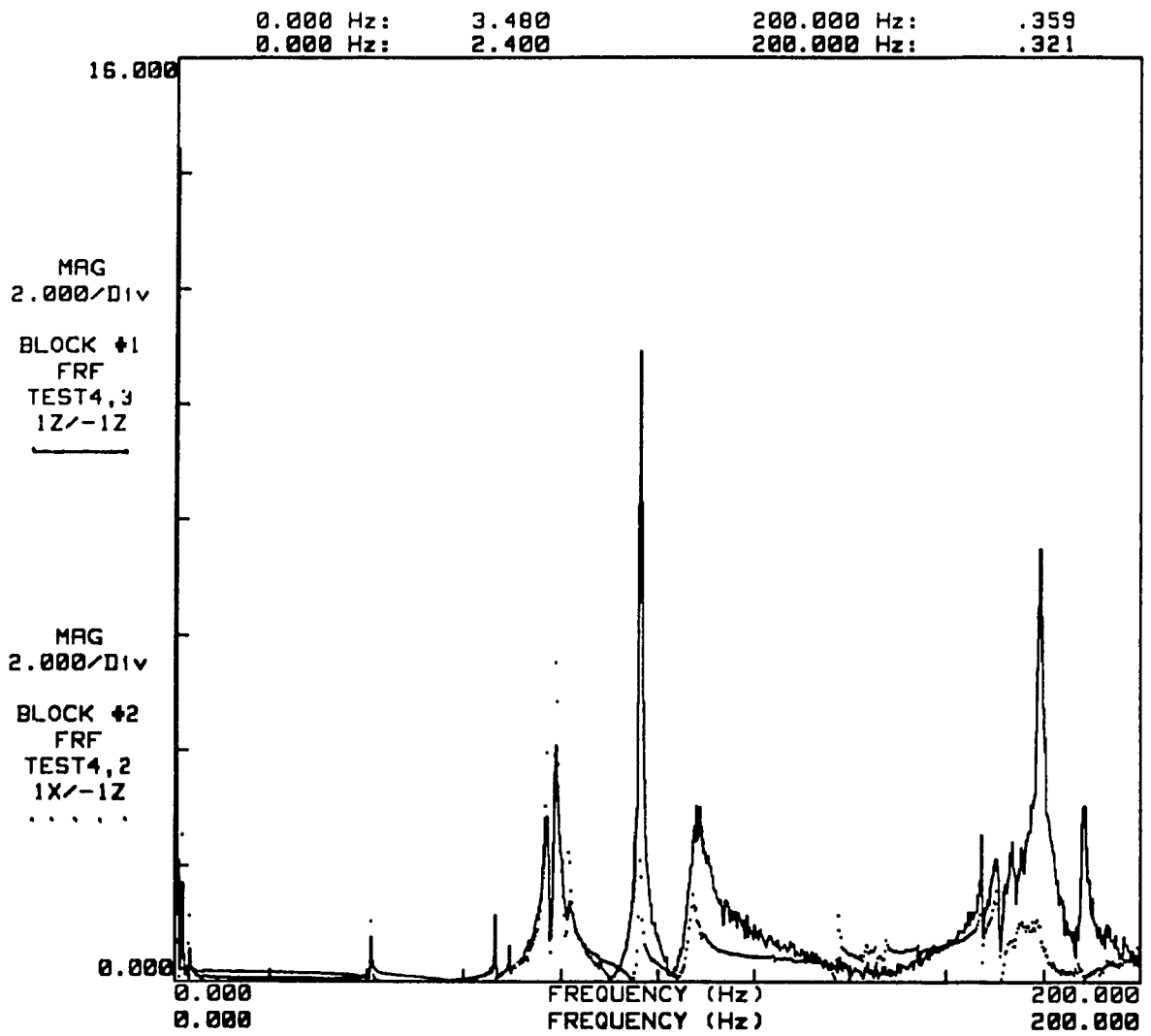


Figure 4-29: Magnitude Comparison of FRF-Measurements Measured at 1Z/-1Z and 1X/-1Z

Figures 4-30 and 4-31 compare the first two and the last two measurements, respectively. We see that they are almost exactly the same.

Finally, for checking the symmetricity, four FRF measurements were also taken at the following DOFs:  $-3Y / -3Y$ ,  $-1Y / -1Y$ ,  $-23Z / -1Y$ , and  $-23Z / -3Y$ . Figures 4-32 and 4-33 compare the first two and the last two measurements respectively. We see that they are almost exactly the same.

Hence it can be concluded that the snowmobile frame is almost a symmetrical structure and satisfies the reciprocity theorem. Also, it can be concluded that the main vibration axis is the Y-axis.

#### **4-2-2 Step 2 - Making the Measurements**

Fifty measurements were taken sequentially at each location in one direction at a time, starting with the vertical direction (Y-axis), and then in the lateral direction (Z-axis).

A total of 10 samples per measurement location were taken to compute the inertance-FRF's. The coherence function and the signal-to-noise ratio were computed before accepting and storing a measurement.

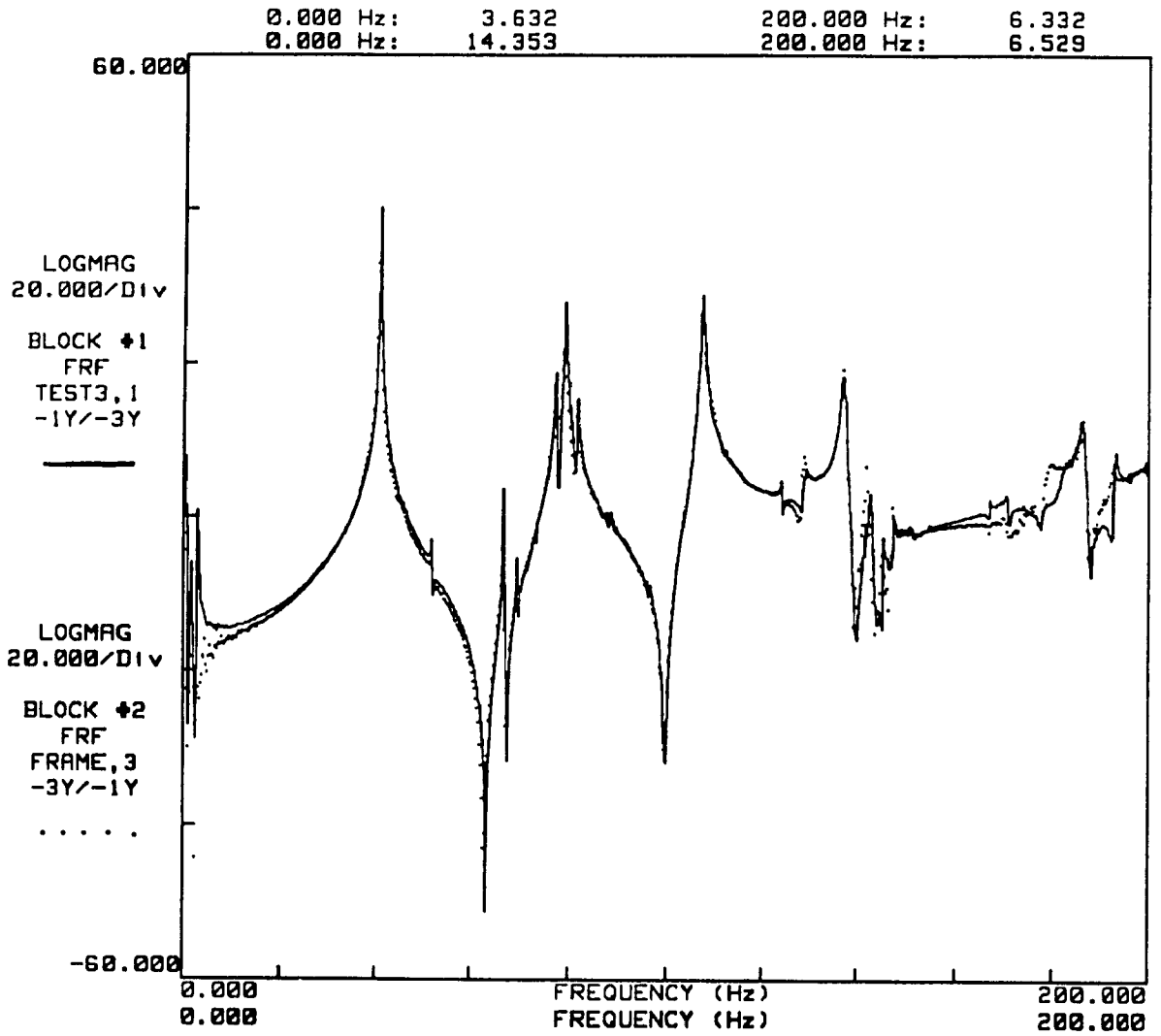


Figure 4-30: Comparing Reciprocity of FRF-Measurements Measured at -1Y/-3Y and -3Y/-1Y

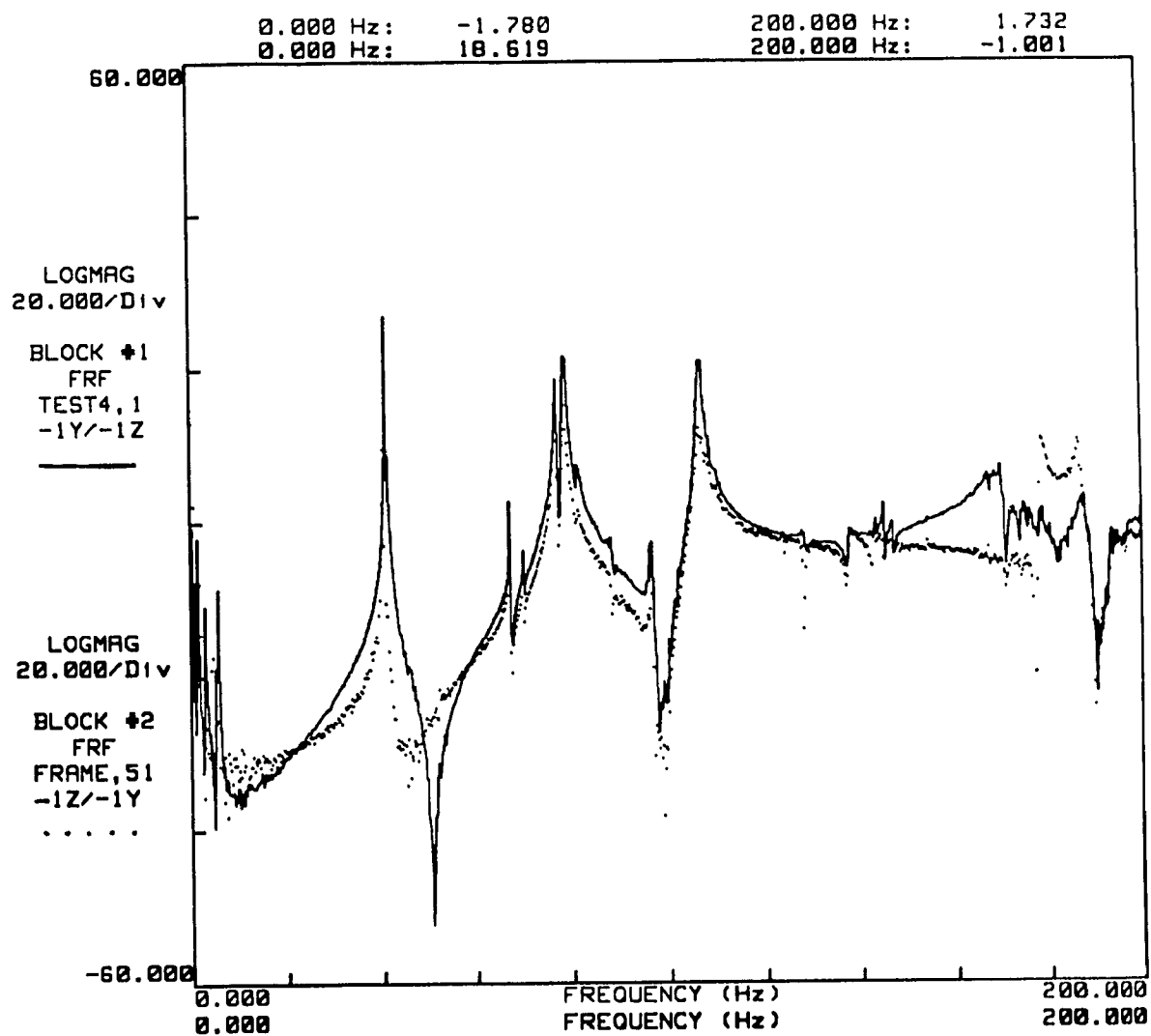


Figure 4-31: Comparing Reciprocity of FRF-Measurements Measured at -1Y/-1Y and -1Z/-1Y

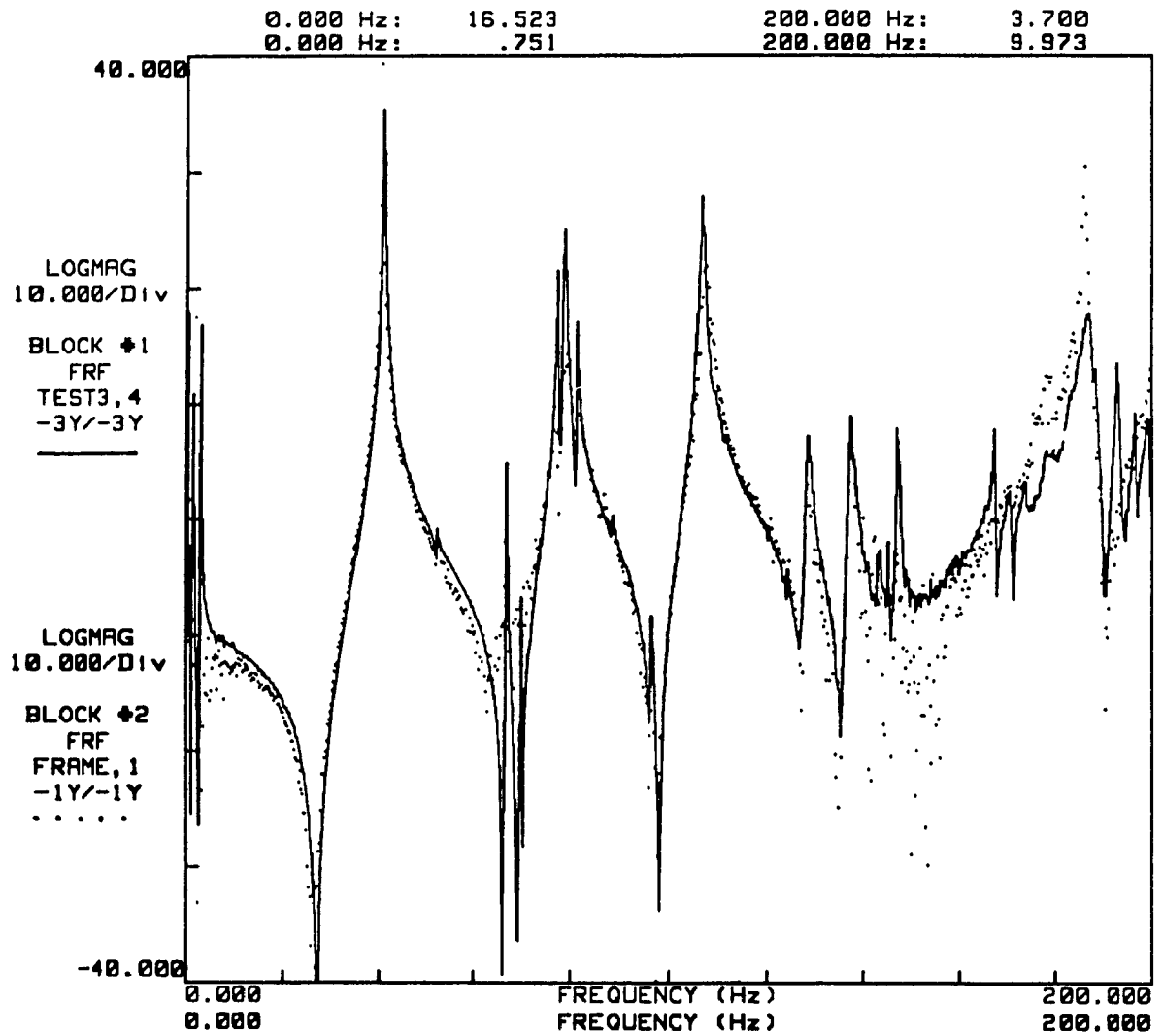


Figure 4-32: Comparing FRF-Measurements Measured at Symmetrical Points: -3Y/-3Y and -1Y/-1Y

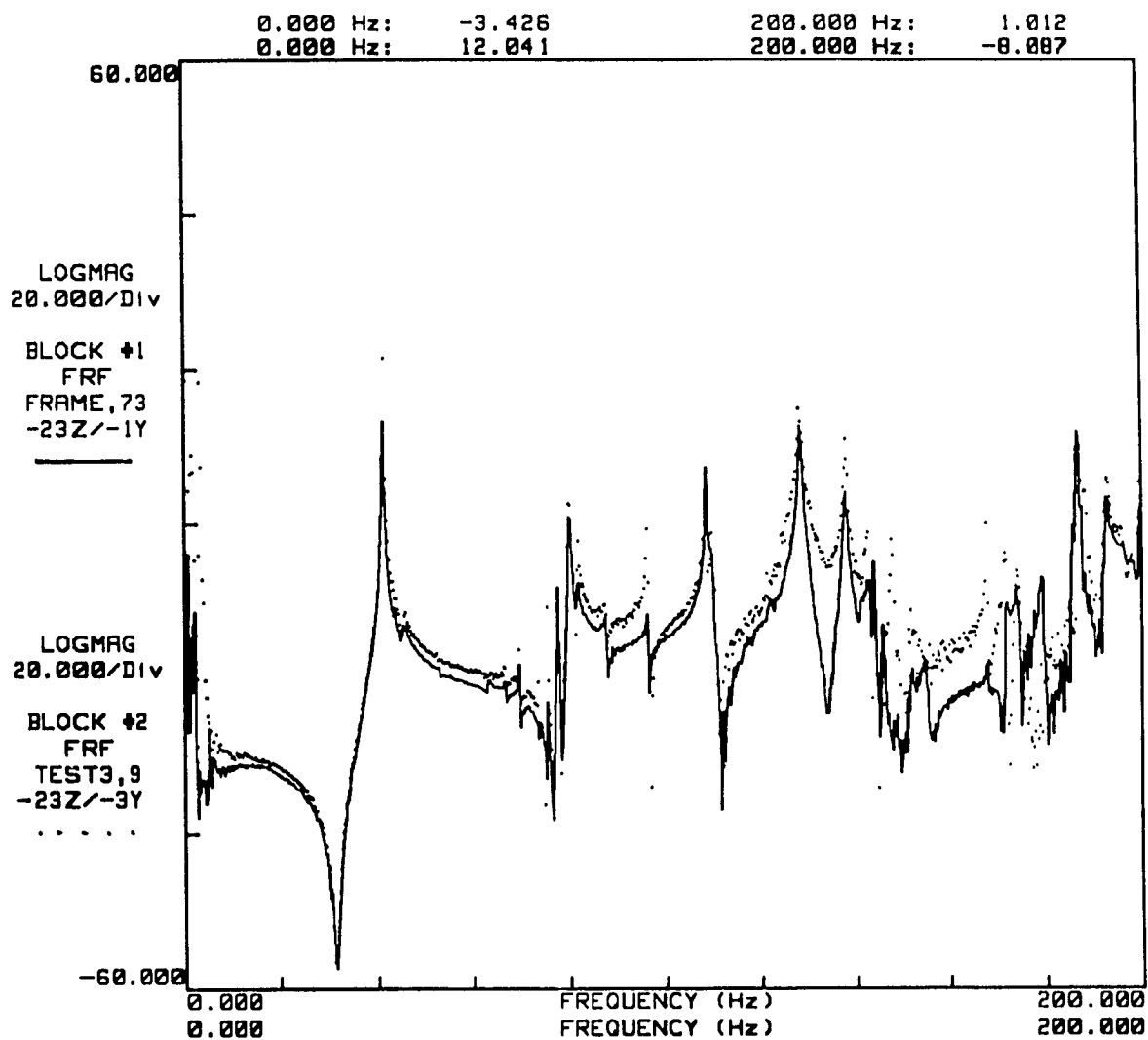


Figure 4-33: Comparing FRF-Measurements Measured at Symmetrical Points:  
-23Z/-1Y and -23Z/-3Y

All the measurements were divided by the previously stored equalization function (Fig. 4.15), for the reasons discussed in Section 4-2-1-5.

In order to easily spot potentially bad measurements and to identify the major modes of vibration, each data set, i.e. the measurements measured along the Y-axis and the Z-axis, is plotted in a waterfall window as shown in Figures 4-34 and 4-35. Basically, it is a three-dimensional plot with frequency along the horizontal axis, the amplitude along the vertical axis, and the measurements along the depth axis. From these plots, we can observe the following:

- There are no indication of bad measurements in each data set
- Both data sets show six dominant peaks within 0 to 200Hz
- The 24<sup>th</sup> measurement in Figure 4-34 shows an additional peak
- The modal density is relatively small
- The FRF amplitude along the Y-axis is larger than along the Z-axis

The six dominant peaks values were quickly identified one at the time. They are approximately in Hertz: 2, 41, 80, 108, 136 and 186. The additional peak value in measurement #24 was identified to be around 31 Hz.

From Section 2-4-18, it is known that the first and second peaks correspond to the highest rigid body and the fundamental flexural modes



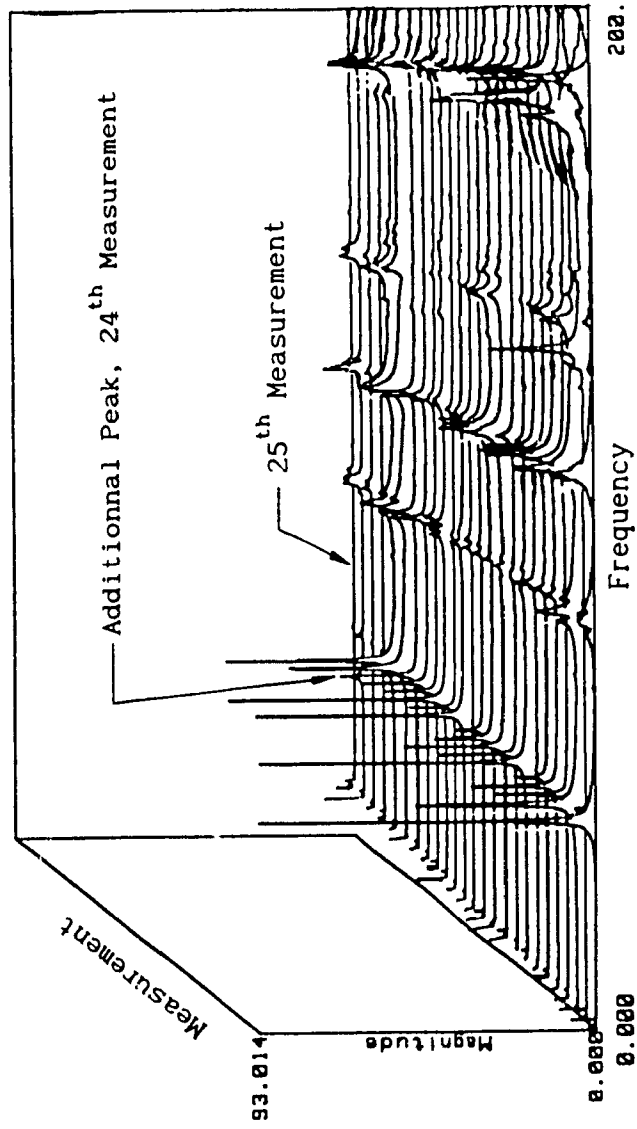


Figure 4-34: 3-D Plot of the Twenty Five Measurements Measured Along the Y-Axis

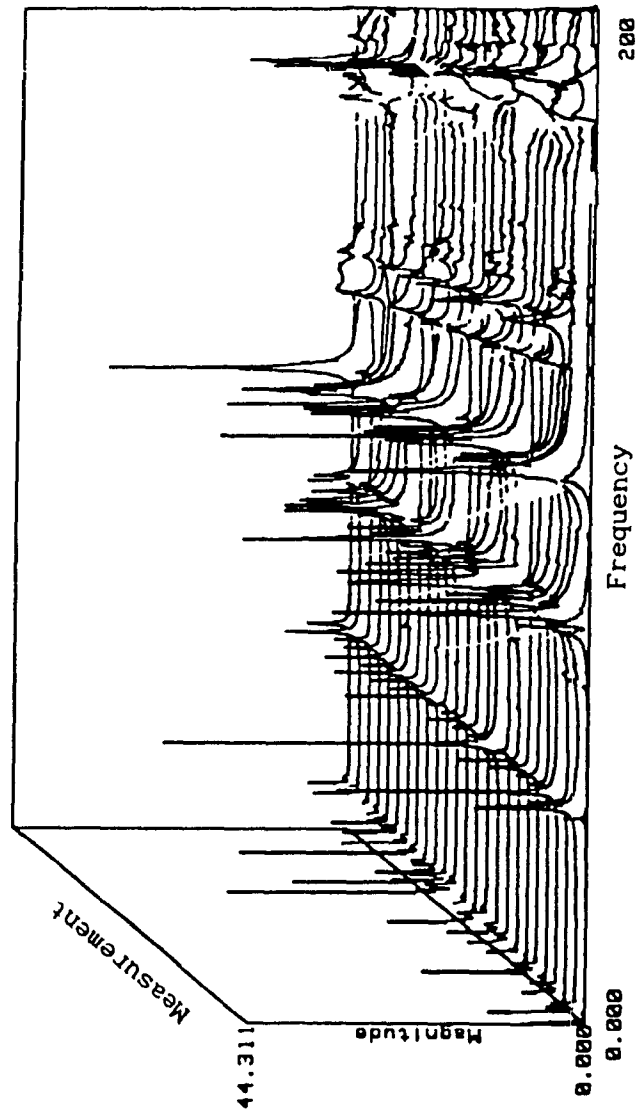


Figure 4-35: 3-D Plot of the Twenty Five Measurements Measured Along the Z-Axis

respectively. Hence, the two dominant modal frequencies of the snowmobile frame are: 41 and 80 Hz.

It can be observed, from these plots, that there is only one mode which exists at 41 Hz, whereas two or more modes seem to exist at the other 4 modal frequencies. This was expected in our structure since it has numerous joints. Hence, there are some closely spaced modes which are often encountered in such complex structures.

Although we mentioned in Section 4-2 that the frequency range of interest was from 0 to 100 Hz, in a practical sense, this structure would never experience, in its working environment, a frequency beyond 60 Hz. Indeed, an engine in a snowmobile would practically never run beyond 3600 RPM, i.e. 60 Hz.

The only reason why the frequency range of interest was selected to be from 0 to 100 Hz is that it provides more peaks in the FRF signal so that it helps one to discuss on the various modal properties. Otherwise, the frequency range of interest would have been selected from 0 to 50 Hz with the FFT analyzer set to 0 to 100 Hz.

An interactive utility program of MODAL 3.0 SE software was used to obtain animated deflection shapes of some of the previously located peaks without going through a formal curve-fitting operation. This utility program is a very useful and quick method to calculate the

complex amplitude at a given frequency for each of the displayed measurements.

From the waterfall plots constructed using the 50 FRF measurements, the deflected mode shapes were obtained at 2, 31, 41 and 80 Hz. The mode shape at 2 Hz shows the vertical rigid body mode. The 31 Hz shows the vertical bending of point 24 only, i.e. the only point of the structure that was moving was point 24 and it was moving along the Y axis (bending in the Z-X plane). Finally, both the 41 and 80 Hz show a longitudinal twist mode.

It should be noted, however, that the modal damping cannot be obtained through this utility program and formal curve fitting has to be carried-out. Also, the results of this investigation would not be sufficient to do structural modifications.

#### **4-2-3 Step 3 - Estimating the Modal Parameters by Curve-Fitting**

Formal curve-fitting estimates first the pole locations and then the residues at all measured DOF's for each of the estimated pole location. Each pole location can be either estimated from any single measurement (local curve-fitting) or from all the measurements (global curve-fitting). This process represents the manipulation of a large amount of data since for each FRF measurement the FFT analyzer gives us

800 complex values. Therefore, manual techniques is not practical and computer-aided techniques are essential.

The Modal 3.0 SE software was utilized to estimate the modal parameters of the snowmobile frame structure. The software has two groups of curve-fitting methods available: Single Degree-of-Freedom (SDOF) and Multiple Degrees-of Freedom (MDOF) methods. They are used for systems with light and heavy modal coupling respectively. Figure 4-36 shows a typical FRF measurement with both light and heavy modal coupling.

The SDOF curve-fitting method is based on SDOF assumptions. There are several SDOF fitting algorithms available in the software such as circle fitting, polynomial, etc. The polynomial fitting algorithm is preferred to any other ones because when comparing the original measurement with the synthesized one, it often gives good results.

The overall SDOF curve-fitting procedure involves three steps. The first step consists of curve-fitting all the modes of interest to calculate the residue using any single FRF measurement for each mode. Usually, the driving FRF measurement along the dominant vibration axis is the one used since this DOF is at the vibration source and consequently this FRF will generally have lower modal density, i.e. clearer peaks. Then one must define a cursor band around each modal frequency. Each of them should be defined to compromise between

### COMBINING SDOF & MDOF METHODS

- use SDOF methods on LIGHTLY COUPLED modes
- use MDOF methods on HEAVILY COUPLED modes

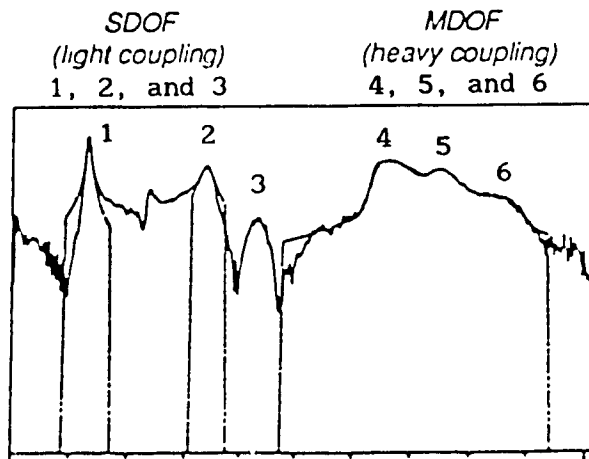


Figure 4-36: Typical FRF Measurement with Both Light and Heavy Modal Coupling [4]

including as many data points as possible, to maximize the statistical estimation, and ensuring that the other modes will not become dominant and the SDOF assumption becomes invalid. The second step consists of estimating the remaining residues based on the estimated pole locations and using the same curve-fitting algorithms and cursor bands. The last step consist of sorting the entire set of residues to obtain a mode shape for each mode.

The overall MDOF curve-fitting procedure is similar to the SDOF curve-fitting and involves all three steps. The only differences are that the cursor band is defined to include two or more modal frequencies, and the curve fitting algorithms are based on MDOF assumptions.

Figure 4-37 shows a typical FRF measurement having four modes. The quality of modal results, from curve-fitting, depends strongly on the user's skill and experience in making the right assumptions. If it is assumed, for example, that the four modes behave like MDOF for the system, i.e. curve-fitting the four modes using one single cursor band with MDOF algorithms, the results will certainly have large errors in the estimated modal parameters. A good assumption would be to define and use, as shown in Figure 4-37, two cursor bands and a combination of SDOF and MDOF algorithms.

The accuracy of the results depends also on the cursor bandwidth used to fit the modes. To illustrate that, the driven FRF measurement

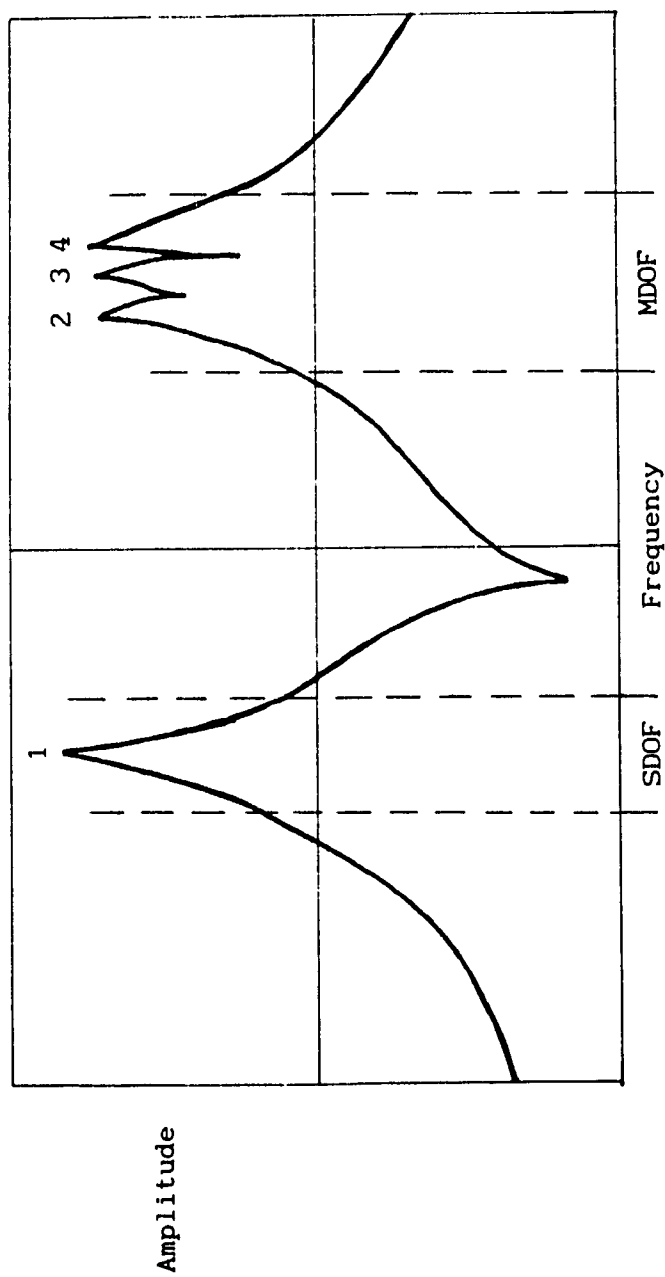


Figure 4-37: Typical FRF Measurement Having Four Modes



at 41, and 108 Hz had been curve-fitted with different cursor bands. SDOF algorithm was used to fit each mode. The modal results are shown in Table 4-4. The table shows the estimated modal parameters, namely, the modal frequency, damping factor, and modal residue (amplitude and phase) for five different cursor bands. The first cursor band was defined so as to have only one spectral line on each side of the peak (minimum cursor band that an operator should try to use). Each subsequent ones was increased by one spectral line on each side of the peak. It can be seen that the modal results change as the cursor band increases and then they become stable. Hence, this simple example shows the importance of defining an adequate cursor band to curve-fit a mode. As a rule of thumb, a negative damping factor should be rejected, and the investigation should be carried-out with increased cursor band.

In addition, curve-fitting can be done in a "local" or "global" sense. The most popular one falls into the category of local fitting. That is, each pole location can be estimated from anyone measurements. Once the pole locations are estimated, they are used to estimate the residue from all the measurements, that is at all DOFs. On the other hand, global curve-fitting evaluates the global parameters (pole locations) based on all measurements using the least square method. It generally estimates the pole locations more accurately. Also, since the residue is often tightly coupled to damping, the estimation of residue will also be generally more accurate. The steps involved in using global curve-fitting in SMS software are given here because they are not

Table 4-4: Modal Results Using Different Cursor Bands

Measurement Number: 1  
 D.O.F.'s: -1Y / -1Y  
 Spectral Resolution: 0,25 Hz

Cursor Band (Hz)	0,50	1,00	1,50	2,00	2,50
------------------	------	------	------	------	------

## 41,3 Hz Mode

Freq. (Hz)	40,50	40,49	40,49	40,49	40,49
Damp. (%)	-108,05u	0,16	0,16	0,16	0,16
Amp. (MPS2/N)-SEC	0,12	76,73	76,52	76,13	73,24
Phase (Deg.)	127,66	4,14	3,24	2,88	2,64

## 108,3 Hz Mode

Freq. (Hz)	***	107,28	108,00	107,96	107,91
Damp. (%)	***	0,93	0,47	0,48	0,44
Amp. (MPS2/N)-SEC	***	468,25	74,57	79,43	72,12
Phase (Deg.)	***	95,14	336,09	345,60	353,83

\*\*\*: Overflow Error

explicitly explained in the SMS manuals. Referring back to Figure 4-37, the steps for global curve-fitting the four modes would be as follow:

Set the cursor band around the first peak (as discussed above),

Give the mode range: 1 to 1,

Give the measurement record range: 1 to n (n = Number of FRF measurements),

Estimate the first pole location based on the n FRF measurements,

Estimate the residue at all DOFs for that mode only,

Set the cursor to encompass the other three peaks,

Give the mode range: 2 to 4,

Give the measurement record range: 1 to n,

Estimate the three pole locations based on n FRF measurements,

Estimate the residue at all DOFs for the three modes.

Hence, the estimation modal parameters can be carried-out in two steps.

Sometimes, it is very difficult to locate the frequency of a particular mode. This is especially true in the case where the modal density is high and the random noise is significant. In that case, an alternative method to the waterfall one is to plot a FRF measurement (receptance or inertance FRF) in four different display formats and then verify that a specific condition is satisfied simultaneously in each of them to recognize a mode. The specific conditions are: a peak in the Log magnitude format display and a phase close to  $\pm 90$  degrees (or a

phase shift) in the Phase format display; a positive or negative amplitude in the Imaginary format display and a magnitude of zero in the Real format display. Note that the last two conditions will be reversed when using the mobility-FRF's. Figures 4-38 to 4-41 show two inertance-FRF measurements (at DOFs 23Z / -3Y and -23Y / -3Y), plotted in those four display formats.

An extension of this method would be to plot all the FRF measurements on the same sheet using anyone of the four display formats. The fifty measured inertance-FRFs of the snowmobile frame was plotted on the same sheet in the Imaginary format display. This is shown in Figure 4-42. Hence, this last plot clearly highlights the major modes of vibration along with the local ones.

Another powerful method to help locating the frequency of a particular mode consists of computing a composite spectrum using all the FRF measurements that will accentuate the modal peaks. SMS software provides the following computation methods:

- 1) Squaring and summing the Imaginary portion of the measurement
- 2) Squaring and summing the Real portion of the measurement
- 3) Squaring and summing the Imaginary and Real portion of the measurement
- 4) Summing the square root of the sum of the Imaginary and Real portion squared

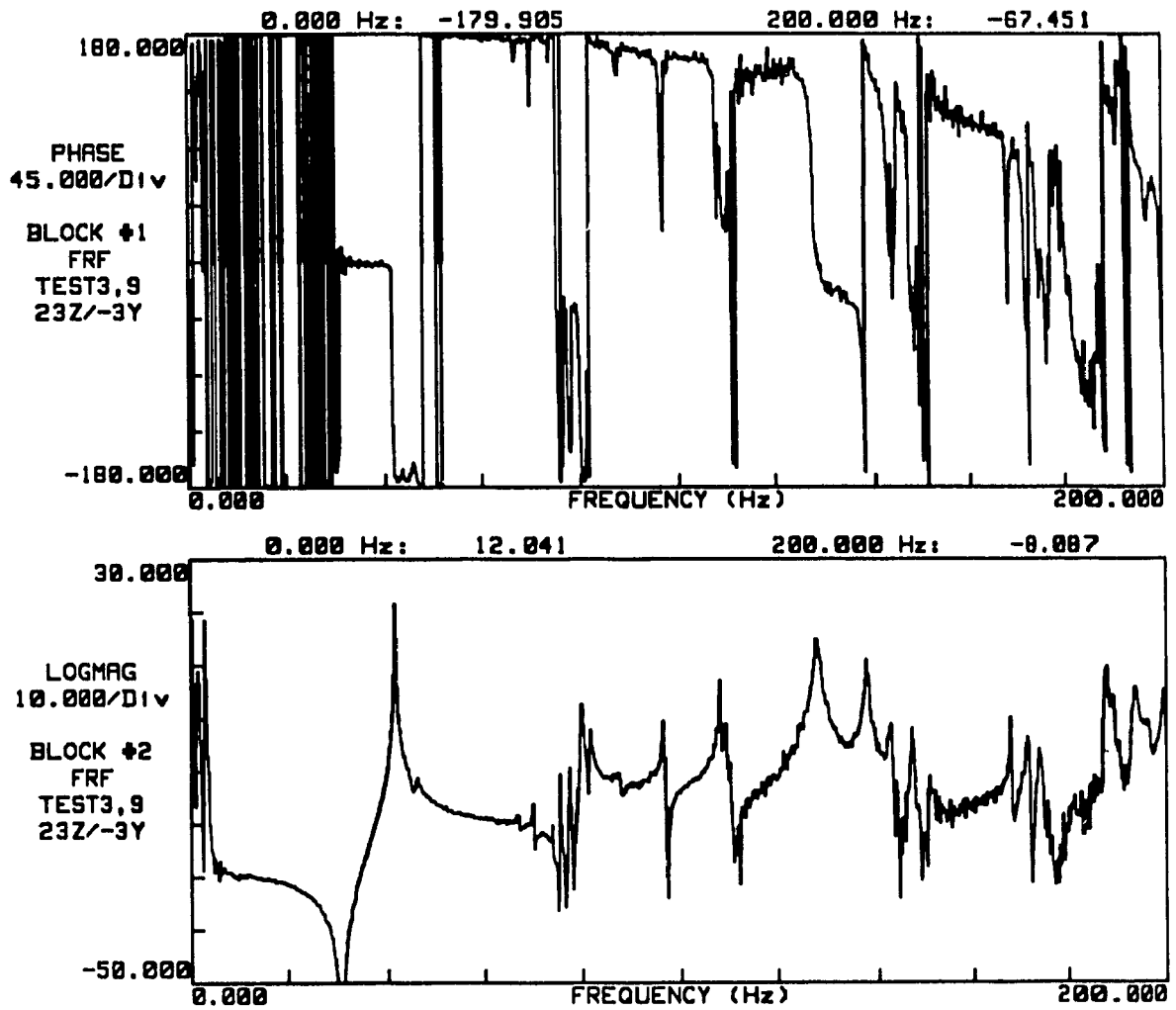


Figure 4-38: Phase and Log-Mag. Display Formats of the Inertance-FRF Measurement Measured at 23Z/-3Y

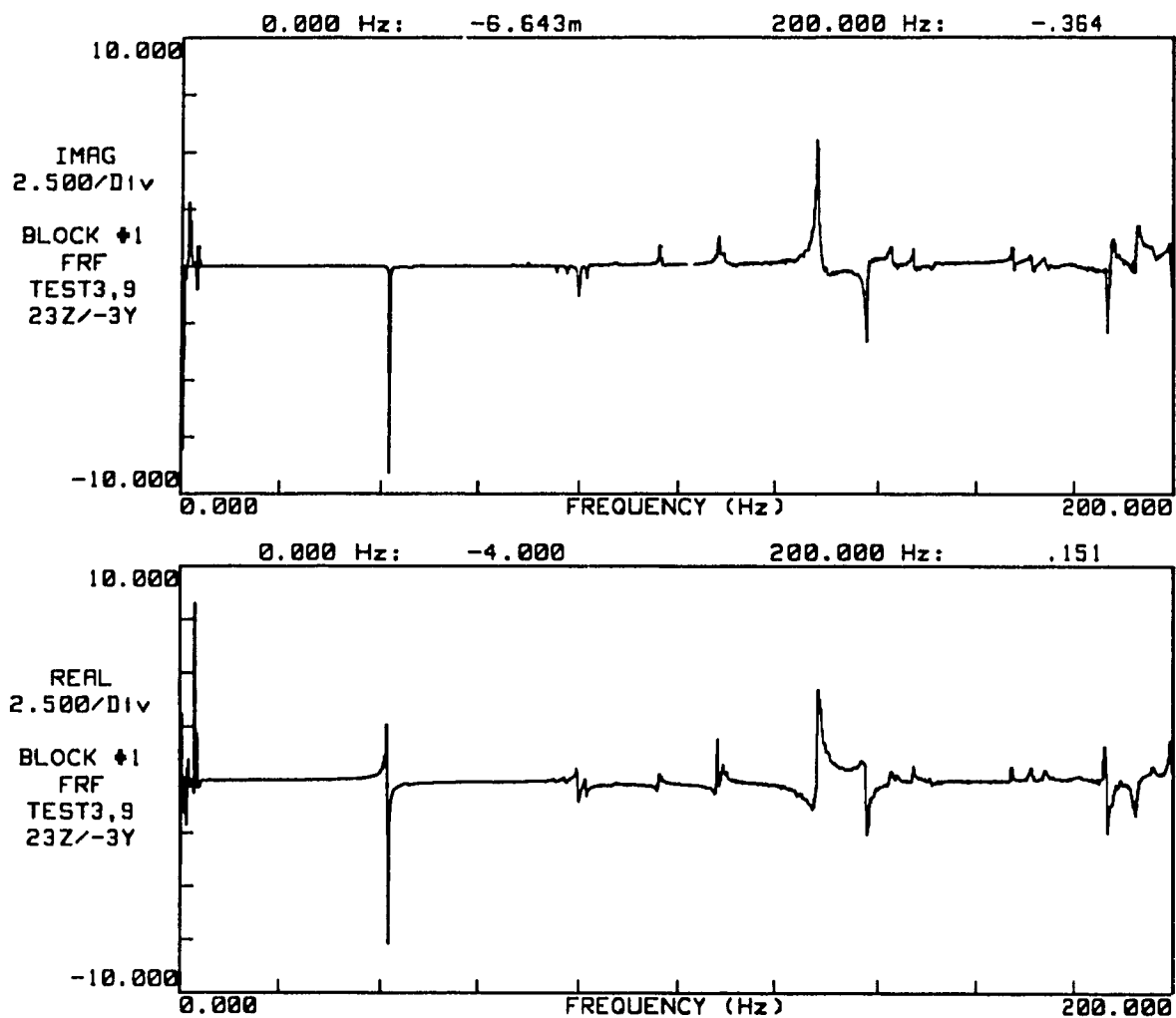


Figure 4-39: Imaginary and Real Display Formats of the Inertance-FRF Measurement Measured at 23Z/-3Y

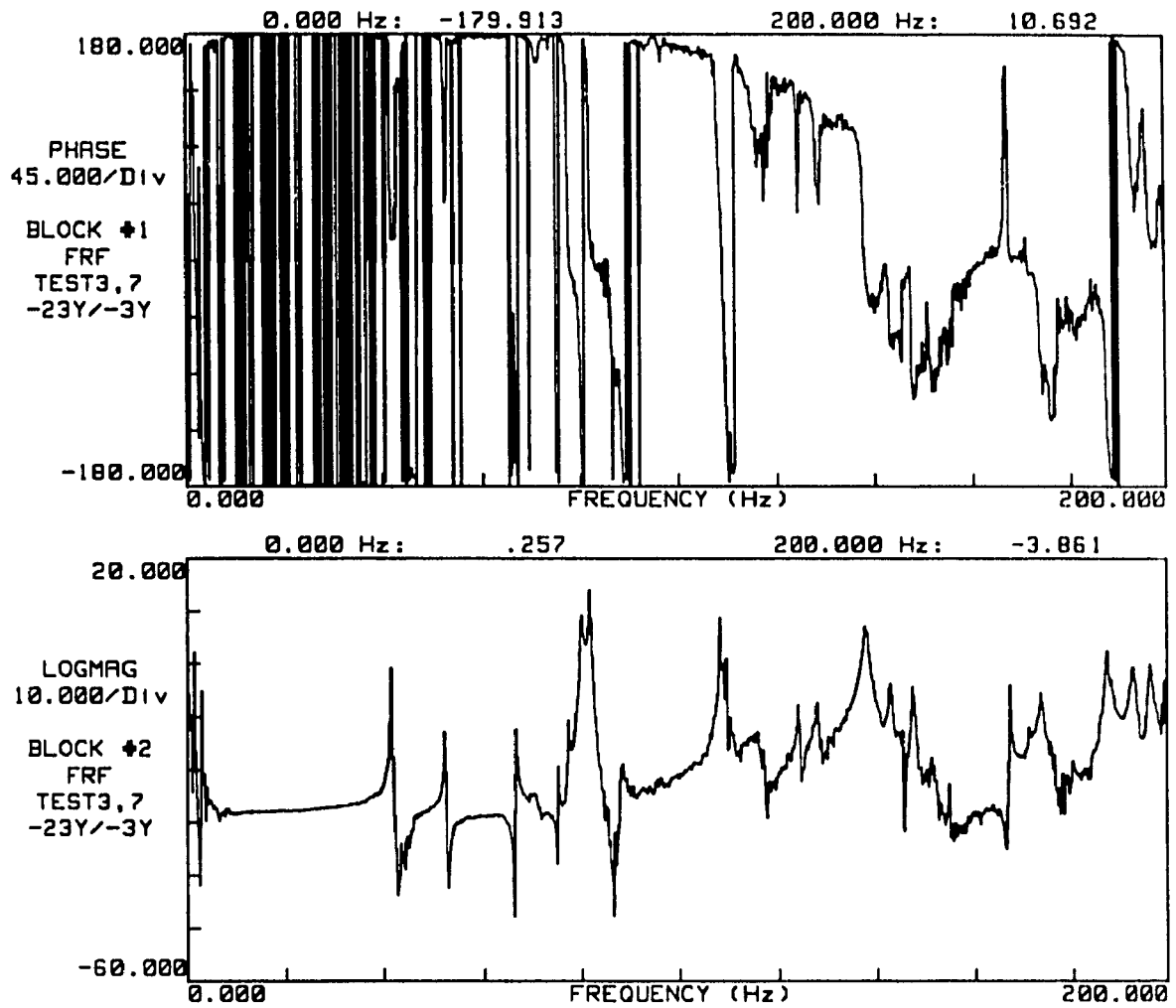


Figure 4-40: Phase and Log-Mag. Display Formats of the Inertance-FRF Measurement Measured at -23Y/-3Y

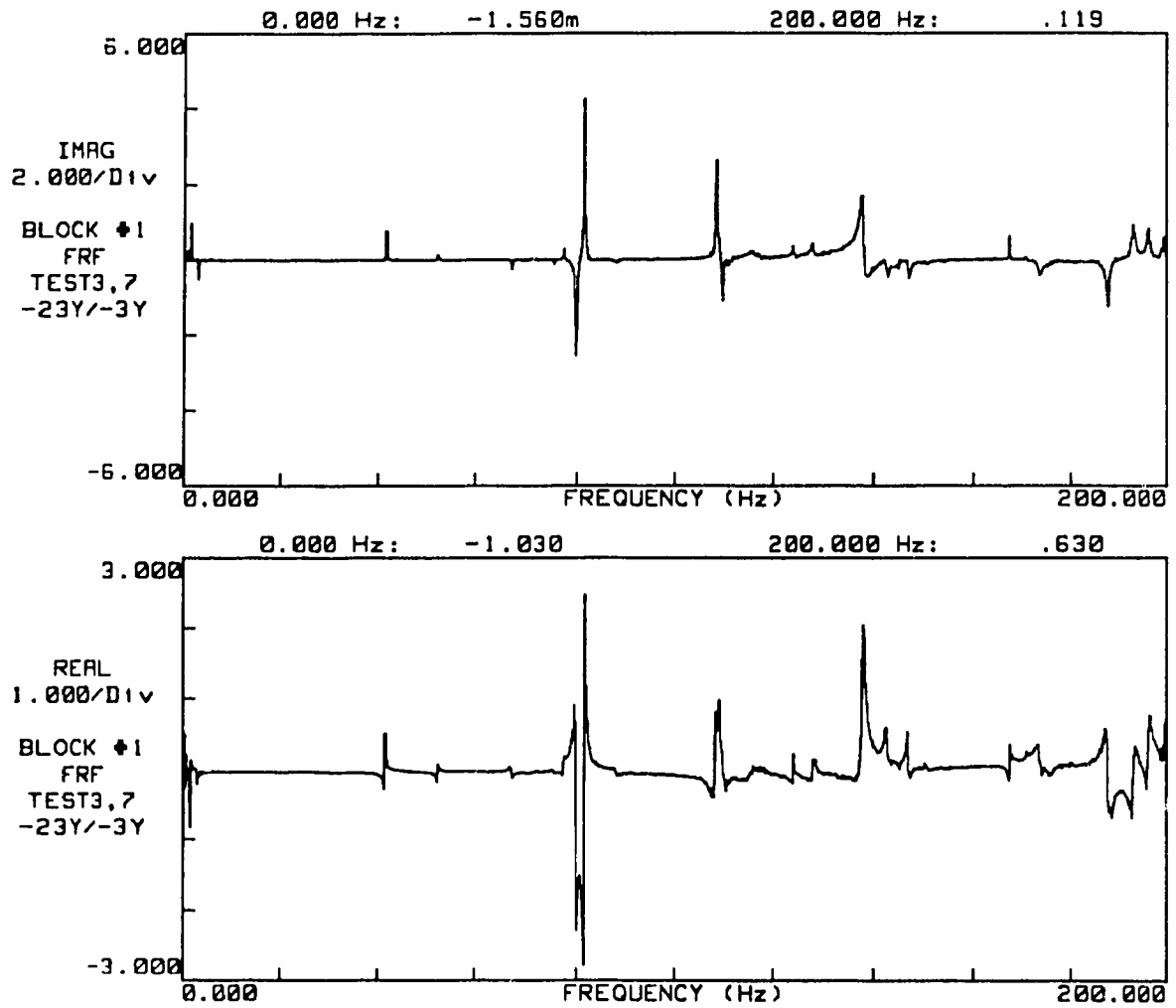


Figure 4-41: Imaginary and Real Display Formats of the Inertance-FRF Measurement Measured at -23Y/-3Y



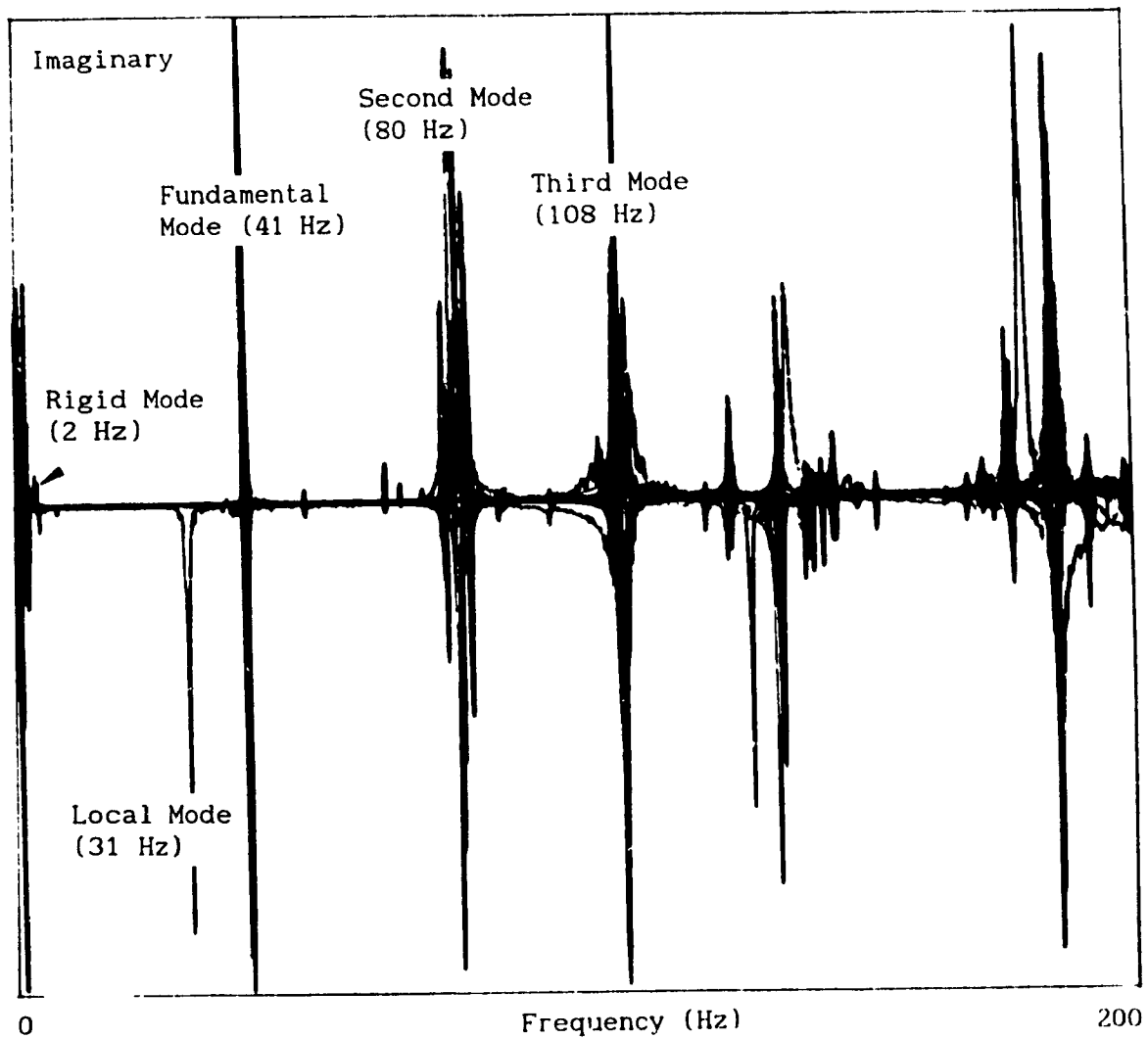


Figure 4-42: Plot of the Fifty FRF Measurements in the Imaginary Display Format

The first and the fourth computation methods were used for all the measurement data and are shown in Figure 4-43 and 4-44.

Hence for the snowmobile frame in the frequency range of interest (0 to 100 Hz), the following conclusions can be drawn:

- The rigid modes are clearly identified
- There is one local mode and its frequency is 31 Hz
- There are three major flexural modes (or modal peaks)
- Their frequencies are 41, 77, AND 79 Hz
- The fundamental frequency is 41 Hz
- The frequency of the highest rigid body mode (2 Hz) satisfies the condition: fundamental flexural frequency > 10 times the highest rigid body frequency

Figures 4-45 and 4-46 compare the synthesized FRF at DOFs -1Y / -1Y obtained from global and local curve-fitting respectively with the measured measurement. Also, Figure 4-47 compares these two synthesized curves and finally Table 4-5 shows the extracted modal values obtained by the two curve-fitting methods. We see that both methods give very similar and accurate frequency estimates. But it seems that the local curve-fitting fits better the amplitude of the second mode (80 Hz one) than the global method. It seems also that the local curve-fitting method closely fits the anti-resonance between mode one and mode two in comparison with the global curve-fitting method. However, SMS states that " if damping is in large error, the residue estimate will also be

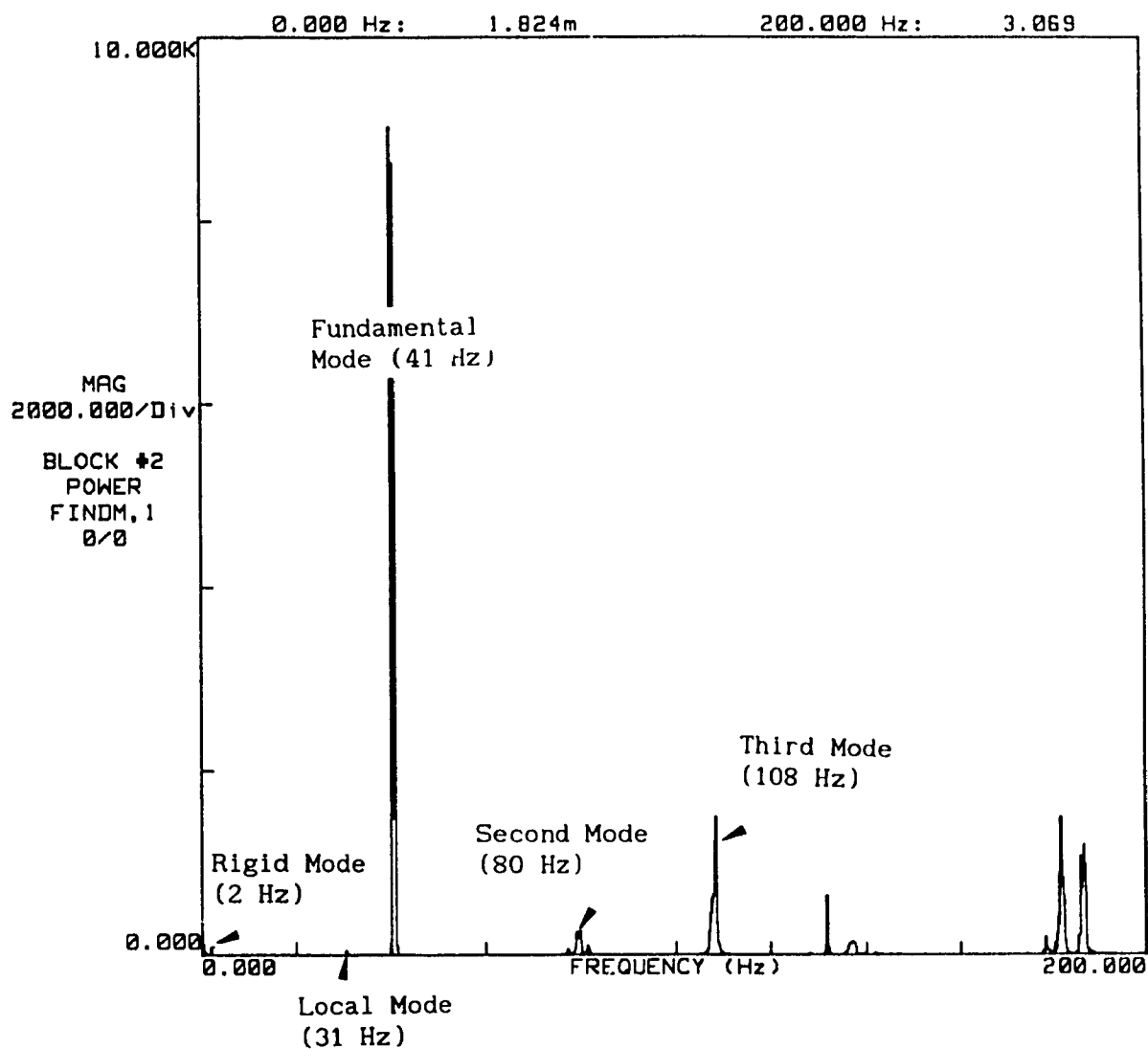


Figure 4-43: Computed Composite Spectrum Using the First Computation Method

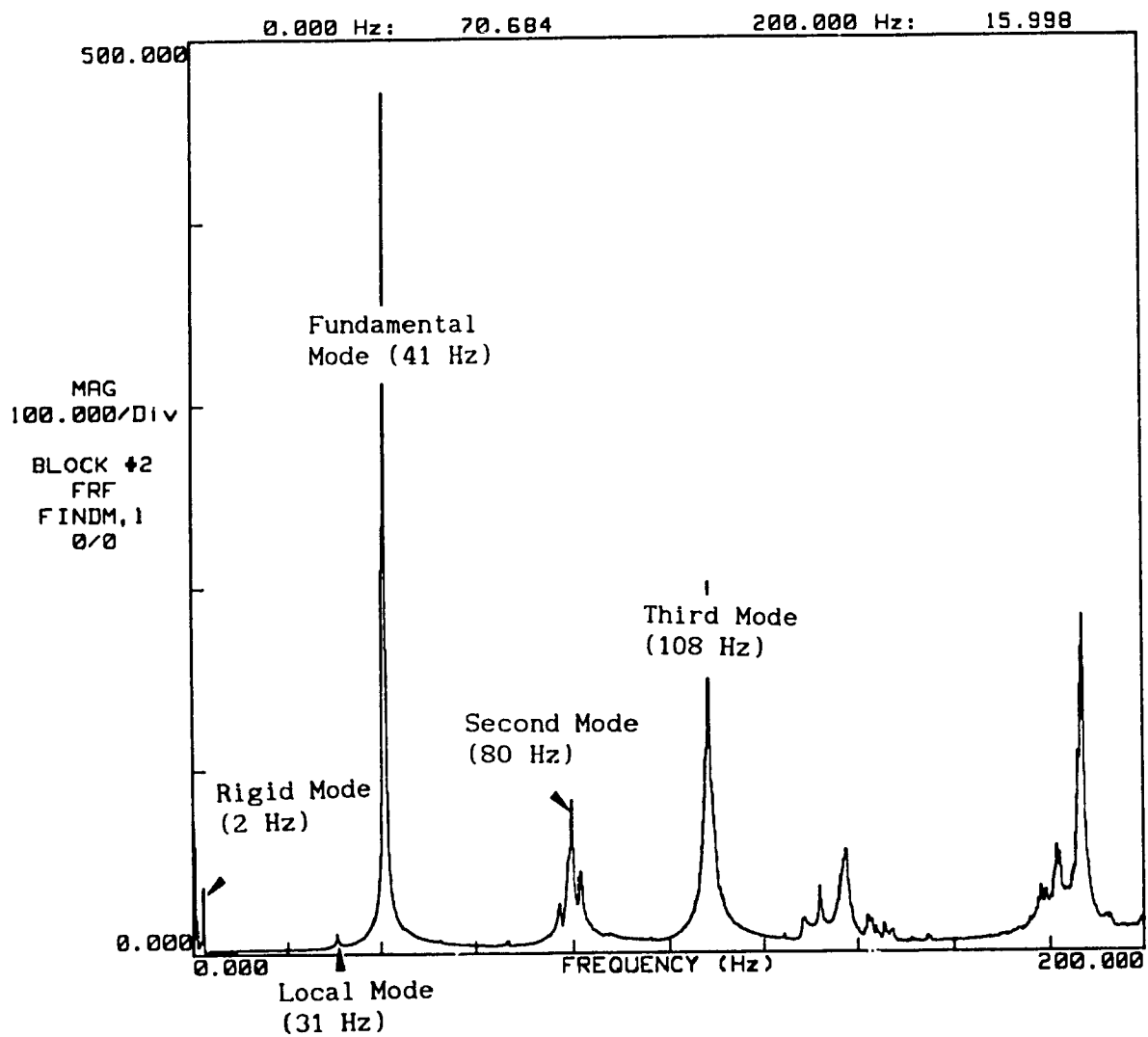


Figure 4-44: Computed Composite Spectrum Using the Fourth Computation Method

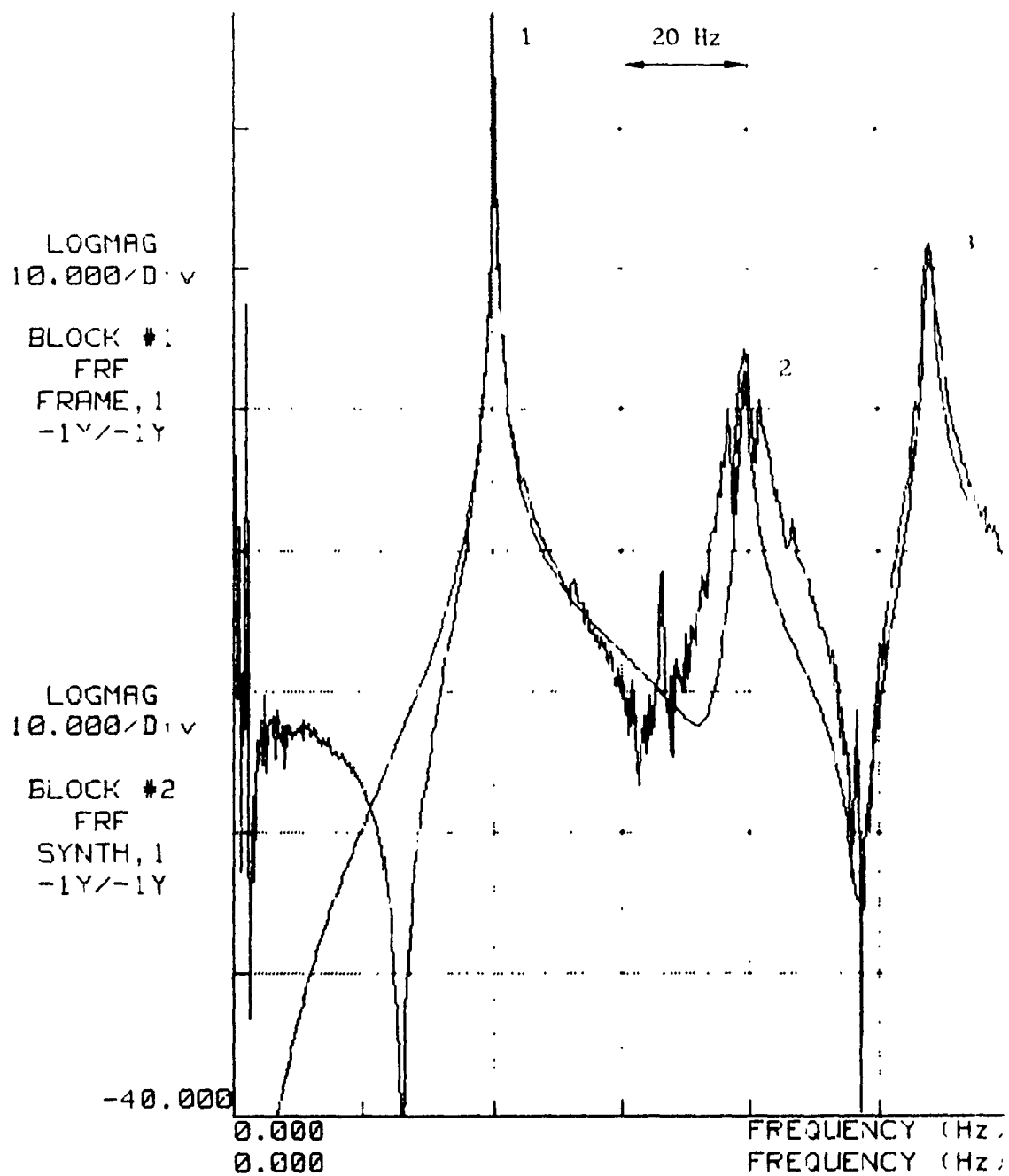


Figure 4-45: Comparison of Measurement at -1Y/-1Y and its Synthesized One Based on Local Curve-Fitting Method

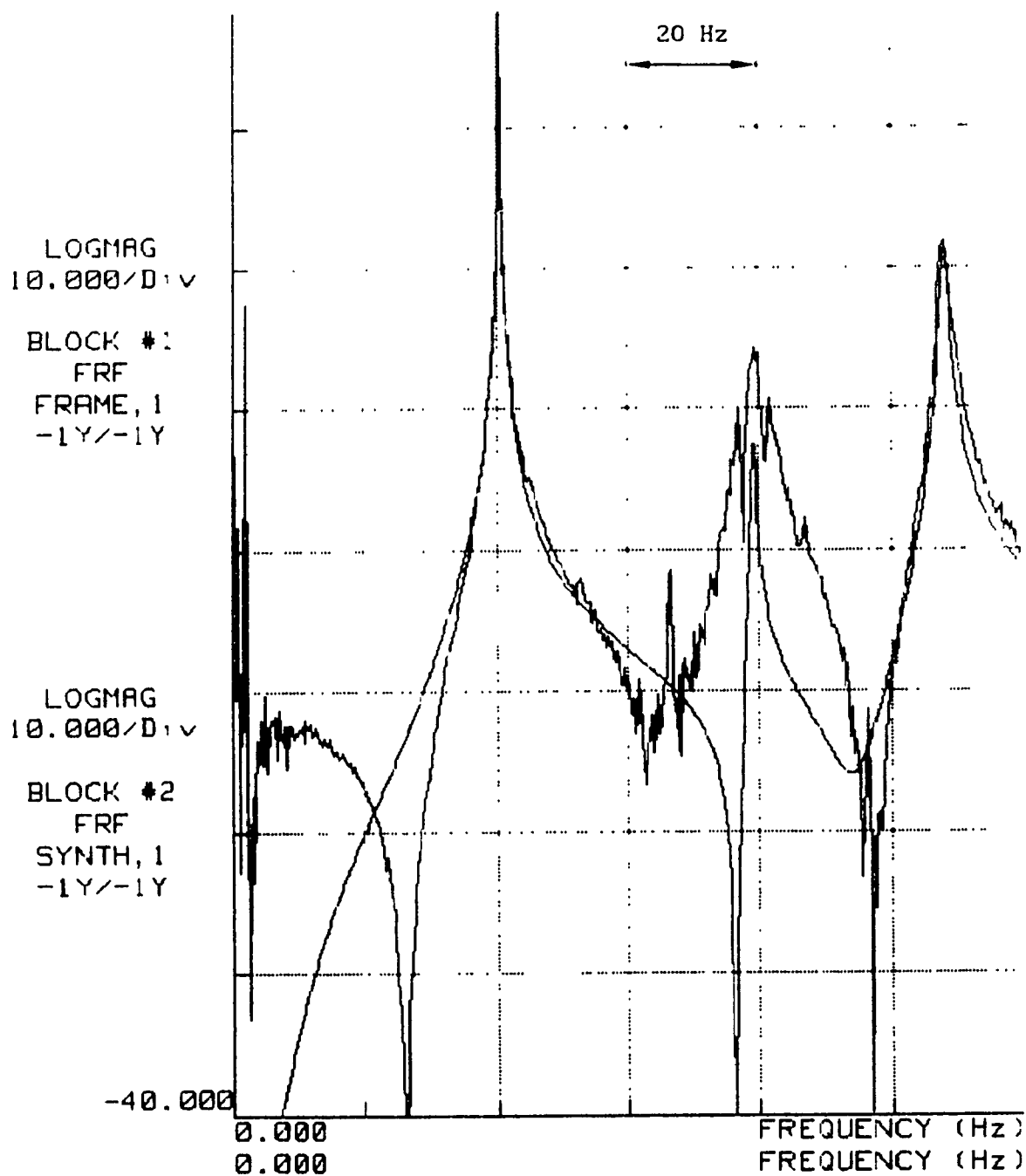


Figure 4-46: Comparison of Measurement at -1Y/-1Y and its Synthesized One Based on Global Curve-Fitting Method

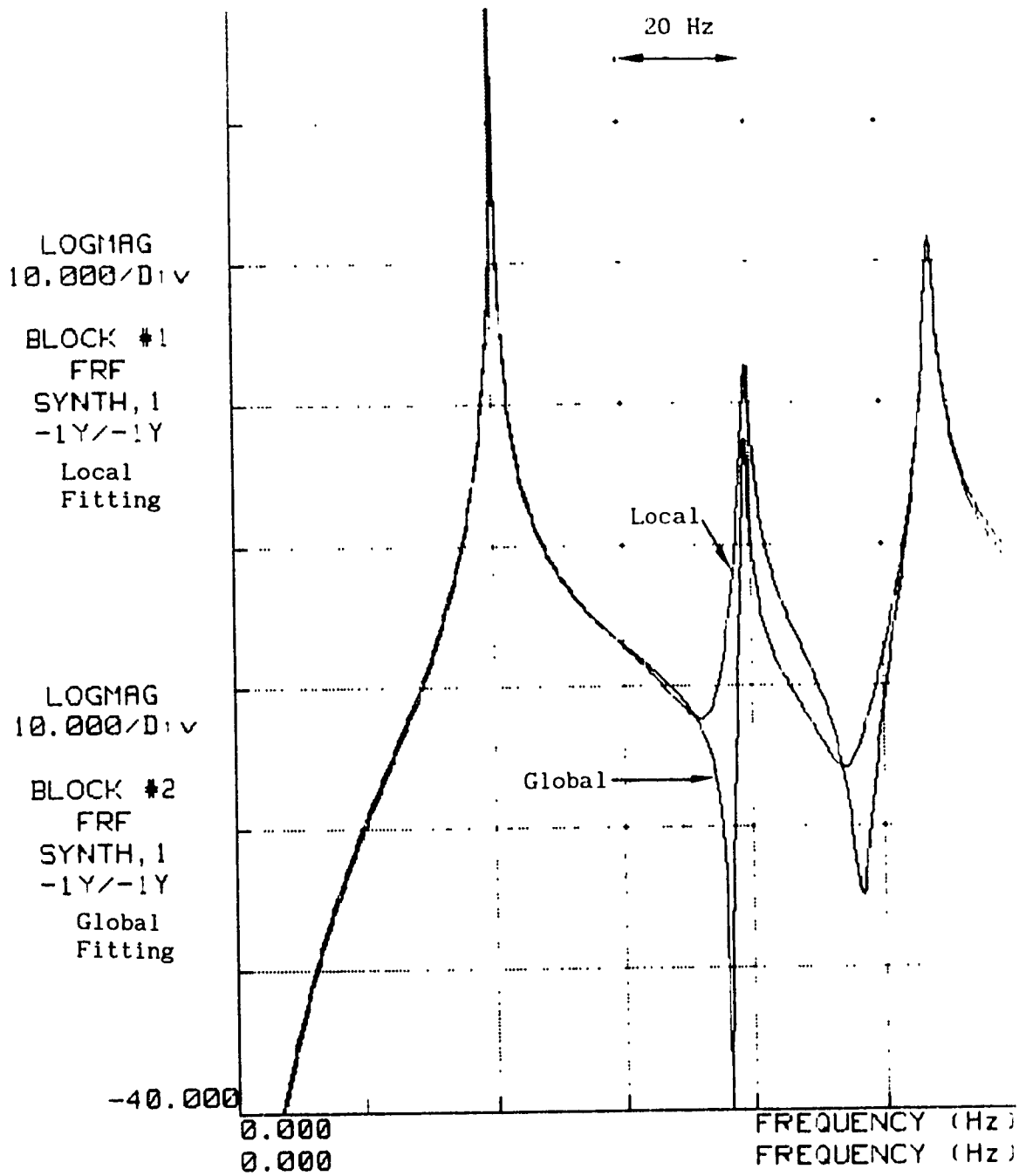


Figure 4-47: Comparison of Synthesized FRF Based on Local and Global Curve-Fitting Methods

Table 4-5: Extracted Modal Parameters: a) Based on Global Curve-Fitting,  
 b) Based on Local Curve-fitting

Global Curve-Fitting						
MEASUREMENT NUMBER: 1						
1.	D.O.F.'s:	-1 Y/	-1 Y	DAMP (%)	FREQ (Hz)	UNITS:MPS2/N -SEC.
MODE						
---	---	---	---	---	---	---
2.	1	40.495	.151	72.808	1.767	
3.	2	79.088	.427	10.530	19.191	
4.	3	107.973	.481	78.411	343.996	

Local Curve-Fitting						
MEASUREMENT NUMBER: 1						
1.	D.O.F.'s:	-1 Y/	-1 Y	DAMP (%)	FREQ (Hz)	UNITS:MPS2/N -SEC.
MODE						
---	---	---	---	---	---	---
2.	1	40.493	.158	76.131	2.880	
3.	2	79.333	.690	28.801	325.707	
4.	3	107.960	.478	79.429	345.600	



in large error even though the curve-fitting function closely matches the measurement data. "

#### 4-2-4 Documenting the Test Results

Two formal curve-fittings were carried-out, first using the FRF data measured along the Y-axis only (25 measurements) and then using all the FRF data, i.e. both the ones measured along the Y-and Z-axes (50 measurements in total).

For both results, local curve-fitting was used. Also both SDOF and MDOF methods with polynomial curve-fitting algorithm were used.

Table 4-6 shows the cursor bands and fit methods used to estimate the pole locations and then the residues at each measured points. FRF measurements measured at DOFs 24 Y / -1Y, -1Y / -1Y, and -3Y / -1Y were used to estimate the pole locations for modes 1, 2, and 3 to 5 respectively.

Table 4-7 shows the estimated frequency and damping values for the five modes.

The residues were sorted to obtain a mode shape for each mode. The unit modal masses and normal modes options of the sorting command were utilized.

Table 4-6: Cursor Bands and Fit Methods Used to Estimate the Pole Locations and the Residues at All Points

```

*** HALF FIT TABLE ***
-----
LOW CURSOR BAND   HIGH CURSOR BAND   FIT METHOD   RESIDUE
-----
1      25.500      45.500      HALF FIT   0.00000
2      26.500      46.500      HALF FIT   0.00000
3      76.750      81.500      MODIFIED   0.00000
-----

```

Table 4-7: Estimated Modal Parameters

```

*** FREQUENCY & DAMPING TABLE ***
-----
MODE   FREQUENCY   DAMPING   LABEL
-----
1      30.725      .565      .174
2      40.494      .156      .064
3      77.064      .226      .220
4      78.805      .504      .397
5      81.222      .220      .134
-----

```

The corresponding mode shapes for using Y only and both Y and Z FRF data are shown in Figures 4-48 to 4-52 and Figures 4-53 to 4-57 respectively along with their values in Tables 4-8 to 4-12 and Tables 4-13 to 4-17. We see that the mode shapes obtained from the Y FRF data are almost identical to the ones obtain from using both Y and Z FRF data, except for modes 3 and 4.

Mode 1 shows a local mode where basically only the rear panel is bending. Mode 2 shows almost a pure longitudinal twist. Modes 3 and 4 are symmetrical bending modes of the lower end section where the symmetrical points are 6 and 12 (see Figures 4-55 and 4-56). The fifth mode shows a combination of the first, third, and fourth modes.

Instead of a shaker excitation, if impact hammer techniques would have been used, similar results can be expected. However, the estimated modal damping would have to be corrected if a weighting function is used to reduce the noise on the response signal as discussed in Chapter 3. To illustrate this, a measurement was taken at DOFs -1Y/-1Y using an impact blow hammer. Both the input and output signals with the defined weighted functions (transient and exponential weighting functions) are shown in Figure 4-58. The computed FRF along with the Coherence function are shown Figures 4-59a and 4-59b, respectively.

The pole location around the 41 Hz modal peak was estimated using that measurement using the SMS software as discussed above. The modal

Figures 4-48 to 4-52

Mode Shapes Based on Y-FRF Data Only

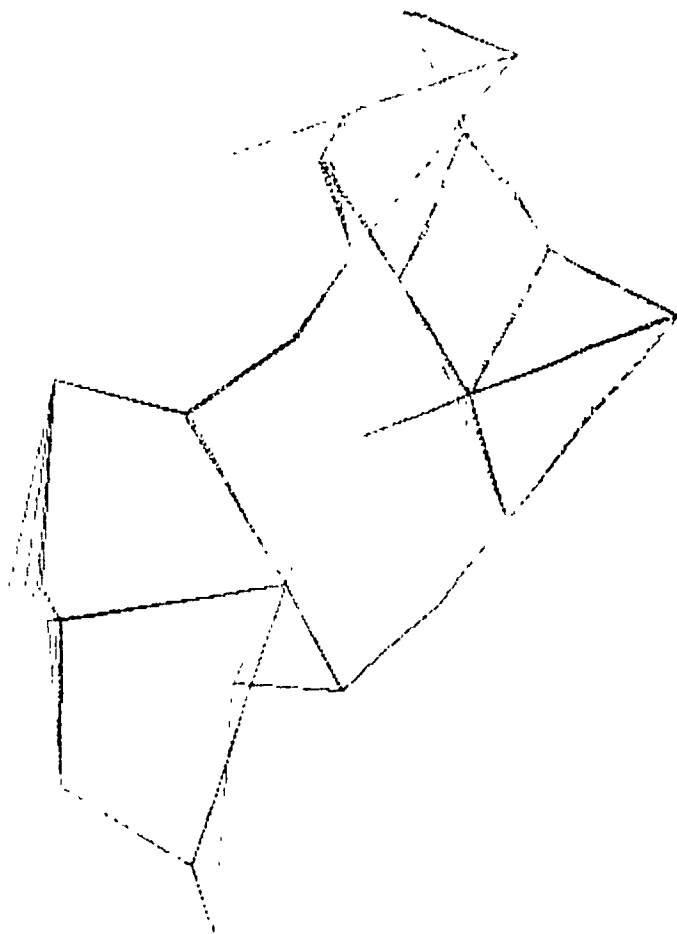


Figure 4-4S: Isometric View - Mode #1 (30,7 Hz)  
Local Bending of Rear Section

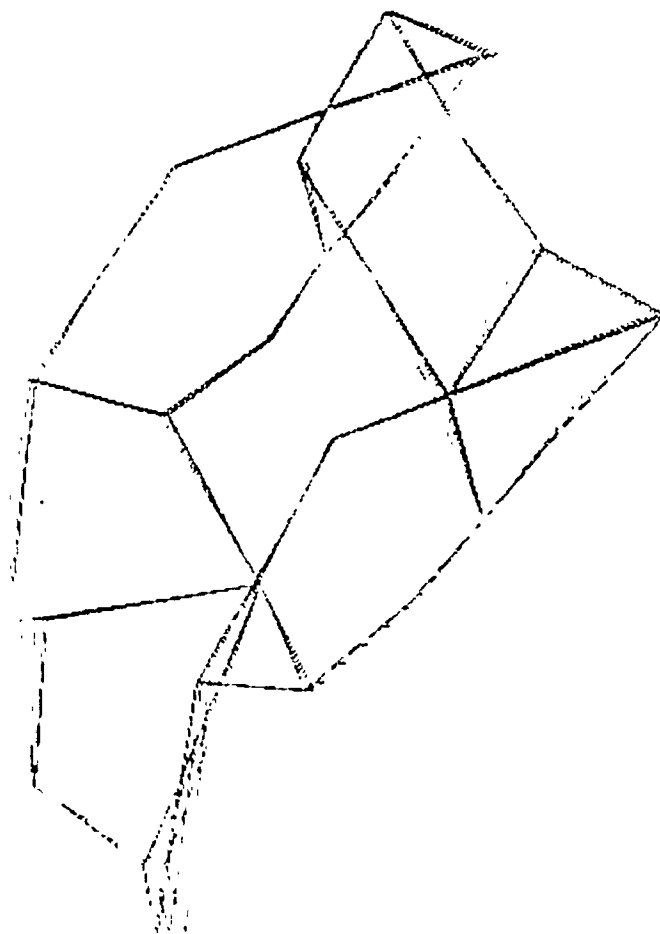


Figure 4-49: Isometric View - Mode #2 (40,5 Hz)  
Longitudinal Twist

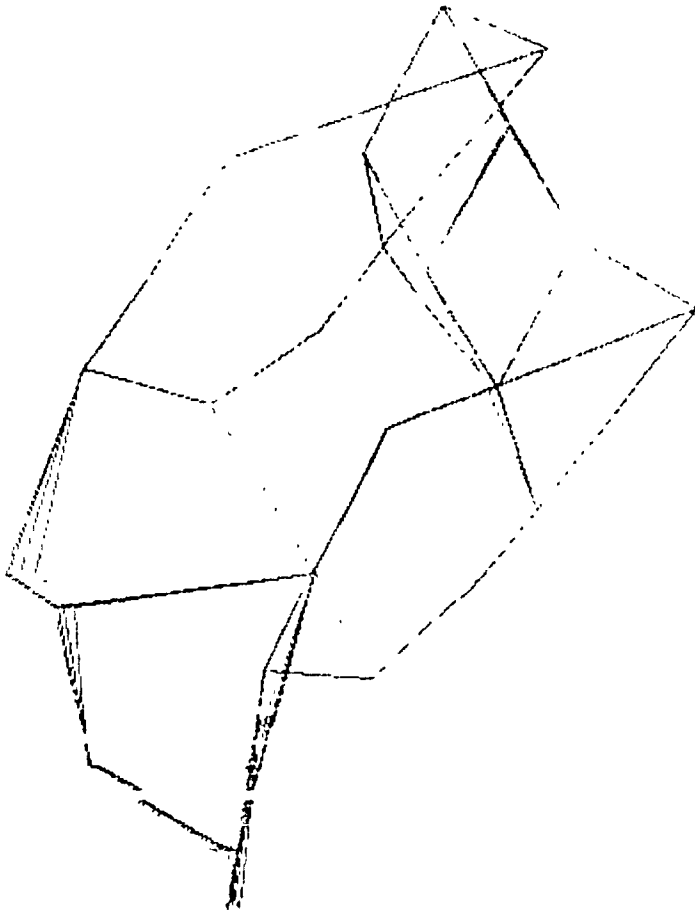


Figure 4-50: Isometric View - Mode #3 (77 : Hz)  
Twisting of Front End Only

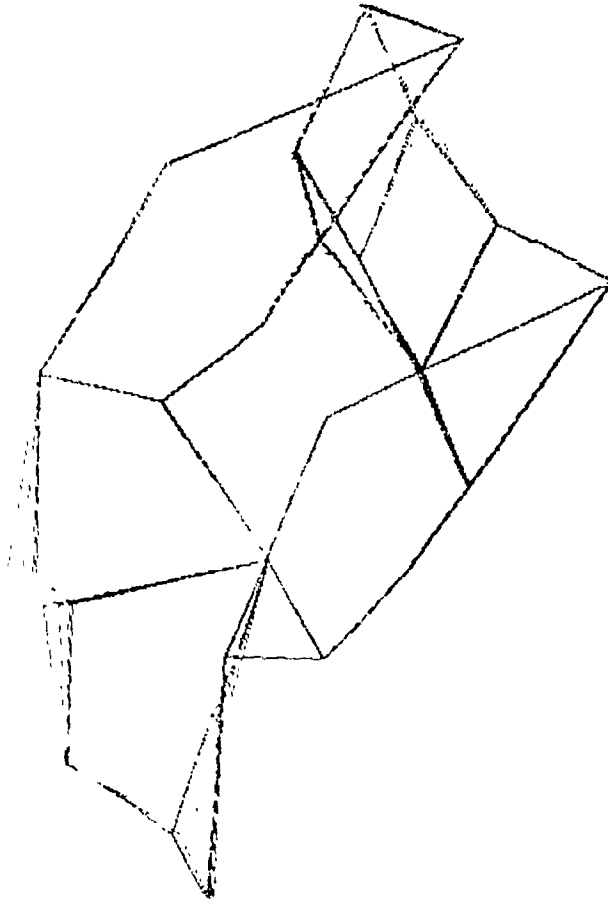


Figure 4-51: Isometric View - Mode #4 (78,8 Hz)  
Twisting of Front End with Small Local Bending of the  
Rear End



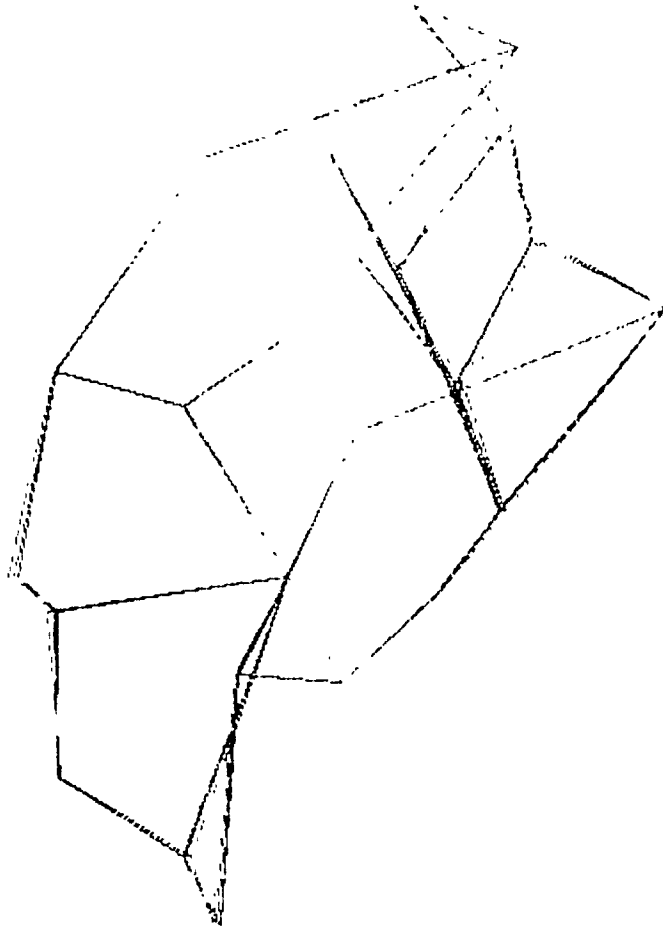


Figure 4-52: Isometric View - Mode #5 (81.2 Hz)  
Twisting of Front End with Local Excitation at a near tip

Figures 4-53 to 4-57

Mode Shapes Based on Y- and Z-FRF Data

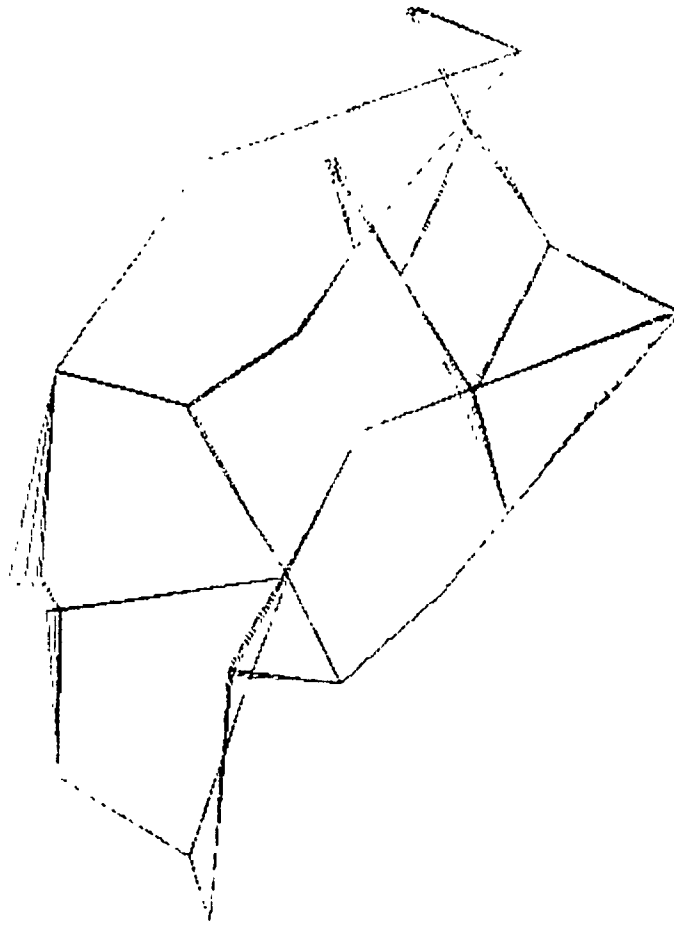


Figure 4-53: Isometric View - Mode #1 (60.7 Hz)  
Local Bending of Rear Section

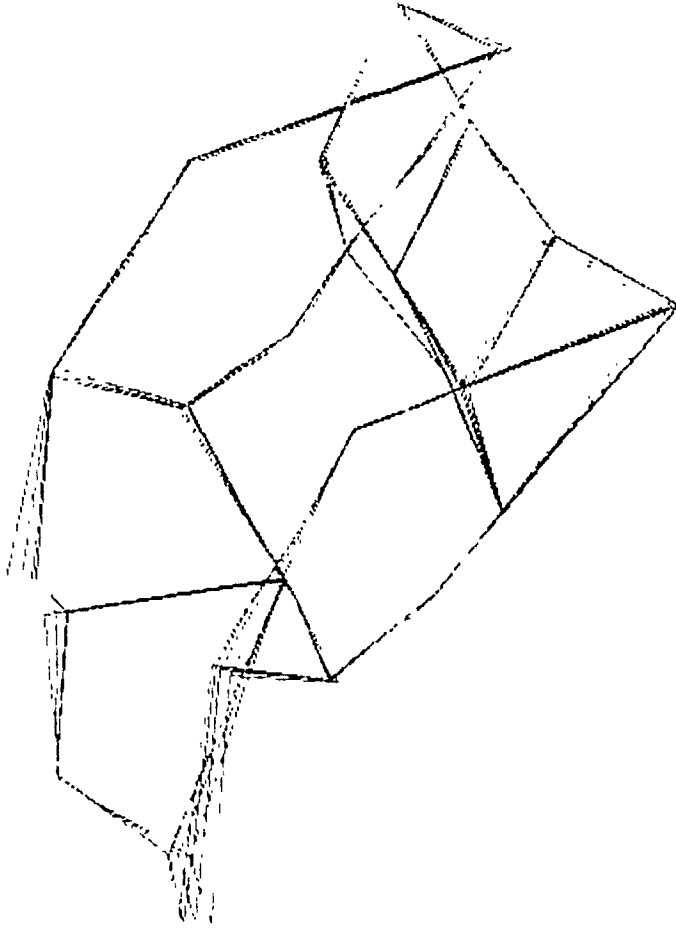


Figure 4-54: Isometric View - Mode #2 (40,5 Hz)  
Longitudinal Twist

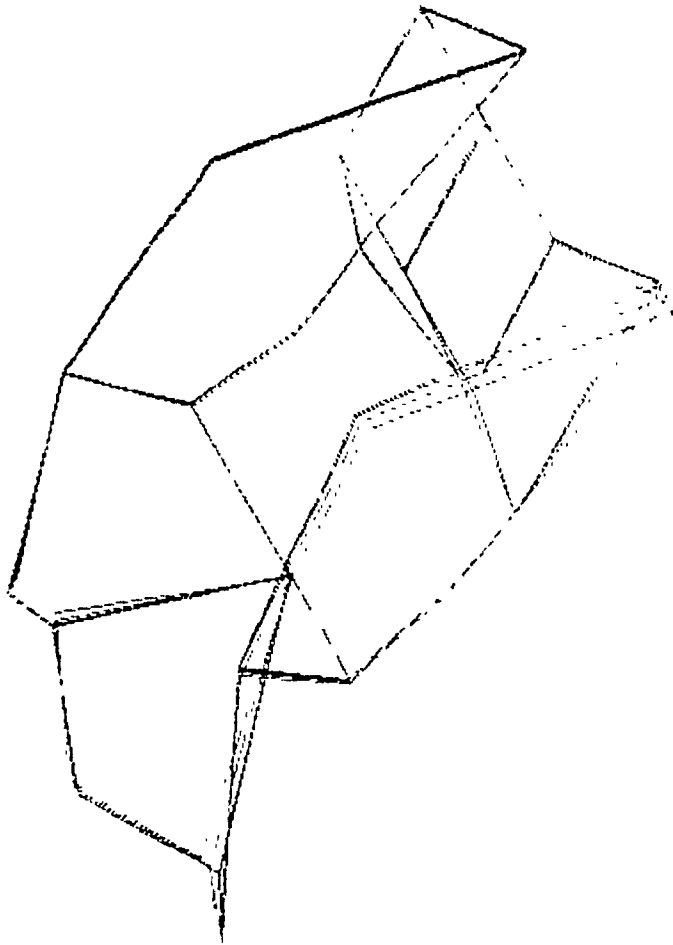


Figure 4-55. Isometric View - Mode #3 (77.1 Hz)  
Local Bending of Left Side Member with Small Twisting of  
Front End

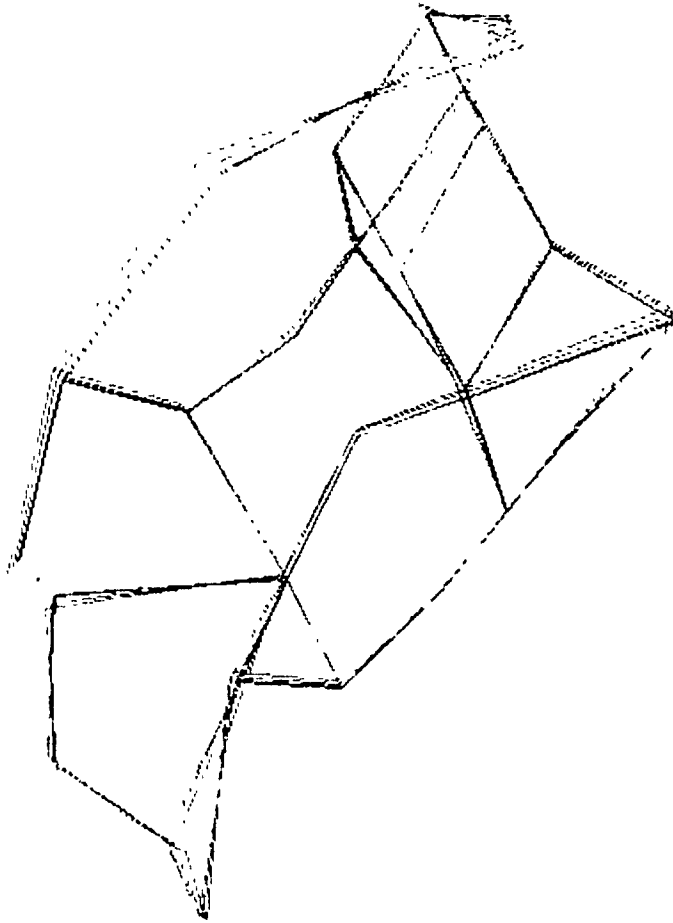


Figure 4-56: Isometric View - Mode #4 (78,8 Hz)  
Local Bending of Right Side Member

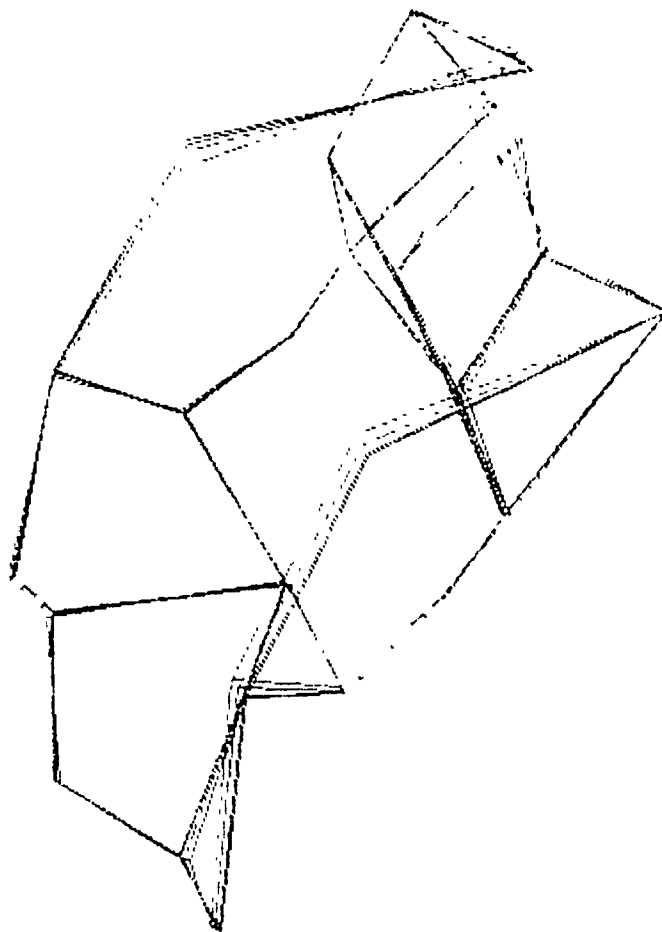


Figure 4-57: Isometric View - Mode #5 (81.2 Hz):  
Combination of Modes 1, 2, and 3

Table 4-8: Mode Shape Values - Mode #1 (Based on Y-FRF Data Only)

MODE NUMBER:			FREQ. Hz :			DAMP. % :			.033		
D.O.F			AMPLITUDE			PHASE					
-----			-----			-----					
1.			.047			0.000					
2.	2 Y		4.511m			0.000					
3.	3 Y		1.242			130.000					
4.	4 Y		.013			130.000					
5.	5 Y		.632			130.000					
6.	6 Y		.631			130.000					
7.	7 Y		910.774u			0.000					
8.	8 Y		.193			0.000					
9.	9 Y		.016			130.000					
10.	10 Y		.067			130.000					
11.	11 Y		.247			0.000					
12.	12 Y		.139			0.000					
13.	13 Y		414.692u			0.000					
14.	14 Y		1.145			130.000					
15.	15 Y		.113			130.000					
16.	16 Y		.173			130.000					
17.	17 Y		.742			130.000					
18.	18 Y		1.035			0.000					
19.	19 Y		1.026			0.000					
20.	20 Y		.062			0.000					
21.	21 Y		1.356			130.000					
22.	22 Y		2.113m			0.000					
23.	23 Y		1.796m			0.000					
24.	24 Y		1.711			0.000					
25.	25 Y		1.373m			130.000					



Table 4-9: Mode Shape Values - Mode #2 (Based on Y-IRF Data Only)

MODE NUMBER: 2		FREQ: 0.47	
	D.O.F.	AMPLITUDE	PHASE
1.	1 Y	.245	0.000
2.	2 Y	.101	0.000
3.	3 Y	.521	0.000
4.	4 Y	.170	100.000
5.	5 Y	.170	100.000
6.	6 Y	.1035	100.000
7.	7 Y	2.201m	100.000
8.	8 Y	.250	0.000
9.	9 Y	.101	0.000
10.	10 Y	.174	0.000
11.	11 Y	.166	0.000
12.	12 Y	.080	0.000
13.	13 Y	4.397m	100.000
14.	14 Y	.251	100.000
15.	15 Y	.080	100.000
16.	16 Y	.233	100.000
17.	17 Y	.100	100.000
18.	18 Y	.100	0.000
19.	19 Y	.100	0.000
20.	20 Y	.273	0.000
21.	21 Y	.400	100.000
22.	22 Y	.210	100.000
23.	23 Y	5.264m	100.000
24.	24 Y	.210	0.000
25.	25 Y	4.267m	100.000

Table 4-10: Mode Shape Values - Mode #3 (Based on Y-FRF Data Only)

MODE NUMBER: 3		DAMP. RATIO: .035	
FREQ. (Hz): 77.064			
D.O.F.	AMPLITUDE	PHASE	
1.	.101	2.000	
2.	.032	180.000	
3.	.032	0.000	
4.	5.522m	180.000	
5.	.014	180.000	
6.	.015	0.000	
7.	.017	180.000	
8.	.039	0.000	
9.	6.027m	180.000	
10.	.036	180.000	
11.	3.364m	0.000	
12.	6.320m	0.000	
13.	.013	180.000	
14.	.030	0.000	
15.	.029	0.000	
16.	0.000	0.000	
17.	.012	180.000	
18.	.019	180.000	
19.	.019	180.000	
20.	.131	180.000	
21.	.194	0.000	
22.	1.123m	0.000	
23.	0.351m	180.000	
24.	.055	2.000	
25.	1.551m	0.000	



Table 4-12: Mode Shape Values - Mode #5 (Based on Y-FRF Data Only)

MODE NUMBER	3	2448.41	.113
REZ. FRE. (Hz)	AMPLITUDE	PHASE	
-----	-----	-----	-----
1.	.153	90.000	
2.	.088	0.000	
3.	.143	90.000	
4.	.213	90.000	
5.	.073	180.000	
6.	.216	180.000	
7.	3.476m	0.000	
8.	.054	180.000	
9.	.020	180.000	
10.	.066	180.000	
11.	6.162m	0.000	
12.	.043	0.000	
13.	.033	0.000	
14.	.042	0.000	
15.	7.003m	180.000	
16.	.237	0.000	
17.	.153	0.000	
18.	4.200m	180.000	
19.	4.200m	180.000	
20.	.121	0.000	
21.	.125	180.000	
22.	7.340m	180.000	
23.	.232	0.000	
24.	.452	180.000	
25.	.065	0.000	

Table 4-13: Mode Shape Values - Mode #1  
(Based on Y- and Z-FRF Data)

MODE NUMBER: 1		DAMP. %: .565	
FREQ. (Hz):	AMPLITUDE	PHASE	
D.O.F.			
1.	.957	0.000	0.000
2.	.111	0.000	130.000
3.	.009	0.000	140.000
4.	.0019	180.000	150.000
5.	0.0004	180.000	160.000
6.	.009	0.000	170.000
7.	.002	180.000	180.000
8.	0.000	180.000	190.000
9.	1.000	180.000	200.000
10.	.001	0.000	210.000
11.	1.000	180.000	220.000
12.	.004	180.000	230.000
13.	.001	0.000	240.000
14.	.001	0.000	250.000
15.	.001	0.000	260.000
16.	.001	180.000	270.000
17.	.001	180.000	280.000
18.	.001	180.000	290.000
19.	.001	180.000	300.000
20.	.001	180.000	310.000
21.	.001	180.000	320.000
22.	.001	180.000	330.000
23.	.001	180.000	340.000
24.	.001	180.000	350.000
25.	.001	180.000	360.000
26.	.001	180.000	370.000
27.	.001	180.000	380.000
28.	.001	180.000	390.000
29.	.001	180.000	400.000
30.	.001	180.000	410.000
31.	.001	180.000	420.000
32.	.001	180.000	430.000
33.	.001	180.000	440.000
34.	.001	180.000	450.000
35.	.001	180.000	460.000
36.	.001	180.000	470.000
37.	.001	180.000	480.000
38.	.001	180.000	490.000
39.	.001	180.000	500.000
40.	.001	180.000	510.000
41.	.001	180.000	520.000
42.	.001	180.000	530.000
43.	.001	180.000	540.000
44.	.001	180.000	550.000
45.	.001	180.000	560.000
46.	.001	180.000	570.000
47.	.001	180.000	580.000
48.	.001	180.000	590.000
49.	.001	180.000	600.000
50.	.001	180.000	610.000
51.	.001	180.000	620.000
52.	.001	180.000	630.000
53.	.001	180.000	640.000
54.	.001	180.000	650.000
55.	.001	180.000	660.000
56.	.001	180.000	670.000
57.	.001	180.000	680.000
58.	.001	180.000	690.000
59.	.001	180.000	700.000
60.	.001	180.000	710.000
61.	.001	180.000	720.000
62.	.001	180.000	730.000
63.	.001	180.000	740.000
64.	.001	180.000	750.000
65.	.001	180.000	760.000
66.	.001	180.000	770.000
67.	.001	180.000	780.000
68.	.001	180.000	790.000
69.	.001	180.000	800.000
70.	.001	180.000	810.000
71.	.001	180.000	820.000
72.	.001	180.000	830.000
73.	.001	180.000	840.000
74.	.001	180.000	850.000
75.	.001	180.000	860.000
76.	.001	180.000	870.000
77.	.001	180.000	880.000
78.	.001	180.000	890.000
79.	.001	180.000	900.000
80.	.001	180.000	910.000
81.	.001	180.000	920.000
82.	.001	180.000	930.000
83.	.001	180.000	940.000
84.	.001	180.000	950.000
85.	.001	180.000	960.000
86.	.001	180.000	970.000
87.	.001	180.000	980.000
88.	.001	180.000	990.000
89.	.001	180.000	1000.000
90.	.001	180.000	1010.000
91.	.001	180.000	1020.000
92.	.001	180.000	1030.000
93.	.001	180.000	1040.000
94.	.001	180.000	1050.000
95.	.001	180.000	1060.000
96.	.001	180.000	1070.000
97.	.001	180.000	1080.000
98.	.001	180.000	1090.000
99.	.001	180.000	1100.000
100.	.001	180.000	1110.000
101.	.001	180.000	1120.000
102.	.001	180.000	1130.000
103.	.001	180.000	1140.000
104.	.001	180.000	1150.000
105.	.001	180.000	1160.000
106.	.001	180.000	1170.000
107.	.001	180.000	1180.000
108.	.001	180.000	1190.000
109.	.001	180.000	1200.000
110.	.001	180.000	1210.000
111.	.001	180.000	1220.000
112.	.001	180.000	1230.000
113.	.001	180.000	1240.000
114.	.001	180.000	1250.000
115.	.001	180.000	1260.000
116.	.001	180.000	1270.000
117.	.001	180.000	1280.000
118.	.001	180.000	1290.000
119.	.001	180.000	1300.000
120.	.001	180.000	1310.000
121.	.001	180.000	1320.000
122.	.001	180.000	1330.000
123.	.001	180.000	1340.000
124.	.001	180.000	1350.000
125.	.001	180.000	1360.000
126.	.001	180.000	1370.000
127.	.001	180.000	1380.000
128.	.001	180.000	1390.000
129.	.001	180.000	1400.000
130.	.001	180.000	1410.000
131.	.001	180.000	1420.000
132.	.001	180.000	1430.000
133.	.001	180.000	1440.000
134.	.001	180.000	1450.000
135.	.001	180.000	1460.000
136.	.001	180.000	1470.000
137.	.001	180.000	1480.000
138.	.001	180.000	1490.000
139.	.001	180.000	1500.000
140.	.001	180.000	1510.000
141.	.001	180.000	1520.000
142.	.001	180.000	1530.000
143.	.001	180.000	1540.000
144.	.001	180.000	1550.000
145.	.001	180.000	1560.000
146.	.001	180.000	1570.000
147.	.001	180.000	1580.000
148.	.001	180.000	1590.000
149.	.001	180.000	1600.000
150.	.001	180.000	1610.000
151.	.001	180.000	1620.000
152.	.001	180.000	1630.000
153.	.001	180.000	1640.000
154.	.001	180.000	1650.000
155.	.001	180.000	1660.000
156.	.001	180.000	1670.000
157.	.001	180.000	1680.000
158.	.001	180.000	1690.000
159.	.001	180.000	1700.000
160.	.001	180.000	1710.000
161.	.001	180.000	1720.000
162.	.001	180.000	1730.000
163.	.001	180.000	1740.000
164.	.001	180.000	1750.000
165.	.001	180.000	1760.000
166.	.001	180.000	1770.000
167.	.001	180.000	1780.000
168.	.001	180.000	1790.000
169.	.001	180.000	1800.000
170.	.001	180.000	1810.000
171.	.001	180.000	1820.000
172.	.001	180.000	1830.000
173.	.001	180.000	1840.000
174.	.001	180.000	1850.000
175.	.001	180.000	1860.000
176.	.001	180.000	1870.000
177.	.001	180.000	1880.000
178.	.001	180.000	1890.000
179.	.001	180.000	1900.000
180.	.001	180.000	1910.000
181.	.001	180.000	1920.000
182.	.001	180.000	1930.000
183.	.001	180.000	1940.000
184.	.001	180.000	1950.000
185.	.001	180.000	1960.000
186.	.001	180.000	1970.000
187.	.001	180.000	1980.000
188.	.001	180.000	1990.000
189.	.001	180.000	2000.000
190.	.001	180.000	2010.000
191.	.001	180.000	2020.000
192.	.001	180.000	2030.000
193.	.001	180.000	2040.000
194.	.001	180.000	2050.000
195.	.001	180.000	2060.000
196.	.001	180.000	2070.000
197.	.001	180.000	2080.000
198.	.001	180.000	2090.000
199.	.001	180.000	2100.000
200.	.001	180.000	2110.000
201.	.001	180.000	2120.000
202.	.001	180.000	2130.000
203.	.001	180.000	2140.000
204.	.001	180.000	2150.000
205.	.001	180.000	2160.000
206.	.001	180.000	2170.000
207.	.001	180.000	2180.000
208.	.001	180.000	2190.000
209.	.001	180.000	2200.000
210.	.001	180.000	2210.000
211.	.001	180.000	2220.000
212.	.001	180.000	2230.000
213.	.001	180.000	2240.000
214.	.001	180.000	2250.000
215.	.001	180.000	2260.000
216.	.001	180.000	2270.000
217.	.001	180.000	2280.000
218.	.001	180.000	2290.000
219.	.001	180.000	2300.000
220.	.001	180.000	2310.000
221.	.001	180.000	2320.000
222.	.001	180.000	2330.000
223.	.001	180.000	2340.000
224.	.001	180.000	2350.000
225.	.001	180.000	2360.000
226.	.001	180.000	2370.000
227.	.001	180.000	2380.000
228.	.001	180.000	2390.000
229.	.001	180.000	2400.000
230.	.001	180.000	2410.000
231.	.001	180.000	2420.000
232.	.001	180.000	2430.000
233.	.001	180.000	2440.000
234.	.001	180.000	2450.000
235.	.001	180.000	2460.000
236.	.001	180.000	2470.000
237.	.001	180.000	2480.000
238.	.001	180.000	2490.000
239.	.001	180.000	2500.000
240.	.001	180.000	2510.000
241.	.001	180.000	2520.000
242.	.001	180.000	2530.000
243.	.001	180.000	2540.000
244.	.001	180.000	2550.000
245.	.001	180.000	2560.000
246.	.001	180.000	2570.000
247.	.001	180.000	2580.000
248.	.001	180.000	2590.000
249.	.001	180.000	2600.000
250.	.001	180.000	2610.000
251.	.001	180.000	2620.000
252.	.001	180.000	2630.000
253.	.001	180.000	2640.000
254.	.001	180.000	2650.000
255.	.001	180.000	2660.000
256.	.001	180.000	2670.000
257.	.001	180.000	2680.000
258.	.001	180.000	2690.000
259.	.001	180.000	2700.000
260.	.001	180.000	2710.000
261.	.001	180.000	2720.000
262.	.001	180.000	2730.000
263.	.001	180.000	2740.000
264.	.001	180.000	2750.000
265.	.001	180.000	2760.000
266.	.001	180.000	2770.000
267.	.001	180.000	2780.000
268.	.001	180.000	2790.000

Table 4-14: Mode Shape Values - Mode #2  
(Based on Y- and Z-FRF Data)

Mode Number	FREQ. (Hz)	DIFF. (s)	DIFF. (in)	PHASE				
1.	1 Y	10.705	0.000	0.000	26.	1.0	1.1	0.000
2.	1 Z	.341	180.000	180.000	27.	4.9	4.9	180.000
3.	2 Y	.668	180.000	180.000	28.	1.0	1.0	180.000
4.	2 Z	2.966	180.000	180.000	29.	1.6	1.6	180.000
5.	3 Y	10.240	180.000	180.000	30.	1.6	1.6	180.000
6.	3 Z	.692	180.000	180.000	31.	5.6	5.6	180.000
7.	4 Y	2.652	180.000	180.000	32.	1.5	1.5	180.000
8.	4 Z	2.701	180.000	180.000	33.	2.5	2.5	180.000
9.	5 Y	2.459	180.000	180.000	34.	1.0	1.0	180.000
10.	5 Z	.452	180.000	180.000	35.	2.1	2.1	180.000
11.	6 Y	1.690	180.000	180.000	36.	1.1	1.1	180.000
12.	6 Z	.640	0.000	0.000	37.	2.1	2.1	0.000
13.	7 Y	.065	180.000	180.000	38.	1.0	1.0	180.000
14.	7 Z	.905	0.000	0.000	39.	2.1	2.1	0.000
15.	8 Y	5.155	0.000	0.000	40.	1.8	1.8	180.000
16.	8 Z	.658	0.000	0.000	41.	0.4	0.4	180.000
17.	9 Y	1.966	0.000	0.000	42.	1.1	1.1	180.000
18.	9 Z	.445	180.000	180.000	43.	1.0	1.0	180.000
19.	10 Y	5.476	0.000	0.000	44.	1.0	1.0	0.000
20.	10 Z	2.796	180.000	180.000	45.	1.2	1.2	180.000
21.	11 Y	3.270	0.000	0.000	46.	1.5	1.5	0.000
22.	11 Z	.505	180.000	180.000	47.	1.7	1.7	0.000
23.	12 Y	1.651	0.000	0.000	48.	1.2	1.2	180.000
24.	12 Z	.664	0.000	0.000	49.	1.0	1.0	180.000
25.	13 Y	.086	180.000	180.000	50.	1.1	1.1	0.000

Table 4-15: Mode Shape Values - Mode #3  
(Based on Y- and Z-FRF Data)

MODE NUMBER: 3      DAMP. (%): .286  
 FREQ. (Hz): 77.004

D.O.F.	AMPLITUDE	PHASE					
1.	1.9.8	0.000	.76.	12.7	1.0.0000		
2.	5.262	0.000	.27.	14.1	0.0000		
3.	.671	180.000	.20.	14.2	1.0.0000		
4.	5.246	0.000	.29.	15.7	0.0000		
5.	5.9.9	0.000	.20.	15.1	1.0.0000		
6.	5.547	0.000	.21.	16.1	0.0000		
7.	.111	180.000	.22.	16.2	1.0.0000		
8.	1.011	0.000	.23.	17.1	1.0.0000		
9.	.259	180.000	.14.	17.4	1.0.0000		
10.	.002	180.000	.25.	17.5	1.0.0000		
11.	.000	0.000	.15.	17.5	1.0.0000		
12.	.000	180.000	.26.	17.6	1.0.0000		
13.	.000	180.000	.16.	17.6	1.0.0000		
14.	.000	0.000	.17.	17.7	1.0.0000		
15.	.000	180.000	.18.	17.8	1.0.0000		
16.	.000	0.000	.19.	17.9	1.0.0000		
17.	.000	180.000	.20.	18.0	1.0.0000		
18.	.000	0.000	.21.	18.1	1.0.0000		
19.	.000	180.000	.22.	18.2	1.0.0000		
20.	.000	0.000	.23.	18.3	1.0.0000		
21.	.000	180.000	.24.	18.4	1.0.0000		
22.	.000	0.000	.25.	18.5	1.0.0000		
23.	.000	180.000	.26.	18.6	1.0.0000		
24.	.000	0.000	.27.	18.7	1.0.0000		
25.	.000	180.000	.28.	18.8	1.0.0000		
26.	.000	0.000	.29.	18.9	1.0.0000		
27.	.000	180.000	.30.	19.0	1.0.0000		
28.	.000	0.000	.31.	19.1	1.0.0000		
29.	.000	180.000	.32.	19.2	1.0.0000		
30.	.000	0.000	.33.	19.3	1.0.0000		
31.	.000	180.000	.34.	19.4	1.0.0000		
32.	.000	0.000	.35.	19.5	1.0.0000		
33.	.000	180.000	.36.	19.6	1.0.0000		
34.	.000	0.000	.37.	19.7	1.0.0000		
35.	.000	180.000	.38.	19.8	1.0.0000		
36.	.000	0.000	.39.	19.9	1.0.0000		
37.	.000	180.000	.40.	20.0	1.0.0000		
38.	.000	0.000	.41.	20.1	1.0.0000		
39.	.000	180.000	.42.	20.2	1.0.0000		
40.	.000	0.000	.43.	20.3	1.0.0000		
41.	.000	180.000	.44.	20.4	1.0.0000		
42.	.000	0.000	.45.	20.5	1.0.0000		
43.	.000	180.000	.46.	20.6	1.0.0000		
44.	.000	0.000	.47.	20.7	1.0.0000		
45.	.000	180.000	.48.	20.8	1.0.0000		
46.	.000	0.000	.49.	20.9	1.0.0000		
47.	.000	180.000	.50.	21.0	1.0.0000		
48.	.000	0.000	.51.	21.1	1.0.0000		
49.	.000	180.000	.52.	21.2	1.0.0000		
50.	.000	0.000	.53.	21.3	1.0.0000		
51.	.000	180.000	.54.	21.4	1.0.0000		
52.	.000	0.000	.55.	21.5	1.0.0000		
53.	.000	180.000	.56.	21.6	1.0.0000		
54.	.000	0.000	.57.	21.7	1.0.0000		
55.	.000	180.000	.58.	21.8	1.0.0000		
56.	.000	0.000	.59.	21.9	1.0.0000		
57.	.000	180.000	.60.	22.0	1.0.0000		
58.	.000	0.000	.61.	22.1	1.0.0000		
59.	.000	180.000	.62.	22.2	1.0.0000		
60.	.000	0.000	.63.	22.3	1.0.0000		
61.	.000	180.000	.64.	22.4	1.0.0000		
62.	.000	0.000	.65.	22.5	1.0.0000		
63.	.000	180.000	.66.	22.6	1.0.0000		
64.	.000	0.000	.67.	22.7	1.0.0000		
65.	.000	180.000	.68.	22.8	1.0.0000		
66.	.000	0.000	.69.	22.9	1.0.0000		
67.	.000	180.000	.70.	23.0	1.0.0000		
68.	.000	0.000	.71.	23.1	1.0.0000		
69.	.000	180.000	.72.	23.2	1.0.0000		
70.	.000	0.000	.73.	23.3	1.0.0000		
71.	.000	180.000	.74.	23.4	1.0.0000		
72.	.000	0.000	.75.	23.5	1.0.0000		
73.	.000	180.000	.76.	23.6	1.0.0000		
74.	.000	0.000	.77.	23.7	1.0.0000		
75.	.000	180.000	.78.	23.8	1.0.0000		
76.	.000	0.000	.79.	23.9	1.0.0000		
77.	.000	180.000	.80.	24.0	1.0.0000		
78.	.000	0.000	.81.	24.1	1.0.0000		
79.	.000	180.000	.82.	24.2	1.0.0000		
80.	.000	0.000	.83.	24.3	1.0.0000		
81.	.000	180.000	.84.	24.4	1.0.0000		
82.	.000	0.000	.85.	24.5	1.0.0000		
83.	.000	180.000	.86.	24.6	1.0.0000		
84.	.000	0.000	.87.	24.7	1.0.0000		
85.	.000	180.000	.88.	24.8	1.0.0000		
86.	.000	0.000	.89.	24.9	1.0.0000		
87.	.000	180.000	.90.	25.0	1.0.0000		
88.	.000	0.000	.91.	25.1	1.0.0000		
89.	.000	180.000	.92.	25.2	1.0.0000		
90.	.000	0.000	.93.	25.3	1.0.0000		
91.	.000	180.000	.94.	25.4	1.0.0000		
92.	.000	0.000	.95.	25.5	1.0.0000		
93.	.000	180.000	.96.	25.6	1.0.0000		
94.	.000	0.000	.97.	25.7	1.0.0000		
95.	.000	180.000	.98.	25.8	1.0.0000		
96.	.000	0.000	.99.	25.9	1.0.0000		
97.	.000	180.000	1.00.	26.0	1.0.0000		

Table 4-16: Mode Shape Values - Mode #4  
(Based on Y- and Z-FRF Data)

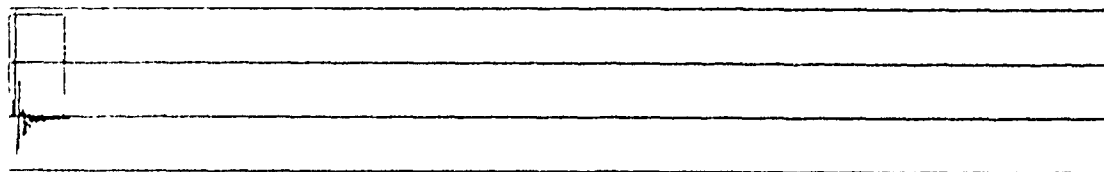
MODE NUMBER: 4		DAMP. (%): .504	
FREQUENCY: 0.005			
D.O.F.	AMPLITUDE	PHASE	
1.	3.271	0.000	0.000
2.	5.698	180.000	0.000
3.	1.736	180.000	0.000
4.	17.503	190.000	0.000
5.	14.658	180.000	0.000
6.	12.558	180.000	0.000
7.	9.917	180.000	0.000
8.	10.990	0.000	0.000
9.	2.172	180.000	0.000
10.	6.980	0.000	180.000
11.	2.116	180.000	0.000
12.	5.505	0.000	0.000
13.	3.027	180.000	0.000
14.	8.875	0.000	0.000
15.	2.069	180.000	0.000
16.	24.762	180.000	180.000
17.	3.259	180.000	180.000
18.	18.858	0.000	180.000
19.	1.563	180.000	0.000
20.	8.480	0.000	180.000
21.	9.917	0.000	0.000
22.	7.077	0.000	0.000
23.	1.031	0.000	0.000
24.	2.730	0.000	180.000
25.	1.257	0.000	180.000
26.			
27.			
28.			
29.			
30.			
31.			
32.			
33.			
34.			
35.			
36.			
37.			
38.			
39.			
40.			
41.			
42.			
43.			
44.			
45.			
46.			
47.			
48.			
49.			
50.			



Table 4-17: Mode Shape Values - Mode #5  
(Based on Y- and Z-FRF Data)

MODE NUMBER: 5		DAMP. (%): .288	
FREQ. (Hz): 51.223			
D.O.F.	AMPLITUDE	PHASE	
1. Y	2.557	180.000	0.000
2. Z	.447	0.000	0.000
3. Y	1.292	0.000	180.000
4. Z	1.757	180.000	180.000
5. Y	2.913	180.000	0.000
6. Z	1.631	180.000	0.000
7. Y	.372	180.000	0.000
8. Z	1.529	180.000	0.000
9. Y	.762	180.000	0.000
10. Z	1.150	0.000	0.000
11. Y	.709	180.000	0.000
12. Z	.115	0.000	0.000
13. Y	.083	0.000	0.000
14. Z	.110	0.000	0.000
15. Y	1.011	180.000	0.000
16. Z	.446	0.000	0.000
17. Y	.600	180.000	0.000
18. Z	.311	180.000	0.000
19. Y	.600	0.000	0.000
20. Z	.311	180.000	0.000
21. Y	.600	0.000	0.000
22. Z	.311	180.000	0.000
23. Y	.600	0.000	0.000
24. Z	.311	180.000	0.000
25. Y	.600	0.000	0.000
26. Z	.311	180.000	0.000
27. Y	.600	0.000	0.000
28. Z	.311	180.000	0.000
29. Y	.600	0.000	0.000
30. Z	.311	180.000	0.000
31. Y	.600	0.000	0.000
32. Z	.311	180.000	0.000
33. Y	.600	0.000	0.000
34. Z	.311	180.000	0.000
35. Y	.600	0.000	0.000
36. Z	.311	180.000	0.000
37. Y	.600	0.000	0.000
38. Z	.311	180.000	0.000
39. Y	.600	0.000	0.000
40. Z	.311	180.000	0.000
41. Y	.600	0.000	0.000
42. Z	.311	180.000	0.000
43. Y	.600	0.000	0.000
44. Z	.311	180.000	0.000
45. Y	.600	0.000	0.000
46. Z	.311	180.000	0.000
47. Y	.600	0.000	0.000
48. Z	.311	180.000	0.000
49. Y	.600	0.000	0.000
50. Z	.311	180.000	0.000

W1 TIME CH A REAL INPUT MAIN Y -127mU  
 Y 51.00 X 0.0ms  
 X 0.0ms + 2s

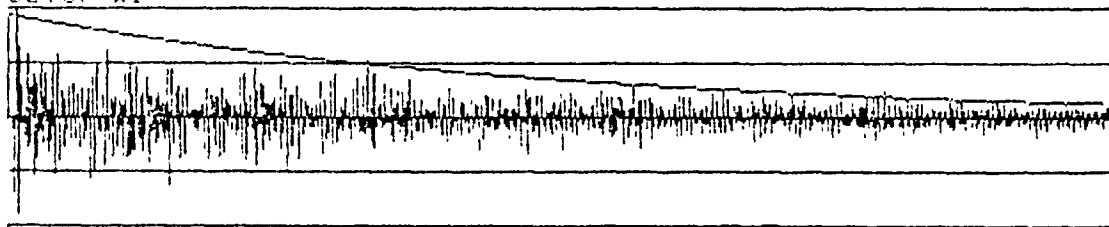


SETUP W1

MEASUREMENT DUAL SPECTRUM AVERAGING  
 TRIGGER CH A +SLOPE LEVEL +0.10 MAX INPUT  
 DELAY TRIG-A -1.0ms CH A-B 0.0ms  
 AVERAGING LIN 2  
 FREQ SPAN 300Hz ΔF 250mHz T 4s ΔT 1.95ms  
 CENTER FREQ BASEBAND  
 WEIGHT CH A TRANSIENT SHIFT 0.0ms LENGTH 99.5ms  
 WEIGHT CH B EXPONENTIAL SHIFT 0.0ms LENGTH 1.0000s  
 CH A 80mV + 3Hz DIR FILT 25 6kHz 230uV/N  
 CH B 2V + 3Hz DIR FILT 25 6kHz 101mV/G  
 GENERATOR DISABLED

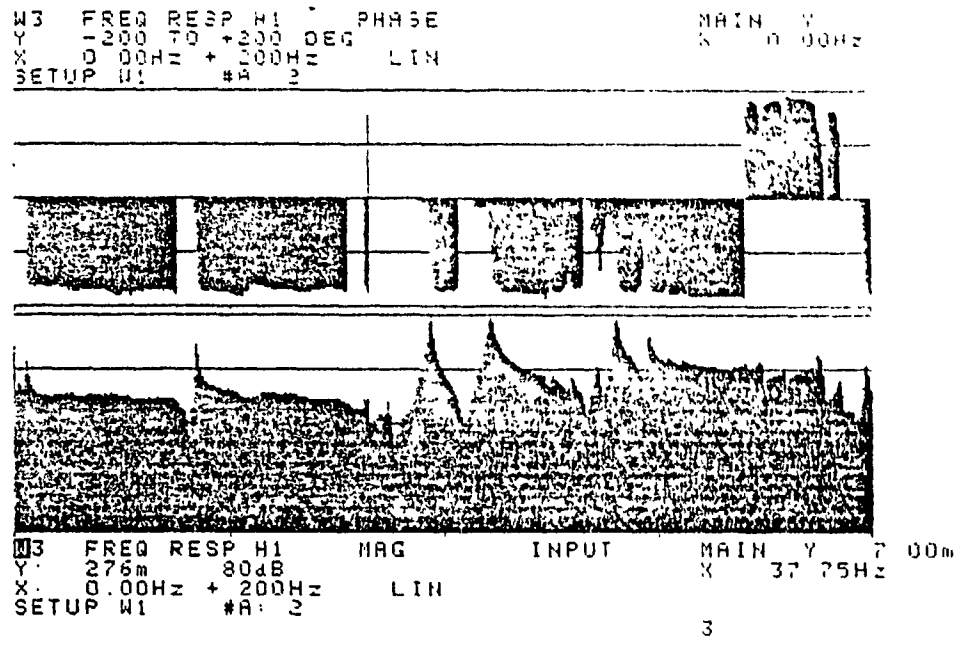
a)

W2 TIME CH B REAL MAIN Y 3.63mU  
 Y 789mU X 0.0ms  
 X 0.0ms + 2s  
 SETUP W1

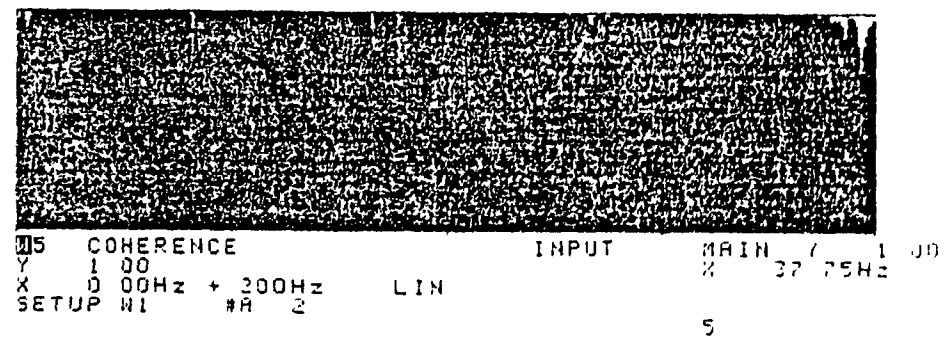


b)

Figure 4-58: Time Signals: a) Impulse Signal with a Rectangular Window, b) Response Signal with an Exponential Window



a)



b)

Figure 4-59: Based on Impact Hammer Techniques:  
 a) FRF Measurement Measured at DOFs -1Y/-1Y,  
 b) Coherence Function Computed at DOFs -1Y/-1Y

frequency and modal damping were estimated to 41,84 Hz and 0,503% respectively. Previously, the modal damping was founded to be 0,158% for that mode (see Table 4-5). The calculations to correct the estimated damping are as follow [6]:

Defining the following terms,

$\tau_{\omega}$  = Width of the exponential window (second), i.e. the time required for the amplitude to decay by a factor of  $e = 2,72$  or 8,7 dB.

$\sigma = 1/\tau$  (rad./sec)

$\sigma_{\text{H}}$  = Estimated modal damping ( $\text{sec}^{-1}$ )

$\omega_{\text{H}}$  = Estimated modal frequency (rad./sec)

$f_{\text{H}}$  = Estimated modal frequency (Hertz)

$\zeta_{\text{H}}$  = Estimated damping factor

$\sigma_{\text{K}}$  = Corrected modal damping ( $\text{sec}^{-1}$ )

We know that,

$$\sigma_{\text{H}} = \zeta_{\text{H}} \omega_{\text{H}} = \zeta_{\text{H}} (2\pi f_{\text{H}}) \quad (4-2)$$

From [6], we have,

$$\sigma_{\text{K}} = \sigma_{\text{H}} - \sigma_{\omega} \quad (4-3)$$

For the example, we have

$$\tau_{\omega} = 1 \text{ sec} ; \quad \zeta_M = 0,503\% ; \quad f_M = 41,84 \text{ Hertz}$$

The corrected damping value can be calculated as follow

$$\sigma_K = \sigma_M - \sigma_{\omega} = \zeta_M (2\pi f_M) - 1/\tau_{\omega} = 0,00503 (83,68\pi) - 1 = 0,322 \text{ rad/sec}$$

or

$$\zeta_K = \sigma_K / \omega_M = \sigma_K / (2\pi f_M) = 0,322 / (83,68\pi) = 0,123\%$$

#### **4-3 Case II: Modal Testing of Large Vehicle Structures**

In case II, experimental modal testing was conducted on the three vehicle structures (rail wagons) shown in Figures 4-2 to 4-4 to evaluate their major modes of vibration.

The objective of each test was to determine the modal parameters (modal frequency, modal damping, and mode shape) in the frequency range of 5 to 25 Hz.

Exploratory vibration testing was carried-out on the first

structure using impact hammer, sledge hammer, and shaker excitation techniques. It was found that both hammer techniques were ill-suited for carrying out the testing. In the case of the impact hammer technique, the input vibration energy was not sufficient enough to get a good signal-to-noise-ratio (at least 20dB) even close to the impacted point. On the other hand, although it is possible to generate high input vibration energy using sledge hammer technique, the local stress levels and deflections were found to be high and also the signal-to-noise-ratio at extreme points of the vehicle structure were small and unacceptable (i.e. far away from the excited point). Also, sledge hammer technique is not recommended for such large structures, since it is a heavy piece of equipment to be carried around to excite all points, and also it is not safe to use when impacting points which had to be reached using a ladder.

An electrodynamic shaker used in the modal testing of the snowmobile frame structure was utilized for the first phase of the testing on one vehicle structure.

The following observations and conclusions were drawn:

- 1) The lateral excitation with the shaker gave higher signal-to-noise ratio compared to the vertical excitation.

- 2) The location at mid-span of the structure in the middle of a window opening (point #43 in Figure 4-60) was found to excite all three directions with high output (acceleration) signals at the extreme points of the structure in the frequency band of interest. Hence, this location was selected as the driving point for the exciter.
  
- 3) The ambient noise at the test site during the normal operation of the plant was found to be too high and interfered on with the vibration response signal. It was decided that in order to get good (high) signal-to-noise ratio, the testing was carried-out when the plant was shut-down.

Prior to actual testing, the modal geometry was prepared in the SMS database using the engineering drawings. The structure was discretized into 70 points and the response signals were planned to be measured along X-, Y-, and Z-axes for all the points, for a total of 210 FRF measurements.

From the initial phase of the testing, two more observations were made. The first one was that the quadrature of the inertance-FRF, along the longitudinal axis (X- direction) on the vehicle structure, was found to be relatively small in comparison with the other two axes, i.e. Y- and Z- directions. The second one was that the time for one FRF measurement, using 3 averages/measurement, was approximately 10 minutes. Based on those observations, the modal geometry of the vehicle structure was reduced from 70 to 43 test points and the measurements were recorded along the Y-and Z-axes for a total of 86 measurements. A schematic

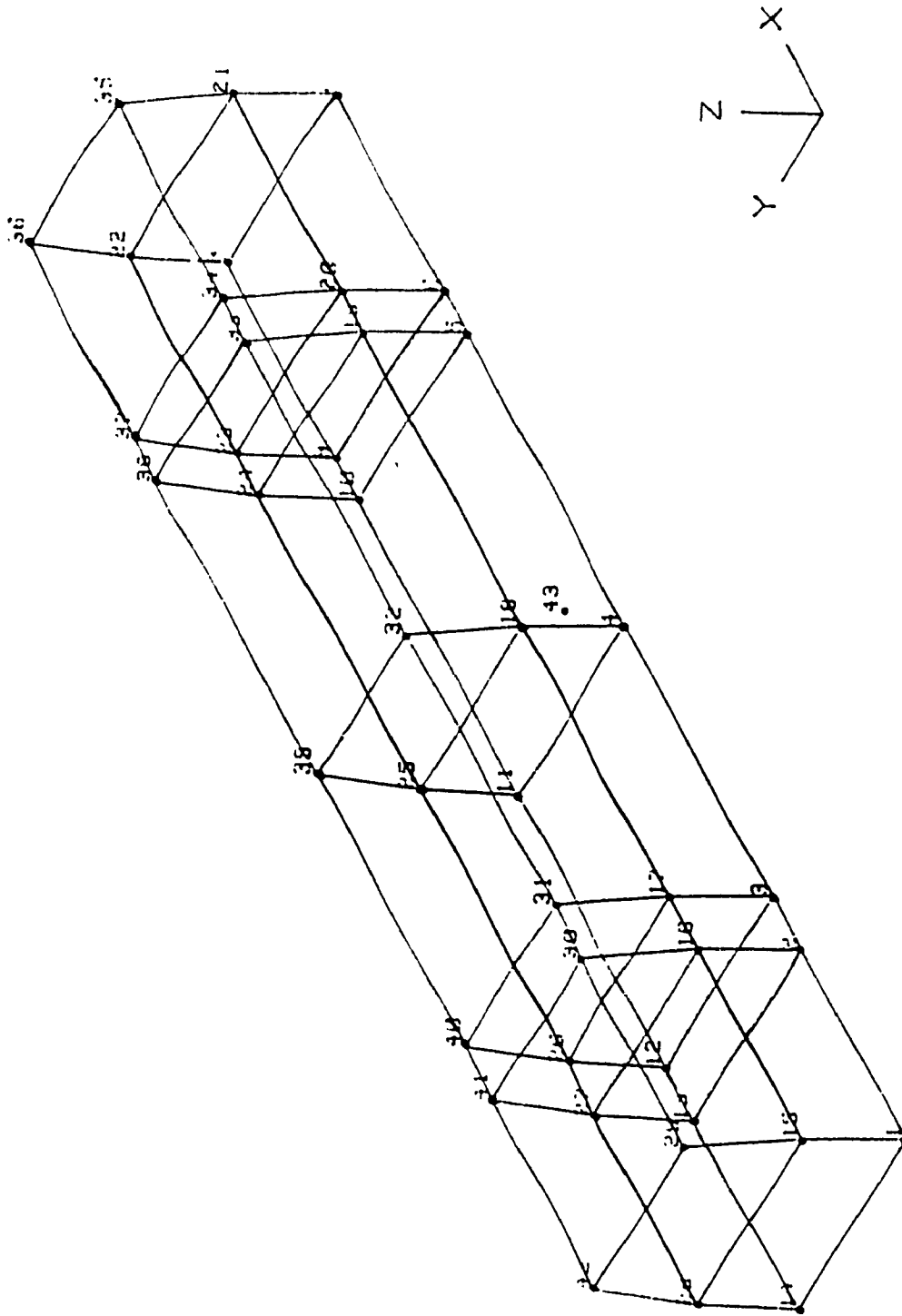


Figure 4-60: Schematic 3-D Model of the First Large Vehicle Structure [17]



three-dimensional model of the vehicle structure is illustrated in Figure 4-61, which includes measurement points and shaker location.

It is important that an equalization process be carried-out not only to compensate the FRF measurements at the analysis stage, for the load-cell calibration and the motion transducer response errors, but to verify that the force transducer-accelerometer system is behaving correctly. Note that it is important for that verification to use the same electrical wires as in the case of the actual testing.

In addition, it is recommended to monitor the measured signals on an oscilloscope and to compute the coherence functions and signal-to-noise ratios to verify for the acceptable quality of the input and output signals prior to storing the FRF functions.

For each vehicle structure, pseudo-random input (0-50 Hz with random phase) was used as the excitation source. A piezoelectric accelerometer and a force transducer were used to measure accelerations along Z-, and Y-directions at the selected measurement points and forces at the actuator attachment point respectively.

The techniques to identify the modal peaks, discussed earlier, were used.

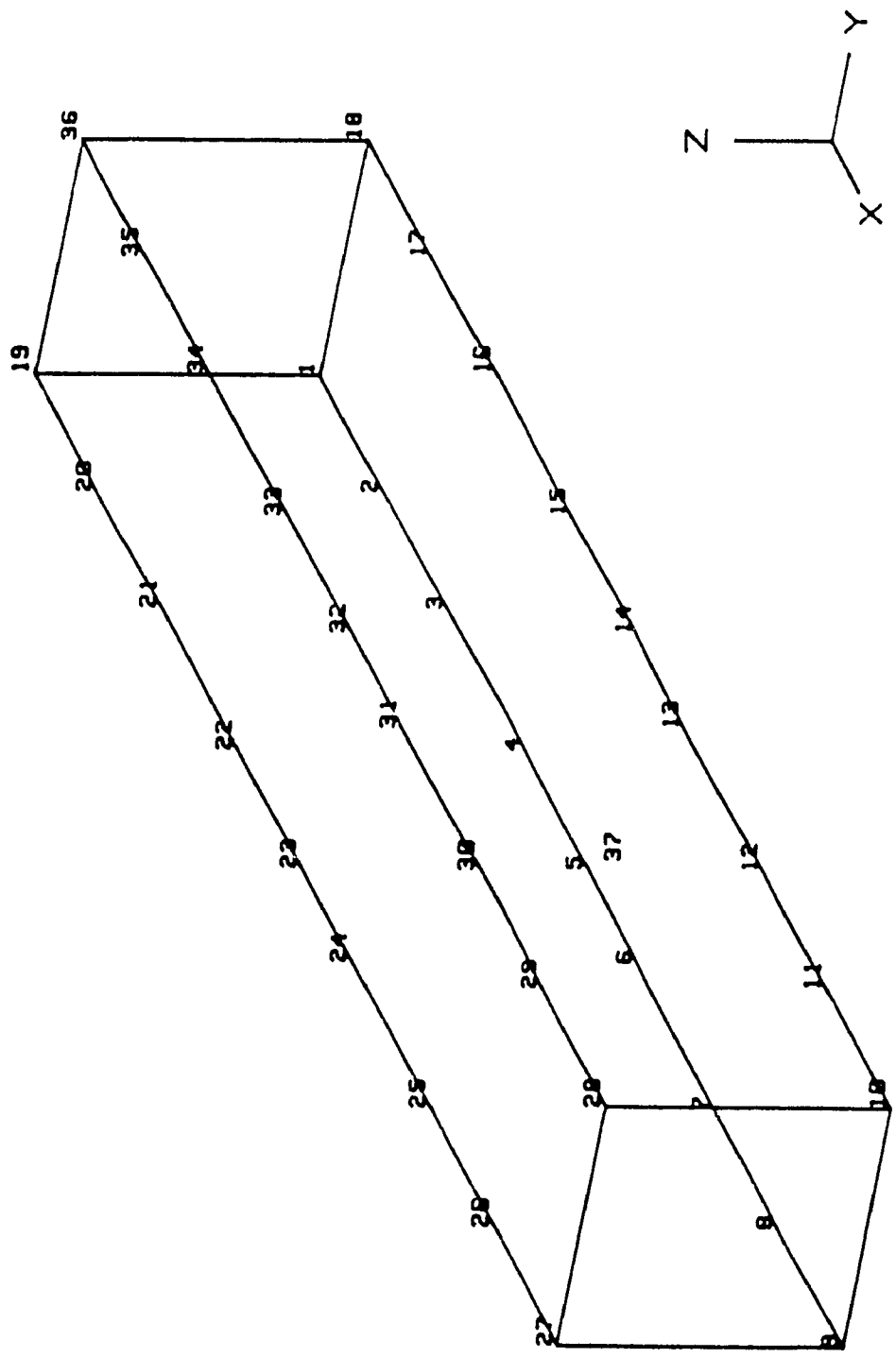


Figure 4-61: Schematic 3-D Model of the Second Large Vehicle Structure for Vertical Excitation [18]

Although the frequency range of interest was from 5 to 25 Hz, the measurements were taken in the bandwidth from 0 to 50 Hz. The reasons for this were to identify the vehicle rigid body modes and any elastic modes in the low frequency range 0 to 5 Hz. Secondly, to recognize any dominant modes in the 25 to 50 Hz region.

The second vehicle structure was discretized into 37 points for measurements in both vertical and lateral directions. The schematic three-dimensional models are illustrated in Figures 4-61 and 4-62 which include measurement points (points 1 to 37) and shaker location (point 37). An electro-hydraulic shaker system made by Ling Electronic Inc. was used to excite the car body. It was first excited vertically by locating the actuator at the mid span of the vehicle structure on its longitudinal beam, i.e. at point 37 acting along Z-axis as shown in Figure 4-61, and 74 FRF measurements were taken. Then, the vehicle structure was excited laterally by hanging the actuator through a crane and attaching it at the mid-span of the car body in the middle of the window opening, i.e. at point 37 acting along Y-axis as shown in Figure 4-62.

In the case of the vertical excitation testing, the servo-controller of the electro-hydraulic actuator was set for a force-feedback so that the actuator maintains a constant force.

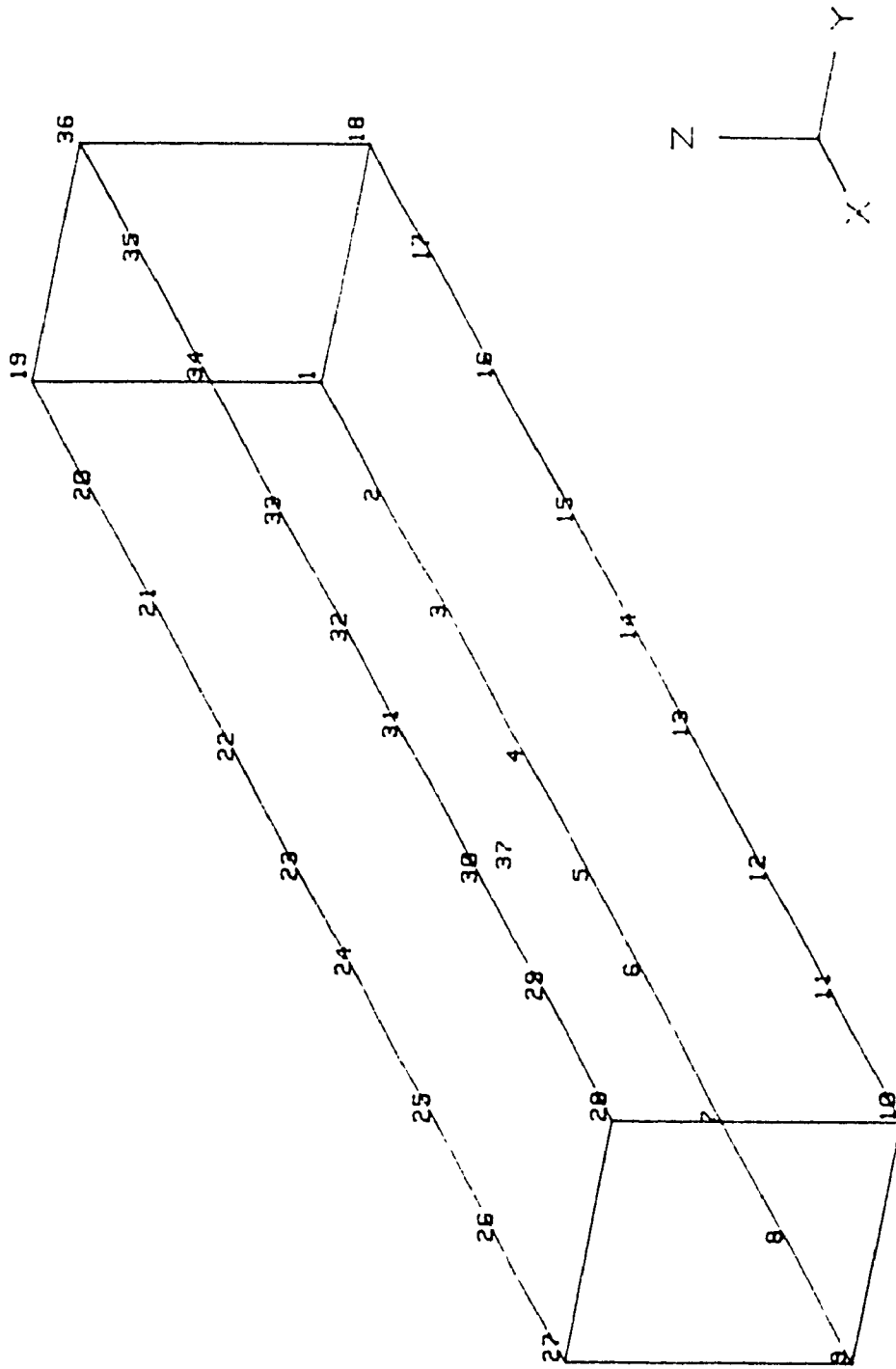


Figure 4-62: Schematic 3-D Model of the Second Large Vehicle Structure for Lateral Excitation. [15]

In the case of the lateral excitation testing, the servo-controller was set with the displacement feedback so that the actuator was vibrating at its mid-position.

It was found that the signal-to-noise ratio for lateral excitation testing was much higher than the ones for vertical excitation testing. It was also found that the modal density of the FRF measurements for the lateral excitation testing was lower than for the vertical excitation testing.

Also, the modal density of the FRF measurements obtained by using an electro-hydraulic shaker was much smaller than the ones obtained using an electro-dynamic shaker. Hence, the modal peaks were identified quickly using the waterfall method discussed earlier.

Both FRF-measurement sets (from vertical and lateral excitation testings) were processed and the estimated modal parameters were found to be identical.

Finally, the third vehicle structure was discretized into 42 points and is illustrated schematically in Figure 4-63, which includes measurement points (points 1 to 42) and shaker driving point location (point 1). The electro-hydraulic shaker was used to excite the structure. It was decided to excite it vertically at the left corner of the end section, i.e. at point 1 (Figure 4-63) acting along Z-axis, and

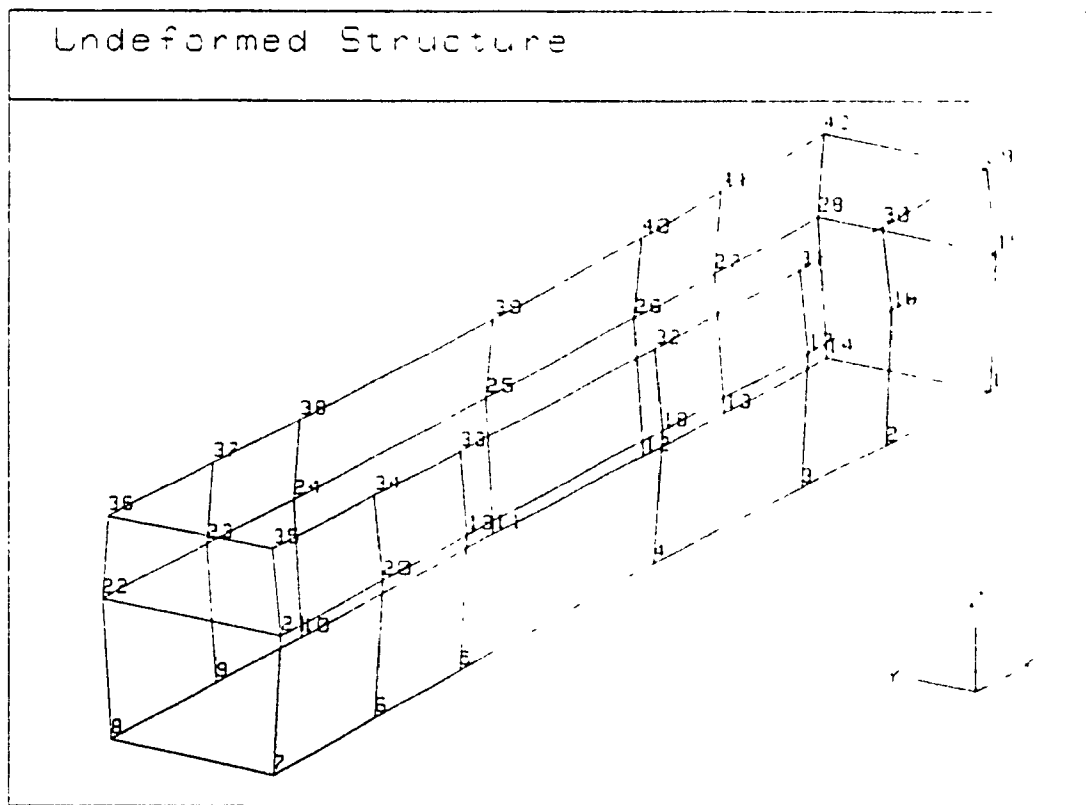


Figure 4-63: Schematic 3-D Model of the Third Large Vehicle Structure [19]

84 FRF measurements (along Y- and Z-axes) were taken.

For the three vehicle structures, the modal parameters were estimated in four steps for each mode using the global curve-fitting method. Firstly, the modal peaks were identified as discussed in the previous sections.

In the second step, the modal frequency, modal damping, and residue were estimated by curve-fitting a single measurement. A Single-Degree-of-Freedom (SDOF) method with polynomial curve-fitting algorithm was used.

In the third step, the remaining measurements for that mode were autofitted to estimate the residues at all the other discretized locations. Finally, the residues were sorted to obtain the mode shapes.

All three vehicle structures were mounted on shop-dolly with appropriate suspensions and simulated payload using lead weights. For the three vehicle structures, the highest rigid body mode-frequency was around 5 Hz. Rolling, bouncing with small roll, and pitching were found to be the rigid body modes for the first, second, and third vehicle structures, respectively. The lowest flexural mode frequency for each vehicle structure was found to be around 8 Hz.

Finally, around 10 flexural modes were found for each vehicle structure. As it is normally expected, all modes were simple modes, such as longitudinal twist, first and second vertical bending, first and second lateral bending, and a combination of two modes, e.g. first vertical bending with small longitudinal twist.

#### 4-4 CONCLUSION

In this chapter, the process involved in carrying-out experimental modal testing, using computer-aided modal analysis software, is discussed in detail. A small vehicle structure was used, as an example, to illustrate the testing procedures, including the measurement and data analysis phases.

The procedures for setting-up the modal testing and making the measurements on the small structure were presented. Then, the modal parameter estimating techniques and the modal results, obtained from the testing of that structure, were also presented.

Finally, heuristic procedures for carry-out modal testing on large vehicle structures were discussed.



CHAPTER 5

MODAL ANALYSIS OF A SNOWMOBILE FRAME STRUCTURE

USING

FINITE ELEMENT ANALYSIS (FEA)

## CHAPTER 5

### MODAL ANALYSIS OF A SNOWMOBILE FRAME STRUCTURE

#### USING

#### FINITE ELEMENT ANALYSIS (FEA)

##### 5-1 General

Modal testing is an experimental testing technique used to identify the major modes of vibration of a test structure within a selected frequency bandwidth. The modal model or frequency domain model can be formulated by measuring the minimum set of data required, i.e. at least one row or column of the FRF (Frequency Response Function) measurements matrix. This model is given in terms of the modal parameters, which are: modal frequency, modal damping and mode shape.

The modal model can be used to carry-out two types of computer analyses. The first type is called structural dynamics modification analysis, and consists of studying the changes in the modal properties (parameters) of a test structure due one or several modifications in its mass, stiffness, and damping. This analysis is very useful to solve a noise or vibration problem since the resonance(s) causing the mechanical amplification of the normal operational forces can be shifted by adding or removing mass, stiffness or damping at strategic locations on the

structure. Alternatively, a tuned vibration absorber (i.e., spring-mass-damper vibrators) can be attached to the structure and fine tuned to get an acceptable structural response. In addition, this analysis is very practical to simulate the test structure in its operational environment (e.g. to add its payload, to connect it to ground or to another structure).

Sinusoidal forced response simulation is the second type of analysis that can be performed using the modal model. Basically, the vibration response of the structure is predicted due to a sinusoidal excitation force acting at one DOF. When the structure is subjected to more than one sinusoidal excitation force acting all at the same frequency, the total response will be the sum of the individual responses. For example, a rotating unbalance can be simulated as two orthogonal sinusoidal excitation forces both acting at the rotating frequency, but  $90^\circ$  out of phase. In the case when the excitation frequencies are different, true vibration response is only feasible for linear system using modal superposition.

However, when designing or optimizing a structure, static and/or dynamic stress analyses are needed, and the modal model cannot be used to carry-out these since they are derivatives of displacements. An analytical model has to be developed and Finite Element Technique is a well accepted method to model a structure and to calculate structural dynamic response. Finite Element Analysis (FEA) requires the creation

of a Finite Element Model (FEM). This model is a mathematical idealization of the structure and is described by nodes, elements, and boundary conditions.

In this chapter, the modelling of a lightweight structure (the snowmobile frame structure) presented in the previous chapter is discussed using FEA. The ANSYS-PC/LINEAR, revision 4.4, was used to model the structure and to carry-out the modal analysis. The results from this analysis are compared to the ones obtained from modal testing and conclusions are drawn.

## 5-2 The ANSYS-PC/LINEAR Finite Element Software

The ANSYS-PC/LINEAR program is a finite element software that runs on 80286 or higher microprocessor-based computers in DOS (Disk Operating System) environment. It is a general purpose finite element code for solving many practical engineering problems (e.g., a structural engineer may have to study the vibration response of a bridge due to moving loads, whereas an electrical engineer may have to study the magnetic potentials of an electric motor).

There are six different structural analysis types in ANSYS program: Static Analysis, Modal Analysis, Transient Dynamic Analysis, Harmonic

Response Analysis, Response Spectrum Analysis, and Random Vibration Analysis. They are all governed by special cases of the same general equilibrium equation:

$$[M]\{\ddot{u}\} + [C]\{\dot{u}\} + [K]\{u\} = \{F(t)\} \quad (5-1)$$

where

$[M]$  = Structure mass matrix (known)

$[C]$  = Structure damping matrix (known)

$[K]$  = Structure stiffness matrix (known)

$\{F(t)\}$  = Time dependent forcing function vector (known)

$\{u\}$  = Nodal displacement vector (unknown)

$\{\dot{u}\}$  = Nodal velocity vector (unknown)

$\{\ddot{u}\}$  = Nodal acceleration vector (unknown)

### 5-2-1 General Finite Element Concepts

Similar to modal testing, the structure is discretized into a number of points called nodes. These nodes should be defined, at least at locations, to accommodate the element types (e.g. 2-D line element, 2-D surface element, 3-D solid element, etc.) selected to model adequately each major structural component of the structure and also at

locations where boundary conditions are applied such as displacement constraints, applied forces, pressures, temperatures, body forces (gravity), etc.. Additional nodes should also be defined at locations where stress values need to be calculated in a fair amount of detail and also at areas where there are discontinuities in the structure.

There are 22 different element types available in the ANSYS-PC/LINEAR, revision 4.4 and are summarized in Figures 5-1 and 5-2. The selection of an element type to model a particular structural member of a structure is based on its mathematical capabilities (shape functions, loading options, etc.), and on its assumptions and restrictions. For example, 2-D truss element type is an uniaxial tension-compression element defined by two nodes with two DOFs at each node and would be appropriate to model a 2-D pin-jointed structure but would not be adequate to model a cantilever beam since bending is not considered in the solution of this element type.

The solution of the FEM is then carried-out firstly by constructing the element matrices  $[M_i^e]$ ,  $[C_i^e]$ , and  $[K_i^e]$  for each individual element "i" of the model. Secondly, each of them are assembled into the global matrices  $[M]$ ,  $[C]$ , and  $[K]$ . This is straightforward since the elements are mathematically connected to each other by their nodes. Then, the resulting global set of simultaneous equations (Equation (5.1)) are solved for the unknowns (displacement DOFs). ANSYS uses the frontal (also called the wavefront) equation method to perform the assembly and








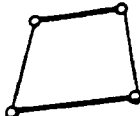
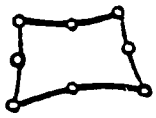
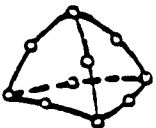
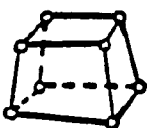

<p><b>2-D Truss</b></p>  <p>STIF1 2 nodes 2-D space DOF: UX, UY F: (S) Axial force only (spar).</p>	<p><b>3-D Truss</b></p>  <p>STIF8 2 nodes 3-D space DOF: UX, UY, UZ F: (S) Axial force only (spar).</p>	<p><b>2-D Elastic Beam</b></p>  <p>STIF3 2 nodes 2-D space DOF: UX, UY, ROTZ F: (S) For bending members with symmetric cross-sections.</p>	<p><b>3-D Elastic Beam</b></p>  <p>STIF4 2 nodes 3-D space DOF: UX, UY, UZ, ROTX, ROTY, ROTZ F: (S) Bending or torsional members with symmetric cross-sections</p>
<p><b>2-D Tapered Unsymmetric Beam</b></p>  <p>STIF54 2 nodes 2-D space DOF: UX, UY, ROTZ F: (S) Cross-section may taper and may be unsymmetric. Each end may be independently offset from node.</p>	<p><b>3-D Tapered Unsymmetric Beam</b></p>  <p>STIF44 2 nodes 3-D space DOF: UX, UY, UZ, ROTX, ROTY, ROTZ F: (S) Cross-section may taper and may be unsymmetric. Each end may be independently offset from node.</p>	<p><b>2-D Triangular Solid</b></p>  <p>STIF2 6 nodes 2-D space DOF: UX, UY F: (S) Plane stress, plane strain, or axisym models.</p>	<p><b>2-D 4-node Quadrilateral Solid</b></p>  <p>STIF42 4 nodes 2-D space DOF: UX, UY F: (S) Plane stress, plane strain, or axisym models.</p>
<p><b>2-D 8-node Quadrilateral Solid</b></p>  <p>STIF42 8 nodes 2-D space DOF: UX, UY F: (S) Plane stress, plane strain, or axisym models.</p>	<p><b>Tetrahedral Solid</b></p>  <p>STIF92 10 nodes 3-D space DOF: UX, UY, UZ F: (S) General application to 3-D solid models</p>	<p><b>8-node Brick</b></p>  <p>STIF45 8 nodes 3-D space DOF: UX, UY, UZ F: (S) General application to 3-D solid models. Generalized plane strain option.</p>	<p><b>4-node Quadrilateral Shell</b></p>  <p>STIF58 4 nodes 8-D space DOF: UX, UY, UZ, ROTX, ROTY, ROTZ F: (S) General thin shell or plate analyses. Membrane-only, bending-only, or both.</p>

Figure 5-1: Element Summary by Types Available In ANSYS-PC/LINEAR








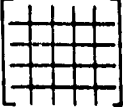


<p>Axisymmetric Shell with Torsion</p>  <p>STIF1 2 nodes 2-D space DOF: UX, UY, UZ, ROTZ F: (S) Axisym analysis of conical shells. Torsional behavior option.</p>	<p>Elastic Straight Pipe</p>  <p>STIF16 2 nodes 3-D space DOF: UX, UY, UZ, ROTX, ROTY, ROTZ F: (S) Axial, bending, and torsion behavior. Flexibility and stress intensification factors. Insulation and corrosion allowance.</p>	<p>Elastic Pipe Tee</p>  <p>STIF17 4 nodes 3-D space DOF: UX, UY, UZ, ROTX, ROTY, ROTZ F: (S) Axial, bending, and torsion behavior. Flexibility and stress intensification factors. Insulation and corrosion allowance.</p>	<p>Elastic Curved Pipe</p>  <p>STIF18 3 nodes 3-D space DOF: UX, UY, UZ, ROTX, ROTY, ROTZ F: Axial, bending, and torsion behavior. Flexibility and stress intensification factors. Insulation and corrosion allowance.</p>
<p>2-D Gap (Interface)</p>  <p>STIF12 2 nodes 2-D space DOF: UX, UY F: Interface for surfaces which may make or break contact.</p>	<p>3-D Gap (Interface)</p>  <p>STIF32 2 nodes 3-D space DOF: UX, UY, UZ F: Interface for surfaces which may make or break contact.</p>	<p>Generalized Mass</p>  <p>STIF21 1 node 3-D space DOF: UX, UY, UZ, ROTX, ROTY, ROTZ F: Lumped mass in dynamic or static analyses.</p>	<p>General Matrix</p>  <p>STIF27 2 nodes 3-D space DOF: UX, UY, UZ, ROTX, ROTY, ROTZ F: Allows user-input of 12 x 12 stiffness and/or matrices</p>
<p>Spring</p>  <p>STIF14 2 nodes 3-D space DOF: UX, UY, UZ, ROTX, ROTY, ROTZ, PRES, TEMP F: Torsional or longitudinal spring, thermal pipe, hydraulic conductance pipe.</p>	<p>Combination</p>  <p>STIF40 2 nodes 3-D space DOF: UX, UY, UZ, ROTX, ROTY, ROTZ, PRES, TEMP F: Spring and gap combination. Break-away or lock-up ability. Bilinear spring stiffness.</p>	<p>Legend:</p> <p>DOF = Degrees of Freedom F = Features S = Stress Stiffening</p>	

Figure 5-2: Element Summary by Types Available In ANSYS-PC/LINEAR



to obtain the solution simultaneously. Additional solution data such as structural stresses are calculated from the derivatives of the shape function. Indeed, strains are obtained from the first derivative of the displacements and stresses from the stress-strain relationships.

The construction of the individual element matrices are derived differently.  $[K_1^e]$ , is derived by using its element shape function and the energy principles. In the case of a consistent element mass matrix,  $[M_1^e]$  is also obtained by using the element shape function in its computation. When concentrated masses are used to replace the element mass (located at the element nodes), a lumped element mass matrix is obtained. In this case,  $[M_1^e]$  is a diagonal matrix (off-diagonal terms are zero) and the sum of the nodal masses equals the total element mass. A reduced element mass matrix will be a lumped one with no rotational DOF. Most ANSYS element types are defaulted to consistent mass matrix which, in general, is recommended, except in two cases [11]:

- When the structural component is small in one (or two) dimension(s) compared to the other dimension(s) - e.g., slender beams, very thin shells.
- For wave propagation problems.

In ANSYS, the element damping matrix,  $[C_1^e]$ , can be specified as a combination of inertial damping, structural damping and discrete damping:

$$[C_1^e] = \text{Inertial damping} + \text{Structural damping} + \text{Discrete damping} \quad (5-2)$$

Generally, friction and hysteretic dampings are the types of damping encountered in structures rather than viscous damping, and are usually approximated by a linear combination of the element mass matrix and of the element stiffness matrix respectively as follow:

$$[C_1^e] = \alpha[M_1^e] + \beta[K_1^e] \quad (5-3)$$

where  $\alpha$  and  $\beta$  are known as Rayleigh damping constants. These constants can be related to the modal damping ratio,  $\zeta_1$ , which are often known or estimated using experimental modal analysis [11]:

$$\zeta_1 = \frac{\alpha}{2\omega_1} + \frac{\beta\omega_1}{2} \quad (5-4)$$

where  $\omega_1$  is the circular modal frequency of  $i^{\text{th}}$  mode in radian per second.

The inertial (or mass) damping is a special case of Equation (5-4) where  $\beta=0$  so that

$$\zeta_1 = \frac{\alpha}{2\omega_1} \quad (5-5)$$

or

$$\alpha = 2\omega_1 \zeta_1 \quad (5-6)$$

A body immersed in oil would be an example of extreme case of inertial damping.

However, in most practical problems, rigid body damping can be ignored,  $\alpha=0$ , so that

$$\zeta_1 = \frac{\beta\omega_1}{2} \quad (5-7)$$

or

$$\beta = \frac{2\zeta_1}{\omega_1} \quad (5-8)$$

where  $\beta$  represents stiffness (or structural) damping.

Equations 5-4, 5-5, and 5-7 are plotted in Figure 5-3. It can be seen that at low frequencies,  $\alpha$ -damping, damped more than  $\beta$ -damping, and at high frequencies,  $\alpha$ -damping damped less than  $\beta$ -damping. Also, the sum of the two damping functions is nearly constant over the frequency range where they intersect. Therefore, given a damping ratio,  $\zeta$ , and a frequency range ( $f_1$  to  $f_2$ ), the following two equations can be solved simultaneously for  $\alpha$  and  $\beta$ .

$$\zeta = \frac{\alpha}{4\pi f_1} + \frac{\beta\pi f_1}{2} \quad (5-9)$$

$$\zeta = \frac{\alpha}{4\pi f_2} + \frac{\beta\pi f_2}{2} \quad (5-10)$$

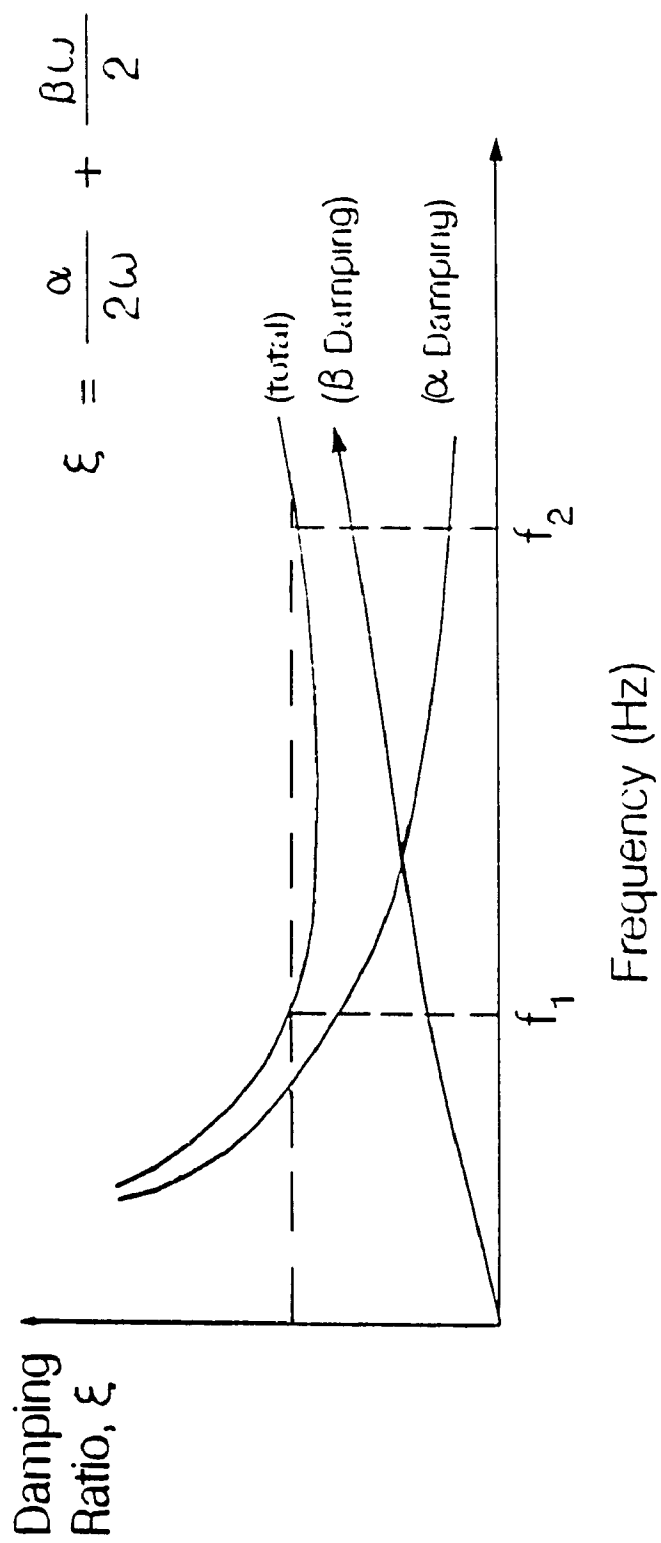


Figure 5-3: Plot of Equations (5-2), (5-3), and (5-3) [11]

### 5-2-2 Understanding Static and Modal Structural Analysis Types

Static analysis is, in general, the first type of analysis which is carried-out when studying or designing a structure. The purpose of that analysis is to evaluate the displacements, stresses, and reaction forces of the structure under applied static loads (applied loads do not vary with time). In this case, Equation (5-1) reduces to:

$$[K]\{u\} = \{F\} \quad (5-11)$$

Modal analysis, also called mode-frequency analysis, is used to evaluate the modal frequencies and mode shapes of a structure. In this analysis type, free, undamped vibrations are assumed, i.e.,  $\{F(t)\} = \{0\}$  and  $[C] = [0]$ . Hence the basic equations to solve are:

$$[M]\{\ddot{u}\} + [K]\{u\} = \{0\} \quad (5-12)$$

For a linear system, free vibrations will be harmonic of the form  $\{u\} = \{U\}\cos(\omega t)$  and Equation 5-12 will reduce to the classical eigenvalue problem:

$$([K] - \lambda[M])\{U\} = \{0\} \quad (5-13)$$

For non-trivial solutions, the determinant of  $([K] - \lambda[M])$  must be zero. The solutions are the eigenvalues,  $\lambda_1$ , and the corresponding

eigenvectors,  $\{U\}_i$ . They represent the natural frequencies of the system ( $\omega_i = \sqrt{\lambda_i}$ ) and the corresponding mode shapes respectively.

### 5-3 Modal Analysis of the Snowmobile Frame Structure Using FEA

The snowmobile frame structure is mostly made of steel pipes of different diameters and wall thicknesses, welded together. Some areas are reinforced with thin steel plates.

The modeling of this structure was particularly difficult because of its complex geometry, and due to the fact that the mass of the structural components itself represents about only 50% of the total mass of the frame. The other 50% of the mass comes from of the welded joints, local components, etc, for which their approximations and assumptions are not straightforward. Also the modeling of these small components could easily increase the FEM size such that it becomes unmanageable. However, since those components are local stiffeners and have very small effect on the modal properties, they were not modelled in ANSYS.

A three-dimensional FEM was constructed with ANSYS/PC/LINEAR, revision 4,4.. The structure was discretized into 27 nodes, of which 25 nodes have the same coordinates and numbering of the points layed-out on

the structure for the experimental modal analysis test and 2 extra nodes on members. Elastic straight pipe (STIF16) and 4-node quadrilateral shell (STIF63) element types were used to model the steel pipes and the steel plates respectively. The FEM developed consists of 41 elements, of which 22 elements were used to model the steel pipes and 19 elements to model the steel plates. Figures 5-4 and 5-5 show the FEM of the frame.

ANSYS/PC/LINEAR was used to carry-out modal analysis under free-free boundary conditions. The FEM was reduced from 162 DOFs (27 nodes times 6 DOFs per node) to 81 DOFs based on Guyan reduction method by specifying three translations on all the nodes as master DOFs shown in Figure 5-6. Three natural frequencies were calculated in the frequency range of 0 to 100 Hz. Their mode shapes are shown in Figures 5-7 to 5-10.

#### **5-4 Comparison between Experimental and Analytical Modal Results**

The natural frequencies and mode shapes of the snowmobile frame structure, obtained through FEA, are compared to those identified during modal testing.

The first deflection mode corresponding to 30,7 Hz (experimental)

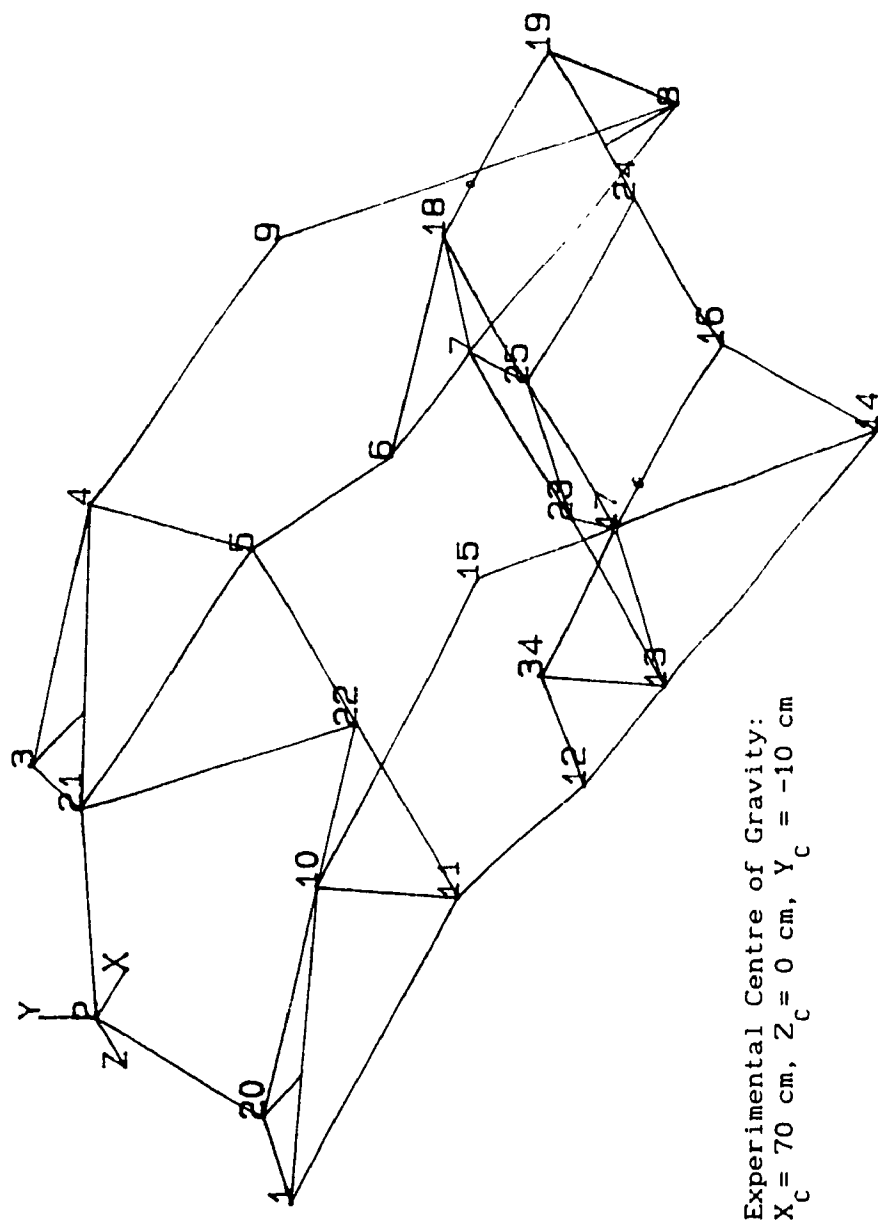


Figure 5-4: FEM of the Snowmobile Frame - Isometric View



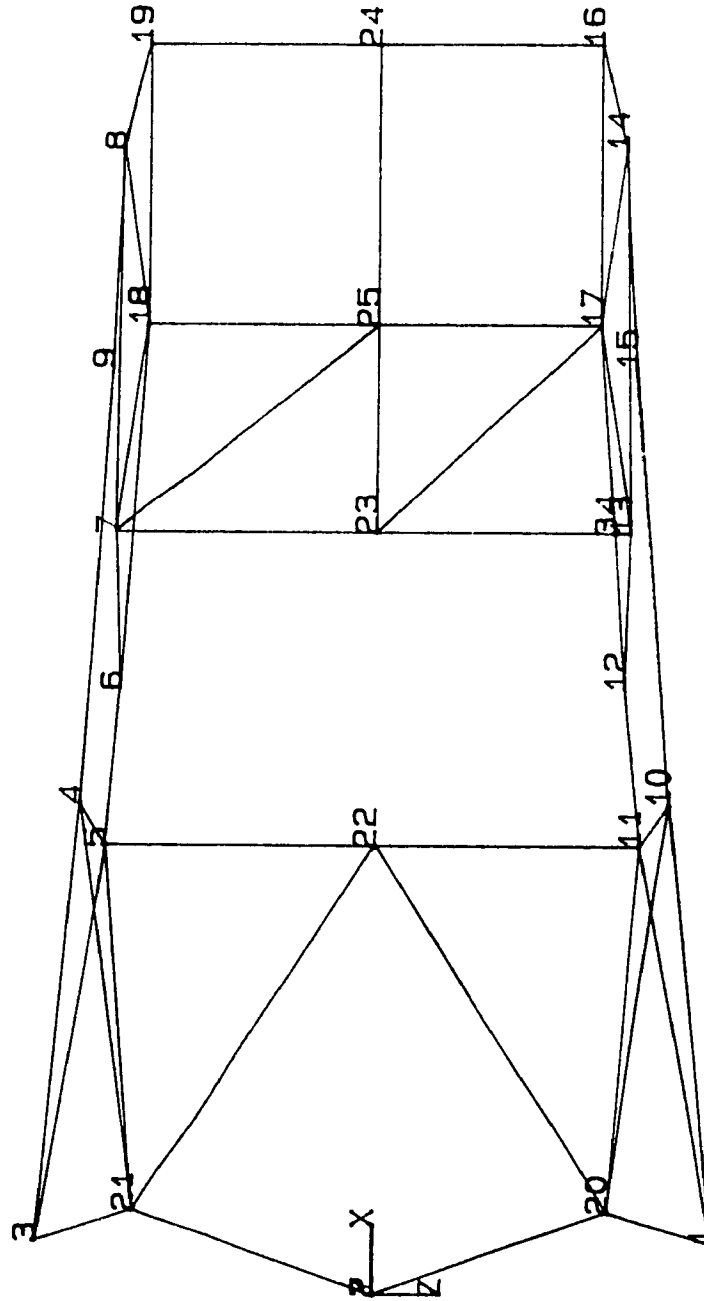


Figure 5-5: FEM of the Snowmobile Frame - Top View

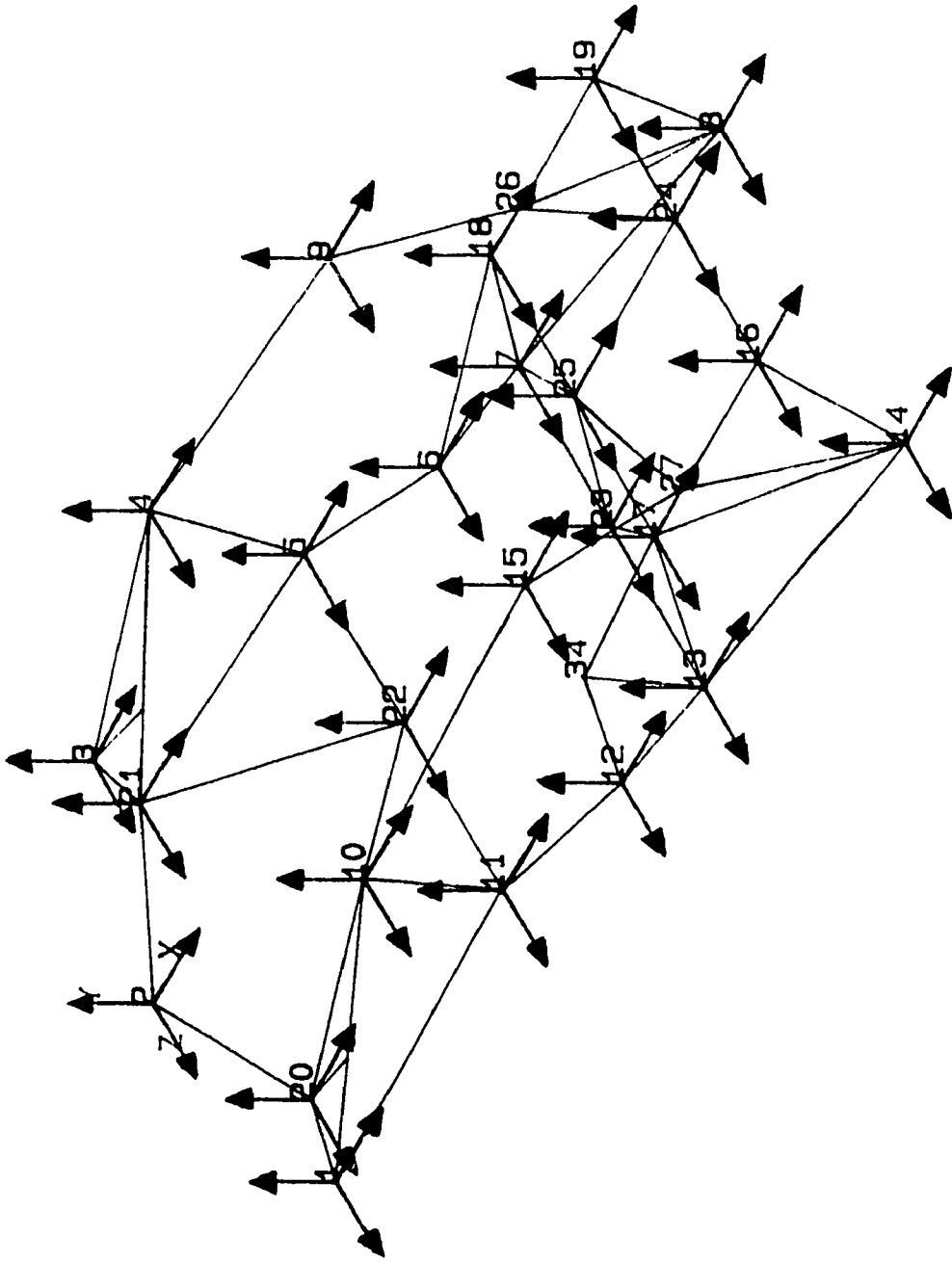


Figure 5-6: Master DOF's Selected for Modal Analysis

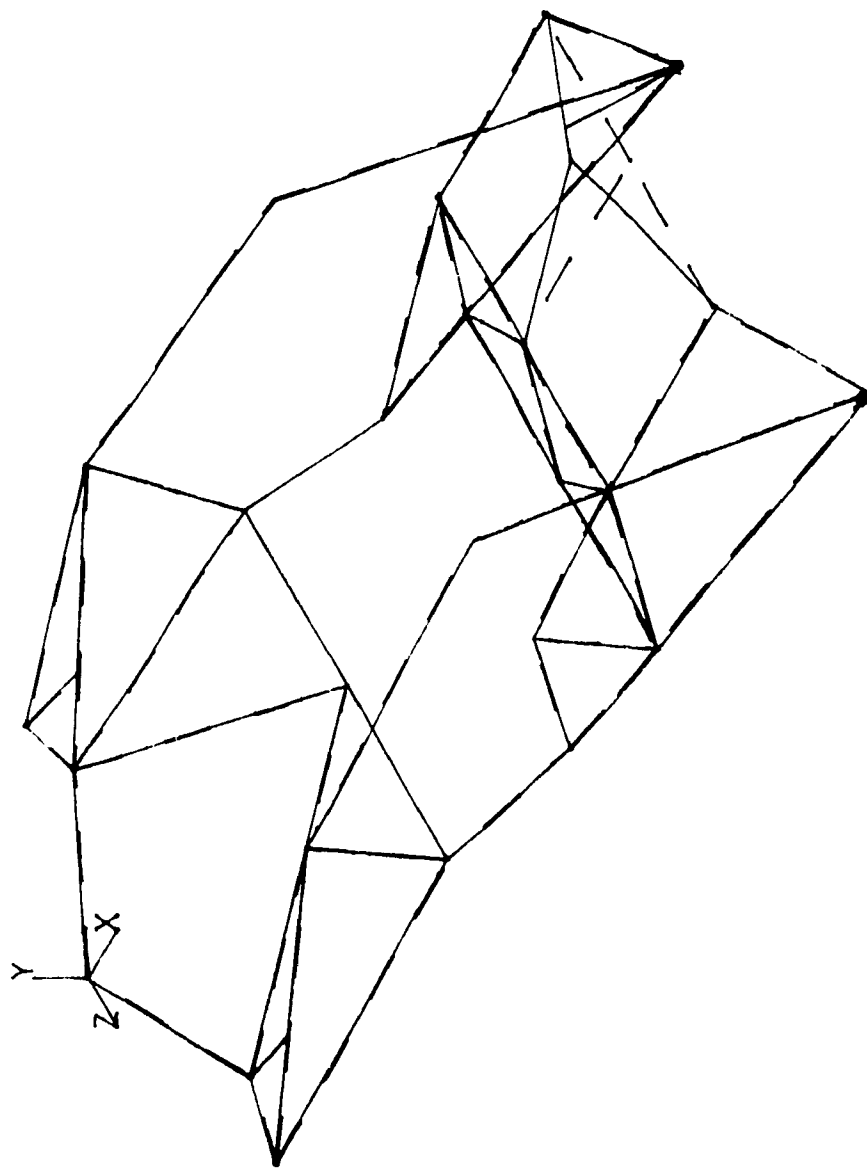


Figure 5-7: Isometric View - Mode #1 (30,3 Hz)  
Local Bending of Rear Section

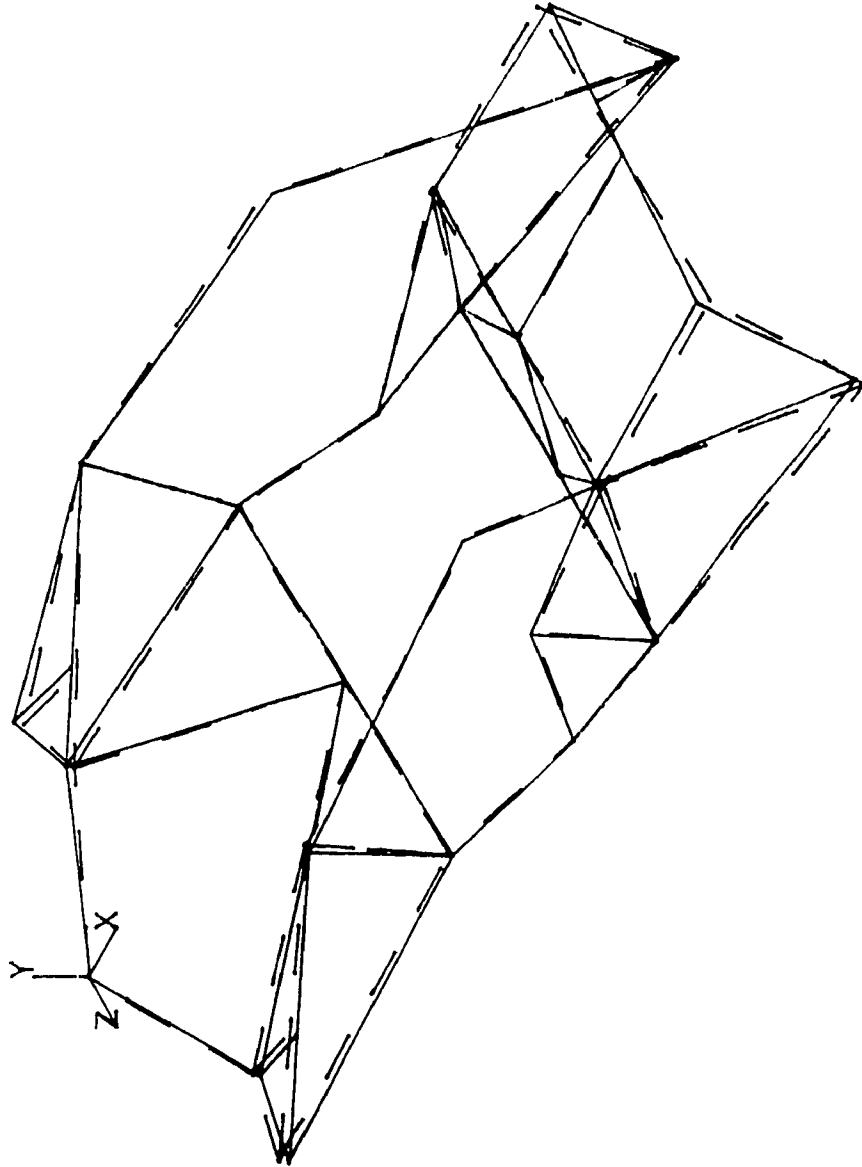


Figure 5-8: Isometric View - Mode #2 (44,7 Hz)  
Longitudinal Twist

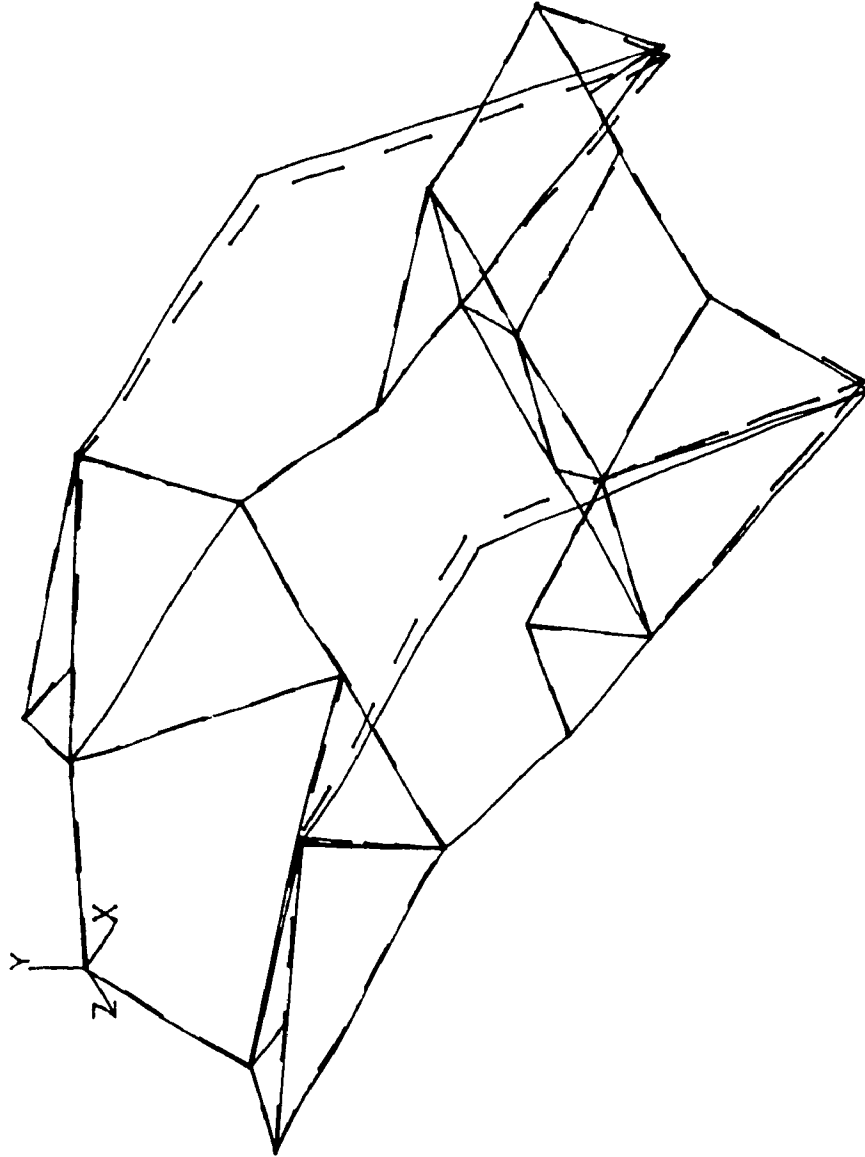


Figure 5-9: Isometric View - Mode #3 (75,5 Hz)  
Lateral Bending of the Side Steel Pipes (Out-of-Phase)

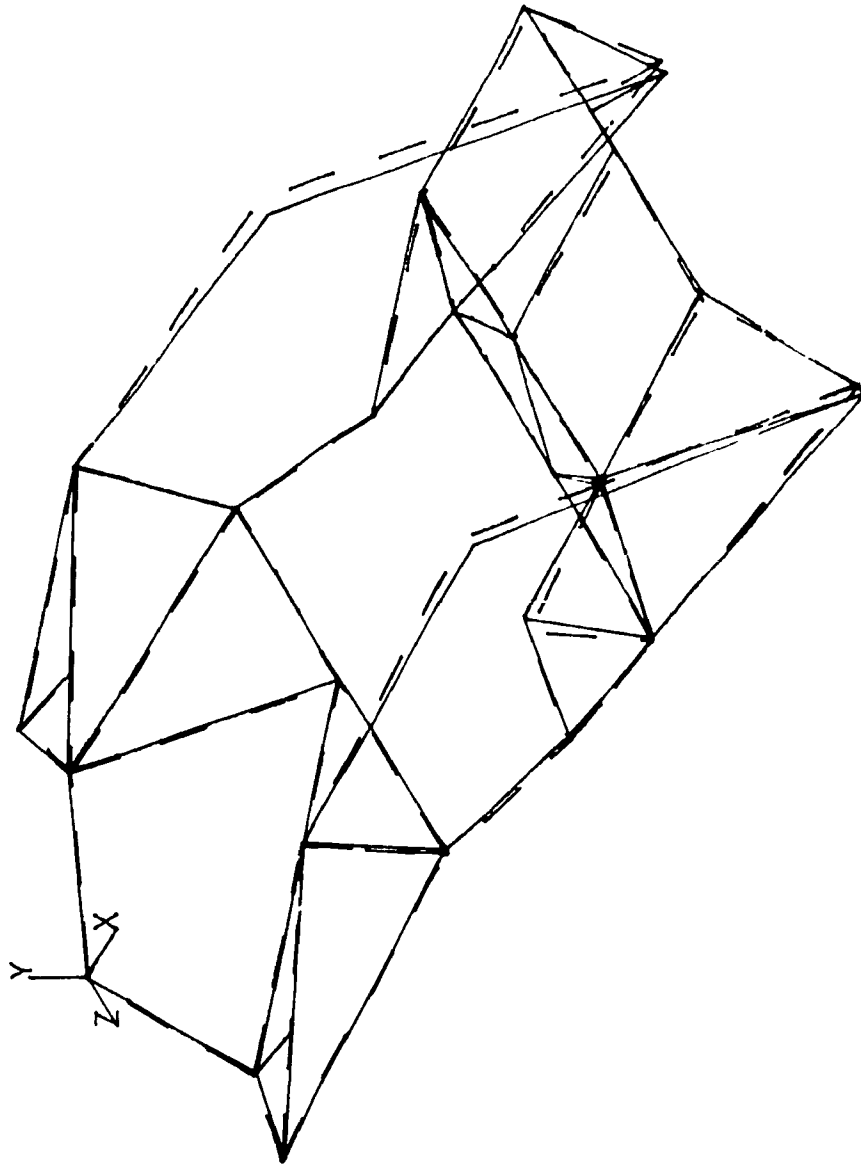


Figure 5-10: Isometric View - Mode #4 (89.2 Hz)  
Lateral Bending of the Side Steel Pipes (In-Phase)

and 30,3 Hz (analytical) are illustrated in Figure 5-7 and Table 4-7 respectively. We can observe that both of them exhibit similar local mode, i.e. bending of the rear panel.

For the second one corresponding to 40,5 Hz (experimental) and 44,7 Hz (analytical), we see that both of them exhibit a longitudinal twist and it corresponds to the fundamental mode of the structure. Those are shown in Figures 4-54 and 5-8, respectively.

Finally, the fifth and the third deflection modes corresponding to 81.2 Hz (experimental) and 75,5 Hz (analytical) are presented in Figures 4-57 and 5-9 respectively. Both of them exhibit bending of the side steel pipes.

In addition to the mode shapes and modal frequency, the center of gravity (centroid of mass) and the total mass of the frame structure obtained from FEA is also compared to those found through experiment. The center of gravity is observed to be within 10% as shown in Table 5-1. But, the total mass estimated by the FEA is approximately 50% of the actual mass. This was expected since local stiffeners were not modelled in ANSYS.

Hence, this close agreement, between the analytical and experimental modal analysis results as well as the centroid of mass provide a high level of dynamic validation to the FE model. Indeed,

Table 5-1: Comparison of Analytical and Experimental Centroid of Mass and Total Mass

	Centroid of Mass (cm)			Total Mass (kg)
	X	Y	Z	
Analytical	65,0	-10,1	0,1	11,0
Experimental	70,0	-10,0	0,0	19,3
Error (%)	7,0	1,0	?	43,0



this analytical model can be used with confidence to carry-out dynamic analysis to calculate dynamic strains and stresses in time or frequency domains

#### 5-5 Conclusion

In this chapter, analytical modal analysis is carried-out on the snowmobile frame structure using FEM/FEA techniques. First, the needs of an analytical model and the general concepts of finite element methods are presented including the procedures to define the damping in the FEM. Finally, experimental and analytical results are compared to validate the FEM model.

## **CHAPTER 6**

### **CONCLUSIONS AND RECOMMENDATIONS FOR FUTURE WORK**

## CHAPTER 6

### CONCLUSIONS AND RECOMMENDATIONS FOR FUTURE WORK

#### 6-1 General

Experimental modal analysis is a powerful testing method which can be used to validate an analytical model, such as a finite element model (FEM). The validation consists of comparing the experimental modal results (modal frequency, modal damping and mode shape) with the ones predicted by the analytical model. Once the confidence in the FEM has been reached, the modal damping of the structure, estimated through modal testing, can be incorporated into the FEM to carry-out structural response analysis.

Another interesting point about this testing method is that the measured data provides another complete model (experimental modal model) which can be used to study the effects of modifying the structure.

In this thesis, theoretical basis, measurement and data analysis methods are provided in order to understand properly the implications and limitations of experimental modal analysis (modal testing) using single excitation technique. Rules of thumb or heuristic knowledge are highlighted to carry-out modal testing on small and large vehicle structures and to construct, with confidence, an experimental modal

model (mathematical model based on test data).

The limitations and assumptions involved in modal testing are presented as well as mathematical definitions upon which the technique is found. Such mathematical background information is important for the practical aspects of the measurement process to be utilized in the testing method.

Discussions are provided on the advantages and disadvantages of different measurement techniques which are currently used for modal testing. Also, rules of thumb are given to minimize the different errors relating to signal processing, such as random and bias errors, aliasing errors, just to name a few.

A small vehicle (snowmobile frame) structure is used as an example to illustrate the step-by-step procedures of modal testing using computed-aided techniques. Different methods are presented to help analyze the measured data and the experimental modal results, namely, the modal frequency, modal damping, and mode shapes. In addition, heuristic knowledge is provided to carry-out modal testing on large vehicle structures.

Finally, an analytical model of the snowmobile vehicle structure, was constructed using ANSYS-PC Linear software. The general concepts of FEM are discussed. Using the FEA software, analytical model analysis was carried-out.

## 6-2 Conclusions and Highlights of the Present Work

It can be concluded that the main steps to carry-out modal testing, using single exciter methods and a computer-aided modal analysis software, can be specified as follows:

### 1) Set-Up the Test Experiment

- Choose the excitation technique
- Mark-out test points on the structure
- Mount the structure
- Set-up the force and response transducers
- Set-up the FFT analyzer
- Calibrate the force/response transducer combination
- Make trial measurements

### 2) Build the Geometrical Model

- Measure the coordinates of the points layed-out on the structure
- Define the model into the computer system

### 3) Take measurements

- Measure and compute a frequency response function at each DOF
- Transfer the FRF measurements into the computer hard-disk

### 4) Estimate Modal Parameters

Identify the modal frequency

Curve-fit the measurements to extract the modal

## 5) Sort the Modal Data

- Generate and animate each mode shape

These points are discussed in detail in the present work. However, the rules of thumb can be summarized as follows:

- Translational DOF's are usually sufficient to describe the motion of a vehicle structure (p. 160);
- If the test consists only of estimating the modal frequencies and modal dampings of the vehicle structure, then only a few DOF's are required (p. 160);
- If the test consists of obtaining a modal model, then sufficient test points must be used to describe all the mode shapes of the vehicle structure within a frequency band of interest (p. 160) - If available, use same coordinates used in the theoretical model;
- At least one row or one column of the FRF matrix is required to carry-out SDM (structural dynamic modification) (p. 161);
- Use masking tape to mark and number the test points onto the structure (p. 160);
- Usually, two measurement directions are sufficient to describe simple mode shapes (p. 165);
- It is preferable to prepare the vehicle structure in a "free-free" condition by mounting it with softy restraints (p. 165);
- Hanging direction should be perpendicular to the primary excitation direction (p. 166);

- Check influence of rigid modes on the flexural rule of thumb (p. 166);
- Shaker testing techniques with pseudo-random wave preferable to hammer testing techniques (p. 167);
- Use an impact blow hammer or a sledge hammer to identify the fundamental frequency and then to verify that the shaker influence is small (p. 187);
- Always conduct a calibration of the force/response transducer combination before actual testing (p. 172);
- Locate exciter at a corner of the vehicle structure so that both symmetric and asymmetric modes can be excited (p. 183);
- "Fun Tak" product works well to hold the accelerometer at the selected points on the vehicle structure (p. 183);
- Select the frequency bandwidth of interest from 0 Hz to twice the one specified in the test requirements (p. 109);
- Compute auto-spectrum, Coherence function, and signal-to-noise ratio to make conclusions (p. 187);
- Symmetricity and reciprocity verifications are not needed unless one wants to assess those assumptions (p. 201);
- Use 3 to 5 averages to verify that the measurement has constant value and its Coherence function is close to unity (p. 108);
- Always use an oscilloscope to monitor both the input and output electrical signals (p. 187);
- Use waterfall window to identify bad measurements (p. 207);
- Use the approach discussed in Section 4-2-3 to identify the modal frequencies and to estimate the modal parameters (p. 211).

Also, the FEM of the snowmobile frame structure is validated by comparing the finite element analysis (FEA) results from modal analysis to the ones obtained from carrying out experimental modal testing on a prototype.

### 6-3 Recommendations for Future Work

Modal validations of the finite element model was carried-out through experimental modal testing. However, prior to its use, higher confidence in the analytical model should be achieved through static validations using strain gages.

Structural Dynamic Modifications (SDM) should be used to investigate the effects on the modal properties by adding secondary structures to the main snowmobile frame structure, such as the motor, skis, rear section, etc. This investigation can be studied using both models (analytical and experimental) and the resultant modal properties from each of them can also be compared.

It would be also interesting to make the actual modifications on the structure and to carry-out again modal testing, and then to compare the modal results with the ones obtained from SDM analysis.

Finally, modal testing using multiple excitation techniques shall be experimented to establish the step-by-step procedure and rules of thumb.



## REFERENCES

## REFERENCES

- [1] Tse, F.S., Morse, I.E., and Hinkle, R.T. " Mechanical Vibrations - Theory and Applications ," Allyn and Bacon Inc., Boston, 1979.
- [2] Ewins, D.J. " Modal Testing: Theory and Practice ," John Wiley & Sons Canada Ltd., Ontario, 1984.
- [3] Zaveri, K. " Modal Analysis of Large Structures - Multiple Exciter Systems ," Brüel & Kjaer, Denmark, 1985.
- [4] " Modal 3.0 SE Version 6.00 Software and Operating Manual ," Structural Measurement Systems Inc., Milpitas, California, 1990
- [5] Dossing, O. " Structural Testing - Part I: Mechanical Mobility Measurements ," Brüel & Kjaer, Denmark, 1988.
- [6] " Instruction Manual: Dual Channel Signal Analyzer - Type 2032 - Familiarization ," Vol. 1, Brüel & Kjaer, Denmark, 1987.
- [7] Inman, D.J. " Vibration with Control, Measurement, and Stability ," Prentice Hall, New Jersey, 19??
- [8] Dossing, O. " Structural Testing - Part II: Modal Analysis and Simulation ," Brüel & Kjaer, Denmark, 1988.
- [9] Serridge, M., and Licht, T.R, " Piezoelectric Accelerometers and Vibration Preamplifiers - Theory and Application Handbook ," Brüel & Kjaer, Denmark, 1987.

- [10] Ramsey, K. " Effective Measurements for Structural Dynamics Testing - Part I ," Modal Analysis: A Collection of Technical Papers, Structural Measurement Systems Inc., April 1989.
- [11] " ANSYS Dynamics Seminar Notes ," DN-S211, Swanson Analysis Systems Inc., Rev. 4.3, Houston, 1989.
- [12] Broch, J.T. " Mechanical Vibration and Shock Measurements ," Brüel & Kjaer, Denmark, 1973.
- [13] Halvorsen, W.G. and Brown, D.L. " Impulse Technique for Structural Frequency Response Testing ," Modal Analysis: A Collection of Technical Papers, Structural Measurement Systems Inc., April 1989.
- [14] " Pamphlet: Shuttle Tourist Car ," Bombardier Inc., 1990.
- [15] " Master Catalogue - Electronic Instruments ," Brüel & Kjaer, Denmark, 1989.
- [16] Lebel, G., and Sankar, S. " Experimental Modal Testing for Evaluating Structural Body Vibration of a Euroshuttle Double Deck Carrier (DDC) Wagon ," Confidential Report, CONCAVE-06-91, CONCAVE Research Centre, Dept. of Mechanical Engineering, Concordia University, Montreal, June 1991.
- [17] Lebel, G., and Sankar, S. " Experimental Modal Testing for Evaluating Structural Body Vibration of a Single Deck Carrier (SDC) Wagon ," Confidential Report, CONCAVE-09-91, CONCAVE Research Centre, Dept. of Mechanical Engineering, Concordia University, Montreal, Sept. 1991.

- [18] Lebel, G., and Sankar, S. " Experimental Modal Testing for Evaluating Structural Body Vibration of a Double Deck Loader (DDL) Wagon ," Confidential Report, CONCAVE-12-91, CONCAVE Research Centre, Dept. of Mechanical Engineering, Concordia University, Montreal, June 1991
- [19] Ramsey, K. " Effective Measurements for Structural Dynamics Testing - Part II ," Modal Analysis: A Collection of Technical Papers, Structural Measurement Systems Inc., April 1989.
- [20] Richardson, M. " Modal Analysis using Digital Test Systems ," Seminar on Understanding Digital Control and Analysis in Vibration Test Systems, Modal Analysis: A Collection of Technical Papers, Structural Measurement Systems Inc., April 1989.
- [21] Shye, K., Vankarsen, C., Richardson, M., and Structural Measurements Systems Inc. " Modal Testing Using Multiple References ," Modal Analysis: A Collection of Technical Papers, Structural Measurement Systems Inc., April 1989.
- [22] Richardson, M., Ramsey, K., and Structural Measurements Systems Inc. " Integration of Dynamic Testing into the Product Design Cycle ," Modal Analysis: A Collection of Technical Papers, Structural Measurement Systems Inc., April 1989.
- [23] Structural Measurement Systems Inc. " An Introduction to Structural Dynamics Modification ," Modal Analysis: A Collection of Technical Papers, Structural Measurement Systems Inc., April 1989.

- [24] Ramsey, K., Structural Measurement Systems Inc., Firmin, A., and H. G. Engineering Ltd. " Experimental Modal Analysis, Structural Modifications and FEM Analysis - Combining Forces on a Desktop Computer ," Modal Analysis: A Collection of Technical Papers, Structural Measurement Systems Inc., April 1989.
- [25] Hebert, M., Kientzy, D., and Structural Measurement Systems Inc. " Applications of Structural Dynamics Modification ," Modal Analysis: A Collection of Technical Papers, Structural Measurement Systems Inc., April 1989.
- [26] Richardson, M., Formenti, D., and Structural Measurement Systems Inc. " Parameter Estimation from Frequency Response Measurements Using Rational Fraction Polynomials ," Modal Analysis: A Collection of Technical Papers, Structural Measurement Systems Inc., April 1989.
- [27] Bourdon, P., Brunelle, J., Hardy, C., and Lavigne, P. " The applications of Experimental Modal Analysis to Transmission Line Hardware ," Proceedings of the 4th IMAC, Los Angeles, CA, 1986.
- [28] Richardson, M., Formenti, D., and Structural Measurement Systems Inc. " Global Curve Fitting of Frequency Response Measurements ," Modal Analysis: A Collection of Technical Papers, Structural Measurement Systems Inc., April 1989.
- [29] Snoeys, R., Sas, P., Heylen, W., and Van Der Auweraer, H. " Trends in Experimental Modal Analysis ," Mechanical Systems and Signal Processing, Vol. 1, No. 1, Jan. 1987, pp. 5-27.

- [30] Dobson, B. J. " A Straight-Line Technique for Extracting Modal Properties from Frequency Response Data ," Mechanical Systems and Signal Processing, Jan. 1987, Vol. 1, No. 1, pp. 29-40.
- [31] Boentgen, R., Behring, A., Allen, B., and Yeh, C. " Dynamic Finite Element and Experimental Modal Analysis of a Trashrack for Use in a High Velocity Flow ," Proceedings of the 4th IMAC, Los Angeles, 1986.
- [32] Braccesi, C., and Carfagni, M. " Using Experimental Modal Analysis to Simulate Structural Dynamic Modifications ," Technical Review, No. 1, 1988, Brüel & Kjaer.
- [33] Sidhu, J., and Ewins, D. j. " Correlation of Finite Element and Modal Test Studies of a Practical Structure ," Proceeding of the 2nd IMAC, pp. 756-762, Orlando, Florida.